UNIVERSIDAD NACIONAL AUTÓNOMA DE MÉXICO

POSGRADO EN CIENCIAS DE LA TIERRA

CENTRO DE GEOCIENCIAS

CHARACTERIZATION OF GEOCHEMICAL AND ENVIRONMENTAL PROCESSES CONTROLING THE STABLE ISOTOPE AND TRACE ELEMENT COMPOSITION OF DRIP WATER AND FARMED CALCITE IN RÍO SECRETO KARST CAVE, LOCATED IN THE YUCATÁN PENINSULA, MÉXICO.

TESIS

QUE PARA OPTAR POR EL GRADO DE:

DOCTORA EN CIENCIAS DE LA TIERRA

PRESENTA:

MARÍA FERNANDA LASES HERNÁNDEZ

TUTORES:

DR. JUAN PABLO BERNAL URUCHURTU
CENTRO DE GEOCIENCIAS, UNAM

DR. MARTIN MEDINA ELIZALDE
UNIVERSITY OF MASSACHUSETTS AMHERST

ASESORA:

DRA. PATRICIA BEDDOWS
NORTHWESTERN UNIVERSITY

Juriquilla, Santiago de Quéretaro, Noviembre 2020

Declaración de Ética Académica

"Declaro conocer el Código de Ética de la Universidad Nacional Autónoma de México, plasmado en la Legislación Universitaria. Con base en las definiciones de integridad y honestidad ahí especificadas, aseguro mediante mi firma al calce que el presente trabajo es original y enteramente de mi autoría. Todas las citas de, o referencias a, las obras de otros autores aparecen debida y adecuadamente señaladas, así como acreditadas mediante los recursos editoriales convencionales".

Maria Fernanda Lases Hernández

A Joaquín por inspirarme a buscar tesoros bajo tierra…

La mejor vida no es la más duradera, sino más bien aquella que está repleta de buenas acciones (Marie Curie).

Aprende a vivir y sabrás morir bien (Confucio).

El corazón quiere lo que quiere, o no le importa (Emily Dickinson).

El mayor peligro que nos depara el futuro es la apatía (Jane Goodall).

Es como si el tiempo diera vueltas en redondo y hubiéramos vuelto al principio... (Gabriel García Márquez).

AGRADECIMIENTOS

Al Dr. Martin Medina Elizalde por acompañarme en mi travesía profesional y personal durante mis estudios de posgrado con gran honestidad, respeto, generosidad y sabiduría, por la amistad que hemos construido y tus profundas enseñanzas que me cambiaron para siempre.

Al Dr. Juan Pablo Bernal Uruchurtu por alentarme a realizar un doctorado y creer en mi desde el principio, por aceptar mi carácter obstinado y libre y darme un espacio en tú vida, toda mi admiración a tú gran profesionalismo y vocación científica.

A la Dra. Patricia Beddows por tantos consejos y enseñanzas a nivel personal y académico, por confiar en mí, escucharme, comprenderme y ser una gran amiga y fuente de inspiración.

A los miembros de mi Jurado evaluador, los doctores Stephen Burns, Matthew Lachniet y Juan Carlos Herguera por invertir su valioso tiempo en revisar mi tesis y realizar sus enriquecedores comentarios y observaciones.

A la familia Río Secreto, son un gran ejemplo de lo que se puede lograr a través de la ciencia ciudadana y se han convertido en mi tribu:

A Tania Ramírez, por confiar y abrirme las puertas para realizar investigación en este sistema de cuevas, tu invaluable ayuda lo hizo posible, y más aún todas la aventuras, locuras, risas, tertulias, discusiones, marchas y borracheras que compartimos fueron imprescindibles en esta travesía. Eres una guerrera Tania, nunca desistas.

A Otto Von Bertrab, por su confianza y ayuda para realizar investigación dentro de este sistema y por su importante labor para preservarlo y compartirlo con la humanidad.

A mi amigo Raúl Padilla por tu genuino interés en mi trabajo de investigación y por hacerme testigo del tuyo, eres un gran naturalista que nos inspira a luchar por la conservación de nuestros ecosistemas.

A Rodrigo Pimienta por toda tu ayuda para documentar y compartir mi aventura en Río Secreto mediante increíbles fotos y videos, además por toda la música de azotea, charlas inspiradoras y nuestro interminable debate filosófico.

A mi querida amiga Lucila Faccioli por tu sinceridad, bondad, por apoyarme en campo y estar siempre pendiente de mis hallazgos en la investigación y de la evolución de mi vida personal.

A Alfredo Ponce Guevara por llevarme por primera vez al sitio de la cueva que más tarde sería conocido como “mi laboratorio”.

Mi agradecimiento más sincero a tantas amigas y amigos del alma que no solo me cambiaron la vida motivándome, con carcajadas y genuinas palabras de aliento y reconocimiento día tras día; sino que además me donaron su tiempo y esfuerzo para ir a la cueva a colectar muestras y mucho más, especialmente a:

Isabel Barradas Martínez, Yuliana Lizardi, Beatriz Karen Mukul Cahum, Mónica Fernández, Alan Borjas, Julio León, Hermelinda Ramos, Driss Castro, Ramón Hernández, Jonathan Sotelo, Edith Anacaren Kumul López, Aurora Dannae Martin, Víctor Rodas, Jimena Bornao, María Balam, Leonardo Lara, Ariel Desentis, Michel Zaidman, Atziri Lemus, Natalia Dixon, Pablo Salce, Ana Galetto, Alejandro Osorio Adoue, Daniele Mare, Guilhermetl Martins, Santiago Ruíz, Carina Carreón, Jorge Atlahua, Fausto German Pech, Héctor Cahum Cahum, Juan de Dios Mukul Cahum, Daniel Solis, Ricardo Careaga, Daniel Sanchéz, Alexandra Valadez, Daniela Trejo, Enrique Estrada , Mina Morsán. Y muchas otras personas que han trabajado en este lugar y lo mantienen funcionando, sin ustedes nada habría sido posible, muchas gracias a todas.

A la Universidad Nacional Autónoma de México y el Programa de Posgrado en Ciencias de la Tierra por el apoyo institucional, en especial por el financiamiento recibido del Programa de Apoyo a Proyectos de Investigación e Innovación Tecnológica a través de los proyectos IN110615 y IN108419.

Al Consejo Nacional de Ciencia y Tecnología por el apoyo de la beca Nacional de doctorado con el CVU no. 440572.

A la National Science Foundation por el apoyo financiero derivado de los siguientes proyectos: NSF Grant #1502836 y NSF Grant # AGS-1702848.

A la National Geographic Society por el apoyo financiero con el Waitt Grant #W457-16 y la Geological Society of America por el Research Grant que me fue otorgado.

A la cDra. Ofelia Pérez Arvizu, la M. en C. Liliana Corona Martínez, el Dr. Carlos Ortega Obregón y la M. en C. Carolina Muñoz Torres por su invaluable ayuda en el trabajo de Laboratorio que desempeñé en los laboratorios del Centro de Geociencias durante mi trabajo de doctorado.

Al Dr. Matthew DeCesare por su ayuda en el trabajo realizado en el Laboratorio de Paloclimatología e Isotópos Estables en Auburn University.

A Peter Sprouse y los espeleólogos que mapearon Río Secreto por compartirme el mapa del sistema, gracias a Edward Mallon por compartirme datos de temperatura generados por el Cave Pearl Project y a CONAGUA por compartirme datos meteorológicos contenidos en esta tesis.

Por último y de suma importancia agradezco enormemente a Dan Venegas Martínez por su colosal apoyo durante este tiempo, una larga lista que va desde crear un entorno de paz y armonía a mi alrededor hasta ayudarme en el campo y el laboratorio. Definitivamente no lo habría logrado sin ti, gracias infinitas por todo.

A mis cuatro perrhijes que me llenaron de amor y energía para enfrentar los retos del doctorado.

A toda mi querida familia que es enorme y muy solidaria, especialmente a mis abuelos Consuelo Ruíz Guzmán y Joaquín Hernández Vargas que en paz descanse por ayudarme a llegar hasta este punto en la vida. A mis amadas madre María del Carmen y hermana Carmen Angélica por su cariño y apoyo incondicional.

CONTENT

Resumen

La reconstrucción de la variabilidad hidroclimática pasada a partir de registros isotópicos de oxígeno (i.e. $\delta^{18}O$) y elementos traza en estalagmitas de regiones tropicales requieren una comprensión de la integración temporal de la cantidad de lluvia y de las características isotópicas y elementales de las aguas de goteo que en última instancia forman las estalagmitas. La principal motivación de este estudio fue determinar los controles hidrológicos de la composición isotópica y de elementos traza del agua de goteo y la calcita para la reconstrucción de la variabilidad de la cantidad de lluvia y la detección de sequías y ciclones tropicales (CTs) a partir de registros de $\delta^{18}O$ y elementos traza en estalagmitas. Este estudio examina la composición isotópica de oxígeno ($\delta^{18}O$) e hidrógeno (δD) de muestras de agua subterránea, lluvia y agua de goteo, recolectadas a intervalos de tiempo desde ~semanales a ~bimensuales, durante cinco años hidrológicos en la cueva kárstica de Río Secreto, localizada en la Península de Yucatán, México. Este estudio presenta también resultados de la variabilidad de concentraciones elementales (i.e. Mg, Ca, Sr, Ba, Cl, Mn, Al y Ti) de muestras de lluvia y agua de goteo recolectadas durante un período de 52 meses que abarcan 4 de los 5 años hidrológicos. Las condiciones ambientales de la cueva y los parámetros geoquímicos del agua de goteo se monitorearon en tres cámaras de la cueva con diferentes grados de ventilación junto con las condiciones de temperatura y humedad relativa en la superficie. Durante los primeros tres años se examinaron 16 sitios de goteo los cuales reflejaron la variabilidad isotópica (δD y $\delta^{18}O$) anual de la lluvia en diversos grados, dependiendo del tamaño de los reservorios de agua contenida en el epikarst y de la complejidad de las rutas de flujo. Durante el cuarto y quinto año hidrológico se modificó el protocolo de muestreo para capturar toda el agua de drenaje de 7 de los 16 sitios de goteo originales, seleccionando los sitios de goteo que representaron mejor el rango completo de la variabilidad elemental, isotópica e hidrológica caracterizada previamente. La variabilidad isotópica observada a escalas temporales desde quincenales hasta interanuales en los valores de $\delta^{18}O$ del agua de cada sitio de goteo puede explicarse a través de diferentes integraciones de la cantidad de lluvia en el dominio del tiempo. Los sitios de goteo en dos cámaras (estaciones A y B) integran desde 4 hasta 15 meses de acumulación de lluvia. En una tercera cámara (estación LF) un sitio de goteo refleja el ciclo isotópico de la lluvia anual con un sesgo hacia valores positivos y otro sitio de goteo refleja los eventos de lluvia más cuantiosos.

Durante la infiltración en el epikarst, la integración de la cantidad de lluvia por los reservorios que abastecen el agua de goteo determina el grado en el que "diluyen" la firma isotópica de un ciclón tropical. Los CTs se pueden detectar particularmente cuando: (1) el volumen de agua del reservorio en el epikarst es bajo, por ejemplo, durante una sequía meteorológica persistente, y; (2) Los CTs tienen una señal isotópica suficientemente distinta en relación con la ya existente en el reservorio previa al evento. Las señales isotópicas de CTs pueden enmascararse o atenuarse cuando las muestras de agua de goteo se colectan durante más de una semana e incluyen eventos de lluvia posteriores al CT.

La relación lineal entre las razones Sr/Ca y Mg/Ca de las aguas de goteo revela interacciones agua/roca tales como la precipitación previa de calcita (PCP) en todos los sitios de goteo analizados. En la cueva de Río Secreto, es posible reconstruir la cantidad de precipitación y detectar las firmas isotópicas de los CTs a partir de registros de $\delta^{18}O$ de estalagmitas. El análisis aquí realizado demuestra que los registros de $\delta^{18}O$, Mg/Ca y Sr/Ca de las estalagmitas tienen más probabilidades de subestimar la magnitud de una sequía a escala anual subsecuente a condiciones hidroclimáticas normales, y más probabilidades de registrar un CT durante sequías de varios años que durante períodos hidroclimáticos normales o particularmente húmedos. Los resultados del monitoreo de las aguas de goteo sugieren que los registros disponibles de $\delta^{18}O$ a partir de estalagmitas de las tierras bajas Maya podrían estar subestimando la intensidad de los eventos de paleo-sequías hasta ahora encontrados, como las sequías del Clásico Terminal asociadas con la desintegración de la civilización Maya.

Adicionalmente, las proporciones de los elementos traza y la variabilidad de $\delta^{18}O$ y de $\delta^{13}C$ fueron determinadas en calcita neoformada de tres sitios de goteo diferentes que creció a diferentes intervalos cubriendo un período de 24 meses, lo cual permitió el cálculo de coeficientes de distribución para Sr, Mg y Ba a partir de valores empíricos.

Se realizó una comparación de estos coeficientes de determinación y de los valores de $\delta^{18}O$ de la calcita neoformada, con los pronosticados por las relaciones de equilibrio publicadas basadas en experimentos de laboratorio de calcita inorgánica y/o en condiciones análogas a las de una cueva, cálculos teóricos y calibraciones *in situ*. Este estudio proporciona la primera evidencia por una calibración *in situ* de la viabilidad del uso de los valores de

$\delta^{13}C$, Mg/Ca y Sr/Ca como indicadores paleoclimáticos de condiciones húmedas y secas registradas en estalagmitas de esta región.

Por último, este estudio ofrece evidencia geoquímica de que la recarga efectiva en el sistema kárstico de la Península de Yucatán no está limitada a los meses en los que la precipitación excede la evaporación, debido a que la alta permeabilidad del substrato permite que la mayor parte de la lluvia "escape" de la re-evaporación y se infiltre rápidamente. Este descubrimiento hidrológico tiene implicaciones importantes para el manejo del agua dulce y para las estrategias de adaptación al cambio climático en la Península de Yucatán.

Abstract

The reconstruction of past hydroclimate variability from trace element and oxygen isotope (i.e. $\delta^{18}O$) records from stalagmites in tropical regions requires an understanding of the temporal integration of rainfall amount and the isotopic and elemental characteristics of drip water that ultimately form stalagmite deposits. The main motivation of this study was to determine the hydrological controls of the isotopic and trace element composition of drip water and calcite in order to reconstruct rainfall variability, droughts and tropical cyclone activity from stalagmite $\delta^{18}O$ and trace element records. This study examined the oxygen ($\delta^{18}O$) and hydrogen (δD) isotopic composition of groundwater, rainfall and drip water samples, collected from ~weekly to ~ bimonthly time intervals, over five hydrological years at Río Secreto Cave, in the Yucatán Peninsula, Mexico. This study also presents results of trace element variability (i.e. Mg, Ca, Sr, Ba, Cl, Mn, Al and Ti) from rainfall and drip water samples collected over a 52-month period spanning 4 of the 5 hydrological years examined. Cave environmental conditions and geochemical parameters of drip water were monitored in three chambers with different degrees of ventilation, along with temperature and relative humidity conditions at the surface. During the first three years 16 drip sites were examined and found to reflect the annual isotopic (δD and $\delta^{18}O$) variability of rainfall to varying degrees, depending on the epikarst water reservoir size and flow path complexity. During the fourth and fifth hydrological year the water sampling protocol was modified in order to capture all the water drained from 7 of the 16 original drip sites, selecting those which better represented the full range of elemental, isotopic and hydrological variability previously characterized. Observed bi-weekly to interannual variability in drip water $\delta^{18}O$ values during the five hydrological years examined can be explained by different integrations of rainfall amount in the time domain. Drip sites in two cave chambers (stations A and B) integrate 4 to 15 months of rainfall accumulation. In a third chamber (station LF) one drip site reflects the annual rainfall isotopic cycle with a positive offset and another, the largest rainfall events. During epikarst infiltration, the integration of rainfall amount by drip water source reservoirs determines the degree to which they "dilute" a TC isotopic signature. TCs can be detected particularly when: (1) the water volume of the reservoir is low, such as during a persistent meteorological drought, and; (2) TCs have a sufficiently distinct isotopic signal relative to

that of the reservoir prior to the event. TC isotopic signals can be masked or attenuated when drip water samples are integrating more than a week and rainfall events proceeding the TC.

Linear relationships between drip water Sr/Ca and Mg/Ca ratios reveal water/rock interactions such as Prior Calcite Precipitation in all drip sites analyzed. In Río Secreto cave reconstructing precipitation amount and detecting the TC isotopic signatures from stalagmite $\delta^{18}O$ records is possible. Our analysis shows that stalagmite $\delta^{18}O$, Mg/Ca and Sr/Ca records are more likely to underestimate the magnitude of annual-scale droughts following normal hydroclimate conditions and more likely to record TCs during multiyear droughts than during normal or wet periods. Drip water monitoring results suggest that available stalagmite $\delta^{18}O$ records from the Maya lowlands might be underestimating the intensity of paleo-drought events, such as the Terminal Classic droughts associated with the disintegration of the Maya civilization.

Aditionally, trace element ratios and $\delta^{18}O$ and $\delta^{13}C$ variability was determined from farmed calcite at three different drip sites during a 24-month period, allowing the calculation of empirical distribution coefficients for Sr, Mg and Ba. These trace element distribution coefficients and farmed calcite $\delta^{18}O$ values, were compared to those predicted by published equilibrium relationships based on laboratory experiments of inorganic calcite and/or under cave-analog conditions, theoretical calculations and *in situ* calibrations. This study provides the first evidence of the feasibility of using $\delta^{13}C$, Mg/Ca and Sr/Ca values as proxies of wet and dry conditions in stalagmites from this region.

Lastly, this study provides evidence that the effective recharge in the Yucatan Peninsula karst system is not limited to the months when precipitation exceeds evaporation, because high bedrock permeability allows rainfall to “escape” evaporation and infiltrate rapidly. This hydrological finding has important implications for freshwater management and adaptation strategies to climate change in the Yucatan Peninsula.

PREFACE

The rapid economic and population growth observed worldwide over the last decades have resulted in the accelerated consumption and destruction of vital resources (forests, fossil fuels, biodiversity) and global climate change. Our understanding of Earth's climate variability has improved substantially, thus providing the knowledge necessary to mitigate the negative impacts of human activities on Earth's ecosystems and climate. The prediction of future climate variability by Earth System Model studies, however, has significant uncertatinty, particularly concerning the magnitude and frequency of future changes in hydroclimate, such as droughts, floods and tropical cyclones. In order to mitigate and adapt to future anthropogenic climate change it is necessary to analyze the history of Earth's climate evolution so as to understand the short-term and long-term drivers of climate variability and to improve model predictions from Earth System Models.

Paleoclimate studies provide an essential tool to predict future climate change and to assess the extent to which human and biological adaptation is realistic under business-as-usual scenarios of anthropogenic greenhouse gas emissions. Recent efforts, in particular, have utilized paleoclimate observations to provide an empirical assessment of climate sensitivity and hydrological responses to shifts in the concentration of atmospheric greenhouse gases and other factors internal to the climate system (Medina-Elizalde et al., 2017; Palaeosens, 2012). Studies of past climates spanning large time scales are based on interpreting geochemical "proxies" that are indicators of past climate variables. Proxies are measured in different natural archives, for example, ice cores, marine and lake sediments, and speleothems (Bradley, 1999).

In the last decades the use of speleothems as archives has considerably increased since they are terrestrial archives of climate and environmental variability that offer many advantages: absolute chronologies that can be obstained via the Uranium series disequilibrium technique, the measurement of multiple proxies within a single sample, their natural abundance throughout the world and, high degree of preservation relative to other terrestrial and marine archives (Fairchild and Baker, 2012). The most widely used speleothems for paleoclimatic reconstructions are stalagmites, which are secondary deposits

of calcium carbonate. The stalagmite formation process is carried out in karst caves, by dissolving $CaCO_3$ above the epikarst and its subsequent re-precipitation in the vadose zone.

Mexico has the longest system of flooded karst caves in the world, which is located in the Yucatan Peninsula (Bauer-Gottwein et al. 2011), where thousands of dolines allow access to flooded and semi-flooded caves that have thousands of stalagmites. Only along the coast of the State of Quintana Roo there is a record of more than 1,300 kilometers of full-mapped caves (QRSS, 2016). Together with its location at the western end of the Tropical Atlantic, the abundance of caves and stalagmites, make the Yucatan Peninsula an ideal region to carry out paleoclimatic and paleoenvironmental reconstructions from speleothems.

The most common used proxy in stalagmites is the ratio of stable oxygen isotopes denoted as $\delta^{18}O$, that has been often interpreted to reflect past hydrological variability in tropical and subtropical regions (Lachniet et al. 2012, 2017; Medina Elizalde et al., 2010, 2016a, 2017). Less frequently used stalagmite environmental proxies have been stable carbon isotopes ($\delta^{13}C$) and trace element ratios (i.e. Mg/Ca, Sr/Ca and Ba/Ca), that have been also interpreted to reflect wet and dry climate conditions (Ridley et al. 2015; Fairchild and Treble, 2009).

Although seldom acknowledged by studies concerning paleohydrological reconstruction based on stalagmite proxy records, it is essential to understand how regional and local processes control the isotopic and trace element composition of meteoric precipitation, drip water and calcite in order to interpret these records properly. Therefore, the process of speleothem formation and their chemical compositions have been monitored in many caves around the world (Baker et al. 2019). Monitoring generally includes long-term measurement of stable isotopes ($\delta^{18}O$, $\delta^{13}C$) (Luo et al. 2014, Moreno et al. 2014, Affolter et al. 2015), pH and minor elements (e.g. Mg, Sr, Ba) (Tremaine and Froelich, 2013; Wassenburg et al. 2020) in drip water and in farmed calcite under controlled conditions. In addition, other important parameters that influence stalagmite formation have been monitored, such as temperature, relative humidity and CO_2 concentration in the cave environment (Riechelmann et al. 2011, Tremaine and Froelich, 2013). Stalagmite formation has a relationship with each of these physicochemical parameters and ultimately their variability over time can also be related to climatic variability. Nevertheless, to test this

assumption and the details of these relationships require an exhaustive long-term monitoring effort and the associated challenge of working frequently inside of a cave environment, often in complete darkness, far from outside air and within a rugged and hazardous terraine.

Due to the favorable characteristics of the Yucatan Peninsula that allowed the generation of several paleoclimate records from stalagmites and the need to test the assumptions implicit in these records, in 2014 I began conducting comprehensive monitoring work in the Rio Secreto karst cave, located in the northeastern Yucatan Peninsula, along the Caribbean coast of the State of Quintana Roo. This pioneering work yielded preliminary results of significant interest within the areas of hydrology and paleoclimatology, which encouraged me to pursue a Doctoral degree in Earth Sciences (Ciencias de la Tierra) at the Centro de Geociencias in the Univesidad nacional Autónoma de México (UNAM) starting in the year 2016. This PhD thesis presents an analysis of the results and the hydroclimate and paleoclimate implications of monitoring work conducted over five hydrological years at unprecedented resolution in many parts of the world and particularly in Mexico. This thesis is organized in three Chapters, which follow the narrative that resulted from the natural evolution of the data-based knowledge generated progressively from this monitoring work. The sequence of these chapters reflect the response to questions that led to new ones and that needed to be answer even at the expense of modifying the sampling protocol in order to best adjust it to the demands of the problem.

Chapter 1 presents the isotopic characterization of rainfall, drip water from 16 drip sites, and groundwater over three hydrological years. Drip water and groundwater is examined from three chambers within the Río Secreto cave system with different degrees of isolation, different temperature and relative humidity variability. This chapter explores the paleoclimatic implications of the isotopic results from groundwater and drip water. Particularly, it examines the role of drip water integration of the rainfall isotopic signal, qualitatively, and the implications of epikarst water reservoir size for the detection of the isotopic signals of drought and tropical cyclone events. This chapter also presents the interpretation of the enviromental parameters monitored such as temperature and relative humidity at distinct sites of the cave with different degree of isolation from the surface environment. An important finding reported in this chapter is the first empirical evidence of the existence of an “amount effect” on a seasonal scale in the Yucatan Peninsula, essential to

support paleorainfall reconstruction from stalagmites. A crucial finding reported here with implications for water management in the Yucatan Peninsula and other regions with similar karst topography, relates to evidence that evapotranspiration plays a negligible role on the effective recharge of groundwater and aquifers, despite that most of this region experiences a deficit of precipitation annually. Lastly, we found two drip water sites from the same chamber separated only 5 meters from each other, which had contrasting patterns of drip water isotopic variability. One of these drip sites, labelled Fénix, seemed to be recording the most intense rainfall events, while the other, labelled LF1, seemed to record closely the isotopic amplitude variability of rainfall at a monthly scale, but seemed biased toward more positive values. These observations from the same chamber represented a conundrum, since on one hand Fenix did not suggest evaporation affected the isotopic composition of drip water, while LF1 suggested it did. Because of the sampling protocol, consisiting of a discrete sampling of drip water for a period of 48 hrs every two weeks, we could not determine whether the isotopic composition of LF1 reflected evaporation or the sampling protocol. I finally note that this chapter was published in the Journal of Geochemica et Cosmochemica Acta in 2019 (Lases-Hernandez et al., 2019).

In Chapter 2, I shifted the sampling protocol to collect continuous water samples in order to be able to calculate an amount-weighted isotopic composition of drip water and test the hypothesis the isotopic compositon of LF1 reflected evaporation the surface. This new sampling protocol also enabled to examine the role of discrete versus continuous water sampling in the characterization of the annual amount-weighted isotopic composition of drip water. Chapter two includes two years of additional hydrological and environmental monitoring of the isotopic composition of 7 of the 16 drip sites previously examined. These drip sites were selected because they represent distinctive isotopic patterns with variable implications for paleoclimate reconstruction. The new monitoring effort: (i) enabled to produce estimates of rainfall integration times and degree of homogenization, stratified by reservoir, of six of these seven drip sites, from bi-weekly, monthly and annual drip water samples, and; (ii) help test the notion that the isotopic composition of drip water at different drip sites converge into a single value when drip water is integrated over a sufficiently long period and provided they reflect the same water source and no other process, such as evaporation, has altered the isotopic composition of the water source. In addition, this study

explored the implications of observed drip water variability and residence times for the detection of significant precipitation reductions (i.e. meteorological droughts) and TCs from stalagmite $\delta^{18}O$ records; and it provides the first instrumental evidence of the existence of a rainfall "amount effect" on interannual timescales for the YP. Chapters 1 and 2 provide therefore a thorough assessment of the processes that affect the isotopic signal of rainfall as it is transferred into drip water sites that ultimately provide the "ingredients" to form a stalagmite and how these processes may affect the interpretation of stalagmite $\delta^{18}O$ records as records of precipitation amount and tropical cyclone activity. However, there is one important aspect that needs to be examined in order to best interpret stalagmite isotope records as environmental and climate records; that is, that stalagmite calcite $\delta^{18}O$ reflects isotopic equilibrium conditions with the isotopic composition of drip water. This Chapter is currently under review in Geochemica et Cosmochimica Acta Journal.

Lastly, Chapter 3 explores the processes that control Mg/Ca, Sr/Ca and Ba/Ca variability of severn drip water sites from Río Secreto cave with samples spanning a 50-month period, based on both sampling protocols, discrete and continuous, and spanning a marked transition from drought to wet conditions. Inaddition this chapter presents results of farmed calcite collected on glass plates over 24 months, providing complimentary $\delta^{18}O$, $\delta^{13}C$ compositions and Mg/Ca, Sr/Ca and Ba/Ca ratios of the solid phase. This chapter presents distribution coefficients for Mg, Sr and Ba, and $\delta^{18}O$ empirical values from drip water and calcite and compares them with those predicted by published thermodynamic relationships based on laboratory experiments of inorganic calcite and/or under cave-analog conditions, theoretical calculations and *in situ* calibrations. This chapter offers the first *in situ* calibration evidence of the feasibility of using $\delta^{13}C$ and X/Ca values as proxies of wet and dry conditions in stalagmites from this region. Lastly, isotopic results of farmed calcite suggest that stalagmites from Rio Secreto cave are likely to reflect isotopic equilibrium conditions, although significant variability exists and there is no consistency regarding published equilibrium equations that best describe the observations.

Until the year 2020, no similar monitoring work exists for the region (Baker et al. 2019), therefore this research lays the foundation to support paleoclimate and also future climate predictions. In addition, this study has implications that are significant for our understanding of aquifer recharge in one of the fastest growing regions in México and Latin

America, that is totally dependent on groundwater for the sustenance of human like and both terrestrial and marine ecosystems, including 25 Protected Natural Areas among wich there are 9 Biosphere Reserves: Arrecifes de Sian Kaan, Banco Chinchorro, Calakmul, Los Petenes, Ría Calestún , Ría Lagartos, Sian Kaan, Tiburón Ballena and Caribe Mexicano.

.

ELSEVIER

Geochimica et Cosmochimica Acta 246 (2019) 41–59

Geochimica et Cosmochimica Acta

Chapter 1. Long-term monitoring of drip water and groundwater stable isotopic variability in the Yucatan Peninsula: Implications for recharge and speleothem rainfall reconstruction

Fernanda Lases-Hernandez et al. 2019 (published article)

Abstract

Hydroclimate interpretations of stalagmite $\delta^{18}O$ records from tropical regions requires an understanding of the temporal integration of rainfall amount and its isotopic composition by drip waters that form stalagmite deposits. This study presents oxygen ($\delta^{18}O$) and hydrogen (δD) isotopic results from over 1200 groundwater, rainfall and drip water samples, collected at ~weekly time intervals, over three hydrological years at Río Secreto Cave, in the Yucatán Peninsula, Mexico. Cave environmental conditions and the isotopic composition of drip water were monitored in three chambers with different degrees of air ventilation, along with temperature and relative humidity conditions at the surface. We examined 16 drips and observed that annual δD and $\delta^{18}O$ variability reflects the isotopic variability of rainfall to varying degrees. The observed annual amplitude of drip water isotopic variability represents between 5% and 95% of that of rainfall, reflecting epikarst water reservoir size and the complexity of flow paths. Drips that closely reflect the isotopic variability of rainfall and best preserve the isotopic signal of individual rainfall events are observed, but they are uncommon. Only two drips out of 16 were found to have potential to record rainfall isotopic shifts associated with tropical cyclones if sampled at weekly resolution. The relationship between δD and $\delta^{18}O$ in drip water suggests that recharge is biased toward the rainy season (June to November), which represents up to 80% of total annual precipitation. We find that over the course of a year most drips reflect the annual $\delta^{18}O$ composition of rainfall, in support of quantitative precipitation estimates from stalagmite $\delta^{18}O$ records. We find evidence that the effective recharge in this cave system is controlled by precipitation amount and that recharge is not limited to the months when precipitation exceeds evaporation.

1.1 INTRODUCTION

Paleoclimate studies provide an essential tool to predict future climate change and to assess the extent to which human and biological adaptation is realistic under business-as-usual scenarios of anthropogenic greenhouse gas emissions. Recent efforts, in particular, have utilized paleoclimate observations to provide an empirical assessment of climate

sensitivity and hydrological responses to shifts in the concentration of atmospheric greenhouse gases and other factors internal to the climate system (Baldini et al., 2016; Medina-Elizalde et al., 2017; Palaeosens, 2012). Stalagmite calcite oxygen isotope ($\delta^{18}O$) records represent one of the most important terrestrial paleoclimate archives used to reconstruct past hydrological variability in tropical and subtropical regions (Akers et al., 2016; Cheng et al., 2016; Fairchild and Baker, 2012; Frappier et al., 2007b, 2014; Kennett et al., 2012; Lachniet et al. 2012, 2017; Medina Elizalde et al., 2010, 2016a, 2017; Medina-Elizalde and Rohling, 2012; Railsback et al., 2017). Hydroclimate records based on stalagmite $\delta^{18}O$ values are often interpreted to reflect the amount effect; the inverse relationship between rainfall amount and rainfall $\delta^{18}O$ described by Dansgaard (1964), which has been observed on seasonal and interannual time scales in low latitude regions (Vuille et al., 2003; Lahniet and Patterson, 2009; Medina-Elizalde et al. 2016a). The implicit assumption is that stalagmite calcite is deposited at or near isotopic equilibrium and that it preserves the variability of $\delta^{18}O$ of meteoric precipitation. This type of data collection requires a continuous commitment and expertise to access and work inside of a cave frequently enough and over an extended period of time. The evaluation of the rainfall/drip water isotopic relationship, nevertheless, is crucial when comparing isotopic variations within a single stalagmite and among different stalagmite $\delta^{18}O$ records and particularly if the goal is to reconstruct precipitation amount quantitatively (e.g. Medina-Elizalde et al., 2010, Lachniet et al., 2012, 2017; Medina-Elizalde and Rohling, 2012). The $\delta^{18}O$ signature of rainfall may be altered between the ground surface and cave drips due to isotopic fractionation in the soil, epikarst and/or vadose zone driven by evaporation (Ayalon et al. 1998; Bradley et al. 2010; Cuthberth et al. 2014; Beddows et al. 2016, Hartmann and Baker, 2017), and by mixing of water reservoirs in the epikarst (Yonge et al., 1985; Ayalon et al., 1998; Williams and Fowler, 2002; McDermott, 2004; Fairchild et al., 2006; Lachniet, 2009; Genty et al., 2014; Hartmann and Baker, 2017). The resolution of a stalagmite $\delta^{18}O$-derived rainfall record, furthermore, is ultimately not determined solely by the stalagmite temporal sampling resolution, but by the time integration of the rainfall signal by drip water. Because of the type of porosity (Worthington and Ford, 2009) and spatial heterogeneity of the water reservoirs and conduits of the vadose zone in a limestone cave, drip water (and thus stalagmites) can potentially integrate the amount-weighted isotopic signal of rainfall accumulated over days (Luo et al. 2014, Duan et al. 2016), a season (Cruz, 2005; Cobb et al., 2007; Fuller et al., 2008; Genty, 2008; Beddows, 2016; Duan et al. 2016), a year or even multiple years (Yonge et al., 1985; Williams and Fowler, 2002; Onac et al., 2008; Genty et al., 2014; Riechelmann et al., 2011, 2017; Czuppon et al. 2018). Drip water information, therefore, is particularly relevant to studies with high-resolution stalagmite $\delta^{18}O$ sampling that seek to characterize seasonal or annual precipitation variability (Medina-Elizalde et al. 2010, 2012; Kennett et al. 2012, Lachniet et al., 2012, 2017) and to discern the negative isotopic anomalies of tropical cyclones (Frappier et al., 2007b). Rainfall events such as subtropical monsoons and tropical cyclones are characterized by particularly low $\delta^{18}O$ compositions, but these events are short lived, lasting from days (cyclones) to a season (monsoons) (Lawrence, 1998, Lawrence and Gedzelman 1996; Gedzelman, 2003; Lachniet, 2009; Lachniet et al. 2017; Vieten et al. 2018). Interpretations of stalagmite $\delta^{18}O$ variations in terms of monsoon intensity and tropical cyclone activity are, therefore, contingent upon the time integration of the rainfall isotopic signal by drip water.

This study characterized the isotopic composition of rainfall, drip water, and groundwater on a weekly basis, over three hydrological years, from three different chambers

of the Río Secreto cave system located in the northeastern Yucatán Peninsula (YP). In addition, we also monitored the cave environment in these chambers, each with a different degree of isolation from the surface environment. This consistent research effort was motivated by improving hydrological interpretations from stalagmite $\delta^{18}O$ records and by enhancing our understanding of the link between precipitation amount and effective groundwater recharge in the YP. Río Secreto cave offered valuable stalagmite rainfall records, including two spanning the Classic and Preclassic Periods in Maya history and the Last Glacial Maximum (23-26 kyr ago) (Medina-Elizalde et al., 2016a, 2017). The monitoring results presented in this study help to better interpret paleoclimate information from stalagmites while guiding sampling protocols for stalagmites from the Río Secreto cave system and other similar karst environments. The authors of this study are currently reconstructing additional paleoclimate records from this cave including one of the oldest stalagmite $\delta^{18}O$ records in the Americas spanning the interval between 300 thousand years (kyr) and 190 kyr before present (BP).

1.2. FIELD SITE

1.2.1. Study site, cave system and climate

The YP has a distinctive annual cycle in precipitation characterized by the *Nortes*, *Dry* and *Rainy* seasons. The *Nortes* cold front season occurs between the months of November and February, the *Dry* season from March to May and the *Rainy* season between June and October. The *Rainy* season, also known as the *hurricane season*, has a bimodal distribution of precipitation with maxima during June and September and a precipitation drop between July and August, known as the midsummer drought (Magaña et al., 1999). Precipitation maxima in the YP occur during September when the Intertropical Convergence Zone reaches its northern most position and when the peninsula experiences the maximum tropical cyclone frequency. Regional models and the NCEP-NCAR Global reanalysis, indicate that the dominant source of moisture for the YP is the Caribbean Sea and is linked to the Caribbean Low Level Jet (CLLJ) (Karmalkar et al., 2011; Mestas-Nuñez et al., 2007; Muñoz et al., 2008; Vuille et al., 2003).

Río Secreto Cave (Secret River Cave) is a shallow horizontally developed karst cave with 42 km of surveyed passages, located in the northeast of the YP in the State of Quintana Roo, Mexico (20° 35.244'N; 87° 8.042'W, Fig. 1.1A; Sprouse et al., 2017). The cave is 5 km south of the city of Playa del Carmen, and the main entrance is five km from the Caribbean coast. Daily guided tours are conducted in small section of the overall cave. The climate of the northeastern YP is sub-humid, with average annual temperature of 25.8˚C and a range of 21-30˚C in monthly temperatures at Playa del Carmen (14 years measured by government meteorological stations, i.e. CONAGUA). Average annual precipitation in Playa del Carmen is 1463 ± 280 mm and more than 70% of precipitation occurs during the rainy season from June to November (Medina-Elizalde et al., 2016b). Summer precipitation is sourced by onshore trade winds off the Caribbean, and tropical storms and cyclones that cross the YP. Winter precipitation comes from humidity-saturated cold fronts (Orellana et al., 2009).

The geology is a highly karstified Pliocene carbonate rising to only 20 m above sea level (López-Ramos, 1975). High bedrock permeability leads to very little runoff and hence the shallow aquifer is recharged only by direct infiltration of precipitation. Caves are common along a 100 km section of the Caribbean coast from Playa del Carmen and south to the town of Tulum, including Sac Actum the world's longest underwater cave system (www.caves.org/project/qrss/qrlong.htm). The Río Secreto cave system lies at and above the water table, with extensive semi-flooded passages, all frequently interrupted by 1-8 m diameter sinkholes that allow ventilation of the system. The exceptional karstification and high hydraulic conductivity of the aquifer result in a water table nearly at sea level, with a shallow hydraulic gradient in the range of 10^{-5} cm per km. (Bauer-Gottwein et al. 2011). The coastal semi-diurnal tides affect the Río Secreto water table up to several cm, while rapid recharge during heavy rainfall can cause a short-term rise of up to 1 m (McMonigal and Beddows, 2014).

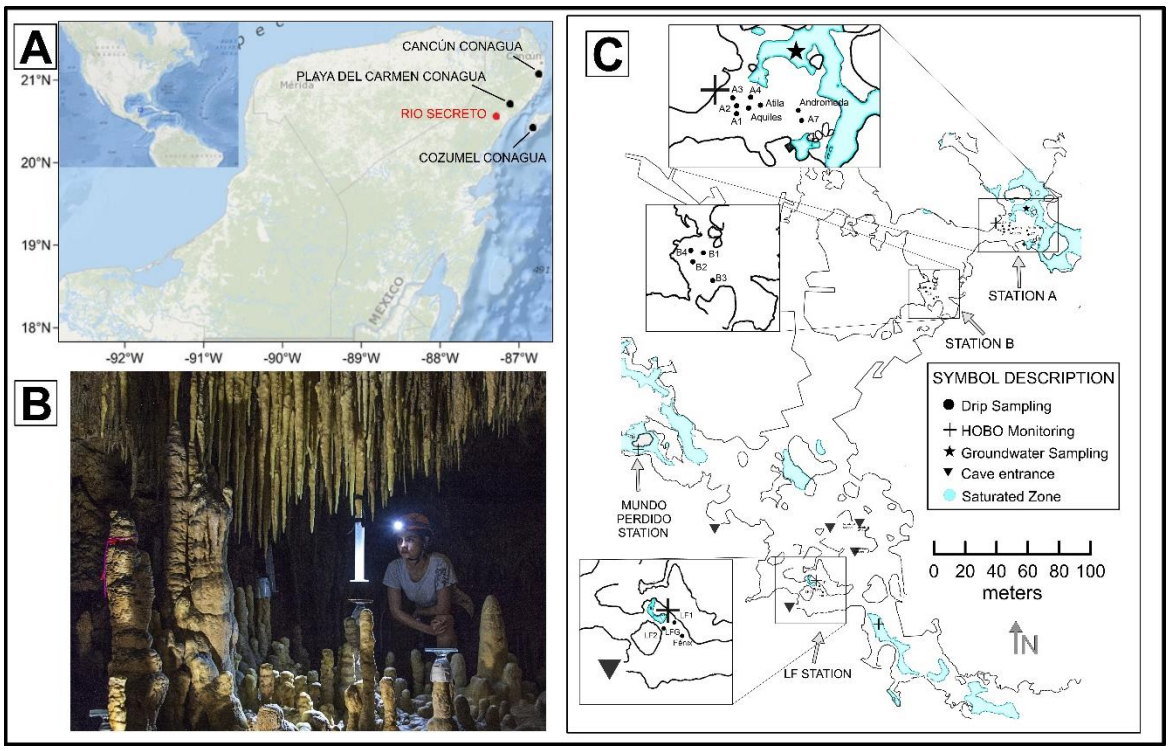

Figure 1.1 (A) Location of Río Secreto cave (red dot) and of the government (CONAGUA) weather stations of Playa del Carmen, Cozumel and Cancún (black dots). (B) Station A, collection of drip water from A4 by hanging a graduated cylinder using Velcro. Visible also is a glass plate on top a stalagmite used to farm calcite. (C) Map of the monitored stations A, B and LF (modified from Sprouse et al. 2017). Note that "Corazón" chamber is off the map located ~ 350 m to the east from station A.

1.2.1.2 Soil and epikarst composition

The ecosystem is a tropical dry forest subject to natural fires, as well as slash-and-burn agriculture practiced by the Maya. The current vegetation cover is young, possibly because the area is in a state of recovery after a forest fire ~ 20 years ago. The bedrock is composed of Pliocene-Pleistocene carbonates that retains much of its porosity, allowing water penetration in addition to the more rapid infiltration through small fractures and secondary porosity features. As mentioned, surface run-off is rare. An "epikarst" has been described as the superficial part of karst areas, where tree roots and karst processes fracture and enlarge rock joints and cracks, creating a more permeable and porous zone over less permeable massive carbonate rock (Bakalowicz, 2012). The vadose zone of Río Secreto cave and of most caves of northeast of YP fit this description and, therefore, all the processes described in this study are being carried out in the epikarst.

The soil above the cave is thin and variable, with pockets rarely reaching 0.5 m between areas of exposed bedrock. Because the roots and the soil penetrate into the bedrock, which is 2-12 meters thick, it is possible to observe them in the ceiling, walls and floor of the cave inside the vadose zone. Roots of some species use fractures to access moisture and the water table in the vadose zone. Some tree species have roots that can help develop or create small fractures that serve as conduits that increase the hydraulic conductivity (Bauer-

Gottwein et al., 2011). Root respiration increases the amount of CO_2 in cave air (Cowan et al., 2013). Where porous carbonates are sub-aerially exposed during times of negative water budgets, shallow re-precipitation of carbonate forms slabs of indurated caliche or calcrete (also kankar and duricrust) (Bautista et al., 2011). Several layers of caliche at and above the water table have been documented along the Caribbean coast (Cabadas-Báez et al., 2010; Ward, 1985) and are likely present above Río Secreto cave. The local vadose zone also includes patches of friable fine-to-medium-grained carbonate, locally called sascab, which may also store water (Bautista et al., 2011). The patchy nature of the bedrock strata and consequently infiltration and storage, are expressed in the heterogeneity of the ceiling of the cave, where ceilings of some sections are decorated with hundreds of distributed stalactites, and conversely, other sections have ceilings devoid of water infiltration.

1.3. METHODS

1.3.1 Precipitation sampling and surface weather monitoring

A total of 36 monthly composite rainfall samples were collected over three years from June 2014 to June 2017. Rainfall samples were collected above the cave at ground level using HDPE 8-liter containers with a Ping-Pong ball over a funnel connected to a hose consistent with IAEA (2014) protocols. Rainfall samples were collected every week and their volume measured using a graduated cylinder. These samples were then aggregated into monthly samples from which an aliquot was taken for $\delta^{18}O$ and δD analysis. From June 2016, we installed a second pluviometer of the same design beside the first one, to collect when possible, samples of individual rainfall events that accumulated between 1 and 7 days. Ground level precipitation at Río Secreto may underestimate the true rainfall amount due to the presence of dense vegetation potentially blocking lateral rainfall associated with large storms. Therefore, in this study we also examine the average of precipitation amount from June 2014 to July 2017 from weather station data from three other locales to compare with our rain gauge data; Playa del Carmen (20°37.200 'N, 87 04.200'W), Cozumel Island (20°31.200 'N, 86°57.000 'W) and Cancún (21° 09,002'N, 86 ° 49,200 'W) (See Fig. 1.1A). In order to estimate the historical recharge in Playa del Carmen we use precipitation amount and evaporation historical data from CONAGUA. Evaporation data was calculated using the Penmann Montheit method.

1.3.2 Monitoring using data loggers

Monitoring of the cave chambers included measurements using HOBO Temperature/HR U23 data loggers of cave air relative humidity (RH) with accuracy ±5% above 90% and air temperature (accuracy of ±0.21°C). Additional cave climate data was collected in the Corazón chamber, and water level data in the "Mundo Perdido" section of the cave (Fig. 1.1C). Cave air RH and temperature data were measured at 4 and 6-hour intervals from April 2012 to July 2017 in Station LF, Station A, and Corazón chambers (See Table 1.1 for more details). From July 2016 to January 2017 another HOBO Temperature/RH U23 was placed outside the cave under the shade 4 m from the ground and 20 m from the cave entrance to record at 3-hour intervals. Cave groundwater temperature 30 cm below the water table was determined at 1 hour intervals from November 2015 to July 2017 in Mundo

Perdido and Station LF phreatic zones by using a HOBO Water Level U20L-01 data logger with accuracy of ±0.44°C (see Fig. 1.1C and Table 1.1).

Daily average temperature data of January 2016 – June 2016 from a Davis Vantage Pro 2 station (accuracy of ±0.5°C and 1% for RH) was used for this study, the station is located in the Planetarium of Playa del Carmen (20°39.045 'N, 87°5.208 'W). An additional Davis Vantage Pro 2 weather station was installed in Río Secreto Nature Reserve above the canopy approximately midway between the coast and the cave main entrance in June 2016.

Table 1.1.1 Summary of temperature data from drips, groundwater and air (°C) inside and outside Río Secreto Cave system.

Station	Sample	Period	Frequency	n	AVG	SD	MIN	MAX
Corazón	Air	April 2012 –May 2014	6 hr	3104	24.8	0	24.7	24.9
	Groundwater	April 2012 –May 2014	3 hr	6208	24.8	0	24.7	24.8
LF	Air	July 2014 – July 2017	6 hr	6840	22.8	1.2	18.8	24.5
	Air	July 2016-July 2017	6 hr	1454	23.7	0.7	24.7	22.6
	Groundwater	Oct 2015 – July 2017	1 hr	13867	22.8	0.9	20.7	24.1
	Drips	July 2014 – July 2017	Weekly	270	23.0	1.9	18.2	24.8
A	Air	July 2014 – July 2017	6 hr	3616	24.5	0.2	23.8	24.9
	Air	July 2016-July 2017	6 hr	1454	24.4	0.2	23.8	24.7
	Groundwater	Oct 2015 – Nov 2015	1 hr	960	24.6	0	24.6	24.6
	Groundwater	July 2014 – July 2017	Weekly	68	24.7	0.1	24.6	24.8
	Drips	July 2014 – July 2017	Weekly	487	24.5	0.3	23.8	25.0
B	Drips	July 2014 – July 2017	Weekly	232	24.6	0.3	24.6	24.8
Mundo Perdido	Groundwater	Dec 2015 – July 2017	1 hour	12902	24.2	0.4	23.0	24.7
Rio Davis Station	Air	July 2016-July 2017	6 hr	1454	26.2	3.4	14.5	33.9

1.3.3 Groundwater and drip water monitoring

The monitored portion of the Río Secreto cave system is shown in Fig. 1.1C. Three chambers were selected as stations for the drip study: Laberinto del Fauno (LF), located close to an entrance and stations A and B located ~200 m from the nearest entrance. The vadose zone bedrock above these 3 chambers is 9-12 m thick. Groundwater sampling began in June 2014 and consisted of weekly measurements of temperature, pH and electrical conductivity at the water table of station A using a HACH multi-parameter probe pre-calibrated with buffer pH 4, 7 and 10 and a sodium chloride standard solution of 491± 2.5 mg/L (1000 ± 10 µS/cm) with accuracy of 0.1 for pH and 0.01 mg/L for TDS. Water samples were also collected in 30 mL Nalgene bottles at a depth of 30 cm for $\delta^{18}O$ and δD analysis. In addition, we selected 16 drip sites associated with stalactites known to be hydrologically active throughout the year to take drip water samples. Each drip was monitored quasi-weekly from June 2014 to June 2017. The sampling protocol in station LF included drip water from 3 individual stalactites labeled LF1, LF2 and Fénix, and an additional point combining drip

water from several stalactites labeled LFG. At station A, drip water from 8 individual stalactites were monitored: A1, A2, A3, A4, A7, Andromeda, Aquiles and Atila. At station B, four individual stalactites were monitored: B1, B2, B3 and B4. The monitoring periods for each drip span slightly different time intervals and only drips LF1, A3 and B1 were sampled continuously over the three-year period. Two of the selected chambers, LF and A, are sites where stalagmites have been collected (Medina Elizalde et al., 2016a; 2017) and most of the 16 drips studied are above active candlestick stalagmites longer than 30 cm. A representative image of the monitoring and sampling sites is provided in Fig. 1.1.

For almost all drips (except LFG, A2 and LF2), drip water was collected by hanging a clean dry 250 mL plastic graduated cylinder from each stalactite using Velcro to ensure that no secondary drips were collected (see Fig. 1.1B). After the accumulation period (~48 hours; See Table A.1), the volume of dripwater collected and its temperature were recorded, the latter, using a ThermoWorks digital thermometer (accuracy of ±1.0°C). Then, sample aliquots were decanted into 15 mL and 30 mL Nalgene bottles for $\delta^{18}O$ and δD analysis. If the collected water volume was sufficient, pH and electrical conductivity were measured using the HACH probe. Drip rate is reported in mL/hr based on total volume divided by the collection interval. If the drip volume of a particular drip was greater than 250 mL and the water sample overflowed the cylinder drip rates were recorded as 8 mL/hr, thus representing a minimum flow but still allowing characterizing infiltration during significant rainfall events.

1.3.4 Stable isotopes

The $\delta^{18}O$ and δD values of groundwater, precipitation and drip water samples collected up to the year 2016 were determined using a Cavity Ring-Down Spectroscopy (CRDS) Picarro Isotope Analyzer, model L1102-i at the University of Massachusetts, Amherst. Reproducibility of in-house standard waters was better than 0.08‰ for $\delta^{18}O$ and 0.4‰ for δD. The $\delta^{18}O$ and δD analyses of groundwater, precipitation and drip water collected after 2016 were performed using a Cavity Ring-Down Spectroscopy (CRDS) Picarro Isotope Analyzer, model L2130-i at Auburn University, Alabama. Long-term reproducibility of in-house Picarro Zero and Mid standard waters in both labs was better than 0.03 ‰ for $\delta^{18}O$ and at 0.2 ‰ for δD. Results are reported in per mil (‰) relative to VSMOW (Vienna Standard Mean Ocean Water).

1.4. RESULTS

1.4.1 Temperatures and relative humidity

A summary of the cave air, dripwater and groundwater temperature data is presented in Table 1.1. During the period between July 2016 and July 2017 the total range of air temperature variation inside the cave was 1–2°C while the total range observed outside the cave spanned 19°C (Fig. 1.2). Groundwater, cave air and drip water temperature variability at station LF was the most pronounced of all the stations. Observed mean annual air temperature outside the cave and at LF and A stations was the same, although the daily air temperature range inside the cave was only a small fraction (<12%) of that observed outside (July 2016-July 2017) (Table 1.1, Supplementary Fig. A.1). Seven months of air temperature data collected at 12 hr. intervals inside LF and outside the cave indicate that LF follows atmospheric

temperature variability within an hour. As noted above, however, LF greatly buffers the atmospheric air temperature range (Supplementary Fig. A.1). Cave drip water and air temperature at stations A and LF were similar, reflecting thermal equilibrium within a 48-hour period maximum (Supplementary Table A.1 and Fig. 1.2)

Río Secreto surface air RH averaged 84% with a range of 68% to 98% during 2016 and 2017. RH at LF station ranged from 89.9% to 100%, with an average of 99.9± 0.8% (n = 5106). At station A, RH ranged from 95.3% to 100%, with average of 99.6 ± 0.9% (n = 3616) (Fig. 1.2). Considering the small uncertainty associated with RH measurements (5%), all the chambers investigated exhibit water vapor saturation conditions.

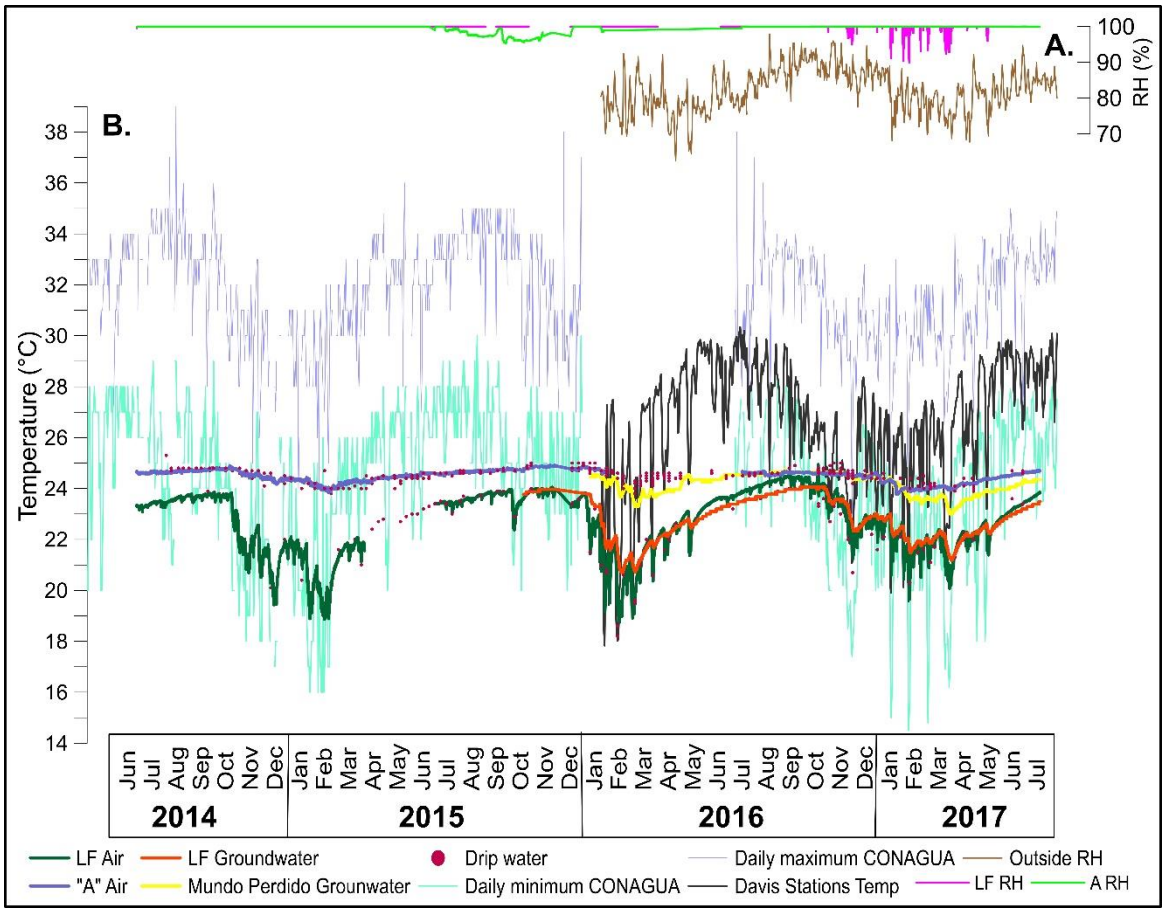

Figure 1.2. (A) Air relative humidity recorded outside and inside Río Secreto cave. (B) Temperatures outside the cave: Daily record of maximum, and minimum temperatures in Playa del Carmen measured by CONAGUA and daily average temperatures measured by two Davis Vantage Weather Stations (See Section 1.3.2). Cave groundwater, drip water, and air temperatures at stations LF, A and "Mundo Perdido" (see Section 1.3.2). Note minimum temperature variability within isolated chambers of stations A and "Mundo Perdido" that contrast with the more significant temperature variability at station LF, located near an entrance. The temperature range in station LF is smaller (~6°C) relative to surface air (19°C). Mean summer temperatures at station LF approximate temperatures in the isolated chambers of stations A and "Mundo Perdido".

1.4.2. Precipitation $\delta^{18}O$ and δD

A total of 66 samples of rainfall were analyzed for $\delta^{18}O$ and δD, including monthly samples (n =36) and samples of individual rainfall events (n=30) (Figs. 3 and 4, Supplementary Fig. A.2). This sample collection included a particularly intense rainfall event on October 21, 2014, representing an accumulation of 150 mm/day, which had the lowest isotopic values found in this study ($\delta^{18}O$= -9.5‰, δD= -61.4‰). This study includes the drought year of 2016, when annual precipitation was 40% lower than the long-term average and nearly half that of the previous year.

Rainfall $\delta^{18}O$ and δD varied from -9.5‰ to +1.5‰ and from -61.4‰ to +17.9‰, respectively (n=66) (Fig. 1.4). Monthly rainfall $\delta^{18}O$ and δD ranged from -7.4‰ to -0.6‰ and from -45.8‰ to 12.3‰, respectively (n=36; Fig. 1.4). The amount-weighted mean isotopic compositions of rainfall calculated from monthly data (n=36) were -3.7‰ and -17.8‰ for $\delta^{18}O$ and δD, respectively. The amount-weighted annual $\delta^{18}O$ composition of rainfall over the study interval, was -4.2‰ (yr. 1), -4.5‰ (yr. 2) and -2.3‰ (yr. 3). The arithmetic average (not amount-weighted) based on monthly samples (n=36) was -2.6‰ and -9.3‰ for $\delta^{18}O$ and δD, respectively (Table 1.2). We stress here, that the arithmetic mean does not truly represent the annual $\delta^{18}O$ composition of rainfall because it weighs all months the same regardless of their relative contribution to the total annual rainfall amount. We include this calculation, however, because it represents one potential end-member of the mean annual drip water $\delta^{18}O$ composition, also estimated without weighing water amounts. More details are provided below.

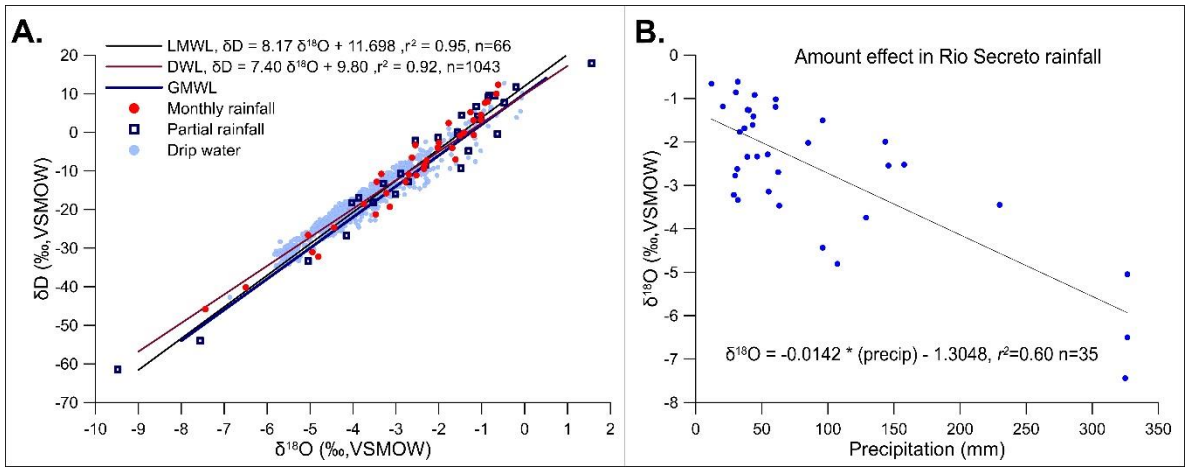

Figure 1.4. A. Comparison of the linear relationship between $\delta^{18}O$ and δD of monthly rainfall samples and samples of individual rainfall events (local meteoric water line, LMWL), and drip waters (drip water line, DWL) of Río Secreto cave. The global meteoric water line (GMWL) is also shown to provide global context. B. Linear relationship between $\delta^{18}O$ and monthly rainfall amount collected in Río Secreto. Both plots present data collected from June 2014 to July 2017.

Table 1.1.2. $\delta^{18}O$ and δD averages and standard deviation of monthly rainfall, drips and groundwater collected from June 2014 to July 2017.

Sample description	n	$\delta^{18}O$				δD			
		AVG	SD	MIN	MAX	AVG	SD	MIN	MAX
Monthly Rainfall									
Arithmetic	36	-2.6	1.6	-7.4	-0.6	-9.3	13.9	-45.8	12.3
Amount-Weighted	36	-3.7	---			-17.8	---		
A1	11	-3.9	0.4	-4.6	-3.0	-19.6	2.7	-22.8	-13.5
A2	94	-4.1	0.5	-5.4	-2.8	-20.4	4.0	-30.1	-9.0
A3	113	-4.2	0.4	-5.3	-3.3	-21.6	2.7	-27.5	-15.2
A4	83	-3.9	0.5	-5.1	-3.1	-19.5	3.5	-29.3	-11.1
A7	62	-4.3	0.4	-4.8	-3.1	-21.9	3.9	-26.9	-12.1
Andrómeda	79	-4	0.3	-4.5	-3.3	-19.7	2.8	-25.4	-13.5
Aquiles	47	-4.5	0.4	-5.6	-3.8	-24.1	2.4	-29.7	-17.9
Atila	56	-4.4	0.3	-5.1	-3.4	-22.6	2.9	-26.3	-13.9
B1	115	-3.6	0.8	-6.9	-2.0	-16.6	5.9	-42.7	-6.0
B2	42	-3.3	0.5	-4.4	-2.5	-13.7	4.5	-24.3	-6.5
B3	44	-3.3	0.6	-5.1	-2.3	-13.9	4.8	-27.8	-4.8
B4	69	-4.1	0.6	-5.4	-2.6	-20.5	4.8	-30.5	-11.3
Fénix	72	-5.5	0.2	-5.8	-4.8	-32.0	1.8	-35.1	-25.6
LF1	94	-2.4	1	-5.0	0	-7.9	8.0	-27.3	12.7
LF2	41	-2.8	1.2	-5.8	-0.2	-12.7	7.5	-31.6	4.3
LFG	21	-2.4	0.9	-4.3	-1.0	-7.2	6.4	-20.2	5.6
Total Drips	1043	-3.9	1	-6.9	0	-18.9	7.4	-42.7	12.7
Groundwater	101	-4.7	0.15	-5.0	-4.2	-26.0	1.4	-28.4	-19.5

A negative relationship between precipitation amount and precipitation $\delta^{18}O$ (i.e. an amount effect) is revealed by our precipitation data on seasonal timescales, as expected in tropical regions (Dansgaard, 1964; Lachniet and Patterson, 2009; Rozanski et al., 1993). The slope of the amount effect relationship in Río Secreto is -0.0142 ‰mm^{-1} (r^2 = 0.6) (Fig. 1.4), very similar to observations from Veracruz, México, and El Salvador; -0.0125 ‰mm-1 and -0.0124 ‰mm^{-1}, respectively (Lachniet and Patterson, 2009).

1.4.3. Groundwater level and isotopic composition

The average $\delta^{18}O$ and δD values of groundwater in Río Secreto cave were -4.7 ± 0.1‰ (1 standard deviation, SD) and -25.5 ± 0.9‰ (1 SD), respectively, from July 2014 to July 2017 (n=78 samples). The $\delta^{18}O$ value of groundwater was within analytical uncertainty of the annual amount-weighted $\delta^{18}O$ composition of rainfall observed in the three-year study period (-4.5‰ to -2.3‰), and the most temporally stable of all the water types analyzed, suggesting it represents the integration of about one or more years of rainfall accumulation (Fig. 1.3, Supplementary Fig. A.2). Groundwater is actively moving through Río Secreto, probably toward the ocean. During the summer when strong rains occur in the region the water table can rise up to 1 m in the course of 1 to 2 days to then gradually lower to base levels within few weeks (McMonigal and Beddows, 2014).

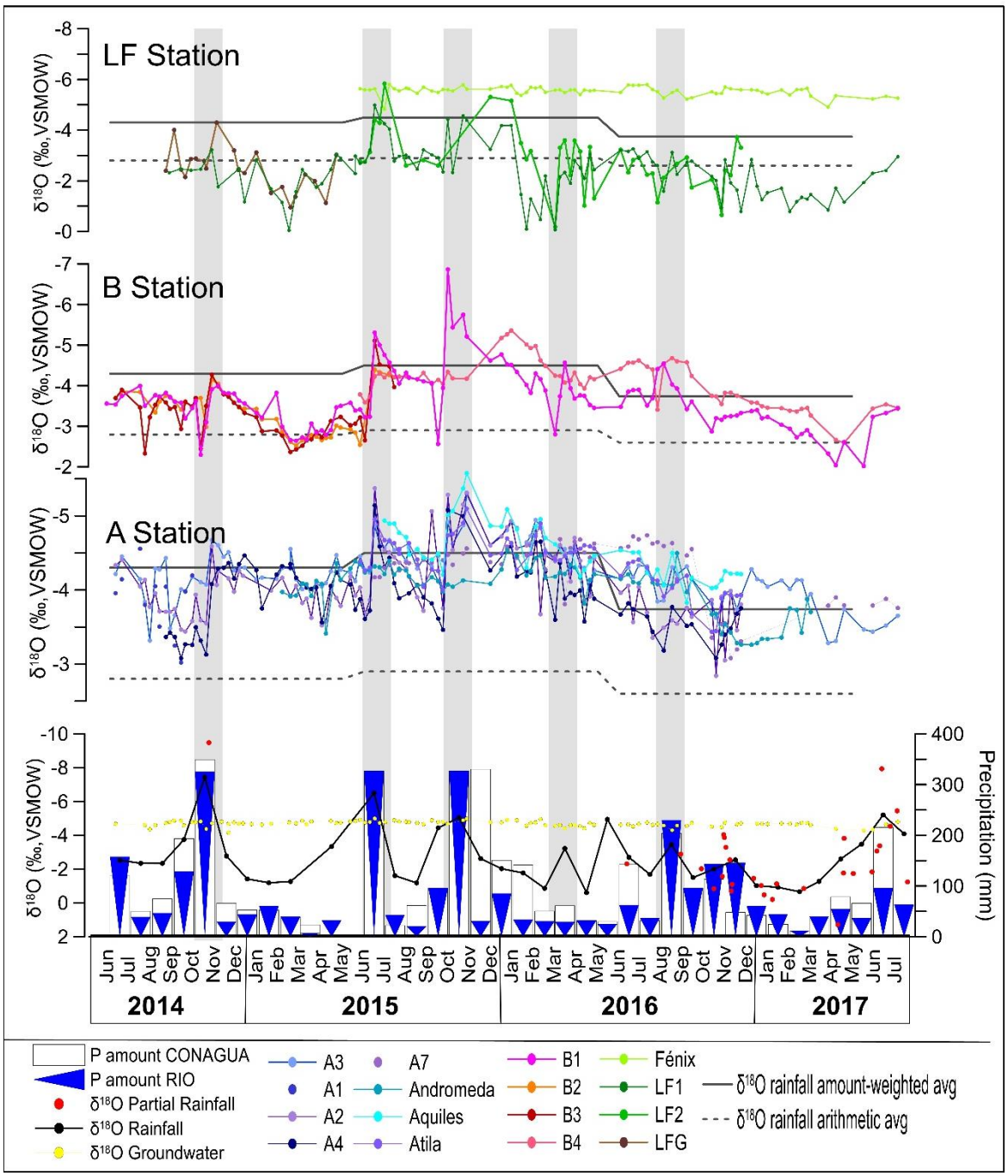

Figure 1.3. Upper three panels: drip water $\delta_{18}O$ data from June 2014 to June 2017 from stations LF, B and A; Note that axes are inverted. Lower panel: (blue triangles) monthly precipitation collected at the location of Río Secreto cave; (white rectangles) monthly precipitation recorded by CONAGUA, including weather stations in Cancún, Playa del Carmen and Cozumel; (black line) precipitation $\delta_{18}O$ from monthly samples, and; (red dots) individual rainfall events (1-7 days)(See section 1.3.1). $\delta^{18}O$ Annual amount-weighted and arithmetic averages of rainfall are shown to ilustrate two end members (See sections 1.4.4 and 1.5.2). Gray bars highlight conspicuous drip $\delta_{18}O$ shifts coeval with rainfall $\delta^{18}O$ changes.

1.4.4. Drip water $\delta^{18}O$ and δD

A total of 1043 samples from 16 different drip sites were analyzed for $\delta^{18}O$ and δD (Supplementary Table A.1, Fig. 1.3 and Fig. A.2). This study examines the annual average and amplitude $\delta^{18}O$ variability of drips, because of its application to hydroclimate reconstructions from speleothems. We note that the annual $\delta^{18}O$ composition of drip water of each site is not from samples that are amount-weighted because our sampling protocol involves the collection of temporally discrete water samples that represent aliquots from a reservoir of unknown size. Thus, the annual mean drip water $\delta^{18}O$ composition that we determine is not expected to perfectly represent the $\delta^{18}O$composition of all the drip water that actually drained over the course of a year. This is analogous to estimating the annual $\delta^{18}O$composition of rainfall from monthly precipitation $\delta^{18}O$data without taking into account the monthly amount of rainfall: this calculation would not provide the true annual $\delta^{18}O$composition of rainfall over the course of that year. We anticipate, therefore, that our sampling protocol would yield a drip annual mean $\delta^{18}O$composition more closely resembling the annual arithmetic mean $\delta^{18}O$composition of rainfall (i.e. amount-unweighted) when a drip integrates rainfall over a short time. Conversely, a drip annual mean $\delta^{18}O$composition resembling the annual amount-weighted $\delta^{18}O$composition of rainfall would be indicative of a reservoir that accumulates rainfall for one year. We note, furthermore, that drip sites that integrate one year of rainfall are expected to show a modest response to rainfall $\delta^{18}O$variability and thus minor $\delta^{18}O$variability during the year. We find drips that fall within these two annual isotopic end members as described below.

1.4.4.1. Station A

With the exception of Fénix, the drip sites with the smallest annual $\delta^{18}O$ variability (~2‰) were those at station A (Figs. 3 and 5). The annual mean $\delta^{18}O$ composition of these drip waters closely resembles the annual amount-weighted $\delta^{18}O$ composition of rainfall during years 1 and 2 (Fig. 1.5). During year 3, drip waters at station A display lower $\delta^{18}O$ values than coeval rainfall, and closely resemble the isotopic composition of rainfall in the previous year (Fig. 1.5).

1.4.4.2. Station B

The mean annual $\delta^{18}O$ composition of drips from station B had values between the annual amount-weighted and unweighted $\delta^{18}O$ composition of rainfall during year 1, and similar to the annual amount-weighted $\delta^{18}O$ composition of rainfall during year 2. Similar to drip waters at station A, during year 3, the mean annual $\delta^{18}O$ composition of drip water at station B is more negative relative to that of rainfall (both amount-weighted and unweighted), and similar to the $\delta^{18}O$ mean composition of rainfall in the previous year (Fig. 1.5). Drip waters from station B show larger $\delta^{18}O$ variability during 2015 (~4‰) than during 2014 and 2016 (~2-3‰).

1.4.4.3. Station LF

Drip Fénix at station LF had the lowest isotopic values and lowest temporal variability of all drip waters ($\delta^{18}O$= -5.5± 0.2‰) (Fig. 1.3, Table 1.2). Fénix has $\delta^{18}O$ values that range from -5.8 to -4.8‰ and are up to ~2‰ lower than the annual amount-weighted $\delta^{18}O$ composition of rainfall (-3.7 ± 1‰, n=3 years). Drips LF1 and LF2, from the same chamber, in contrast, show the largest $\delta^{18}O$ variability (~6‰) of all the drips examined in this study. LF1 and LF2

$\delta^{18}O$ variability (~6‰) closely resembles that of rainfall over the same time interval (9‰) (Fig. 1.3 and Fig. A.3). It is notable that these drip sites are located only 5m away from Fénix (Fig. 1.1C). The mean annual $\delta^{18}O$ compositions of LF1 and LF2 are close to the mean $\delta^{18}O$ value of rainfall (unweighted) during all three years (Fig. 1.5).

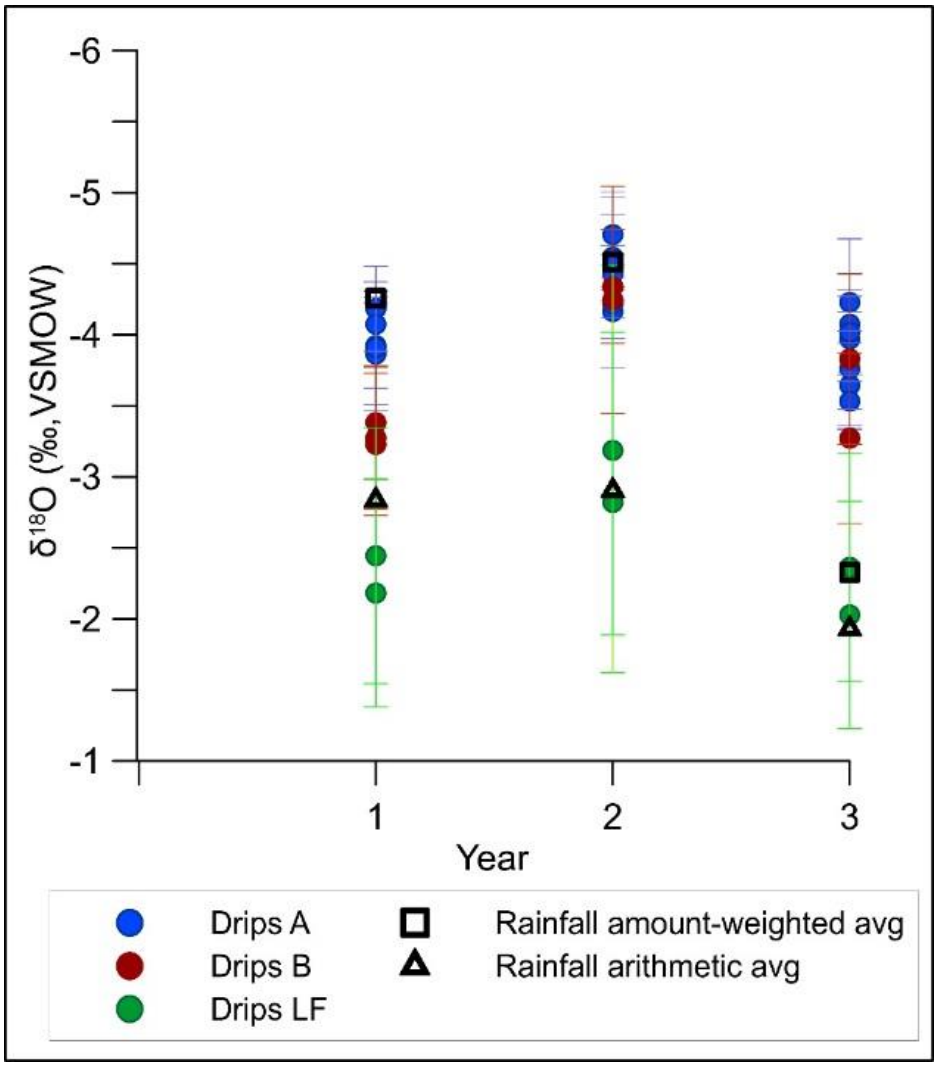

Figure 1.5. Río Secreto amount-weighted and unweighted (arithmetic) annual drip water and rainfall $\delta^{18}O$ data; Note that axis is inverted. Values were calculated from June 2014 to May 2015 (year 1), June 2015 to May 2016 (year 2) and June 2016 to May 2017 (year 3). Only drip data with more than 15 data points per year were included (see Supplementary Table A.3). Drips at station A have a similar isotopic composition to the amount-weighted $\delta^{18}O$ composition of rainfall during year 1 and 2. Drips at station B have an isotopic composition in between the amount-weighted and unweighted $\delta^{18}O$ composition of rainfall. Lastly, drips at station LF have an isotopic composition similar to the mean $\delta^{18}O$ composition of rainfall, unweighted. During year 3 the YP experienced a drought reflected by a positive shift in the isotopic composition of rainfall (black triangle and square shown in year 3). Bar errors of 1 SD are showed for drip waters.

1.4.5 Discharge variability of cave drips

In order to examine the infiltration of rainwater into the karst system and its relationship with the isotopic composition of drip water, drip rates were determined throughout the three-year monitoring effort. Drip rate variability ranged from 0.01 mL/hr. to more than 16 mL/hr, including all drips (Supplementary Table A.1). Despite discharge rates increasing in most drips during the rainy season, marked differences among them were observed (Fig. 1.6). In some cases, an increase in drip discharge immediately followed individual rainfall events (e.g. Drips B1, A3, Fénix). However, other drip discharge lagged rainfall amount shifts by a few weeks and to three months (e.g. Drips A7, Andromeda, Aquiles and Atila). We note that a similar lag between drip discharge and rainfall amount has been documented for Río Secreto cave at station A, via a calibration study of automatic drip sensors (Beddows and Mallon, 2018).

We determined the hydrological behavior of the drips using the maximum discharge and the coefficient of variation (i.e. the quotient of the standard deviation over the mean drip rate value expressed as a percentage) of the discharge according to the classification of Fairchild et al. 2006 (Fig. 1.7). We found that several of the drips that maintain a high and temporally constant drip rate seasonally can be classified as Seepage flow (e.g., A7, Andromeda, B4, Fénix, A3). Atila, Aquiles, A4, B1, B2, B3 and LF1 drips are classified as Seasonal Drips, i.e. drips that have both the lowest and highest drip rates of those examined. We note that the observed drip rate variability associated with B1 was distinct from all the other drips which suggests a threshold response to rainfall amount, as an "overflow" drip (Smart and Friederich, 1987; Arbel et al., 2010; Bradley et al., 2010).

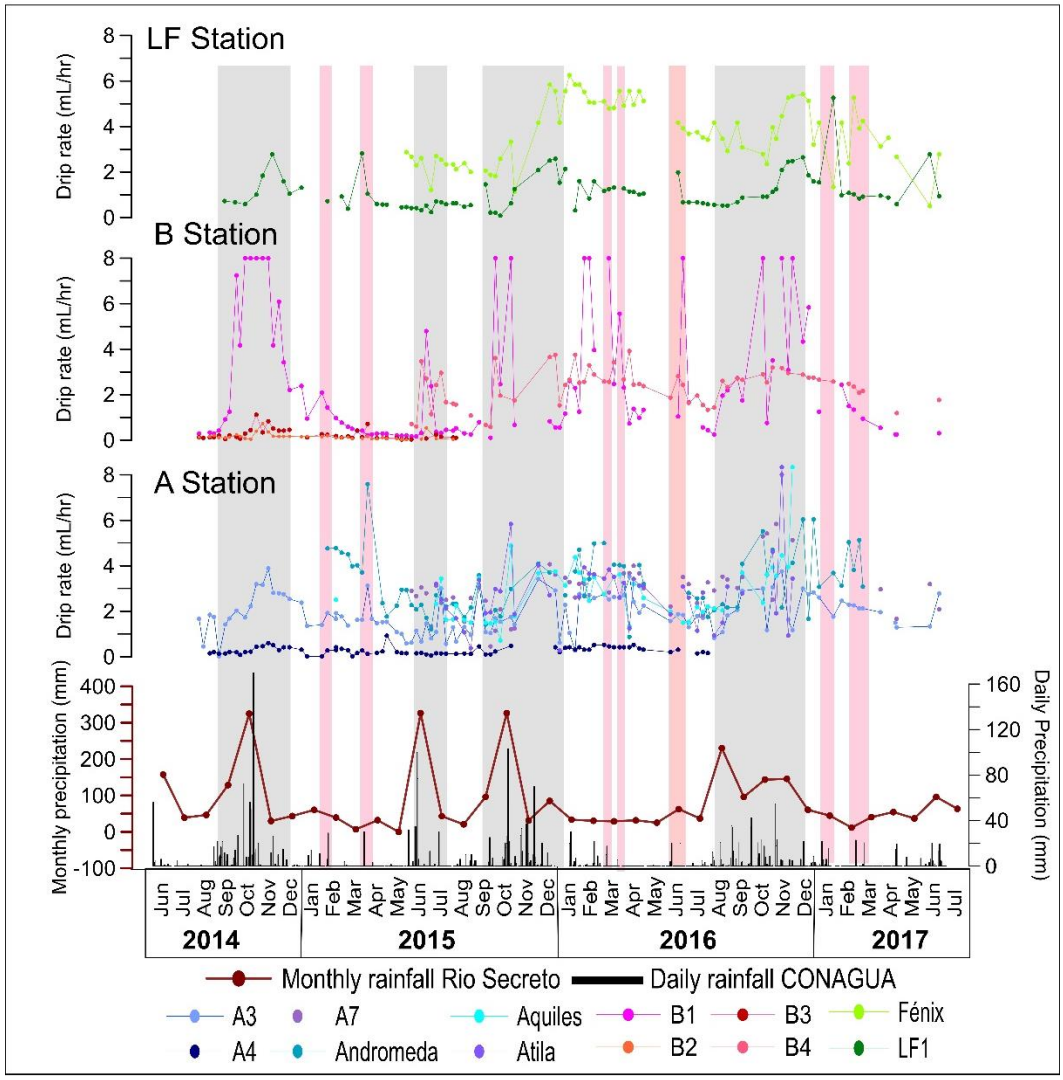

Figure 1.6. Upper Panel: Drip rate in mL/hr at stations LF, B and A. Lower Panel: Monthly rainfall amount collected near the main entrance of Río Secreto cave (red line) and daily rainfall amount recorded by CONAGUA (2017) in Playa del Carmen. Gray bars highlight drip rate increases during the rainy season. Pink bars highlight drip rate increases in response to individual rainfall events.

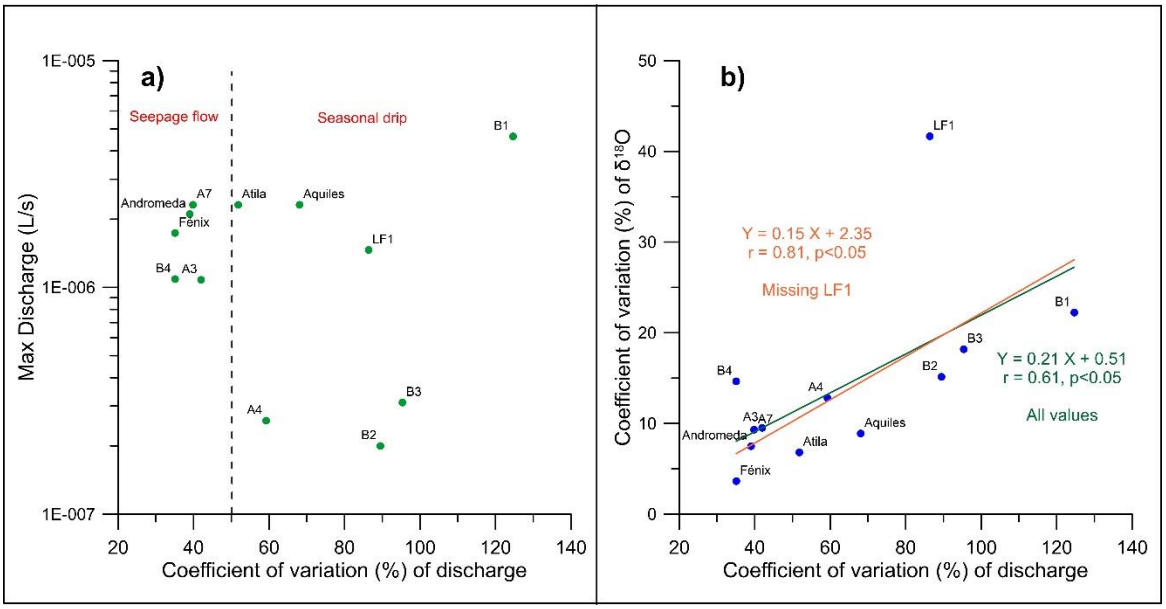

Figure 1.7. (a) Hydrological behavior of Rio Secreto cave drip sites expressed in terms of maximum discharge versus variability in discharge defined by Fairchild et al. (2006). (b) Comparison between drip $\delta^{18}O$ and discharge rate variability. All data correspond to the period between July 2014 and July 2017.

1.5 DISCUSSION

1.5.1 Temperature and cave ventilation

The observed modest variability of cave air, dripwater and groundwater temperatures at stations A and B is consistent with their isolation from the cave exterior. There is no difference between mean cave air and mean surface air temperatures (Fig. 1.2), reflecting the thermal equilibrium with surface heating by conduction (Smerdon et al., 2003), as has been reported in many caves around the world (Rau et al., 2015). Temperature variability in LF Station (groundwater, air and drip waters) in contrast with the isolated chambers (stations A and B) is more pronounced and closely follows seasonal air surface temperature variability, although with an amplitude modulation (Fig. 1.2 and Supplementary Fig. A.1.). An amplitude-modulated response of cave air temperature to surface air temperature may result from the "chimney effect"; the predominant effect of seasonal air circulation within a cave with two or more entrances. Cave temperature is expected to be constant over the course of a year in a closed environment, but variable when the cave is open to surface air. In this case, differences of temperature and air density between the surface and cave environments drives cave ventilation due to pressure disequilibrium (Wigley and Brown, 1976; Oh and Kim, 2011). Ventilation in Río Secreto cave is enhanced during the winter season, when the surface-to-cave air temperature contrast increases, thus cooling the cave. Due to the high heat capacity and thermal inertia of groundwater relative to air within the cave, its temperature variability is more modest (~3°C) than air temperature (~6°C). We note that later in the summer when the highest air surface temperature is reached (~34°C), LF reaches a maximum air temperature similar to the annual mean temperature observed in the more isolated chambers (24.5°C). Temperature in LF station does not increase beyond this point and does not reach typical, higher peak summer surface air temperature because it becomes thermally isolated like stations A and B. "Mundo Perdido" is another section of the cave that represents temperature variations between LF and the isolated chambers A and B. This chamber is

located near an opening to the surface but not as close as LF is from a similar opening (Fig. 1.1). Groundwater at this location, as expected, shows larger temporal temperature variability than the isolated chambers but lower than station LF (Fig. 1.2, Table 1.1). Comparing coeval air temperatures at LF and A stations and outside temperature measured using data loggers, we find that cooling by ventilation is occurring also on a daily basis; we did not detect a lag in the temperature cave-surface coupling (Fig. A.1. Supplementary). In some caves temperature changes have been related to visitations (Frisia et al., 2011, Baldini et al 2006; Vieten et al., 2016), but the close coupling between surface air and cave temperatures and the minimum annual variability at station A does not support this scenario for Río Secreto (Table1, Fig. 1.2 and Fig. A.1. Supplementary). Río Secreto cave represents over 40 km passages, and tourist activity in the system consists of about 12 visitors at a time traversing about 1 km of cave, and rarely spending more than 5 minutes in any chamber of the system.

1.5.2 Infiltration and transmission of the rainfall isotopic signature

Due to the thin ~10 m permeable vadose zone above Río Secreto cave, infiltration of rainfall from the surface to stalactites (drip waters) occurs rapidly as suggested by our isotopic and discharge data. Different infiltration patterns, however, are observed among and within the 3 studied chambers. Because drip water data represents a brief interval of time (~ 48 hours, every one or two weeks), we cannot calculate an annual amount-weighted isotopic composition for each drip and directly assess the degree to which drip water integrates the rainfall amount and isotopic signals, as mentioned previously. We observed, however, that the isotopic composition of drip water has annual values that fall between two end members: (1) drip waters whose annual mean $\delta^{18}O$values are close to the annual amount-weighted $\delta^{18}O$composition of rainfall, and; (2) drip waters whose annual mean $\delta^{18}O$values are close to the arithmetic average isotopic composition of rainfall (amount-unweighted). Drip waters from stations A, B and LF fall at or within these two end members. Fénix seems to be an exception and is discussed in more detail below.

When considering discharge rates, we find that changes in drip flow and drip isotopic values are not always coeval with rainfall changes even within an individual drip site. For instance, the isotopic composition and drip rates of LF1 and B4 peaked at the same time in association with some rainfall amount maxima events, but lagged other similar rainfall events by weeks (e.g. June 2015) to months (e.g. October 2015) (Figs 3 and 6). We find a significant correlation between the total variability of drip discharge and $\delta^{18}O$ composition ($r = 0.61$, $p<0.05$). LF1 is a particular case that has significant variability of both drip rate and $\delta^{18}O$ values in comparison with the other drips. Removing the information from this drip, yields a more significant correlation ($r = 0.81$, $p<0.05$) (Fig. 1.7) between drip rate and $\delta^{18}O$ variability: the greater the drip rate variability, the greater the associated $\delta^{18}O$ variability. In karst systems drips are fed by a combination of preferential flows (fissure and conduit) and through the matrix (seepage) converging between discrete water storages (Bradley et al., 2010). As a result of the complexity of the conduits through which water infiltrates and flows, water feeding each drip has a specific seepage behavior even when drips are only a few meters apart, such as in the case of Fénix and LF1 and LF2 (See Section 1.4.5).

Figure 8 shows our proposed conceptual models to illustrate the different flow patterns as a function of reservoir size and infiltration flow, at stations A, B and LF. These

conceptual models seek to explain drip rate and isotopic observations, as explained in more detail below.

Drip waters at station A integrate at least a year of rainfall accumulation and this reflects a larger epikarst water reservoir relative to the other two stations (Fig. 1.8). This inference is supported by the observation of modest annual drip $\delta^{18}O$ variability relative to that of rainfall and an annual mean $\delta^{18}O$ composition resembling the annual amount-weighted $\delta^{18}O$ composition of rainfall during years 1 and 2 (Fig. 1.5). The drips of station A are classified as both seepage and seasonal flow, with maximum drip rates above 10^{-6} (L/s). An exception is A4, which seems to be fed by matrix flow (Figs. 7 and 8).

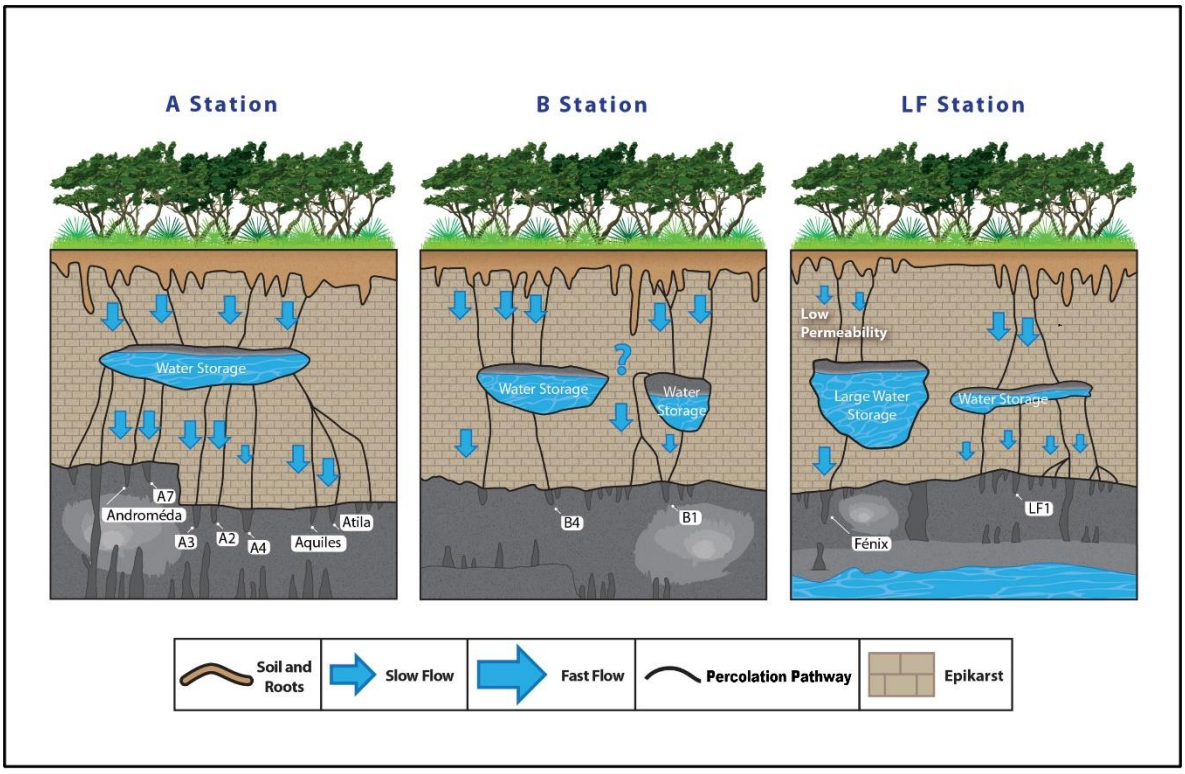

Figure 1.8. Río Secreto conceptual model of infiltration of rainwater through the karst vadose zone at stations A, B and LF (modified from Hartmann and Baker, 2017). This was constructed based on drip rate and isotopic responses of the most widely monitored drips on a quasi-weekly time scale, from August 2014 to July 2017 (Table 1.2). We consider the infiltration pathways as a combination of matrix flow (i.e. slow flow) and preferential flow (i.e. fast flow) between discrete water storages. Station A is suggested to have a relatively large reservoir since its drips have average isotopic values very close to the annual amount-weighted $\delta^{18}O$ composition of rainfall. Station LF is proposed to have two reservoirs: the smallest one with discharge points for LF1; the drip that most closely resembles the isotopic amplitude of rainfall (Fig. A.2), and; the largest reservoir with few discharge points that supply Fénix, the drip with constant isotopic signature that preferably allows the infiltration of very low isotopically events (intense rainfall events). We propose at least two different reservoirs for station B: one reservoir associated with B4 that behaves similar to the reservoir of station A, and one reservoir for B1 the drip that shows a threshold response to rainfall amount; an overflow drip (see Section 1.4.2).

At station B, drip waters show larger isotopic variability than at station A and an annual $\delta^{18}O$ values that fall between the annual amount-weighted and unweighted mean $\delta^{18}O$ composition of rainfall, during years 1 and 2 (Fig. 1.5). This suggests an integration of rainfall accumulation of few months and less than a year, suggesting a smaller reservoir than at

station A (Fig. 1.8). We also note that differences in reservoir effects are observed within B station drips. Drips B4 and B1, for instance, located 1 meter apart, show a consistent $\delta^{18}O$ difference of about 0.5‰. B4 also presents marked differences in drip rate variability in comparison with B1, B2 and B3, suggesting they are associated with two different reservoirs (Figs. 3, 7, 8 and Table 1.2).

At station LF, with the exception of Fénix, drip waters show the largest isotopic variability, closely reflecting that of rainfall, with an annual $\delta^{18}O$ composition similar to the mean $\delta^{18}O$ composition of rainfall (unweighted). These observations suggest an integration of few weeks of rainfall accumulation, thus reflecting the smallest water reservoir of all stations. As expected, during year 3 when the YP experienced a drought, the only drips that capture the high rainfall $\delta^{18}O$ values associated with this drought are those from station LF (Fig. 1.5). Conversely, drip waters from stations A and B reflecting a larger integration time and, therefore, a larger water reservoir size, show more isotopic 'inertia' to a rainfall isotopic shift. This isotopic inertia is clearly expressed in year 3, when the $\delta^{18}O$ values of these drip waters increase by ~0.5 per mil relative to the previous year, despite the ~2 per mil positive change in precipitation $\delta^{18}O$ associated with this drought (Fig. 1.5). Drip waters that resemble the monthly and seasonal isotopic variability of rainfall have been found in previous studies but with a greater degree of amplitude modulation than it is observed in this study (Li et al., 2000, Cruz, 2005, Cobb et al., 2007, Luo et al., 2014, Beddows et al., 2016, Duan et al., 2016).

Results from Fénix, located ~5 m from LF1, LF2 and LFG, show the smallest flow rate variability and the lowest average isotopic values of all drip waters (Figs. 3, 7 and Table 1.2). Fénix drip rates suggest a discharge flow coeval with seasonal rainfall changes, but its mean isotopic values are 1 to 2‰ lower than the annual amount-weighted $\delta^{18}O$ composition of rainfall. Constant isotope composition of Fénix reveals that the residence time of its reservoir is greater than three hydrological years, and it is likely a very large reservoir with few discharge points. Drip waters with constant $\delta^{18}O$ that can have variable discharges have been documented and result from a complicated system of infiltration flows that always have a long water residence time (Duan et al. 2016). We propose that the low permeability of the epikarst above Fénix allows primarily infiltration only of intense rainfall events that exceed a certain volume threshold. Observed rainfall $\delta^{18}O$ values associated with intense rainfall events are sufficiently negative to explain Fénix's low isotopic values (Fig. 1.4). However, it is possible that due to this low permeability the water that infiltrates during any rainfall event does not have enough volume to significantly modify the isotopic signature of a very large reservoir such as the Fénix reservoir, so it remains constant. Comparing with the other drip waters, the coefficient of variation of discharge and $\delta^{18}O$ both are very low at Fénix (35% and 4%, respectively; Fig 7). This result implies that amongst all drip waters studied at Río Secreto cave, Fénix is the only one whose stalagmite does not reflect the annual or sub-annual rainfall variability, but would likely integrate several years of rainfall.

1.5.2.1. Deuterium excess variability

The deuterium excess defined by Dansgaard (1964) as d-excess = $\delta D - 8*\delta^{18}O$, is a value that depends on the temperature and relative humidity in the moisture source region (Merlivat and Jouzel, 1979). Figure 9 shows that the d-excess of the local rainfall at Río Secreto has a

variability that is not controlled by temperature but likely controlled by the contributions of moisture from different sources on seasonal and interannual timescales. For instance, most of the rainfall that falls in this region originates from the tropical Caribbean with an influence also from the Tropical Pacific (Vuille et al., 2003). However, there are other contributions from the North Pacific that can modify the isotopic signature of local rainfall and therefore its d-excess (Vuille et al., 2003). Most of the d-excess values of local precipitation are above the global average value of 10 ‰ (Craig, 1961), indicating that most of the water masses were formed in regions with relative humidity higher than 85%. The d-excess variability of rainwater follows the same trend as that of drip water in Río Secreto cave during the three hydrological years, suggesting the transmission of d-excess from rainfall to drip water is happening rapidly. The d-excess variability of rainfall is modulated by drips from station A to a larger extent than those from station LF. Abrupt changes in d-excess are coeval with abrupt changes in drip rates from station B, providing evidence of a rapid response of the system to changes in the amount of precipitation (Supplementary Fig. A.4.). Surprisingly, the d-excess of groundwater and drip water of Fénix shows weekly variability, which indicates that although both reservoirs are likely very large, and therefore maintain a very stable composition of $\delta^{18}O$, both are influenced by moisture source changes. Groundwater and Fénix d-excess variability is modest, however, compared to the other drips and rainfall (Fig. 1.9).

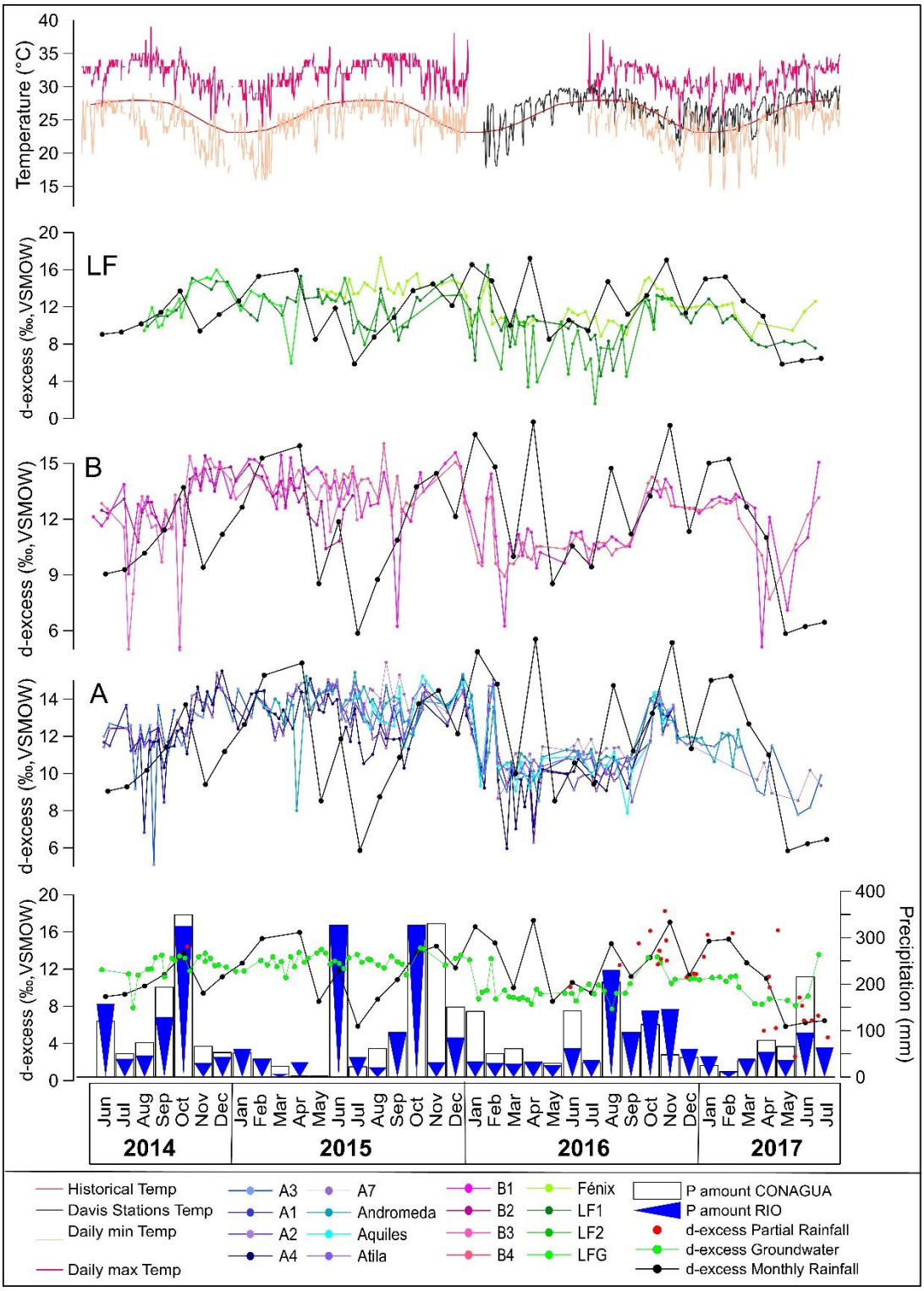

Fig. 1.9. Upper Panel shows the minimum, maximum, average and historical temperatures of Playa del Carmen. LF, B and A panels show the d-excess data from rainfall and drip waters at each of these stations. Lower Panel shows precipitation amount collected at Río Secreto cave and by CONAGUA in Cancún, Playa del Carmen and Cozumel (See section 3.1), and the d-excess from rainfall and groundwater.

1.5.3 Local Meteoric Water Line and the role of evaporation

Figure 4 shows linear relationships between $\delta^{18}O$ and δD of local rainfall (i.e. local meteoric water line, LMWL) and of drip waters (i.e. drip water line DWL). The observed LMWL (slope = 8.17‰, 95% confidence interval, CI,= 7.7-8.6‰) is very close to the global meteoric water line (GMWL, slope = 8‰) (Craig, 1961; Rosanski et al., 1993). The slope of the DWL, however, is lower and statistically distinct (slope = 7.40‰, CI 95%= 7.3-7.5‰) from the LMWL. We propose that the lower slope of the DWL relative to the LMWL does not reflect evaporation of drip water, but that drip waters preferentially incorporate summer/rainy season precipitation (June-Nov), which makes up 80% of total annual rainfall. A LMWL including only the rainy season (slope=7.6 ‰, CI 95% = 6.7-8.5‰) is statistically indistinguishable from the DWL (7.4‰), supporting this inference (Supplementary Table A.2). Furthermore, linear relationships between $\delta^{18}O$ and δD of 12 out of 15 drip sites have slopes statistically similar to that of the rainy season LMWL (Table A.2). Exceptions were Aquiles, A3 and Fénix, probably due to their different water residence times and integration periods relative to rainfall variability (See Supplementary Table A.2). Fénix has a very shallow slope since the composition of $\delta^{18}O$ is practically constant, and its values are located above the GMWL. There are several lines of evidence that suggest evaporative processes did not control the isotopic composition of drip water: (i) drip water isotopic values are similar to the LMWL; (ii) a drip water isotopic composition is similar to that of coeval rainfall; (iii) drip water mean annual $\delta^{18}O$ compositions from stations A and B closely resemble the annual amount-weighted $\delta^{18}O$ composition of rainfall; (iv) drip water average $\delta^{18}O$ composition from Fénix is 1-2‰ more negative than the annual amount-weighted $\delta^{18}O$ composition of rainfall, and; (v) cave air relative humidity was at or near 100% during the entire recorded period.

1.5.4 Groundwater

As previously mentioned, the isotopic composition of groundwater is consistent with the annual amount-weighted isotopic composition of rainfall. The temporal isotopic stability of groundwater in the Río Secreto system over the three hydrologic years studied suggests that it integrates several years of rainfall. It is well known that groundwater integrates long-term rainfall events (e.g. 5-10 years) which is reflected in its isotopic composition (Clark and Fritz, 1997, Wassenaar et al., 2009).

1.5.5 Effective recharge

In regions of little surface runoff, such as the YP, the conventional approach to estimate an effective recharge has been to use precipitation (P) minus evapotranspiration (E) (Gondwe et al. 2010, Bauer-Gottwein 2011). Based on this approach, instrumental weather data suggests that effective recharge in most of the YP would occur from only June to November, and that some locales would experience no recharge throughout the year (Lases-Hernández, 2013). Playa del Carmen in particular would experience effective recharge only during the months of June, September, October and November, representing ~16% of total annual rainfall (Supplementary Table A.4). This result is consistent with independent estimates of effective recharge in the YP based on P-E (15-17% of total annual precipitation) (Gondwe et al. 2010, Bauer-Gottwein 2011).

This conventional approach to estimate effective recharge, however, does not take into consideration the permeability of the local karst. In the case of the YP, where regional

permeability is high and varies significantly (Bauer-Gottwein et al., 2011), these estimates are expected to underestimate recharge, as suggested by independent approaches (Thomas 1999; Beddows 2004). Our study provides compelling evidence that the true recharge in the Río Secreto Cave system closely reflects precipitation amount and not P-E. This inference is supported by: (i) annual drip water $\delta^{18}O$ composition similar to the annual amount-weighted $\delta^{18}O$ composition of rainfall at stations A and B (Fig. 1.5); (ii) annual $\delta^{18}O$ values of drip waters at station LF, which show a strong flow response to individual precipitation events, almost identical to the annual mean $\delta^{18}O$ composition of rainfall (unweighted) over three consecutive years (Fig. 1.5); (iii) drip water stable isotopic variability in all stations following that of rainfall throughout the year, even during months where P-E is negative (Supplementary Table A.4), and; (iv) drip rate variability at all stations responding to rainfall amount variability throughout the year. This inference is in agreement with previous studies that determined the effective recharge in the northeastern YP based on field measurements, which also suggest that the conventional approach to estimate effective recharge (i.e. P-E) underestimates the true recharge (Thomas 1999; Beddows 2004). The expectation *a priori* that effective recharge simply reflects the precipitation to evapotranspiration balance is, therefore, unrealistic in some karstic regions with high permeability, e.g., the northeastern YP.

1.5.6 Paleoclimate implications

Our results have implications for paleo-rainfall reconstruction from stalagmite $\delta^{18}O$ records, which offer a unique opportunity to reconstruct the history of precipitation, monsoon intensity and tropical cyclone activity going back thousands of years. (Burns, 2004; Frappier et al., 2007b; Medina-Elizalde et al., 2010; Wang et al., 2001, 2007). Rarely, however, have these studies included information on how the rainfall isotopic signal is transferred to cave drip water, which are the values ultimately recorded in speleothems. This information is important in assessing how much time is integrated into the drip water isotopic signal for a given stalagmite. The results from this study suggest that individual drip waters can represent a range of integration of the isotopic composition of rainfall, and therefore, of rainfall accumulation. In addition, this study shows that significant variability among drips may be observed when sampling locations are only few meters apart.

We observe two basic time-integration modes of rainfall as reflected by the isotopic composition of drip waters. In one, drip waters isotopic values closely record individual rainfall events albeit with a slight amplitude modulation. In the second, drip waters isotopic values represent an entire year or more of rainfall accumulation. Additionally, we find that a drip can integrate several years of large precipitation events (e.g. Fénix). In light of this evidence, particular caution needs to be applied when stalagmite $\delta^{18}O$ records are sampled at subannual time scales. At this temporal resolution, stalagmites may represent cumulative rainfall amounts from individual rainfall events (e.g. LF1) or integrate over a year or longer (e.g. A3). Subannual sampling resolution of a stalagmite almost never provides an accurate representation of the true seasonal cycle of precipitation. Furthermore, out of the 16 drips examined in this study perhaps only two, LF1 and LF2, could be potentially suitable for reconstructing the history of tropical cyclones *sensu* Frappier et al. (2007a). Amplitude reduction of the isotopic signal of short-lived rainfall events is expected in nearly all cases, however, which would greatly lessen the negative isotopic anomalies characteristic of

tropical cyclones (Lawrence and Gedzelman, 1996; Lawrence et al., 1998; Gedzelman, 2003; Vieten et al., 2018).

The observation that most drip waters record the amount-weighted $\delta^{18}O$ composition of precipitation when integrated over a year or longer provides support to quantitative reconstructions of annual precipitation variability (Bar-Matthews and Ayalon, 2004; Lachniet et al., 2012, 2017; Medina-Elizalde et al., 2017; Medina-Elizalde and Rohling, 2012). A potential bias in these records could be produced, however, when stalagmite $\delta^{18}O$ values reflect a long-term integration of a summer-biased drip, such as Fénix. Our study suggests that this type of drip, at least in Río Secreto cave, is uncommon. Another potential bias could occur in association with drought years when summer monsoon precipitation fails, as we document in this study for the year 2016. In this case, due to the isotopic inertia of drips fed by relatively large water reservoirs, stalagmite $\delta^{18}O$ could underestimate the magnitude of a drought during year one and would be expected to record the full magnitude of multiyear drought with a delay of at least one year. Finally, because the cave can experience ventilation in some chambers and some drips are seasonal, more detailed studies with farmed calcite should be carried out to assess potential seasonal stalagmite growth biases.

1.6. CONCLUSIONS

We monitored surface and cave physicochemical conditions, including the $\delta^{18}O$ and δD of over 1200 groundwater, drip water and rainfall samples in the Río Secreto cave system, located in the Yucatán Peninsula, México, for three consecutive years. Isotopic data from drip water is interpreted to reflect two end-members of integration of rainfall amount: approximating the annual amount-weighted isotopic composition of rainfall or the annual arithmetic average isotopic composition (unweighted). Drip waters represent different integration times of rainfall accumulation with a lag from few days to up to three months and can be placed within the context of these two end-members. The intra-annual isotopic amplitude variability of 16 drips examined represents 5% to 95% of the observed isotopic amplitude of rainfall. Drip waters that do not modulate the isotopic amplitude of rainfall and that preserve the isotopic signal of individual rainfall events are, however, rare. Only 2 drips out of 16 were found to have potential to record the negative rainfall isotopic excursions associated with tropical cyclones if sampled at weekly resolution, but these still underrepresent the isotopic magnitude of individual rainfall events. Because the isotopic composition of drip waters approximates either the annual arithmetic average of rainfall (small reservoir effect) or the annual amount-weighted isotopic composition of rainfall (larger reservoir effect) when integrated over a year, quantitative rainfall reconstructions from stalagmite $\delta^{18}O$ records are feasible on annual or longer resolutions (e.g. *sensu* Medina-Elizalde and Rohling, 2012). Stalagmite $\delta^{18}O$ sub-annual variability, however, is likely to underestimate the seasonal variability of rainfall amount due to amplitude modulation of the rainfall isotopic signal during infiltration into the cave environment. We found that an individual drip may record the most intense rainfall events that occur during the summer season or, alternatively, may integrate over three years of rainfall accumulation. Isotopic inertia associated with most drip waters results in an underestimation of the magnitude of a drought that lasts one year, and a delay of at least one year in recording multiyear droughts by stalagmite $\delta^{18}O$ records. Lastly, we provide evidence that the effective recharge in the YP karst system is not limited to the months when precipitation exceeds evaporation. This important hydrological finding has implications for freshwater management and adaptation strategies to climate change in the YP.

APPENDIX A. SUPPLEMENTARY MATERIAL Supplementary data to this article can be found online at https://doi.org/10.1016/j.gca.2018.11.028.

REFERENCES

Baldini L.M., Baldini J.U.L., McElwaine J., Frappier A.B., Asmerom Y., Liu K.B., Prufer,K., Ridley H.E., Polyak V., Kennett D.J., Macpherson C.G., Aquino V.V., Awe J. and Breitenbach S.F.M. (2016) Persistent northward North Atlantic tropical cyclone track migration over the past five centuries. *Sci. Rep*. **6**,37522.

Baldini J. U., Baldini L. M., McDermott F. and Clipson, N. (2006) Carbon dioxide sources,sinks, and spatial variability in shallow temperate zone caves: evidence from Ballynamintra Cave, Ireland. *J Caves Karst Stud* . **68**, 4-11.

Bar-Matthews, M., and Ayalon A. (2004). Speleothems as paleoclimate indicators, a case study from Soreq cave located in the Eastern Mediterranean region, Israel. In: *Past Climate Variability through Europe and Africa* (eds. R.W., Gasse, F,. and Stickley, C.E) Kluer Academic Publishers Dordrecht, The Netherlands. pp. 343-362

Bauer-Gottwein P., Gondwe B.R., Charvet G., Marín L.E., Rebolledo-Vieyra M. and Merediz-Alonso, G. (2011) the Yucatan Peninsula karst aquifer, Mexico. *Hydrogeol. J.* **19**, 507–524.

Bautista F., Palacio-Aponte G., Quintana P. and Zinck J.A. (2011) Spatial distribution and development of soils in tropical karst areas from the Peninsula of Yucatan, Mexico. *Geomorphology*. **135**, 308–321.

Beddows P.A. (2004) Groundwater hydrology of a coastal conduit carbonate aquifer: Caribbean coast of the Yucatán Peninsula, México. PhD thesis, Sch. of Geogr. Sci. Univ. of Bristol, UK.

Beddows P. A. and Mallon E. K. (2018). Cave Pearl Data Logger: A Flexible Arduino-Based Logging Platform for Long-Term Monitoring in Harsh Environments. *Sensors*, **18**, 530.

Beddows P.A., Mandić M., Ford D.C. and Schwarcz H.P. (2016) Oxygen and hydrogen isotopic variations between adjacent drips in three caves at increasing elevation in a temperate coastal rainforest, Vancouver Island, Canada. *Geochim. Cosmochim. Acta*. **172**, 370–386.

Bradley C., Baker A., Jex C. N. and Leng M. J. (2010) Hydrological uncertainties in the modelling of cave drip-water $\delta^{18}O$ and the implications for stalagmite palaeoclimate reconstructions. *Quat. Sci. Rev.* **29**, 2201–2214

Burns S. J. (2004) Indian Ocean climate and an absolute chronology over Dansgaard/Oeschger events 9 to 13. *Science*. **305**,1567-1567.

Cabadas-Báez H., Solleiro-Rebolledo E., Sedov S., Pi-Puig T. and Gama-Castro J. (2010) Pedosediments of karstic sinkholes in the eolianites of NE Yucatán: A record of Late Quaternary soil development, geomorphic processes and landscape stability. *Geomorphology*. **122**, 323–337.

Cheng H., Edwards R.L., Sinha A., Spötl C., Yi L., Chen S., Kelly M., Kathayat G., Wang X., Li X., Kong X., Wang Y., Ning Y., Zhang H., 2016. The Asian monsoon over the past 640,000 years and ice age terminations. *Nature.* **534**, 640–646.

Clark I. D. and Fritz P. (1997) *Environmental Isotopes in Hydrogeology*. CRC/Lewis, New York, p. 328, ISBN: 9781566702492.

Cobb K. M., Adkins J. F., Partin J. W. and Clark B. (2007) Regional-scale climate influences on temporal variations of rainwater and cave dripwater oxygen isotopes in northern Borneo. *Earth Planet. Sci. Lett*. **263**, 207–220.

CONAGUA. Comisión Nacional del Agua. Servicio Meteorológico Nacional, México. Available at http://smn.cna.gob.mx/. Data obtained in 2017.

Cowan B. D., Osborne M. C. and Banner J. L. (2013). Temporal variability of cave-air CO_2 in central Texas. *J Cave Karst Stud*. **75**, 38.

Craig H. (1961) Isotopic variations in meteoric waters. *Science*. **133**, 1702–1703

Cuthbert M. O., Baker A., Jex C. N., Graham P. W., Treble P., Andersen M. S. and Acworth R. I. (2014) Drip water isotopes in semi-arid karst: implications for speleothem paleoclimatology. *Earth Planet. Sci. Lett.* **395**, 194–204.

Cruz F. (2005) Stable isotope study of cave percolation waters in subtropical Brazil: implications for paleoclimate inferences from speleothems. *Chem. Geol*. **220**, 245–262.

Czuppon G., Demény A., Leél-Őssy S., Óvari M., Molnár M., Stieber J., Kiss K., Kármán K., Surányi G. and Haszpra L.(2018). Cave monitoring in the Béke and Baradla caves. (Northeastern Hungary): implications for the conditions for the formation cave carbonates. *Int. J. Speleol*. **47**, 13–28.

Dansgaard, W. (1964) Stable isotopes in precipitation. *Tellus.* **16**, 436-468.

Duan, W., Ruan, J., Luo, W., Li, T., Tian, L., Zeng, G., Zhang, D., Bai, Y., Li, J., Tao, T., Zhang, P., Baker, A. and Tan, M. 2016. The transfer of seasonal isotopic variability between precipitation and drip water at eight caves in the monsoon regions of China. *Geochim. Cosmochim. Acta*. **183**, 250–266.

Fairchild I. and Baker A. (2012) *Speleothem Science*. Wiley- Blackwell.

Fairchild I. J., Tuckwell G. W., Baker, A. and Tooth, A. F. (2006) Modelling of dripwater hydrology and hydrogeochemistry in a weakly karstified aquifer (Bath, UK): implications for climate change studies. *Journal of Hydrol*. **321**, 213-231.

Frappier A., Knutson T., Liu K. B., and Emanuel K. (2007a) Perspective: coordinating paleoclimate research on tropical cyclones with hurricane-climate theory and modelling: Tellus, **59**, 529–537.

Frappier A.B., Sahagian D., Carpenter S.J., González L.A. and Frappier, B.R. (2007b) Stalagmite stable isotope record of recent tropical cyclone events. *Geology* **35**, 111–114.

Frisia S., Fairchild I. J., Fohlmeister J., Miorandi R., Spöt, C. and Borsato A. (2011) Carbon mass-balance modelling and carbon isotope exchange processes in dynamic caves. *Geochim Cosmochim Acta*. **75**, 380-400.

Fuller L., Baker A., Fairchild I. J., Spo¨ tl C., Marca-Bell A., Rowe P. and Dennis P. F. (2008) Isotope hydrology of dripwaters in a Scottish cave and implications for stalagmite palaeoclimate research. *Hydrol. Earth Syst. Sci*. **12**, 1065–1074.

Genty D. (2008) Palaeoclimate research in Villars Cave (Dordogne, SW-France). *Int. J. Speleol.* **37**, 173–191.

Genty D., Labuhn I., Hoffmann G., Danis P. A., Mestre O., Bourges F., Wainer K., Massault M., Van Exter S., Re´gnier E., Orengo P., Falourd S. and Minster B. (2014) Rainfall and cave water isotopic relationships in two South-France sites. *Geochim. Cosmochim. Acta.* **131**, 323–343.

Gedzelman S., Hindman E. and X. Zhang (2003) Probing hurricanes with stable isotopes of rain and water vapor. *Mon. Wea. Rev*. **131**, 1112–1127.

Gondwe B. R., Lerer S., Stisen S., Marín L., Rebolledo-Vieyra M., Merediz-Alonso G., & Bauer-Gottwein P. (2010) Hydrogeology of the south-eastern Yucatan Peninsula: new insights from water level measurements, geochemistry, geophysics and remote sensing. *J of Hydrol*. **389**, 1–17.

Hartmann A. and Baker A. (2017) Modelling karst vadose zone hydrology and its relevance for paleoclimate reconstruction. *Earth-Sci. Rev*.**172**, 178–192.

IAEA (2014) *IAEA/GNIP precipitation sampling guide.* Available at http://www-naweb.iaea.org

Karmalkar A. V., Bradley R. S. and Diaz H. F. (2011) Climate change in Central America and Mexico: regional climate model validation and climate change projections. *Clim Dyn*. 37(3-4), 605.

Kennett D.J., Breitenbach S.F., Aquino V.V., Asmerom Y., Awe J., Baldini J.U., Bartlein P., Culleton B.J., Ebert C. and Jazwa C. (2012) Development and disintegration of Maya political systems in response to climate change. *Science.* **338**, 788–791.

Lachniet M.S. and Patterson W.P. (2009) Oxygen isotope values of precipitation and surface waters in northern Central America (Belize and Guatemala) are dominated by temperature and amount effects. *Earth Planet. Sci. Lett.* **284**, 435–446.

Lachniet M. S., J. P. Bernal, Y. Asmerom, V. Polyak, and D. Piperno (2012) A 2400-yr Mesoamerican rainfall history links climate and cultural change in Mexico. *Geology.* **40**, 259–26

Lachniet M.S., Asmerom Y., Polyak V. and Bernal J.P. (2017) Two millennia of Mesoamerican monsoon variability driven by Pacific and Atlantic synergistic forcing. *Quat. Sci. Rev.* **155**, 100–113.

Lases-Hernández F. (2013) Análisis Temporal y Espacial de la Influencia de los Ciclones Tropicales en la Precipitación de la Península de Yucatán. Master Thesis, Centro de Investigación Científica de Yucatán, México.

Lawrence J. R. (1998) Isotope spikes from tropical cyclones in surface waters: Opportunities in hydrology and paleoclimatology. *Chem. Geol.* **144**, 153–160.

Lawrence J. R. and Gedzelman S.D. (1996) Low stable isotope ratios of tropical cyclone rains,*Geophys. Res. Lett.* **23**, 527–530.

Li B., Yuan D., Qin J., Lin Y. and Zhang M. (2000) Oxygen and carbon isotopic characteristics of rainwater, drip water and present speleothems in a cave in Guilin area, and their environmental meanings. *Sci. China Ser. D-Earth Sci*. **43**, 277–285.

López-Ramos E.(1975) Geological summary of the Yucatan Peninsula. In *The Ocean Basins and Margins, The Gulf of Mexico and the Caribbean* (eds. A.E.M. Nairn, F.G. Stehli). Plenum Press, NY, USA. pp. 257–282

Luo W., Wang S., Zeng G., Zhu X. and Liu W. (2014) Daily response of drip water isotopes to precipitation in Liangfeng Cave, Guizhou Province, SW China. *Quat. Int.* **349**, 153–158.

Magaña V., Amador J. A. and Medina S. (1999) The midsummer drought over Mexico and Central America. *J Climate*. **12**, 1577-1588.

McDermott F. (2004) Palaeo-climate reconstruction from stable isotope variations in speleothems: a review. *Quat. Sci. Rev*. **23**, 901–918.

McMonigal K. and Beddows P.(2014) Calcite rafts - Rapid deposition of transgressive infill cave sequences as a new paleo sea level proxy. 2014 GSA Annual Meeting in Vancouver, British Columbia (19–22 October 2014). Vancouver, BC. Canada. # 43-2 (abstr.).

Medina-Elizalde M. and Rohling E.J. (2012) Collapse of Classic Maya civilization related to modest reduction in precipitation. *Science.* **335**, 956-959.

Medina-Elizalde M., Burns S.J., Lea D.W., Asmerom Y., von Gunten L., Polyak V., Vuille M. and Karmalkar A. (2010) High resolution stalagmite climate record from the Yucatán Peninsula spanning the Maya terminal classic period. *Earth Planet. Sci. Lett.* **298**, 255-262.

Medina-Elizalde M., Burns S.J., Polanco-Martinez J., Lases-Hernández F., Bradley R., Wang H. –C. and Shen C. –C. (2017) Synchronous precipitation reduction in the American Tropics associated with Heinrich 2. *Sci. Rep.* **7**, 11216.

Medina-Elizalde M., Burns S.J., Polanco-Martínez J.M., Beach, T., Lases-Hernández F., Shen C. –C. and Wang H. –C. (2016a) High-resolution speleothem record of precipitation from the Yucatan Peninsula spanning the Maya Preclassic Period. *Glob. Planet. Change*. **138**, 93–102.

Medina-Elizalde, M., Polanco-Martínez, J.M., Lases-Hernández, F., Bradley, R. and Burns, S. (2016b) Testing the "tropical storm" hypothesis of Yucatan Peninsula climate variability during the Maya Terminal Classic Period. *Quat. Res.* **86**, 111–119.

Mestas-Nuñez A. M., Enfield D. B. and Zhang, C. (2007) Water vapor fluxes over the Intra-Americas Sea: Seasonal and interannual variability and associations with rainfall. *J Climate*. **20**, 1910-1922.

Muñoz E., Busalacchi A. J., Nigam S. and Ruiz-Barradas, A. (2008). Winter and summer structure of the Caribbean low-level jet. *J Climate*. **21**, 1260-1276.

Oh Y.H. and Kim G. (2011) Factors controlling the air ventilation of a limestone cave revealed by 222 Rn and 220 Rn tracers. *Geosci. J.* **15**, 115–119.

Onac B. P., Pace-Graczyk K. and Atudirei V. (2008) Stable isotope study of precipitation and cave drip water in Florida (USA): implications for speleothem-based paleoclimate studies. *Isot. Environ. Health Sci.* **44**, 149–161.

Orellana R., Espadas C., Conde C. and Gay C. (2009) Atlas. Scenarios Climate Change in the Yucatán Peninsula.: In *Problemas del desarrollo*, (ed. E. Iglesias) Centro de Investigación Científica de Yucatán (CICY). Mérida, México 43(168), pp.191–193.

Paillard D.L., Labeyrie L. and Yiou P. (1996)) Macintosh program performs time-series analysis. *Eos. Trans.* AGU **77**, 379.

Palaeosens P. M. (2012) Making sense of palaeoclimate sensitivity: *Nature*, **491**, 683-691.

Railsback L.B., Liang F., Vidal-Romaní J.R., Garrett K.B., Sellers R.C., Vaqueiro-Rodríguez M., Grandal-d'Anglade A., Cheng H. and Edwards R.L. (2017) Radiometric, isotopic, and petrographic evidence of changing interglacials over the past 550,000 years from six stalagmites from the Serra do Courel in the Cordillera Cantábrica of northwestern Spain. *Palaeogeogr. Palaeoclimatol. Palaeoecol.* **466**, 137-152.

Rau G.C., Cuthbert M.O., Andersen M.S., Baker A., Rutlidge H., Markowska M., Roshan H., Marjo C.E., Graham P.W., Acworth R.I. (2015) Controls on cave drip water temperature and implications for speleothem-based paleoclimate reconstructions. *Quat. Sci. Rev.* **127**, 19-36

Riechelmann D. F. C., Schro¨der-Ritzrau A., Scholz D., Fohlmeister J., Spo¨ tl C., Richter D. K. and Mangini A. (2011) Monitoring Bunker Cave (NW Germany): a prerequisite to interpret geochemical proxy data of speleothems from this site. *J. Hydrol*. **409**, 682–695.

Riechelmann S., Schröder-Ritzrau A., Spötl C., Riechelmann D.F.C., Richter D.K., Mangini A., Frank N., Breitenbach S.F.M. and Immenhauser A. (2017) Sensitivity of Bunker Cave to climatic forcings highlighted through multi-annual monitoring of rain-, soil-, and dripwaters. *Chem. Geol.* **449**: 194–205.

Rozanski K., Araguas-Araguas L. and Gonfiantini R. (1993) Isotopic patterns in modern global precipitation. In *Climate Change in Continental Isotope Records* (eds. P.K. Swart, K.C. Lohman, J. McKenzie and S. Savin). American Geophysical Union Monograph 78. pp. 1–36

Smart P.L. and Friederich H. (1987) Water movement and storage in the unsaturated zone of a maturely karstified aquifer, Mendip Hills, England. In *Proceedings of the Conference on Environmental Problems in Karst Terrains and their Solutions*. National Water Well Association, Dublin Ohio. pp. 59–87.

Smerdon J.E., Pollack, H.N., Enz, J.W. and Lewis, M.J. (2003) Conduction-dominated heat transport of the annual temperature signal in soil. Journal of Geophysical Research: Solid Earth 108.

Sprouse P,. Stan A., Ediger G., Graham K., Lloyd C., Moore D., Rincón J. (cartoonists). Addison A., Bordignon M., Bryant M., Burgos J., Cahun H., Alanis A., Ediger G., Ferreira A., Gouila C., Munguía M., Ramírez T., Rojo R., Solignac G., Sprouse P., Sprouse T, Vela G., Vela J., Von Bertrab O., Yañez G., Zabaleta M., Zappitello M., Zappitello S. and others (topographers) (2017) Map of the Pool Tunich System. Playa del Carmen, Quintana Roo, Mexico. Contact <Peter@zaraenvironmental.com>.

Thomas C. (1999) Aspects hydrogéologiques du Yucatan (Mexique). *Karstologia*, **34**, 9–22.

Vieten, R., Warken S., Winter A., Schröder-Ritzrau A., Scholz, D. and Spötl C. (2018). Hurricane Impact on Seepage Water in Larga Cave, Puerto Rico. *J Geophys Res Biogeosci*. **123** , 879-888

Vieten R., Winter A., Warken S. F., Schröder-Ritzrau A., Miller T. E. and Scholz D. (2016) Seasonal temperature variations controlling cave ventilation processes in Cueva Larga, Puerto Rico. *Int J Speleol.* **45**, 7.

Vuille M., R.S. Bradley, R. Healy, M. Werner, D.R. Hardy, L.G. Thompson and. Keimig F. (2003) Modeling $\delta^{18}O$ in precipitation over the tropical Americas: 2. Simulation of the stable isotope signal in Andean ice cores. *J. Geophys. Res.* **108**, 4175.

Wang X., A.S. Auler, R.L. Edwards, H. Cheng, E. Ito, Y. Wang, X. Kong, and Solheid M. (2007) Millennial-scale precipitation changes in southern Brazil over the past 90,000 years: *Geophys. Res. Lett*. **34**, L23701.

Wang Y. J., Cheng H., Edwards R. L., An Z. S., Wu J. Y., Shen C. C., and Dorale J. A. (2001) A high-resolution absolute-dated Late Pleistocene monsoon record from Hulu Cave, China. *Science*. **294**, 2345-2348.

Ward W.C., (1985) Quaternary geology of northeastern Yucatan Peninsula. In *Geology and Hydrogeology of the Yucatan and Quaternary Geology of Northeastern Yucatan Peninsula* (eds. A.E. Weidie, W.C. Ward and, W. Back),. New Orleans Geological Society, New Orleans, LA, pp. 23–95.

Wassenaar L.I., Van Wilgenburg S.L., Larson K. and Hobson K.A. (2009) A groundwater isoscape (δD, $\delta^{18}O$) for Mexico. *J. Geochem. Explor.* **102**, 123-136.

Williams P. P. W. and Fowler A. (2002) Relationship between oxygen isotopes in rainfall, cave percolation waters and speleothem calcite at Waitomo, New Zealand. *J. Hydrol. New. Zeal*. **41**, 53–70.

Wigley T.M.L. and Brown M.C. (1976) In *The physics of caves*. (eds. T.D. Ford, C.H.D. Cullingford), The Science of Speleology, Academic Press, London, pp. 329-358.

Worthington S. R. H. and Ford D. C. (2009) Self-organized permeability in carbonate aquifers. *Ground Water* **47**, 326–336.

Yonge C., Ford D., Gray J. and Schwarcz H. (1985) Stable isotope studies of cave seepage water. *Chem. Geol.* **58**, 97–105.

Chapter 2. Drip water $\delta^{18}O$ variability in the northeastern Yucatán Peninsula, Mexico: Implications for tropical cyclone detection and rainfall reconstruction from speleothems

Lases-Hernandez et al. 2020 (accepted for publication in GCA Journal)

Abstract

This study examines the oxygen isotopic composition ($\delta^{18}O$ values) of drip water, rainfall, and groundwater in the Río Secreto cave system, located in the Yucatán Peninsula, Mexico. The main motivation of this study was to determine the implications of drip water hydrology for the reconstruction of rainfall, droughts and tropical cyclone activity from stalagmite $\delta^{18}O$ records. Monitoring of environmental and isotopic conditions was conducted for two years, from June 2017 to April 2019. This study provides the first instrumental evidence of an "amount effect" on interannual timescales in the Yucatán Peninsula. Observed bi-weekly to interannual variability in drip water $\delta^{18}O$ values can be explained for individual drips by different integrations of rainfall amount in the time domain. Drip sites in two chambers (Stations A and B) integrate 4 to 15 months of rainfall accumulation. In a third chamber (Station LF) one drip site reflects the annual rainfall isotopic cycle with a positive offset and another, the largest rainfall events. During epikarst infiltration, the integration of rainfall amount by drip water source reservoirs determines the degree to which they "dilute" a tropical cyclone (TC) isotopic signature. TCs can be detected particularly when: (1) the water volume of the reservoir is low, such as during a persistent meteorological drought, and; (2) TCs have a sufficiently distinct isotopic signal relative to that of the reservoir prior to the event. TC isotopic signals can be masked or attenuated when drip water samples integrate more than a week and if significant rainfall events proceed the TC. In Río Secreto cave reconstructing precipitation amount and detecting the TC isotopic signatures from stalagmite $\delta^{18}O$ records is possible. Our analysis shows that stalagmite $\delta^{18}O$ records are more likely to underestimate the magnitude of annual-scale droughts following normal hydroclimate conditions and more likely to record TCs during multiyear droughts than during normal or wet periods. Drip water monitoring results suggest that available stalagmite $\delta^{18}O$ records from the Maya lowlands might be underestimating the intensity of paleo-drought events, such as the Terminal Classic droughts associated with the disintegration of the Maya civilization. This study complements the results from Lases-Hernandez et al. (2019) comparing two different sampling protocols of drip water collection. This study shows that a discrete sampling protocol is expected to approximate the amount-weighted isotopic composition of a drip, as long as it is conducted at a temporal resolution higher than the rainfall integration time by the drip reservoir. We highlight the importance of conducting multiyear monitoring of drip water and rainfall in order to interpret stalagmite $\delta^{18}O$ as a paleoclimate proxy.

2.1. INTRODUCTION

The frequency and intensity of precipitation extremes are expected to increase globally as human greenhouse gas emissions (GHG) continue to rise over the 21st century (Huntington, 2006; Williams et al., 2007; Wild et al., 2008; Chou et al., 2009; Dery et al.,

2009; O'Gorman and Schneider, 2009; Lu and Fu, 2010; Seager et al., 2010; Wu et al., 2010; Kao and Ganguly, 2011; Muller et al., 2011; Durack et al., 2012). Intergovernmental Panel of Climate Change (IPCC-AR5) projections of precipitation variability in response to GHG forcing over the 21st century show large uncertainties, particularly in regions between tropical and subtropical climates. Paleoclimate studies have the potential to help reduce these uncertainties by providing empirical estimates of precipitation responses to shifts in internal modes of climate variability and the atmospheric composition of GHGs.

Stalagmite calcite or aragonite oxygen isotope ($\delta^{18}O$ value) records represent one of the most promising terrestrial paleoclimate archives with the potential to yield semi-quantitative records of precipitation variability and records of tropical cyclone (TC) activity in tropical and subtropical regions (e.g. Wang et al., 2001; Frappier et al., 2007a; Fleitmann et al., 2009; Medina-Elzalde et al., 2010; Kennett et al., 2012; Partin et al, 2012; Akers et al., 2016; Baldini et al., 2016; Medina-Elizalde et al., 2017) .

In these regions, stalagmite $\delta^{18}O$ records have been interpreted either explicitly or implicitly to reflect the "amount effect"; that is, the inverse relationship between rainfall amount and rainfall $\delta^{18}O$ described by Dansgaard (1964), that occurs on seasonal and interannual time scales in low and mid-latitude regions (Vuille et al., 2003; Lachniet and Patterson, 2009; Medina-Elizalde et al. 2016a; Lases-Hernández et al. 2019). The working hypothesis of stalagmite hydrological records from these regions is often that calcite and aragonite deposited under isotopic equilibrium conditions preserve the rainfall $\delta^{18}O$ composition thus recording rainfall amount (Burns et al., 2003; Medina-Elizalde et al., 2010). This approach assumes that other potential effects on rainfall $\delta^{18}O$ within these regions may be negligible such as temperature, evaporation, source moisture $\delta^{18}O$ and plant transpiration (Fairchild and Treble, 2009; Wang et al., 2017; Wang et al., 2001).

Although seldom acknowledged in studies of paleohydrological records based on stalagmites, the isotopic relationship between rainfall and drip water is crucial when comparing relative isotopic variations within a single stalagmite and among different stalagmite $\delta^{18}O$ records, and particularly if the goal is to reconstruct precipitation amount quantitatively (e.g. Medina-Elizalde et al., 2010; Lachniet et al., 2012, 2017; Medina-Elizalde and Rohling, 2012; Aharon and Dhungana, 2017; Medina-Elizalde et al., 2017). The $\delta^{18}O$ signature of rainfall may be altered between the ground surface and the cave interior due to processes including isotopic fractionation in the soil, epikarst and/or vadose zone, driven by evaporation (Ayalon et al. 1998; Bradley et al. 2010; Cuthberth et al. 2014; Beddows et al. 2016, Hartmann and Baker, 2017), and by mixing with other meteoric water reservoirs in the epikarst, which essentially attenuates the isotopic signal of a rainfall event (Yonge et al., 1985; Ayalon et al., 1998; Williams and Fowler, 2002; McDermott, 2004; Fairchild et al., 2006; Lachniet, 2009; Genty et al., 2014; Hartmann and Baker, 2017). The resolution of a stalagmite $\delta^{18}O$-derived rainfall record, importantly, is not determined solely by the stalagmite sampling resolution, but also by the time integration of the rainfall signal during drip water infiltration (Lases-Hernandez et al., 2019). Drip-specific infiltration pathways can potentially integrate the amount-weighted isotopic signal of rainfall accumulated over days (Luo et al. 2014, Duan et al. 2016), a season (Cruz, 2005; Cobb et al., 2007; Fuller et al., 2008; Genty, 2008; Beddows, 2016; Duan et al. 2016), a year or even multiple years (Yonge et al., 1985; Williams and Fowler, 2002; Onac et al., 2008; Genty et al., 2014; Riechelmann et al., 2011, 2017; Czuppon et al., 2018; Jean-Baptiste et al., 2019).

Moreover, the drip sites within a single cave can exhibit different responses to the same isotopic signal of the rainfall infiltrating water (Trebel et al. 2013; Moerman et al. 2014; Pérez-Mejías et al. 2018; Llases-Hernández et al. 2019)

Drip water isotopic information, therefore, is critical to validate studies with high-resolution stalagmite $\delta^{18}O$ records that seek to characterize seasonal to interannual precipitation variability (Medina-Elizalde et al. 2010, Medina-Elizalde and Rohling, 2012; Kennett et al. 2012, Lachniet et al., 2012, 2017) or to discern the negative isotopic anomalies of TC rainfall (Frappier et al., 2007a; Baldini et al. 2016).

The present study presents new drip water isotopic data from drip sites monitored from June 2017 to April 2019 in the Río Secreto cave system, located in the northeastern coast of the Yucatán Peninsula (YP), Mexico (Fig 2.1). These drip sites are 7 of the 16 previously examined by Lases-Hernandez et al., 2019 (hereafter LH19), and were selected because they represent distinctive isotopic patterns with variable implications for paleoclimate reconstruction. In this study we applied a new sampling protocol different from that of LH19 which: (i) enabled the characterization of all the water discharged at these 7 drip sites over two years; (ii) help test the influence of LH19's sampling protocol on a positive isotopic bias observed at a drip site with a small reservoir size (labelled LF1) (details in Section 2.2.2); (iii) enabled estimates of rainfall integration times and degree of homogenization, stratified by reservoir, of six of these seven drip sites, from bi-weekly, monthly and annual drip water samples, and; (iv) help test the notion that the isotopic composition of drip water at different drip sites converge into a single value when drip water is integrated over a sufficiently long period and provided they reflect the same water source and no other process, such as evaporation, has altered the isotopic composition of the water source. In addition, this study explores the implications of observed drip water variability and residence times for the detection of significant precipitation reductions (i.e. droughts) and TCs from stalagmite $\delta^{18}O$ records. Lastly, we provide the first instrumental evidence of the existence of a rainfall *amount effect* on interannual timescales for the YP.

2.2. FIELD SITE

2.2.1. Study site, cave system and climate

The annual precipitation cycle in the YP is recognized to have three distinctive seasons known as Dry, Rainy and Nortes. The *Dry* season corresponds to the months from March to May when the region experiences the lowest amount of precipitation in the course of the year. The *Rainy* season, concurrent with the so-called "hurricane season", has a bimodal distribution of precipitation with precipitation peaks in June and September and a midsummer drought, or *Canícula*, during July and August (Magaña et al., 1999). During the *Rainy* season the Intertropical Convergence Zone (ITCZ) and its belt of convective activity reach their northernmost position producing peak precipitation in the month of September coeval with maximum tropical cyclone frequency affecting the YP. The *Nortes* season happens during the months of November and February and is characterized by the influence of northern cold fronts which bring cold weather and isotopically distinctive rainfall into the YP.

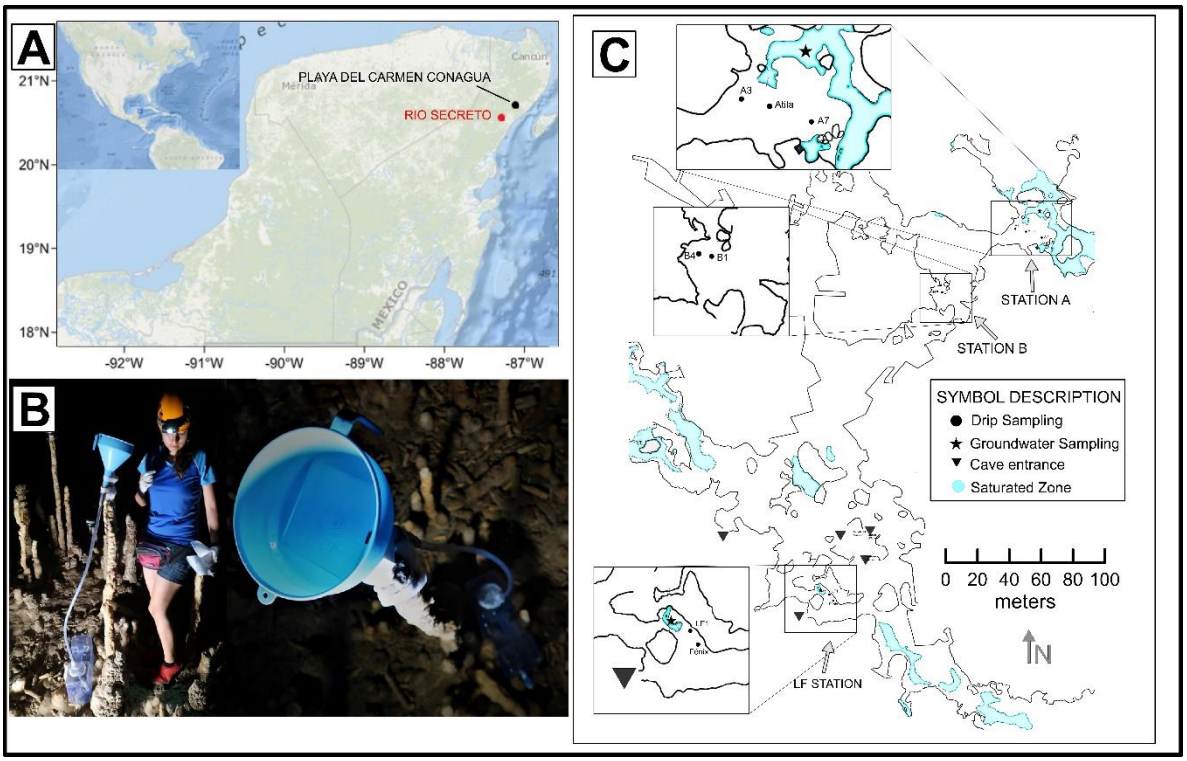

Figure 2.1. (A) Location of Río Secreto cave (red dot) and weather tation of Playa del Carmen (CONAGUA) (black dot). (B) Example of collection of drip water system at A7 drip site, visible also is a glass plate inside the funnel used to farm calcite (See Section 2.3.2). (C) Map of the monitored Stations A, B and LF (modified from Sprouse et al. 2017).

The Río Secreto ("Secret River") cave is a semi-flooded karst system located in the northeast of the YP in the State of Quintana Roo, Mexico (20° 35.244'N; 87° 8.042'W, Fig. 1). The karst cave system is mostly horizontally developed and with an extension larger than 42 km surveyed by Sprouse et al. (2017). The cave is 5 km south of the city of Playa del Carmen, and the main entrance is five km from the Caribbean coast. Río Secreto cave has been used for tourism purposes since the year 2008, although only about 10% of the cave is used for this purpose. Río Secreto cave is located less than 10 km away from the CONAGUA (National Water Office) meteorological station located in Playa del Carmen city. Average annual precipitation in Playa del Carmen is 1390 ± 280 mm (14-year monthly averages 1998-2011; Table E in Supplementary Material). More than 70% of total annual precipitation occurs during the *Rainy* season from June to November and therefore recharge is also biased to these months (Medina-Elizalde et al., 2016b; Lases-Hernández et al., 2019).

The bedrock at Río Secreto cave is composed by Pliocene-Pleistocene carbonates that retain much of its primary porosity, although infiltration is given mostly through small fractures and secondary porosity features. The vadose zone of Río Secreto cave and of most caves in the northeastern YP is within the epikarst and the bedrock thickness is from 2 to 12 m (Lases-Hernández et al., 2019). The water table in Rio Secreto is located ~15 m from the surface and has a very low hydraulic gradient in the range of 10^{-5} cm per km (Bauer-Gottwein et al., 2011). Río Secreto cave has several sinkholes with a diameter from 1 to 8 meters that allow access to the cave and its ventilation. The overlaying soil is very thin and

heterogeneous, with soil pockets <0.5 m deep between frequent areas of exposed bedrock (Lases-Hernández et al., 2019).

2.2.2 Previous study in the Río Secreto cave system

LH19 determined the isotopic composition of drip water, groundwater, and rainfall from three different chambers within the Rio Secreto cave system. These chambers were labeled Station Laberinto del Fauno (LF) and Stations A and B. Monitoring of environmental conditions inside and outside the cave included the measurement of air temperature and relative humidity as well as drip water and groundwater temperatures from 2012 to 2017. Stations A and B are isolated and characterized by having constant temperatures similar to the annual average air temperature outside (~24.5°C). Station LF presents more variable annual variability of groundwater and air temperature (total range of ~3°C and ~6°C, respectively) and air temperature coupled with temperature variability outside. Buoyancy-driven ventilation occurring mainly during winter season produces seasonal temperature variability inside these chambers with a larger effect on the most exposed chamber, the LF Station, as expected (LH19). Relative humidity at Stations A and LF was near to 100% during the 2014-2017 period.

LH19 characterized the oxygen isotopic composition at 16 cave drip sites from these three chambers and results showed that drip sites modulated the amplitude of rainfall $\delta^{18}O$ variability to different degrees. The study by LH19 did not estimate quantitatively the time-integration of rainfall amount by each drip water reservoir, as presented in this current study. At all drip sites (with the exception of drip site labelled Fénix) drip water isotopic compositions were between two end members: (1) drip waters whose annual mean $\delta^{18}O$ values were close to the annual amount-weighted $\delta^{18}O$ composition of rainfall (e.g. drip sites labelled A3, A7, Atila, B1, B4), and; (2) drip waters whose annual mean $\delta^{18}O$ values were close to the arithmetic annual average isotopic composition of rainfall (e.g. LF1). LH19 showed that drip waters whose $\delta^{18}O$ values resemble the annual amount-weighted $\delta^{18}O$ composition of rainfall also presented low intra annual isotopic variability, concluding that they reflect a water reservoir big enough to accumulate rainfall during several months with physical homogenization controlling the water isotope signature over this timescale. Conversely, a small reservoir was inferred for a drip site whose annual mean water $\delta^{18}O$ values was close to the arithmetic annual average isotopic composition of rainfall (e.g. LF1), and that best tracks the $\delta^{18}O$ variability of individual rainfall events. LH19 proposed that these results reflected the sampling protocol consisting of a bi-weekly collection of discrete drip water samples accummulated over 48 hours. According to this hypothesis, the annual average $\delta^{18}O$ composition of drip water would be close to the annual amount-weighted $\delta^{18}O$ composition of rainfall when their reservoirs were large, and close to the unweighted annual average $\delta^{18}O$ composition of rainfall when their reservoirs were small (Fig. 1.5 in LH19). This is because a large reservoir already integrates the cumulative isotopic signal of many rainfall events and therefore a discrete sample would reflect such temporal integration. In contrast, a small reservoir implies that a discrete sample represents only few rainfall events and an annual isotopic average based on discrete samples would therefore be biased; just like an annual average isotopic composition of rainfall, that does not weigh the amount of individual rainfall events, would be biased relative to the annual amount-weighted isotopic

composition of rainfall (Fig. 1.5 in LH19). This hypothesis was supported by evidence that evaporation, a factor that can also potentially shift LF1 $\delta^{18}O$ positively, was likely negligible, as suggested by: (i) drip water isotopic values similar to the coeval local meteoric water line; (ii) the isotopic composition of drip water at various drip sites similar to that of rainfall; (iii) drip water mean annual $\delta^{18}O$ compositions from Stations A and B closely resembling the annual amount-weighted $\delta^{18}O$ composition of rainfall; (iv) drip water average $\delta^{18}O$ composition from drip site labelled Fénix 1-2‰ more negative than the annual amount-weighted $\delta^{18}O$ composition of rainfall, and; (v) cave air relative humidity at or near 100% during the entire recorded period.

One motivation of this work is to test whether the positive isotopic offset of drip site LF1 relative to the annual amount-weighted $\delta^{18}O$ composition of rainfall reflects an artifact of the discrete sample protocol, by adopting a continuous sampling method. We note that if the positive isotopic bias of LF1 were a reflection of the sampling protocol and not evaporation, a stalagmite from this drip would be ideal to identify the short-lived fluxes from TCs.

The drip site labelled Fénix, located ~5 m from LF1, presented a conondrum as it showed the lowest variability and the most depleted isotopic values of the 16 drip sites investigated. Fénix's drip rates suggested a discharge flow coeval with seasonal rainfall amount changes, but its $\delta^{18}O$ values showed negligible variability (<0.4 ‰) and an isotopic composition 1 to 2‰ more depleted than the annual amount-weighted $\delta^{18}O$ composition of rainfall. To explain Fénix's lack of isotopic variability and negatively biased isotopic composition, LH19 hypothesized that the epikarst above Fénix was thin enough to allow primarly infiltration of large rainfall events with their associated depleted $\delta^{18}O$ values resulting from an *amount effect*. Due to Fénix's very large reservoir, on the other hand, these rainfall events did not have enough volume to modify significatly the reservoir's isotopic signature, thus explaining its characteristic low isotopic variability over time. In this study we continued monitoring Fénix in order to better understand its long-term response to rainfall $\delta^{18}O$ variability, particularly during times of drought.

Lastly, LH19 document that drip discharge typically lagged rainfall amount shifts by few weeks and up to three months. According to the methodology of Fairchild et al. (2006), the drip sites we monitor in this study, A3, A7, B4 and Fénix are drips that maintain a high and temporally constant drip rate seasonally and are thus classified as "Seepage flow". The other three drip sites we monitor, Atila, B1 and LF1, exhibit higher discharge variability thus corresponding to "Seasonal Drips" (Fig. 1.7 in LH19).

2.3. METHODS

2.3.1 Rainfall sampling

Thirty five rainfall samples were collected between July 2017 and April 2019, using two HDPE 8-liter containers with a connected funnel that had a Ping-Pong ball in it to help prevent potential isotope exchange and water loss from the containers through evaporation, following previous protocols (Lases-Hernández et al. 2019). Rainfall samples include 22 that integrate 9 to 59 days labeled "monthly rainfall" and 13 samples that integrate 1 to 41 days

labeled "partial rainfall" (Fig. 2.2). Sample periods of rainfall accumulation are presented in the Supplementary Table A. In addition to rainfall amount data collected at the Río Secreto Nature Reserve, we present coeval rainfall amount data recorded by a meteorological station in the city of Playa del Carmen, located 4 Km away from Río Secreto (20°37.200´0N, 87° 04.200´0W). This additional rainfall data offers a broader perspective of spatial variability in this region (Supplementary Table A at Appendix A).

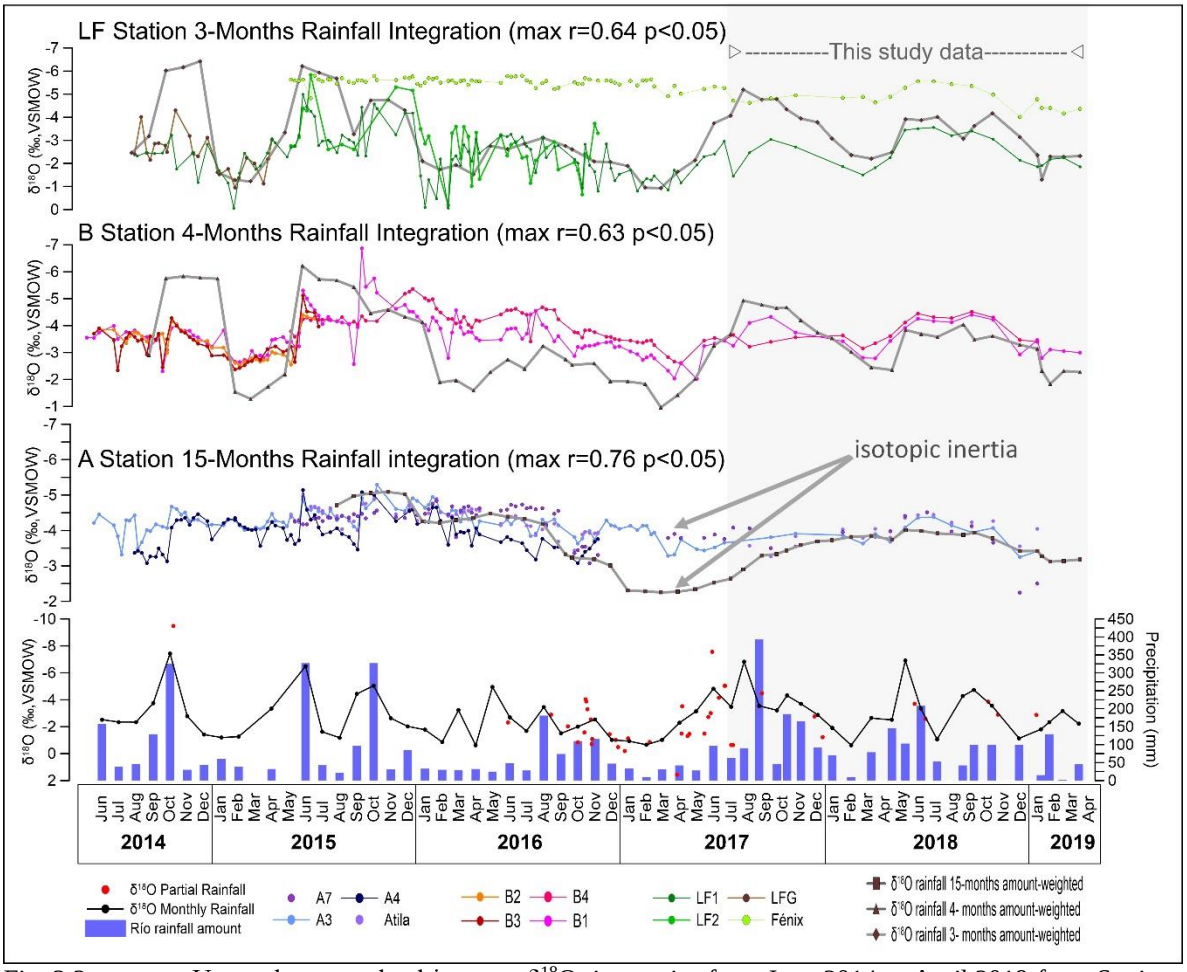

Fig. 2.2 Upper three panels: drip water $\delta^{18}O$ time series from June 2014 to April 2019 from Stations LF, B and A. Superimposed; time series of rainfall amount-weighted $\delta^{18}O$ values integrated over specific time intervals for each station (black lines) (See Sections 2.3.3.2, 2.4.4 and 2.5.2; Fig. B and Table G at appendix A). Lower panel: Rio Secreto rainfall $\delta^{18}O$ composition of monthly samples (black line) and discrete rainfall events (red dots), and rainfall amount (blue rectangles) (See Section 2.3.1). Note that all the $\delta^{18}O$ axis values are inverted and represent different value ranges. Data before July 2017 are from Lases-Hernández et al. (2019).

2.3.2 Drip water and groundwater sampling

Río Secreto Cave drip water $\delta^{18}O$ and discharge rate variability were previously characterized on a ~bi-weekly basis from monitoring 16 stalactites in three different chambers by LH19 (see Section 2.2.2). In this study, we selected and monitored 7 of these 16 drip sites, that best represent the types of isotopic variability patterns previously described. Specifically for this study, drip water was collected from two stalactites labeled LF1 and

Fénix (located in LF Station), three stalactites labeled A3, A7 and Atila (A Station), and 2 stalactites labeled B1 and B4 (B Station) (Fig. 2.1). Drip water samples from these 7 stalactites represent 3 to 61 days of water accumulation over the same 22-month period that rainfall water data was collected (Table B at Appendix A).

Drip water from each drip site was collected using a plastic funnel connected with a hose to an HDPE 8-liter container. Connections were sealed following each collection using three layers of Parafilm and one layer of silver tape to avoid evaporation and isotope exchange with ambient water vapor. After water accumulated in the container, one drip water aliquot was taken into a 30 mL Nalgene bottle through the container's spigot to avoid interaction between water and air during sample transfer. Before deployment of the water collection system, all its plastic components were washed with a 10% solution of ultra clean HNO_3, rinsed three times with deionized water, and finally thoroughly dried. After each sample aliquot was collected the total water volume in the collector was quantified using a graduated cylinder. The collection system was fully cleaned and dried as described above, before being reinstalled to collect a new drip water sample. Nitrile gloves were used to manipulate components during sampling work. We point out that within the funnels we placed 10 x10 cm frosted glass plates in order to farm calcite. Glass plates were previously washed with a 10% solution of ultraclean HNO_3 and rinsed three times with deionized water. During the visits to the cave, discrete groundwater samples from LF and A Stations were also collected directly from cave pools, 30 cm from the surface, using 30 mL Nalgene bottles (Fig. 2.1), the dates of sampling can be found in Table E at Appendix A. The isotopic results of farmed calcite will be reported in a subsequent manuscript.

2.3.3 Analytical methods and Data Interpretation

2.3.3.1. Stable isotope composition

The $\delta^{18}O$ and δD composition of groundwater, meteoric precipitation and drip water samples were determined using a Cavity Ring-Down Spectroscopy (CRDS) Picarro Isotope Analyzer, model L2130-i at Auburn University, Alabama. Long-term reproducibility of in-house Picarro "Zero" and "Mid" standard waters measurements were better than 0.03 ‰ for $\delta^{18}O$ and at 0.2 ‰ for δD. Results are reported in per mil (‰) relative to VSMOW (Vienna Standard Mean Ocean Water).

2.3.3.2. Integration of rainfall amount by drip water

In order to determine how much time of rainfall accumulation the drips integrate (Fig. 2.2), we used a simple inverse modeling approach to calculate the weighted $\delta^{18}O$ composition of rainfall that explains the observed drip water $\delta^{18}O$ baseline values and variability in each chamber (See Fig. B at Appendix A). The weighted $\delta^{18}O$ composition of rainfall is based on the sum of all the rainfall events starting from that closest or coeval to the time integrated by each drip water sample collected, and moving back in time integrating previous rainfall events, until the observed drip water $\delta^{18}O$ variability can be explained. The rationale for this approach is that drip water can reflect only rainfall events that are coeval (fast permeability) and/or preceding the time of collection, depending on the reservoir size. The larger the

reservoir size, the larger the expected integration time of rainfall amount by drip water samples. Note that in reality the reservoir does not reflect the time domain *per se*, but an amount of rainfall that accumulated over a given amount of time, which is known to vary from intraseasonal to interannual timescales. Ideally, this analysis would be based on characterizing the precipitation amount and isotopic composition of every single rainfall event. Practically, that was not possible for us, and rainfall $\delta^{18}O$ samples integrate precipitation between 1-59 days. Our protocol, however, was sufficient to closely approximate the integration time of drips from the three chambers examined at Río Secreto Cave (Section 2.4.4; Fig. 2.2).

2.3.3.3. Convergence of drip water $\delta^{18}O$ values

If different drip sites integrate rainfall amount accumulated over different periods of time, depending on the size of their reservoirs, their drip water $\delta^{18}O$ values are expected to be different at a given point in time. Nevertheless, the amount-weighted $\delta^{18}O$ composition of drip water at different locations integrated over a sufficiently long period should converge into a single value, provided that no other effect, such as evaporation, has altered the isotopic composition of the water source. In order to test this notion, we calculated the amount-weighted $\delta^{18}O$ composition of each drip, integrating consecutively from 2 to 22 months of water accumulation, in order to find the integration time of convergence. We note that this study allows us to perform this integration because all the drip water that drained over two years was collected for each of seven drip sites (see Supplementary Tables A and B). We also calculate amount-weighted and unweighted $\delta^{18}O$ compositions of each drip site to compare each other (Table 2.1).

Table 2.1. Statistical summary of rainfall, drip water and groundwater $\delta^{18}O$ and δD collected at Rìo Secreto Cave during July 2017-April 2019

Sample	n	$\delta^{18}O$ AVG	$\delta^{18}O$ 1SD	$\delta^{18}O$ MIN	$\delta^{18}O$ MAX	δD AVG	δD 1SD	δD MIN	δD MAX	$\delta^{18}O$ Amount Weighted AVG	δD Amount Weighted AVG	Number available volume data
Monthly Rainfall	22	-3.2	1.6	-6.9	-0.6	-12.8	14.5	-46.6	6.8	-3.3	-15.3	22
B4	16	-3.8	0.5	-4.5	-3.2	-18.5	2.3	-21.9	-14.4	-3.9	-19.5	13
B1	20	-3.6	0.6	-4.4	-2.8	-16.6	5.1	-27.1	-9	-3.9	-19.5	18
Atila	16	-4	0.3	-4.4	-3.3	-20.6	0.9	-22.1	-18.9	-4	-20.5	15
A7	14	-3.7	0.7	-4.5	-2.2	-18.9	5.2	-24	-7.7	-3.8	-20	11
A3	14	-3.9	0.3	-4.4	-3.2	-19.1	2	-22.1	-15.3	-4	-19.4	11
LF1	20	-2.5	0.7	-3.6	-1.4	-9	5.2	-16.2	-1.4	-2.5	-9.2	16
Fénix	20	-4.8	0.4	-5.6	-4	-27.4	2.8	-30.5	-22.6	-4.9	-27.5	18
LF Station Pond	12	-3.5	0.7	-4.4	-2.3	-18.1	3.4	-23.3	-13.1			
A Station Groundwater	13	-4.6	0.3	-5	-4.2	-26.7	1	-29.1	-25.2			

2.4. RESULTS

This study presents results for the hydrological years spanning June 2017-May 2018 and June 2018-April 2019, which represent the fourth and fifth year (hereafter referred to as Y4 and Y5) of a continuous monitoring effort that was initiated during the hydrological year June-2014-May 2015 (LH19). We place our results in the context of evidence from the previous three hydrological years (hereafter referred to as Y1, Y2 and Y3) which established the long-term relationship between precipitation amount and its isotopic composition, and in turn how Y4 and Y5 results relate to temporal variability in the isotopic composition of drip water. Also, this study centers preferentially on $\delta^{18}O$ (and not δD), because of its application as a proxy of precipitation in stalagmite records from tropical and subtropical regions.

2.4.1 Precipitation amount, $\delta^{18}O$ and δD composition

The records of rainfall amount from Río Secreto and the government meteorological station in Playa del Carmen (i.e. CONAGUA) were similar to each other during the five hydrological years of monitoring (Supplementary Table A). Precipitation amount during the hydrological year Y4 was particularly large (1513 mm/yr) relative to the previous year when the YP experienced a summer drought (748 mm/yr) and slightly greater than the long-term annual average (1998-2011= ~1400 mm/yr; Supplementary Table E). Precipitation amount during Y5 was also significantly lower than the average and represents another drought year (798 mm/yr). A drought year in this study, therefore, is understood as a hydrological year when annual rainfall amount represented 53%-57% (Y3 and Y5, respectively) of the instrumental 14-year annual average rainfall amount (1998-2011; Supplementary Table E).

The $\delta^{18}O$ and δD annual amount-weighted isotopic compositions of rainfall were, respectively -4.1‰ and -22.5‰ during Y4, and -2.9‰ and -9.5‰, during Y5. The $\delta^{18}O$ composition of rainfall during Y4 is therefore significantly more negative than the previous year Y3 (-2.3 ‰) and proceeding year Y5 (-2.9‰), when the YP experienced significant summer droughts and positive rainfall $\delta^{18}O$ anomalies. During both years, rainfall $\delta^{18}O$ and δD varied from -6.9‰ to -0.6‰ and from -46.6‰ to +6‰, respectively (n=35) (Fig. 2.2); this is almost the same intra-annual $\delta^{18}O$ amplitude variability reported for the three previous hydrological years by LH19 (~6.8‰ for $\delta^{18}O$). Monthly rainfall $\delta^{18}O$ values show two distinctive negative excursions reaching peak values of ~ -7 ‰ occurring in July/August 2017 and May/June 2018 relative to the preceding samples, reflecting the low rainfall isotopic signal of tropical cyclones Franklin and Alberto. Lower rainfall isotopic values are observed in association with the rainy seasons (June-Sept) and relatively more positive with the dry seasons (March-May), consistent with observations of previous years and the amount effect relationship characterized on seasonal timescales by LH19.

We found a negative relationship between the annual amount-weighted $\delta^{18}O$ composition of rainfall and annual rainfall amount during the 5 hydrological years (slope of -0.0019 ‰ per mm, r^2=0.37), revealing the existence of an interannual amount effect. If we remove from this linear regression the data from Y4 -which represents an anomalously wet year-, we found a significantly stronger interannual amount effect (slope of -0.0066 ‰ per mm, r^2=0.82; Fig 2.3A). The amount effect slope value from this study is very similar to that

observed in Cuba (Fig. 2.3B) and to those suggested by climate models with isotope tracers (Vuille et al., 2003).

2.4.2 Drip $\delta^{18}O$ variability

All drip water isotopic data are reported in Supplementary Table B and a statistical summary is presented in Table 2.1. A total of 127 samples from 7 different drip sites were analyzed for $\delta^{18}O$ and δD. These samples represent uninterrupted periods of drip water accumulation from 3 to 61 days over the time interval from July 2017 to April 2019. In addition, we collected a total of 5 discrete samples during two visits to the cave from hollow inverted-funnel-shaped stalactitic speleothems that discharged a large volume of water after few hours of the occurrence of strong rainfall events (also called showerhead). Drip water $\delta^{18}O$ and δD varied from -5.6‰ to -1.4‰ and from -30.5‰ to -1.4‰, respectively. The lowest isotopic values correspond to Fénix drip site and the most positive to LF1 drip site (Fig. 2.2).

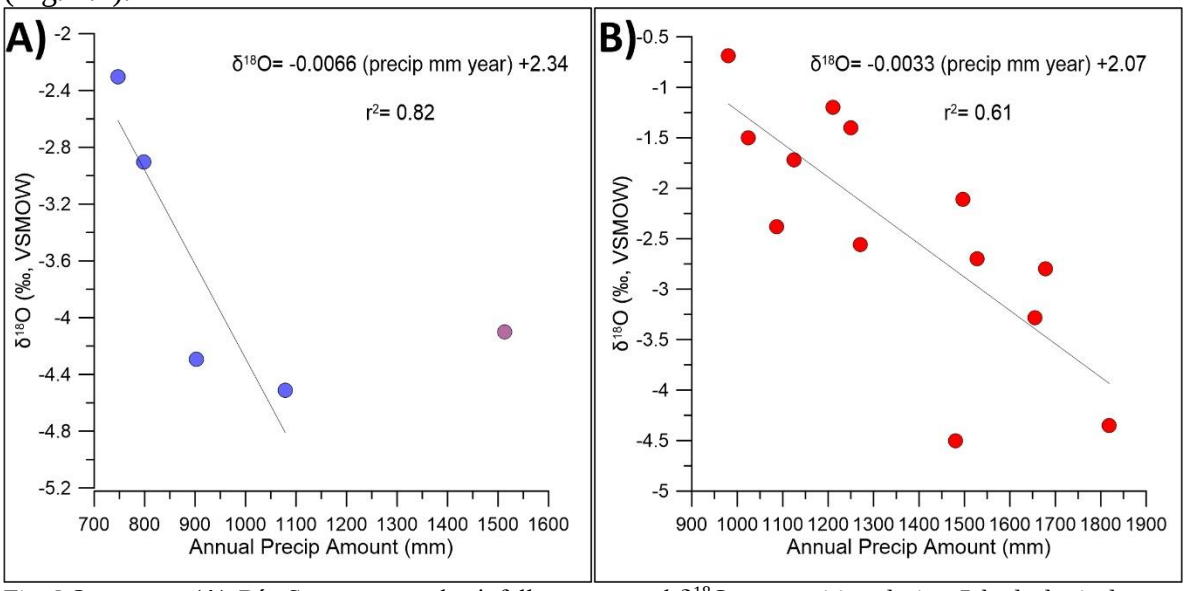

Fig. 2.3. (A) Río Secreto annual rainfall amount and $\delta^{18}O$ composition during 5 hydrological years (See Sections 2.4.1 and 2.5.1). Note that the outlier point is not considering for the linear regression. Data of three hydrological years is from Lases-Hernández et al. 2019. (B) Havana, Cuba annual rainfall amount and $\delta^{18}O$ composition during 12 hydrological years (IAEA-GNIP, 2002-2015). Linear regressions between annual precipitation amount and $\delta^{18}O$ composition from each location are shown.

2.4.2.1 Local Meteoric Water Line and Drip Water Line

The Global meteoric Water Line is the established linear correlation between $\delta^{18}O$ and δD of meteoric precipitation that follows the relationship $\delta D = 8\ \delta^{18}O + 10‰$ at a global scale (Craig, 1961; Rozanski et al. 1993). At a regional level it can vary because local effects can influence the isotopic composition of rainfall and therefore a Local Meteoric Water Line (LMWL) should be established by data spanning at least one hydrological cycle (Clark and Fritz, 1997). LH19 characterized the LMWL finding a slope of 8.2 for rainfall within the period Y1-Y3. The LMWL for the period Y4-Y5 has a slope of 8.8, slightly higher than that found for the previous period (Table C in Supplementary material). However, a comparison

between the $\delta^{18}O$ and δD values of drip water from this study with the coeval LMWL, shows that practically none of the drip water values deviate markedly from the LMWL. Moreover, drip water $\delta^{18}O$ and δD values plot very close to those of rainfall samples that represented rainfall amounts higher than 90 mm, which together represent 80% of total rainfall amount during the period Y4-Y5 (Fig. C at Appendix A).

2.4.3. Drip water $\delta^{18}O$ amplitude

We examine the drip $\delta^{18}O$ amplitude observed in this study based on cumulative drip water samples in light of the previous monitoring work by LH19 based on the collection of discrete water samples. At A Station, the $\delta^{18}O$ amplitude variability of drip sites A3, A7 and Atila was 1.6‰, 1.6‰ and 1.2‰, respectively (Y1-Y3), and 1.2‰, 2.8‰ and 1.2‰, respectively, during this study period. At B Station, the $\delta^{18}O$ amplitude variability range (2 SD) of drip sites B1 and B4 was 3.2‰ and 2.4‰, respectively (Y1-Y3), and 2.4 ‰ and 2‰, respectively during this study period (Y4-Y5). At LF Station, LF1 and Fénix showed an amplitude range of 4‰ and 0.8‰ (2 SD respectively) during the three years preceding this study and a range of 2.8‰ and 1.6‰, respectively, during this study period.
As determined in LH19, drips from the three different chambers reflect the $\delta^{18}O$ amplitude variability of rainfall to different extents. Across the five years of monitoring in Río Secreto cave the largest drip water $\delta^{18}O$ value range is observed at LF1 site (5‰), followed by drip sites from Station B (4‰) and lastly drip sites from Station A (2‰). Fénix is an exception in that it records the lowest amplitude variability of all drip sites (~1‰) and its $\delta^{18}O$ values are consistently more negative than those of average rainfall. The observed drip water $\delta^{18}O$ amplitude variability (≤4 ‰) for Y4 and Y5 is smaller than that of rainfall (6‰) for this period, as was previously reported for Y1-Y3 by LH19.

2.4.4. Drip water isotopic integration of rainfall and convergence

As noted above, monitored drips from all three chambers integrate a longer time interval than monthly $\delta^{18}O$ rainfall variability (~6‰, 2SD). As described in the methods Section 2.3.3.3, we can determine the integration time of rainfall amount necessary to explain the observed drip water $\delta^{18}O$ composition. Figure 2.2 shows the different time integrations of rainfall amount that can explain most of the variability in drip water $\delta^{18}O$ observed in Stations LF, A and B. As expected from the observed difference in the $\delta^{18}O$ amplitude variability of drip water among the three different chambers, the shortest integration time corresponds to LF1 (2-3 months) and the longest to drip sites at Station A (15 months). Drip water at Station B represents rainfall integration times between these two end members (4 months). Note that our approach explains not only the observed drip water $\delta^{18}O$ variability, but also closely approximates the absolute values, with some exceptions. LF1 $\delta^{18}O$ values tend to be more positive than those of rainfall during Y1, Y2 and Y4 and drip sites from Stations B and A tend to be more negative during the drought years Y3 and Y5 (Fig. 2.2).

Because the various drip locations represent different integration times of rainfall, their observed $\delta^{18}O$ composition is not the same at a given point in time, even when they ultimately reflect the isotopic composition of the same rainfall source. Provided drip water is integrated over a sufficiently long interval, however, the $\delta^{18}O$ composition from all drip sites should converge into a single value reflecting the isotopic composition of the source; if

it remained unaltered by evaporation or some other process. In order to find the integration time of convergence we calculated the amount-weighted $\delta^{18}O$ composition of each drip, integrating consecutively from 2 to 22 months of water accumulation (Fig. 2.4). The results of this analysis indicate that drip water from Stations A and B converge into a single $\delta^{18}O$ value after an integration time of about 11-15 months, and that LF1 and Fénix are isotopically distinctive. Of all the drip sites, LF1 integrated $\delta^{18}O$ values are the most positive and those from Fénix the most negative, consistently (Fig. 2.4).

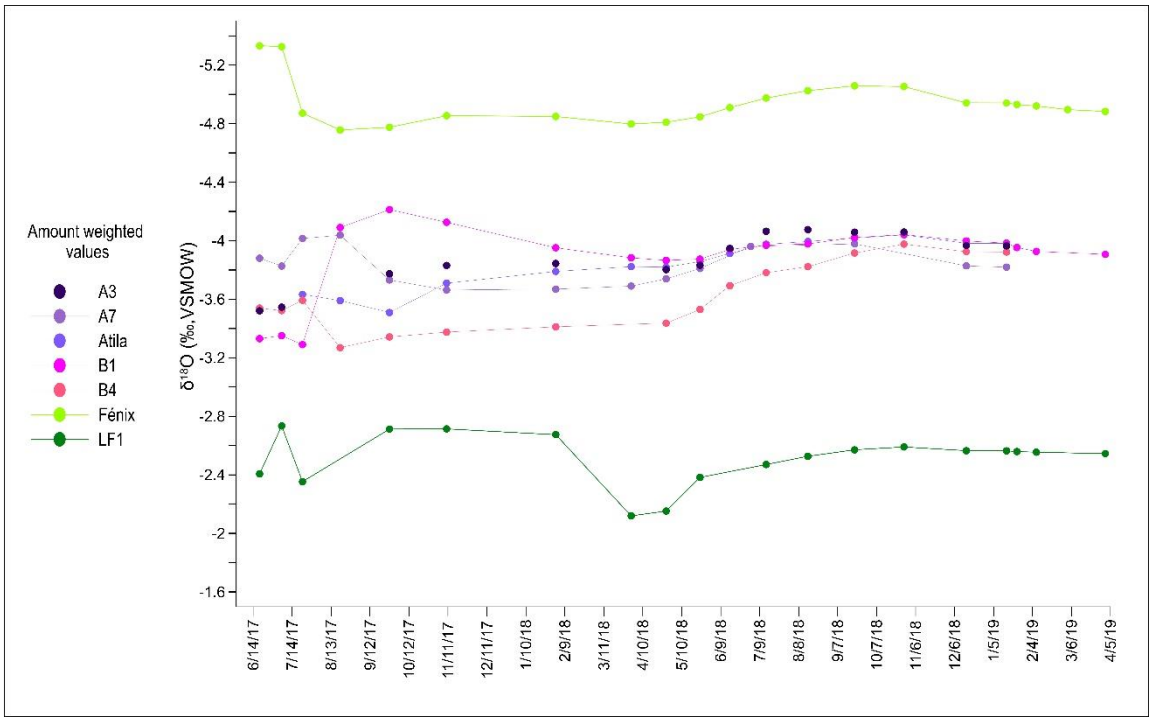

Fig. 2.4. Río Secreto amount weigthed $\delta^{18}O$ composition of drip water for this study (Y4 and Y5). The first values (6/14/17) represent the $\delta^{18}O$ composition of drip water during the first month, the second values represent the amount weigthed $\delta^{18}O$ composition integrating the first and the water sample collected subsequently (7/14/17), the third values represent the amount weigthed $\delta^{18}O$ composition integrating the first three samples, and so on (See Sections 2.3.3.3 and 2.4.4). As described in the main text, each sample represents the total water accumuated over a specific time interval which may differ among drip sites and can be from about a month or longer.

In Table 2.2 we present a summary of the isotopic and discharge characteristics of the 7 drips analyzed in this study, based on the data from 5 hydrological years. We found that the drip sites that have higher $\delta^{18}O$ variability and closer to that of rainfall are those that have a shorter rainfall accumulation time and therefore probably have smaller reservoirs (e.g. LF1, B1 and B4). However, short rainfall integration times and greater variability may be associated with discharges classified as seepage flow (e.g. B4 site) and also seasonal drips (e.g. LF1, B1) (Table 2.2). The opposite can also occur; long rainfall integration times can correspond to both, seasonal drips (e.g. Atila) and a seepage flow (e.g. A3 and A7).

Table 2.2. Summary of isotopic and discharge characteristics of 7 drip sites based on 5 year data for the period June 2014-April 2019 from Río Secreto cave. All results and inferences are explained in detail in Sections 2.4 and 2.5. To perform calculations, data before July 2017 was obtained from Lases-Hernández et al. (2019).

Sample	$\delta^{18}O$ AVG	$\delta^{18}O$ 1SD	$\delta^{18}O$ range	% of $\delta^{18}O$ rainfall range	$\delta^{18}O$ (n)	drip rate avg (mL/h)	drip rate 1 SD (mL/h)	drip rate max (mL/h)	drip rate range (mL/h)	drip rate (n)	Classification	Rainfall integration time (months)	Isotopic convergence time (months)
A3	-4.2	0.4	2.1	31	116	2.4	1.7	10.8	10.5	115	Seepage flow	15	11
B4	-4	0.6	2.8	41	79	3	1.9	9.7	9.1	74	Seepage flow	4	15
A7	-4.2	0.5	2.6	38	69	3.3	1.4	8.3	8	67	Seepage flow	15	11
Atila	-4.3	0.4	1.8	26	63	3.2	1.9	11.8	11.5	55	Seasonal drip	15	11
Fénix	-5.4	0.4	1.8	26	86	3.9	1.9	15.3	14.8	87	Seasonal drip		
LF1	-2.4	1	4.9	72	102	1.2	1.2	9.2	9.1	99	Seasonal drip	1 to 3	
B1	-3.6	0.7	4.9	72	135	3.4	4.3	25.1	25	117	Seasonal drip	4	11

2.4.5. Annual drip water $\delta^{18}O$

The new monitoring effort consisting of cumulative samples allow us to determine an annual amount-weighted $\delta^{18}O$ composition of each drip site and place the information from previous years in the context of the last five years of rainfall information.

Because of the discrete sampling protocol followed by LH19, it was not clear whether drips LF1 and LF2 (not investigated here), which had the most positive annual $\delta^{18}O$ compositions of all 16 drip sites, reflected evaporation processes or that the discrete sampling protocol did not allow accurate characterization of their annual amount-weighted $\delta^{18}O$ composition. We note that drips LF1 and LF2 showed the largest $\delta^{18}O$ amplitude variability of all drip sites and the closest to that of rainfall. Therefore, as mention before, averaging the isotopic composition of discrete drip water samples would be equivalent to calculating the average annual $\delta^{18}O$ composition of rainfall without weighing sample amount. In fact, the annual $\delta^{18}O$ composition of these drips closely resembled the annual amount-unweighted $\delta^{18}O$ composition of rainfall during Y1-Y3 (LH19).

We find that during Y4 and Y5 the annual amount-weighted and unweighted $\delta^{18}O$ composition of drip water was the same to within 0.1‰ in six of the seven drip sites examined (Table 2.1). LF1 is persistently more positive (~1-2‰) than the amount-weighted and unweighted $\delta^{18}O$ composition of rainfall and all other drip sites from Stations A and B (Table 2.1). This result concerning LF1 is similar to what was observed during the previous three years (Y1-Y3) suggesting that this drip site reflects precipitation variability but also is influenced by evaporation at the surface as it is discussed in Section 2.5.4, below.

2.4.6. Interannual variability of drip water and rainfall $\delta^{18}O$

Figure 2.5 shows a comparison of the annual amount-weighted $\delta^{18}O$ composition of rainfall during Y1-Y5 relative to the annual $\delta^{18}O$ composition of drip water during Y1-Y3 (amount-unweighted) and years Y4-Y5 (amount-weighted). As pointed out above, with the exception of LF1, the amount-unweighted and weighted $\delta^{18}O$ composition of drip water were almost the same during Y4 and Y5. Therefore, despite the previous sampling protocol being

discrete, it is possible that the annual $\delta^{18}O$ composition of drips during Y1-Y3 also approximates their amount-weighted $\delta^{18}O$ composition, probably because of the high sampling frequency (bi-weekly) in combination with the reservoir integration.

During Y1, Y2 and Y4, the annual isotopic composition at drips sites from Stations A and B are similar to the annual $\delta^{18}O$ composition of rainfall (Fig. 2.5). During the drought years Y3 and Y5, however, when the annual isotopic composition of rainfall shifts to become 1-2 ‰ more positive than their corresponding preceding years, the isotopic composition at these drip sites are typically more negative than those of rainfall. More specifically, During Y3, the isotopic composition of rainfall shifted by +2 ‰ relative to Y2 whereas drips from A and B Stations only shifted by +0.5 ‰ and ~+1‰, respectively (Fig. 2.5) (LH19). During Y5 the isotopic composition of rainfall shifted by +1‰ relative to Y4. Drips from Station A remained practically unchanged or shifted negatively only slightly by ~-0.2‰ from Y4 to Y5. Drip B4, in contrast shifted negatively by ~-0.7‰, as if still catching up with the wet negative isotopic year Y4, whereas drip B1, remained unchanged from Y4 to Y5. Exceptions to these patterns are drip sites LF1 and Fénix. LF1 annual $\delta^{18}O$ values vary in the same direction as annual shifts in rainfall $\delta^{18}O$ (except in Y5) but they are consistently more positive than rainfall and the other drip sites (Fig. 2.5). Annual isotopic composition of Fénix shows a progressive interannual positive shift from Y2 to Y5 and its absolute $\delta^{18}O$ values are consistently 1-3‰ more negative than those of rainfall amount-weighted composition for Y2-Y5 (Fig. 2.5).

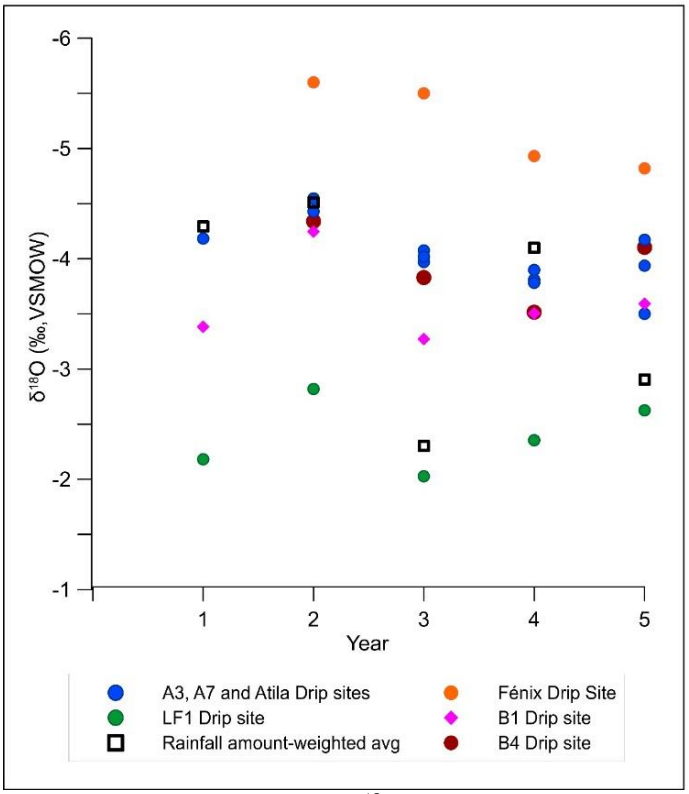

Fig. 2.5 Río Secreto annual amount-weigthed $\delta^{18}O$ composition of rainfall and drip water at Stations A, B and LF. Values were calculated from June 2014 to May 2015 (year 1), June 2015 to May 2016 (year 2), June 2016 to May 2017 (year 3), June 2017 to May 2018 (year 4) and June 2018 to April 2019 (year 5). Values of A3, A7, Atila and B4 drip sites at year 5 only integrate the $\delta^{18}O$ averages of 8 months (See Section 2.4.6). Data of the three first hydrological years are from Lases-Hernández et al. (2019).

2.4.7. Discharge

All the primary data of drip water discharge rate and volume changes over time are reported in Supplementary Table B. An important aspect of this study is that it characterizes the total volume of drip water that drained over the full two-year period examined (i.e. Y4 and Y5). During this sampling interval we observe discharge rates that are more variable that those reported by LH19 following a discrete sample collection protocol. The reason for this difference is that this more comprehensive study allows proper characterization of maximum discharge rates. LH19 used graduated cylinders to collect drip water over a 48-hour period, and when water drained during intervals of maximum discharge the containers may have been overfilled (Section 1.3.3 in LH19). Maximum discharge rates characterized by the protocol by LH19 was 8 mL/hour, whereas this study shows maximum discharge rates of up to 25 mL/hr. We note, however, that only 17 out of 112 samples collected had discharge rates equal or higher than 8 mL/hr. suggesting that LH19's protocol represents a good approximation of typical drip rates while under-representing rare more extreme infiltration events. However, we want also to point out that during Y4 the rainfall amount was higher than during the 3 previous years, therefore the high drip rates characterized at this study may be related to the sampling methodology but also to the increase of recharge into the epikarst during year 4. In this study, we reexamine the hydrological behavior of 7 drips according to the classification of Fairchild et al. (2006), determined by LH19 by examining the first three hydrological years (Fig. 1.7 at LH19). We confirm their classification for six out of the seven drips sites studied during years 4 and 5, the exception being Fénix, previously classified as Seepage Flow (Fig. 1.7 at LH19) and now reclassified as a Seasonal drip (Fig. A at Appendix A). Lastly, we find that there is no significant linear relationship (95% confidence interval) between drip water $\delta^{18}O$ and discharge rates, at all 7 drip sites monitored during Y4 and Y5, with the exception of A3 (r^2=0.35, p=0.043).

2.4.8 Groundwater $\delta^{18}O$ variability

A total of 25 samples of groundwater from standing water at Stations LF (12 samples) and A (13 samples) were collected from August 2017 to January 2019 and analyzed for $\delta^{18}O$ and δD (Supplementary Table C). In comparison to monitored drips located in the LF chamber, the $\delta^{18}O$ composition of groundwater from Station LF is more negative than that of drip water from LF1 and more positive than Fénix. LF groundwater is also isotopically more positive than drip water at all other drip sites from Stations A and B, and groundwater from Station A (by up to 1.5‰). The underground pool at Station A is deeper and clearly connected with the rest of the groundwater system. We have observed that during periods of water table rising in the Río Secreto Cave system, groundwater in LF rises as well, but in contrast with Station A, LF is close to a collapsed sinkhole and thus exposed to ventilation. Therefore, it was not surprising to find that the water table in LF chamber is highly variable and likely experiences evaporation. However, when plotting $\delta^{18}O$ and δD values of LF groundwater, most of them do not deviate markedly form the LMWL calculated for this study (Fig. C at Appendix A).

2.4.9. $\delta^{18}O$ composition of tropical cyclones

This study characterizes the isotopic signature of two weak tropical cyclones (TCs) that influenced the YP: Franklin (1-9 August 2017), which had a $\delta^{18}O$ value of -6.8‰ and a local rainfall flux of 89 mm, and Alberto (25-26 May, 2018) with a $\delta^{18}O$ of -6.9‰ and 102 mm of rainfall (Figs. 2.7 and 2.8). Franklin made landfall over the YP with tropical storm intensity and weakened until re-emerging in the Gulf of Campeche to become a hurricane, while Alberto skirted the YP coast as it developed into a subtropical depression before intensifying to a tropical storm over the Gulf of Mexico. These two locally-weak TC events produced precipitation with the lowest isotopic values found in this study: a negative isotopic shift of ~4 ‰ relative to the isotopic composition of rainfall accumulated over the month prior to the events. In addition, rainfall associated with these TCs had $\delta^{18}O$ compositions distinctively more depleted (2-4‰) than rainfall events that were not associated with TCs, of similar or even higher amount fluxes. TC Michael (5-8 October, 2018), whose rainfall was very strong in other regions (e.g. Florida), did not produce significant rainfall in the study area.

2.4.10. Response of $\delta^{18}O$ dripwater to tropical cyclones

The influence of TCs Franklin and Alberto on the isotopic composition of drip water can be observed at some drip sites even when the sample protocol implemented in this study involved ~monthly water accumulations (Figs. 2.7 and 2.8). Specifically, the negative rainfall $\delta^{18}O$ composition associated with Franklin is reflected as a negative $\delta^{18}O$ departure from background levels of -1‰ and -0.9‰ in LF1 and B1 drip sites, respectively (Supplementary Table D). This event, however, is not observed at the other five drip sites because of the lower-resolution sampling protocol. While rainfall was collected from August 1-9, 2017, exactly when Franklin affected the locale, drip water was collected over a full month (from August 2 to September 8, 2017).

Regarding TC Alberto, rainwater and drip water were collected during the same period of time (14 May-4 June 2018). With this higher drip water collection frequency, the distinctively low $\delta^{18}O$ signature associated with Alberto was registered within weeks as a negative shift of -1.2 ‰ by LF1, and of ~-0.5 ‰ by the other 6 drip sites (Fig. 2.8; Table D at Appendix A). Therefore, Franklin's distinctive rainfall negative isotopic signal was likely dampened by other rainfall events occurring over that period.

We point out that during the previous weekly to bi-weekly sampling protocol of drip water performed by LH19, the isotopic response of drip sites to TC rainfall was recorded by drip sites from all chambers, with the exception of Fénix. An example is the negative rainfall isotopic shift associated with TC Hanna (October 21, 2014), which is the most negative rainfall water sample (-9.5‰) recorded in Río Secreto during the five hydrological years (Supplementary Table A). Because Hanna´s rainfall amount was only 79 mm whereas the total amount of rainfall in October 2014 was 325 mm, the isotopic shift if comparing September 2014 monthly rainfall to Hanna´s rainfall was of -5.8‰, while the isotopic shift from September to October 2014 monthly rainfall was only -3.7‰, making it clear that it is necessary to monitor at least at weekly basis in order to capture the full shift associated with TC´s rainfall in both rainfall and drip water samples (Fig. 2.6; Supplementary Tables A and

D). During September-October 2014 Río Secreto drip water monitoring included only 6 drip sites, three of them examined also in the present study, and all of these presented a negative shift of up to -1.8‰ associated with Hanna TC rainfall (Fig. 2.6 and Table D at Appendix A). As another example, high-resolution sampling of drip water from nine drip sites, including five of the seven examined in the present study, allowed detection of the low $\delta^{18}O$ shift associated with TC Bill rainfall (June 9-16, 2015). Drip water $\delta^{18}O$ at these nine drip sites shifted by up to -2.1‰ relative to the background (Table D at Appendix A). This response was particularly noteworthy because the sample containing rainfall from TC Bill represented the accumulation of one month of rainfall (June) and its isotopic composition was 3.2‰ more negative than the sample of the previous month (April). In this case, however, the high-resolution cave sampling protocol allowed the detection of the isotopic signature of this TC in drip water. Because the rainfall sample of TC Bill itself was not measured, the shift in rainfall $\delta^{18}O$ of monthly samples underestimates the shorter term influence of this cyclone on drip water $\delta^{18}O$ (Table D at Appendix A).

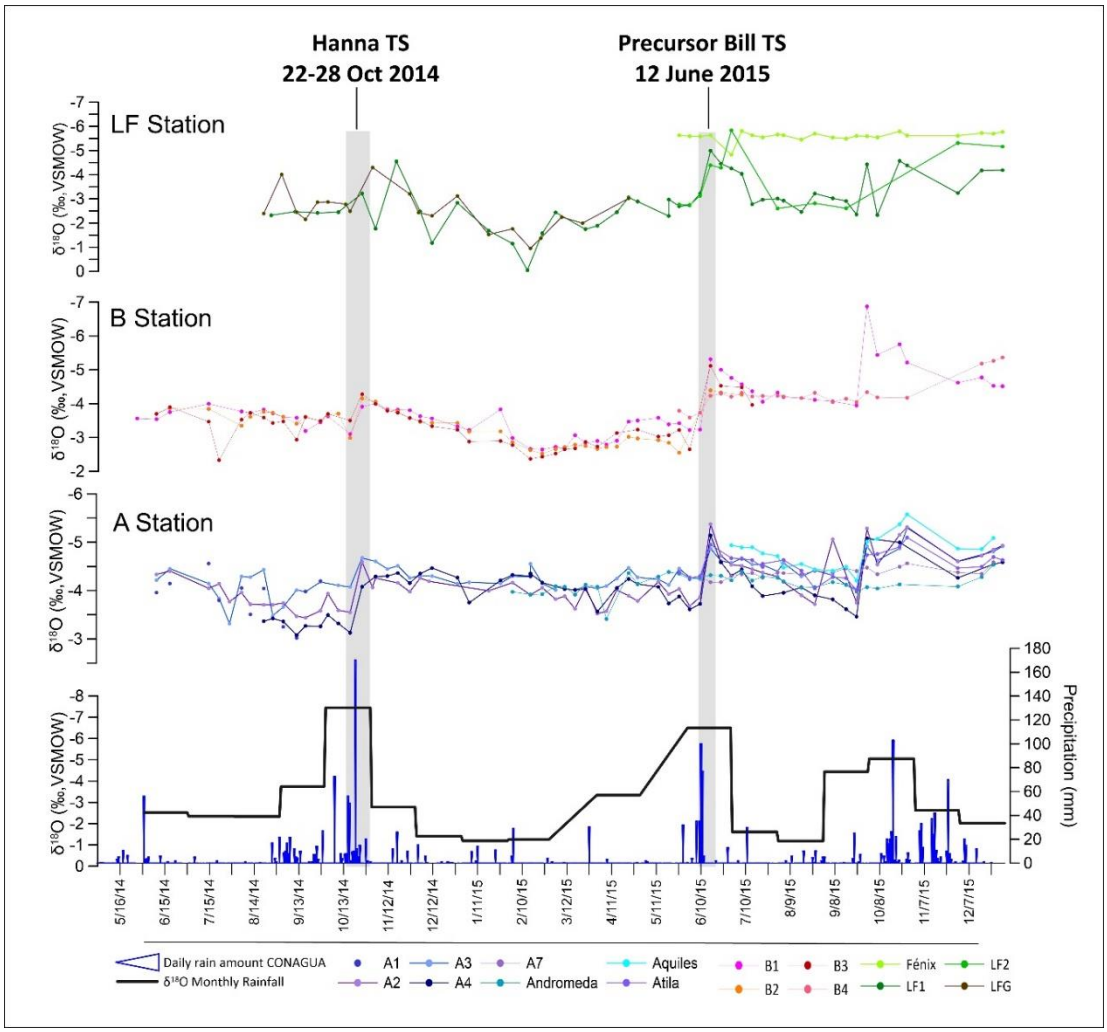

Fig. 2.6. Upper three panels: drip water $\delta^{18}O$ time series from June 2014 to December 2015 (Y1 and Y2) from Stations LF, B and A. Lower panel: monthly rainfall $\delta^{18}O$ values (black line) and amount of daily precipitation from CONAGUA government station (Fig. 2.1A). Note that the Y axis values are inverted. Gray bars highlight the time interval when tropical cyclones influenced the site. Data was obtained from Lases-Hernández et al. (2019).

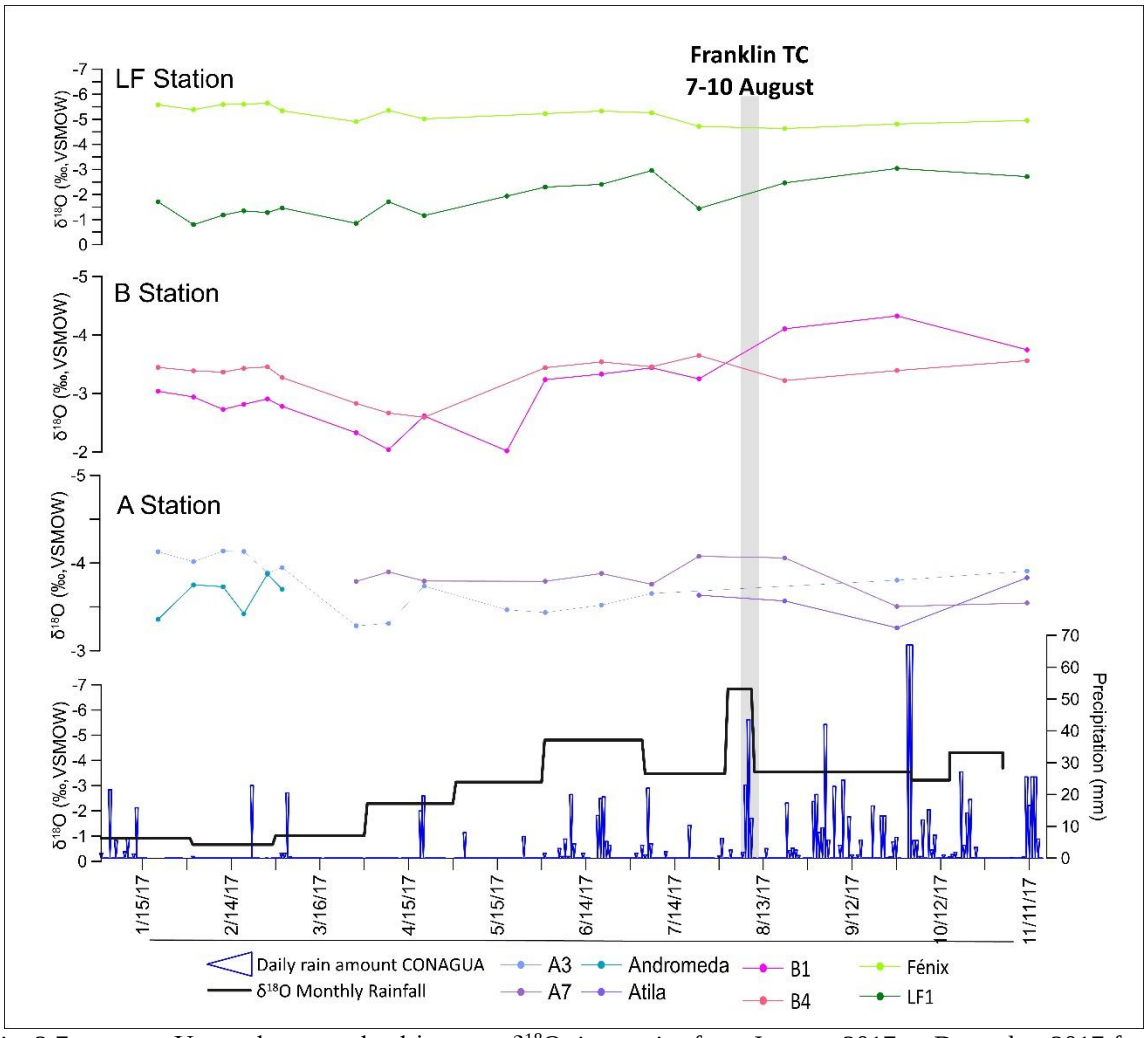

Fig. 2.7. Upper three panels: drip water $\delta^{18}O$ time series from January 2017 to December 2017 from Stations LF, B and A. Lower panel: monthly rainfall $\delta^{18}O$ values (black line) and daily rainfall amount from CONAGUA weather station (Fig. 2.1A). Y axis values are inverted. Gray bar highlight the time interval when Franklin tropical cyclone influenced the site. Data previous to July 2017 was obtained from Lases-Hernández et al. (2019).

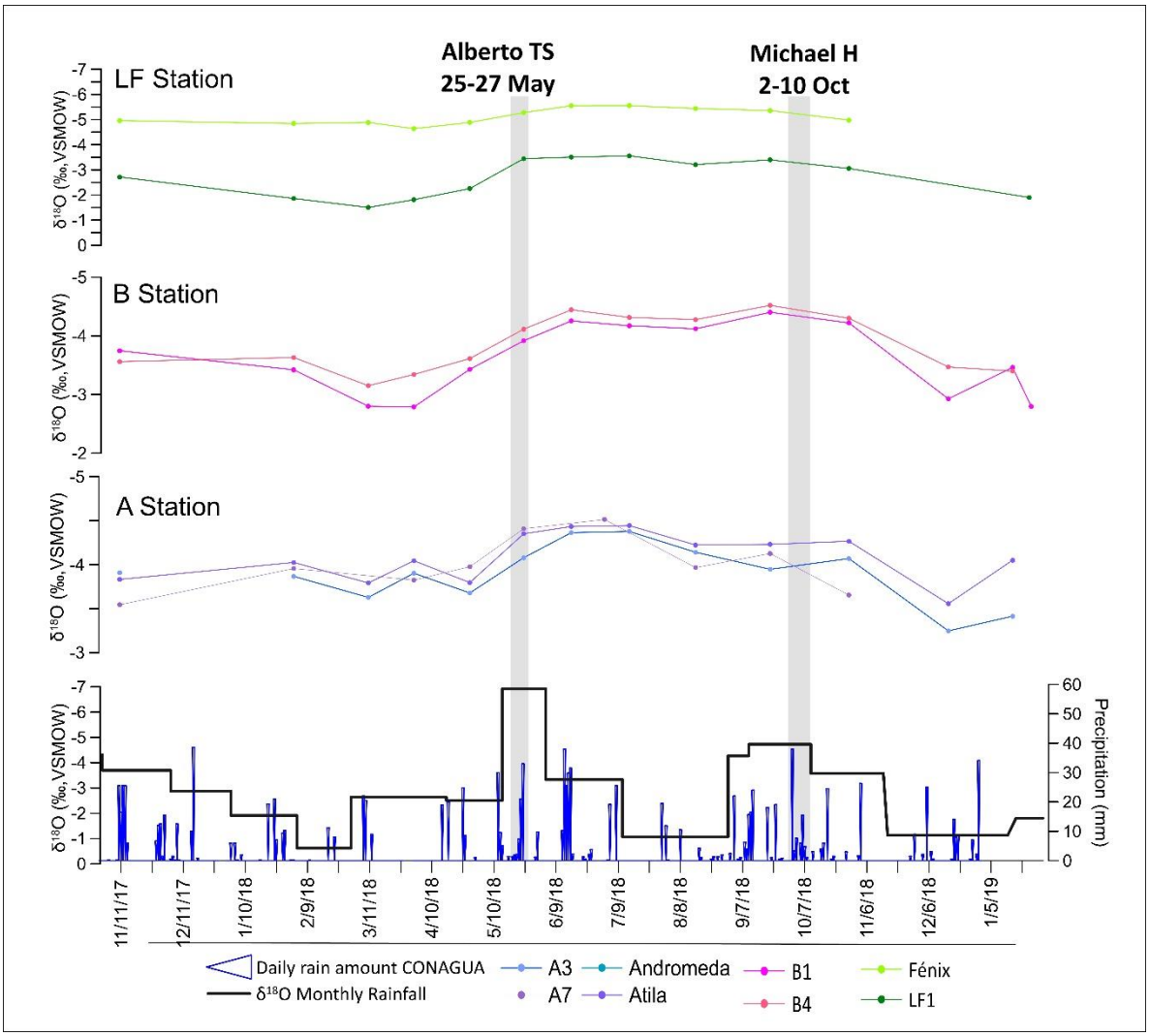

Fig. 2.8 Upper three panels: drip water $\delta^{18}O$ time series from November 2017 to April 2019 from Stations LF, B and A. Lower panel: monthly rainfall $\delta^{18}O$ values (black line) and daily rainfall amount from CONAGUA weather station (Fig. 1A). Y axis values are inverted. Gray bars highlight the time interval when tropical cyclones influenced the site.

2.5. DISCUSSION AND IMPLICATIONS FOR PALEOCLIMATE STUDIES

2.5.1. *Amount effect* on interannual and seasonal timescales

The isotopic amount effect, whereby higher precipitation amount is associated with lower rainfall isotopic ratios is recognized to exist in tropical and subtropical regions from seasonal to interannual timescales (Dansgaard, 1964; Rozanski et al., 1993; Araguas-Araguas et al., 2000; Vuille et al., 2003). Studies with instrumental records of precipitation that report an amount effect on interannual timescales are scant, however, even though it is a desirable precondition to reconstruct precipitation amount variability from stalagmite $\delta^{18}O$ records. To our knowledge, in addition to evidence from models (i.e. Vuille et al., 2003), studies demonstrating an amount effect on interannual timescales based on instrumental records are scarce. Bar-Matthews and Ayalon (2004) characterized the amount effect on interannual

timescales in the eastern Mediterranean region and report a slope of -0.005 ‰ mm^{-1} (similar to this study). Maher et al. (2012) also report interannual covariance between rainfall amount and $\delta^{18}O$ values on various Chinese and Indian locations based on IAEA-GNIP data spanning the interval between 1961 and 2003.

Atmospheric general circulation models (i.e. ECHAM-4 and GISS II) used to analyze interannual variability of $\delta^{18}O$ in precipitation in the tropical Americas suggest a significant amount effect on interannual timescales for the YP and Caribbean (Vuille et al., 2003). These models detect an amount effect on interannual timescales in simulations spanning between 16 to 44 years (1979-1994) which is somewhat validated by model comparisons with decadal or longer IAEA instrumental isotope records (Vuille et al., 2003). The nearest IAEA station to Playa del Carmen is the one from Havana, Cuba. Examination of the relationship between annual precipitation amount and $\delta^{18}O$ from Havana indicates an amount effect on interannual timescales (n=12 years, r^2=0.61, Fig. 2.3). The present study presents the first instrumental evidence in support of an amount effect on interannual timescales for the YP. As mentioned in Section 2.4.1 the correlation between annual rainfall amount and the amount weighted isotopic composition of 4 of 5 years was strong (i.e. Y1,Y2,Y3 and Y5). However, Y4 exhibited higher $\delta^{18}O$ values than expected from the linear correlation of those four years (Fig. 2.3; Section 2.4.1). The relatively high annual $\delta^{18}O$ composition during Y4 can be related to mesoscale convective complexes with disorganized convection (Kurita, 2013) as well as the origin and transport of the low-level vapor feeding the convective system that may affect the amount effect (Risi et al. 2008; Rao et al. 2008). In order to improve our understanding of the driving factors of the amount effect on interannual time scales in this region a detailed continuous monitoring effort would be required. We aim at continuing this monitoring effort to help better describe the amount effect on interannual timescales in the region.

During Y4 and Y5, the protocol of this study precludes determining the amount effect on seasonal timescales because of the variable sample time integrations from 3 to 59 days of rainfall. The existence of an amount effect on seasonal timescales in this region, however, has been observed by previous studies (Medina-Elizalde et al., 2016a; Lases-Hernandez et al., 2019).

2.5.2 Reservoir integration times are relatively fast in Río Secreto cave

In this study we find that most drips retain most of the isotopic amplitude variability observed during the previous discrete sampling protocol (48 hr. water accumulation every 1-2 weeks) (Lases-Hernandez et al., 2019). The reservoirs associated with six of seven drip sites examined integrate between 3 and 15 months of rainfall accumulation. Of course, time is not *per se* the determining factor, but instead the amount of rainfall over time. The observed integration times imply that: (i) drips record preferentially monthly and longer rainfall $\delta^{18}O$ variability; (ii) water discharged at a drip site over few weeks does not represent coeval precipitation, but a combination of coeval and prior precipitation; (iii) even when drip water samples represent short-term isotopic amount-unweighted sample aliquots (e.g. 48 hr.), they can still approximate an annual amount-weighted $\delta^{18}O$ composition at each drip site, as it is observed in this study and; (iv) the longer the integration time and reservoir size, the longer the expected tendency to remain isotopically unchanged (i.e. higher isotopic inertia). We

observe that drip sites at Station A and Fénix, with the longest integration times, have the highest isotopic inertia, lagging and underestimating interannual changes in precipitation $\delta^{18}O$ (Fig. 2.5). Finally, we acknowledge that the estimated integration times do not explain all the drip water $\delta^{18}O$ absolute values because the integration time is not stationary, as previously pointed out by Lases-Hernandez et al., (2019).

When we compare the integration times observed in Río Secreto with those observed in caves elsewhere, we find that the transmission of the isotopic composition of rainfall to drip water is relatively fast. Genty et al. (2014) for example, applied a similar approach to ours (i.e. integration of amount-weighted $\delta^{18}O$ composition of rainfall) and calculated water residence times from 32 to 140 months in drips from shallow galleries in two caves of southern France; Villars and Chauvet caves. Recently, Genty et al. (2014) results were supported by Jean-Baptiste et al. (2019) via a tritium dating of drip water study. In Soreq cave, Israel, it takes between 26 and 36 years for rainwater to reach galleries 10-50 meters below the surface (Kaufman et al., 2003), while it takes only 2-4 years for rainwater to reach 10-30 m deep galleries in Bunker Cave, Germany (Kluge et al., 2010). We note that similar integration times of few months found in this study have also been observed in Borneo where precipitation $\delta^{18}O$ variability is strongly influenced by ENSO (Moerman et al., 2014). Evidently, the comparison of the integration times observed in Río Secreto with those in other caves, highlights the significant potential of this cave for the refining reconstruction of interannual precipitation variability from stalagmite oxygen isotope records and improving proxy uncertainty characterization.

2.5.3 Implications for stalagmite $\delta^{18}O$ records

The annual $\delta^{18}O$ composition of drip water at Stations A and B was similar to the annual isotopic composition of rainfall during years 1, 2 and 4, but not during the drought years, Y3 and Y5 (Fig. 2.5). This pattern results from the isotopic inertia associated with the observed rainfall integration times by reservoirs described above. The large isotopic inertia observed in drip sites Fénix and B4 is clearly expressed as a lag of over one year relative to the positive isotopic annual shifts of rainfall (Fig. 2.5).

The isotopic response of drips from Stations A and B observed during the transition between the wet year Y2 and the drought year Y3 offers a key opportunity to estimate the integration time of one year of drip water accumulation. This is important for high-resolution paleo-rainfall reconstructions from stalagmite $\delta^{18}O$ records. Because of the observed integration times, an annually-resolved stalagmite $\delta^{18}O$ record reflecting the isotopic composition of drips from Stations A and B, would not be expected to reflect only coeval rainfall. Similarly to our approach to assess weekly and monthly drip water isotopic variability, we determined the integration time of rainfall necessary to explain the observed annual isotopic composition of drips from Station A and B1, during Y3. This integration time is 30 months for Station A drip sites and 24 months for drip B1. The implications of these results for paleoclimate reconstructions from stalagmite $\delta^{18}O$ records are significant. These results imply that the annual isotopic composition of drips at Stations A and B1 are similar to that of rainfall during years 1, 2 and 4 simply because the precipitation amount and associated isotopic composition of those years represent the norm, and not because, as is

generally assumed implicitly, the drips are exactly integrating a coeval year of rainfall amount.

During consecutive drought years, the volume of an epikarst drip water source reservoir is expected to decline and, as a result, the drip $\delta^{18}O$ composition would rise slowly compared to rainfall $\delta^{18}O$ values (because of the amount effect) and the capacity for pre-drought water to generate isotopic inertia in dripwater $\delta^{18}O$ values would decline. In this case, a copious rainfall event with an isotopic signature distinctive from that of the reservoir (e.g. from a TC) would be clearly expressed in drip water. In contrast, during consecutive "normal" or wet years, the volume of a reservoir is expected to be relatively large and have a low isotopic signature (the result of the amount effect). The reservoir would have high potential for isotopic inertia and thus remain unaffected by sparse and "normal" rainfall events and mask the negative isotopic signal of TCs.

Stalagmite $\delta^{18}O$ records are therefore expected to register the timing and magnitude of shifts from a drought year to a wet year more accurately than the transition from a wet to a drought year, as observed in this dripwater study. If this is a common regional behavior, stalagmite $\delta^{18}O$ records from the Maya Lowlands may underestimate the magnitude of the droughts associated with the disintegration of the Maya civilization during the Pre-Classic Period (C.E. 100-200) (Medina-Elizalde et al., 2016a) and the Terminal Classic Period (C.E. 750-950) (Medina-Elizalde et al., 2010, Medina-Elizalde and Rohling, 2012, Kennett et al., 2012). Hydroclimate records based on the hydrogen and carbon isotopic composition of leaf wax lipids actually suggest that droughts during the Classic Period were more severe than suggested by other hydroclimate records, including stalagmite $\delta^{18}O$ records (Douglas et al., 2015). The results of this study can help explain this difference.

Due to the central importance of individual drip water reservoirs and routing hydrological characteristics, the timing of the onset and end of drought events as reflected in stalagmite $\delta^{18}O$ records can be expected to differ by months to years. This instrumental study shows that stalagmite sensitivity to TC $\delta^{18}O$ signals is also differentially affected by background hydroclimate, as was inferred by Frappier (2013). Increased isotopic contrast and event rainfall amount relative to epikarst reservoir storage during and following droughts will tend to increase stalagmite $\delta^{18}O$ record sensitivity to TC events. The isotopic effect of TC events during droughts may be difficult to distinguish from drought cessation, unless isotopic shifts are sufficiently anomalous from values expected under normal wet conditions. During wet periods, both brief dry spells and TCs signals in stalagmite $\delta^{18}O$ records are more difficult to distinguish from background, and isotopic inertia from large-volume epikarst reservoirs enhances the tendency to underestimate rainfall variability. The implications of these results should be carefully considered when interpreting stalagmite $\delta^{18}O$ records from locales where the reservoir integration time is large, in those records, slight isotopic variability may be a reflection of much larger shifts in precipitation than suspected. Observing such non-linear effects in this essential paleoclimate proxy system indicates a critical need for further observational and modeling work to re-visit uncertainty analysis and data interpretation for low-latitude $\delta^{18}O$-based paleo-rainfall proxies.

2.5.4. The LF1 and Fénix anomaly

LF1 represents the drip site with the isotopic amplitude variability closest to that of rainfall, on a weekly and monthly basis. Unfortunately, it fails to capture the absolute rainfall isotopic values. LH19 presented several lines of evidence that surface evaporation and evaporation within LF Station were expected to be minimal: (i) drip water mean annual $\delta^{18}O$ compositions from Stations A and B closely resembled the annual amount-weighted $\delta^{18}O$ composition of rainfall; (ii) drip water average $\delta^{18}O$ composition from Fénix, located in Station LF, was 1-3‰ more negative than the annual amount-weighted $\delta^{18}O$ composition of rainfall, and; (iii) Station LF air relative humidity was at or near 100% during the entire recorded period (Y1-Y5). We know now that the observed positive composition of LF1 is not an artifact of the sampling protocol as previously proposed, because the new protocol confirms previous results. In this study, we provide new evidence that indicates that groundwater in LF Station may experience evaporation inside the chamber. However, the $\delta^{18}O$ and δD composition of LF1 and Fénix do not deviate markedly from the LMWL (Section 2.4.2.1 and LH19) suggesting that evaporation inside the chamber did not affect their isotopic compositions. Surface evaporation does not seem to influence Stations A and B drip sites, because they closely reflect the isotopic composition of rainfall (Y1, Y2, Y4). LF1 may have, however, a unique source routing configuration, perhaps receiving water from the overflow of a surface or shallow water pool exposed to evaporation, rather than reflecting direct infiltration, as the other drip sites.

For four consecutive years, Fénix, shows the most negative and stable isotopic composition of all drips. We support LH19's inference that this drip site reflects a large reservoir size preferentially incorporating large rainfall events with the lowest isotopic compositions, which typically happen during the summer rainy season (June-October). We recognize that a stalagmite $\delta^{18}O$ record reflecting the isotopic composition of such a drip site as Fénix, would tend to overestimate annual precipitation amount and be insensitive to drought, leading to underestimations of the magnitude of rapid precipitation reductions.

2.5.6 The transmission of the tropical cyclone signals

Rainfall associated with TCs is frequently distinguished by its characteristic depleted isotopic values relative to other tropical rainfall systems (Gedzelman, 2003). This is likely related to TC anatomy as their isotopic composition becomes more depleted towards their core (Gedzelman et al. 2003; Munksgaard et al. 2015). TC isotopic composition has been also related to their physical evolution, as well as their synoptic-scale meteorological setting; e.g. the proportion of convective to stratiform precipitation (Munksgaard et al. 2015; Aggarwal et al. 2016). As mentioned in Section 2.4.9, the amount of precipitation related to TCs characterized in this study does not explain their particularly depleted isotopic compositions. Therefore, under specific conditions described below, they may be distinguished as TC activity in a $\delta^{18}O$ stalagmite record from this location.

Clearly, the *Achilles heel* of TC detection in a stalagmite $\delta^{18}O$ record is not the stalagmite sampling resolution, since the sampling techniques are readily available (Frappier et al. 2007a, 2007b), it lies in the relationship between the volume and isotopic composition of a drip water reservoir and the amount and isotopic composition of rainfall from a TC. At

a single drip site, even TC with relatively weak precipitation amount and weak isotopic signal are expected to be more easily detected during times of persistent drought or when reservoirs are smaller and have an enriched isotopic composition. These conditions make the depleted TC isotopic signal to stand out from background, thus having a greater influence on the isotopic composition of drip water that can persist longer over time.

We examined our full five-year monitoring data in order to identify rainfall and drip water isotopic shifts associated with TCs (Figs 2.6, 2.7 and 2.8). LF1 and B1 drip sites that have the shortest integration times reflect the largest isotopic response associated with the negative rainfall isotopic shifts of four TCs (Franklin, Alberto, Bill and Hannah, Figs. 6, 7 and 8, Supplementary Table D). On the other hand, Fénix and A7 drip sites, as expected from their long reservoir integration times, and negative isotopic compositions, reflected the weakest the influence of these TCs (Figs. 2.6, 2.7 and 2.8, Supplementary Table D). For future studies aimed at paleotempestology, stalagmites with small drip source reservoirs like LF1 are more sensitive to TC $\delta^{18}O$ signals than those with large reservoirs. Stalagmites with drip source reservoirs like Fénix with low $\delta^{18}O$ values and biased towards infiltration from heavy rainfall events, have poor isotopic contrast for TC detection, and are thus poor candidates for paleotempestology.

Lastly, as suggested by LH19 and shown in this study, the detection of TC rainfall fluxes is possible even when reservoir integration times vary from 3 to 15 months. How do we reconcile the observation of these relatively long residence times with the rapid isotopic shifts associated with TCs observed on weekly drip water samples? We can use our estimates of integration times to examine whether the observed negative shifts in drip water reflect the full mixing of TC rainfall with drip water reservoirs. Integration times provide the amount of rainfall (reservoir size in mm) that explains the $\delta^{18}O$ composition of drip sites prior to TC events. For this analysis, we examine TC Alberto ($\delta^{18}O$= -6.9‰, rainfall amount =103 mm) because drip water and rainfall samples associated with this event were coeval, the event took place during a drought year with smaller epikarst water storage and greater rainfall $\delta^{18}O$ contrast, and the event is well represented by various drip water sites. We find that the expected drip water isotopic shifts from mixing TC Alberto rainfall with reservoir water from LF1, B1 and A3 is similar to the observed isotopic shifts (Supplementary material Table F). This suggests that even a weak TC with significant rainfall amount (~100 mm) and a sufficiently distinct negative isotopic signature relative to that of the reservoir prior to the event can be detected across drip reservoirs that integrate 3 to 15 months of rainfall accumulation. Furthermore, the magnitudes of drip water isotopic shifts associated with a TC are inversely related to reservoir integration times, as observed previously by Lases-Hernandez et al, (2019). This instrumental study supports that a low TC rainfall $\delta^{18}O$ signal impacts all drip locations to various extents, and that the magnitude and duration of the integrated $\delta^{18}O$ signal recorded in drip waters and stalagmite records will depend on epikarst reservoir hydrological characteristics, integrated hydroclimate, and sampling resolution, in agreement with Frappier (2013).

2.6 CONCLUSION

In Río Secreto cave, the observed $\delta^{18}O$ variability of five out of seven drip sites can be explained by integrating from 4 to 15 months of rainfall accumulation. Our integration approach explains not only the observed drip water $\delta^{18}O$ variability, but also closely approximates the absolute values. The isotopic composition of these five drip sites, with different reservoir sizes, converge into the same value after 15 months of drip water accumulation, reflecting the rainfall source and relatively fast residence times. Exceptions are Fénix, which reflects mostly wet season summer rainfall, and LF1, which closely matches the rainfall isotopic variability representing ~3 months of rainfall integration. LF1 annual average and amount-weighted $\delta^{18}O$ compositions are consistently more positive than the annual amount-weighted $\delta^{18}O$ composition of rainfall, due to evaporation processes above the cave. The observed residence times of reservoirs feeding drip sites in the Río Secreto cave system are relatively short compared to caves elsewhere.

Due mostly to epikarst reservoir size, agreement between coeval isotopic compositions of rainfall and drip water on an annual scale, does not necessarily reflect the assumption that drip water records coeval annual rainfall amount. In Río Secreto cave, drip sites show a tendency to best register the annual amount-weighted composition of rainfall and its interannual variability during typical rainfall years. Most drip sites fail to faithfully record a drought year (precipitation reduction by 50% from long-term average) when it follows a normal hydrological year but they are expected to approximate multiyear droughts more faithfully, as the isotopic inertia from the reservoir weakens. Speleothem $\delta^{18}O$-based proxy records would be therefore expected to underestimate the magnitude of intermittent annual droughts but probably properly characterize multi-year droughts.

We find evidence of the existence of an *amount effect* on interannual timescales in the YP in support of model results and therefore, reconstruction of precipitation variability from stalagmite $\delta^{18}O$ records on interannual timescales is possible in samples from the Río Secreto cave. As mentioned above, however, interannual rainfall reconstructions from stalagmite $\delta^{18}O$ records would not necessarily reflect the same time integration of rainfall amount; that is, annual stalagmite $\delta^{18}O$ values could represent over two years of rainfall amount depending on the drip water reservoir size.

This study shows that even within the same cave system, some drip sites may reflect the isotopic composition of rainfall quite accurately, while others may be biased by their drainage characteristics. We find one drip site biased towards the largest rainfall events while another is positively biased by evaporation processes. After integrating the amount of rainfall over the time, drip water results suggest that a stalagmite from Río Secreto cave sampled at a monthly resolution may reflect from 3 to 15 months of rainfall accumulation, and sampled at an annual resolution, over 2 years of rainfall accumulation. Monitoring the isotopic composition of drip water is therefore important in order to characterize the extent to which the isotopic composition of drip water reflects rainfall, especially if studies aim at resolving seasonal and annual precipitation change.

In order for a stalagmite to capture individual tropical cyclones the following conditions are necessary: 1) drip water forming stalagmites must show weekly variability

close to that of rainfall and stalagmite calcite or aragonite should be sampled at ~weekly resolution; 2) TCs must contribute with significant amount of rainfall relative to normal rainfall events preceding the TC, and with an isotopic signal sufficiently distinct from that of the reservoir. TC $\delta^{18}O$ signatures are retained in drip water, but after about a month, depending on the case, a new rainfall event large enough will dilute the TC signal. This is important because in the tropics when a study's goal is to characterize the isotopic signatures of TCs and/or hydroclimate extremes in general, drip water studies must be conducted at weekly resolution. A discrete sampling protocol is expected to approximate the amount-weighted isotopic composition of a drip, as long as it is conducted at a temporal resolution higher than the rainfall integration time by the drip reservoir (e.g. bi-weekly). This study complements the results from Lases-Hernandez et al. (2019) and highlights the importance of conducting multiyear monitoring of drip water and rainfall in order to interpret stalagmite $\delta^{18}O$ as a paleoclimate proxy

REFERENCES

Aggarwal P. K., Romatschke U., Araguas-Araguas L., Belachew D., Longstaffe F. J., Berg P., Schumacher C. and Funk A. (2016) Proportions of convective and stratiform precipitation revealed in water isotope ratios. *Nature Geosci* **9**, 624-629.

Aharon P. and Dhungana R. (2017). Ocean-atmosphere interactions as drivers of mid-to-late Holocene rapid climate changes: Evidence from high-resolution stalagmite records at DeSoto Caverns, Southeast USA. *Quat. Sci. Rev.* **170**, 69-81.

Akers P. D., Brook G. A., Railsback L. B., Liang F., Iannon G., Webster J. W., Reeder P. P., Cheng H. and Edwards R. L. (2016) An extended and higher-resolution record of climate and land use from stalagmite MC01 from Macal Chasm, Belize, revealing connections between major dry events, overall climate variability, and Maya sociopolitical changes. *Palaeogeogr. Palaeoclimatol. Palaeoecol* **459**, 268–288.

Araguás-Araguás L., Froehlich K. and Rozanski K. (2000). Deuterium and oxygen-18 isotope composition of precipitation and atmospheric moisture. *Hydrol. Process.* **14**(8), 1341-1355.

Ayalon A., Bar-Matthews M. and Sass E. (1998) Rainfall-recharge relationships within a karstic terrain in the Eastern Mediterranean semi-arid region, Israel: $\delta^{18}O$ and dD characteristics. *J. Hydrol.* **207**, 18–31.

Baldini L. M., Baldini J. U. L., McElwaine J., Frappier A. B., Asmerom Y., Liu K. B., Prufer K., Ridley H. E., Polyak V., Kennett D. J., Macpherson C. G., Aquino V. V., Awe J. and Breitenbach S. F. M. (2016) Persistent northward North Atlantic tropical cyclone track migration over the past five centuries. *Sci. Rep*. **6**, 37522.

Bar-Matthews M. and Ayalon A. (2004) Speleothems as palaeoclimate indicators, a case study from Soreq Cave located in the Eastern Mediterranean Region, Israel. In: *Past Climate Variability through Europe and Africa. Developments in Paleoenvironmental Research*, vol 6. (eds: Battarbee R.W., Gasse F., Stickley C.E. eds). Springer, Dordrecht, pp 364-391.

Beddows P. A., Mandic´ M., Ford D. C. and Schwarcz H. P. (2016) Oxygen and hydrogen isotopic variations between adjacent drips in three caves at increasing elevation in a temperate coastal rainforest, Vancouver Island, Canada. *Geochim. Cosmochim. Acta* **172**, 370–386.

Bradley C., Baker A., Jex C. N. and Leng M. J. (2010) Hydrological uncertainties in the modelling of cave drip-water $\delta^{18}O$ and the implications for stalagmite palaeoclimate reconstructions. *Quat. Sci. Rev.* **29**, 2201–2214.

Burns S. J., Fleitmann D., Matter A., Kramers J. and Al-Subbary A. A. (2003) Indian Ocean climate and an absolute chronology over Dansgaard/Oeschger events 9 to 13. *Science* **301** (5638), 1365-1367.

Clark I. D. and Fritz P. (1997) Environmental Isotopes in Hydrogeology. CRC/Lewis, New York, p. 328, ISBN: 9781566702492.

Cobb K. M., Adkins J. F., Partin J. W. and Clark B. (2007) Regional-scale climate influences on temporal variations of rainwater and cave dripwater oxygen isotopes in northern Borneo. *Earth Planet. Sci. Lett.* **263**, 207–220.

Craig H. (1961) Isotopic variations in meteoric waters. Science **133**,1702–1703.

Cruz F. (2005) Stable isotope study of cave percolation waters in subtropical Brazil: implications for paleoclimate inferences from speleothems. *Chem. Geol.* **220**, 245–262.

Cuthbert M. O., Baker A., Jex C. N., Graham P. W., Treble P., Andersen M. S. and Acworth R. I. (2014) Drip water isotopes in semi-arid karst: implications for speleothem paleoclimatology. *Earth Planet. Sci. Lett.* **395**, 194–204.

Czuppon G., Demény A., Leél-Őssy S., Óvari M., Molnár M., Stieber, J., Kiss K., Kármán K., Surányi G. and Haszpra, L. (2018). Cave monitoring in the Béke and Baradla caves (Northeastern Hungary): implications for the conditions for the formation cave carbonates. *Int. J. Speleol.* **47**, 13–28.

Dansgaard W. (1964) Stable isotopes in precipitation. Tellus 16, 436–468.

Déry S.J., M.A. Hernández-Henríquez, J.E. Burford and. Wood E.F (2009), Observational evidence of an intensifying hydrological cycle in northern Canada. *Geophys. Res.* **36**, L13402. 10.1029/2009GL038852

Douglas, P. M., Pagani, M., Canuto, M. A., Brenner, M., Hodell, D. A., Eglinton, T. I., & Curtis, J. H. (2015). Drought, agricultural adaptation, and sociopolitical collapse in the Maya Lowlands. *Proc Natl Acad Sci.* **112**(18), 5607-5612.

Duan W., Ruan J., Luo W., Li T., Tian L., Zeng G., Zhang D., Bai Y., Li J., Tao T., Zhang P., Baker A. and Tan M. (2016) The transfer of seasonal isotopic variability between precipitation and drip water at eight caves in the monsoon regions of China. *Geochim. Cosmochim. Acta* **183**, 250–266.

Durack P. J., Wijffels S. E. and Matear R. J. (2012). Ocean salinities reveal strong global water cycle intensification during 1950 to 2000. *Science* **336**(6080), 455-458.

Fairchild I. and Treble P. (2009) Trace elements in speleothems as recorders of environmental change. *Quat. Sci. Rev.***28**, 449-468.

Fairchild I. J., Tuckwell G. W., Baker A. and Tooth A. F. (2006) Modelling of dripwater hydrology and hydrogeochemistry in a weakly karstified aquifer (Bath, UK): implications for climate change studies. *J. Hydrol.* **321**, 213–231.

Frappier A. B., Sahagian D., Carpenter S. J., González L. A. and Frappier B. R. (2007a) Stalagmite stable isotope record of recent tropical cyclone events. *Geology* **35**, 111–114.

Frappier A., Knutson T., Liu K. B., and Emanuel K. (2007b) Perspective: coordinating paleoclimate research on tropical cyclones with hurricane-climate theory and modelling: *Tellus* **59**, 529–537.

Frappier, A. B. (2013). Masking of interannual climate proxy signals by residual tropical cyclone rainwater: Evidence and challenges for low-latitude speleothem paleoclimatology. *Geochemi. Geophys. Geosyst.*, **14**(9), 3632-3647.

Fuller L., Baker A., Fairchild I. J., Spo¨ tl C., Marca-Bell A., Rowe P. and Dennis P. F. (2008) Isotope hydrology of dripwaters in a Scottish cave and implications for stalagmite palaeoclimate research. *Hydrol. Earth Syst. Sci.* **12**, 1065–1074.

Gedzelman S., Hindman E. and Zhang X. (2003) Probing hurricanes with stable isotopes of rain and water vapor. *Mon. Wea. Rev*. **131**, 1112–1127.

Genty D. (2008) Palaeoclimate research in Villars Cave (Dordogne, SW-France). *Int. J. Speleol.* **37**, 173–191.

Genty D., Labuhn I., Hoffmann G., Danis P. A., Mestre O., Bourges F., Wainer K., Massault M., Van Exter S., Re´gnier E., Orengo P., Falourd S. and Minster B. (2014) Rainfall and cave water isotopic relationships in two South-France sites. *Geochim. Cosmochim. Acta*. **131**, 323–343.

Hartmann A. and Baker A. (2017) Modelling karst vadose zone hydrology and its relevance for paleoclimate reconstruction. *Earth-Sci. Rev.* **172**, 178–192.

Huntington H. G. (2006). A note on price asymmetry as induced technical change. *Energy J*. **27** (3), 1-7.

Jean-Baptiste, P., Genty, D., Fourré, E., & Régnier, E. (2019). Tritium dating of dripwater from Villars Cave (SW-France). *J. Appl.* **107**, 152-158.

Kao S. C. and Ganguly, A. R. (2011). Intensity, duration, and frequency of precipitation extremes under 21st-century warming scenarios. *JGR-Atmospheres* **116**(D16)

Kaufman A., M. Bar-Matthews, A. Ayalon and Carmi I. The vadose flow above Soreq Cave, Israel: a tritium study of the cave waters *J. Hydrol.* **273**,155-163

Kennett D. J., Breitenbach S. F., Aquino V. V., Asmerom Y., Awe J., Baldini J. U., Bartlein P., Culleton B. J., Ebert C. and Jazwa C. (2012) Development and disintegration of Maya political systems in response to climate change. *Science* **338**, 788–791.

Kluge T., Riechelmann D.F.C., Wieser M., Spotl C., Sultenfuss J., Schroder-Ritzrau A., S. Niggemann and Aeschbach-Hertig W. (2010) Dating cave drip water by tritium *J. Hydrol.* **394**, 396-406

Kurita N. (2013) Water isotopic variability in response to mesoscale convective system over the tropical ocean. *J. Geophys. Res. Atmos.* **118** (10), 376–10 390.

Lachniet M. S. and Patterson W. P. (2009) Oxygen isotope values of precipitation and surface waters in northern Central America (Belize and Guatemala) are dominated by temperature and amount effects. *Earth Planet. Sci. Lett.* **284**, 435–446.

Lachniet M. S., Asmerom Y., Polyak V. and Bernal J. P. (2017) Two millennia of Mesoamerican monsoon variability driven by Pacific and Atlantic synergistic forcing. *Quat. Sci. Rev.* **155**, 100–113.

Lachniet M. S., Bernal J. P., Asmerom Y., Polyak V. and Piperno D. (2012) A 2400-yr Mesoamerican rainfall history links climate and cultural change in Mexico. *Geology* **40**, 259–326.

Lases-Hernandez F., Medina-Elizalde M., Burns S. and DeCesare M. (2019). Long-term monitoring of drip water and groundwater stable isotopic variability in the Yucatán Peninsula: Implications for recharge and speleothem rainfall reconstruction. *Geochim. Cosmochim. Acta* **246**, 41-59.

Lu R. and Fu, Y. (2010). Intensification of East Asian summer rainfall interannual variability in the twenty-first century simulated by 12 CMIP3 coupled models. *J. Clim.* **23**(12), 3316-3331.

Luo W., Wang S., Zeng G., Zhu X. and Liu W. (2014) Daily response of drip water isotopes to precipitation in Liangfeng Cave, Guizhou Province, SW China. *Quat. Int.* **349**, 153–158.

Magaña V., Amador J. A. and Medina S. (1999) The midsummer drought over Mexico and Central America. *J. Climate.* **12**, 1577–1588.

Maher B. A. and Thompson R. (2012). Oxygen isotopes from Chinese caves: records not of monsoon rainfall but of circulation regime *J. Quat. Sci.* **27**(6), 615-624.

Martínez-Botí, M. A., Foster, G. L., Chalk, T. B., Rohling, E. J., Sexton, P. F., Lunt, D. J., Pancost R. D., Badger M. P. S. and Schmidt, D. N. (2015). Plio-Pleistocene climate sensitivity evaluated using high-resolution CO2 records. *Nature* **518**(7537), 49.

McDermott F. (2004) Palaeo-climate reconstruction from stable isotope variations in speleothems: a review. *Quat. Sci. Rev.* **23**, 901–918.

Medina-Elizalde M. and Rohling E. J. (2012) Collapse of Classic Maya civilization related to modest reduction in precipitation. *Science* **335**, 956–959.

Medina-Elizalde M., Burns S. J., Lea D. W., Asmerom Y., von Gunten L., Polyak V., Vuille M. and Karmalkar A. (2010) High resolution stalagmite climate record from the Yucatán Peninsula spanning the Maya terminal classic period. *Earth Planet. Sci. Lett.* **298**, 255–262.

Medina-Elizalde M., Burns S. J., Polanco-Martínez J. M., Beach T., Lases-Hernández F., Shen C.-C. and Wang H.-C. (2016a) High-resolution speleothem record of precipitation from the Yucatán Peninsula spanning the Maya Preclassic Period. *Glob. Planet. Change* **138**, 93–102.

Medina-Elizalde, M., Polanco-Martínez, J.M., Lases-Hernández, F., Bradley, R. and Burns, S. (2016b) Testing the "tropical storm" hypothesis of Yucatán Peninsula climate variability during the Maya Terminal Classic Period. *Quat. Res.* **86**, 111–119.

Medina-Elizalde M., Burns S. J., Polanco-Martinez J., Lases- Hernández F., Bradley R., Wang H.-C. and Shen C.-C. (2017) Synchronous precipitation reduction in the American Tropics associated with Heinrich 2. *Sci. Rep.* **7**, 11216.

Moerman, J. W., Cobb K. M., Partin J. W., Meckler A. N., Carolin S. A., Adkins J. F., Lejau S., Malang J., Clark B. and Tuen, A. A. (2014). Transformation of ENSO-related rainwater to dripwater $\delta^{18}O$ variability by vadose water mixing. *Geophys. Res. Lett.* ***41***(22), 7907-7915.

Müller C., Cramer W., Hare W. L. and Lotze-Campen H. 2011 Climate change risks for African agriculture **108,** 4313–5

Munksgaard N.C., Zwart C., Kurita N., Bass A., Nott J. and Bird M.I. (2015) Stable isotope anatomy of tropical cyclone Ita, North-Eastern Australia, April 2014. *Plos One* **10**, e0119728.

O'Gorman P. A. and Schneider T. (2009). The physical basis for increases in precipitation extremes in simulations of 21st-century climate change. *Proc. Natl Acad. Sci.* **106** (35), 14773-14777.

Onac B. P., Pace-Graczyk K. and Atudirei V. (2008) Stable isotope study of precipitation and cave drip water in Florida (USA): implications for speleothem-based paleoclimate studies. *Isot. Environ. Health Sci*. 44, 149–161.

Palaeosens P. M. (2012) Making sense of palaeoclimate sensitivity. *Nature* **491**, 683–691.

Partin, J. W., Jenson J. W., Banner J. L., Quinn, T. M., Taylor F. W., Sinclair D., Hardt B., Lander M. A., Bell T., Miklavič B., Jocson J. M. and Taboroši D. (2012) Relationship between modern rainfall variability, cave dripwater, and stalagmite geochemistry in Guam, USA. *Geochemi. Geophys. Geosyst.* **13**(3).

Pérez-Mejías C., Moreno A., Sancho C., Bartolomé M., Stoll H., Osácar M. C., Cacho I. and Delgado-Huertas A. (2018) Transference of isotopic signal from rainfall to dripwaters and farmed calcite in Mediterranean semi-arid karst. *Geochim. Cosmochim. Acta* **243**, 66-98.

Rao T. N., B. Radhakrishna, R. Srivastava, T. M. Satyanarayana, D. N. Rao and R. Ramesh (2008) Inferring microphysical processes occurring in mesoscale convective systems from radar measurements and isotopic analysis *Geophys. Res. Lett*. **35**(9).

Risi, C., Bony, S. and Vimeux, F. (2008) Influence of convective processes on the isotopic composition ($\delta^{18}O$ and δD) of precipitation and water vapor in the tropics: 2. Physical interpretation of the amount effect. *J. Geophys. Res. Atmos.* **113**(19) 148-227.

Riechelmann D. F. C., Schröder-Ritzrau A., Scholz D., Fohlmeister J., Spötl C., Richter D. K. and Mangini A. (2011) Monitoring Bunker Cave (NW Germany): a prerequisite to interpret geochemical proxy data of speleothems from this site. *J. Hydrol.* **409**, 682–695.

Riechelmann S., Schröder-Ritzrau A., Spötl C., Riechelmann D.F.C., Richter D.K., Mangini A., Frank N., Breitenbach S.F.M. and Immenhauser A. (2017) Sensitivity of Bunker Cave to climatic forcings highlighted through multi-annual monitoring of rain-, soil-, and dripwaters. *Chem. Geol.* **449**: 194–205.

Rozanski K., Araguas-Araguas L. and Gonfiantini R. (1993) Isotopic patterns in modern global precipitation. In *Climate Change in Continental Isotope Records* (eds. P.K. Swart, K.C. Lohman, J. McKenzie and S. Savin). American Geophysical Union Monograph 78. pp. 1–36

Seager R., Kushnir Y., Nakamura J., M. Ting and Naik N. (2010), Northern Hemisphere winter snow anomalies: ENSO, NAO and the winter of 2009/10, *Geophys. Res. Lett.* **37**, L14703. doi:10.1029/2010GL043830

Sprouse P,. Stan A., Ediger G., Graham K., Lloyd C., Moore D., Rincón J. (cartoonists). Addison A., Bordignon M., Bryant M., Burgos J., Cahun H., Alanis A., Ediger G., Ferreira A., Gouila C., Munguía M., Ramírez T., Rojo R., Solignac G., Sprouse P., Sprouse T, Vela G., Vela J., Von Bertrab O., Yañez G., Zabaleta M., Zappitello M., Zappitello S. and others (topographers) (2017) Map of the Pool Tunich System. Playa del Carmen, Quintana Roo, Mexico. Contact <Peter@zaraenvironmental.com>.

Treble P. C., Bradley C., Wood A., Baker A., Jex C. N., Fairchild I. J., Gagan M. K., Cowley J. and Azcurra C. (2013) An isotopic and modelling study of flow paths and storage in Quaternary calcarenite, SW Australia: implications for speleothem paleoclimate records. *Quat. Sci. Rev*. **64**, 90-103.

Vieten, R., Warken S., Winter A., Schröder-Ritzrau A., Scholz, D. and Spötl C. (2018). Hurricane Impact on Seepage Water in Larga Cave, Puerto Rico. *J Geophys Res Biogeosci*. **123** , 879-888

Vuille M., Bradley R. S., Healy R., Werner M., Hardy D. R., Thompson L. G. and Keimig F. (2003) Modeling $\delta^{18}O$ in precipitation over the tropical Americas: 2. Simulation of the stable isotope signal in Andean ice cores. *J. Geophys. Res.* **108**, 4175.

Wang X., Edwards R. L., Auler A. S., Cheng H., Kong X., , Wang Y., Cruz F. W., Dorale, J. A. and Chiang H. W. (2017) Hydroclimate changes across the Amazon lowlands over the past 45,000 years. *Nature* **541**, 204-207.

Wang Y. J., Cheng H., Edwards R. L., An Z. S., Wu J. Y., Shen C. C. and Dorale J. A. (2001) A high-resolution absolute-dated Late Pleistocene monsoon record from Hulu Cave, China. *Science* **294** (5550), 2345-2348.

Williams J.W., Jackson S.T. and Kutzbacht J.E. (2007) Projected distributions of novel and disappearing climates by 2100 AD. *Proc. Natl. Acad. Sci.* **104**, 5738–5742.

Williams P. P. W. and Fowler A. (2002) Relationship between oxygen isotopes in rainfall, cave percolation waters and speleothem calcite at Waitomo, New Zealand. J. *Hydrol. New. Zeal.* **41**, 53–70.

Wu, T., Yu R., Zhang F., Wang Z., Dong M., Wang L., Xian J., Chen D. and Li, L. (2010). The Beijing Climate Center atmospheric general circulation model: description and its performance for the present-day climate. *Clim. Dyn.* **34**(1), 123.

Chapter 3. Prior Calcite Precipitation in the karst Río Secreto Cave, northeastern Yucatán Peninsula, México.

3.1 INTRODUCTION

Secondary cave carbonate precipitates – or speleothems - are widely used globally to reconstruct hydroclimate and wide ranging paleo-environmental characteristics (Fairchild ad Baker, 2012). In low latitudes the most common proxy for wet-dry conditions is the stable oxygen isotope composition ($\delta^{18}O$) of stalagmite calcite or aragonite, which has been shown to reflect paleo-monsoon variability (Breitenbach et al., 2010; Luo et al., 2013; Duan et al., 2014; Zhan et al., 2016; Bernal et al., 2016), and precipitation amount variability (Medina-Elizalde et al., 2010, 2017; Kennett et al., 2012; Lachniet et al. 2012, 2017). The carbon stable isotope composition ($\delta^{13}C$) of speleothem calcite and aragonite, on the other hand, is less commonly considered for paleoclimate and paleonvironmental reconstruction due to more complex processes potentially involved in controlling its absolute values and variability through time (Hansen et al., 2019). Stalagmite-calcite $\delta^{13}C$ records can reflect changes in vegetation (Genty et al., 2003; Mischel et al., 2016), temperature variability (Scholz et al. 2012) and also CO_2 variability driven by seasonal ventilation (Tremaine et al., 2011). Importantly, in the Yucatan Peninsula stalagmite $\delta^{13}C$ records have been interpreted to reflect wet and dry conditions in stalagmites from Belize, although the underlying processes controlling the relationship between stalagmite $\delta^{13}C$ and precipitation amount are still unclear (Ridley et al., 2015).

A number of studies have used the ratio of trace elements to Ca in speleothems (i.e. X/Ca ratio) as proxies for local environmental conditions (Fairchild and Treble, 2009). Only a subset of these studies include in-cave calibrations aiming at understanding the relationship between variations in X/Ca relative to $\delta^{18}O$ and processes in the soil, epikarst and within the vadose (e.g. Tremaine and Froelich, 2013; Wassenburg et al., 2020). Distinct geochemical processes modulate the relative abundance of trace elements in dripwater and stalagmites, such as Prior Calcite Precipitation (Sinclair et al., 2012), incongruent calcite dissolution (Sinclair, 2010), mixing between two or more input flows (e.g. sea spray), or influence of bedrock sources (Tremaine et al., 2016). Of these controls on trace element incorporation, only PCP can be typically linked to external atmospheric conditions (Bernal et al., 2016).

During dry conditions, epikarst cavities are typically unwetted, and overal epikarst water has a longer residence time (Williams, 2008). The dry conditions allow for CO_2 degasing, promoting calcite precipitation inside air filled cavities. During the rainy season, CO_2 degassing if impeeded in the wetted, or even saturated epikarst, residence time in the epikarst is shorter, and thus calcite precipitation rates are lower.

The sequential calcite precipitation along flow paths within the epikarst cavities prior to stalagmite formation is known as Prior Calcite Precipitation (PCP; Fairchild et al. 2000), and PCP is expected to be a main modulator of the ratios of Mg/Ca, Sr/Ca, and Ba/Ca in drip water in a rapid infiltration cave system (Treble et al., 2016; Bernal et al., 2016). The incorporation of trace elements to calcite depends on its distributtion coeficcient (D_x) which is defined as:

$$D_X = (X/Ca)_{crystal} / (X/Ca)_{solution} \quad \text{Eq. 1}$$

X	concentration of element X
Ca	calcium concentration
$(X/Ca)_{crystal}$	ratio for calcite
$(X/Ca)_{solution}$	ratio for drip water

The larger the Dx is, the X element will remain preferentially in the solid calcite phase. The lower the Dx, the element will remain preferentially in solution (Fairchild and Treble, 2009).

Sinclair et al. (2012) show that drip water Mg/Ca and Sr/Ca evolve during PCP, such that ln(Sr/Ca) vs ln/Mg/Ca) will be positive linearly correlated, with a correlation slope given by $(D_{Sr-1})/ (D_{Mg-1})$ where D_{Sr} and D_{Mg} are the partition coefficients for Sr and Mg respectively. This correlation is independent of all other parameters, and is not affected by host rock or dripwater composition making it potentially diagnostic for PCP (Sinclair et al. 2012). A review of 23 cave drip water studies found that 91% of them exhibited positive covariation of Sr/Ca and Mg/Ca ratios, and the PCP slope predicted for ln (Sr/Ca) vs. ln(Mg/Ca) was 0.88 ± 0.13 (Sinclair et al. 2012). A wider range of slopes was found by Wassenburg et al. (2020), ranging from 0.71 (or even shallower) up to 1.45, from varying initial drip water Mg/Ca and Sr/Ca ratios as well as D_{Sr} and D_{Mg}, and from the common ion effects between Mg and Sr. In stalagmites, the molar ratios of these elements should linearly covary in the ln space with a slope of 1.02 ± 0.08, when variability is modulated by PCP, based on a similar approach applied by Bernal et al. (2016) with experimentally derived distribution coefficients for Sr/Ca and Ba/Ca at 25ºC by Day and Henderson (2013).

The PCP slope does have known environmental controls. D_{Mg} and D_{Sr} are temperature dependent based on laboratory and cave studies (Katz, 1973; Gascoyne, 1983; Mucci and Morse, 1990; Huang and Fairchild, 2001; Wassenburg et al. 2020). Furthermore, D_{Sr} and D_{Ba} are both dependent on speleothem growth rate based on laboratory calcite and in speleothem studies (Lorens, 1978, 1981; Mucci and Morse, 1983; Ishikawa and Ichikuni, 1984; Tesoriero and Pankow, 1996; Huang and Fairchild, 2001; Treble et al. 2003, 2005; Gabitov and Watson, 2006).

The implicit assumption for the use of $\delta^{18}O$, $\delta^{13}C$ and X/Ca ratios compositions is that stalagmites are being deposited under thermodynamic equilibrium with drip water and, therefore, calcite is preserving the isotopic or chemical variability from the drip water source over time (Fairchild ad Baker, 2012).

This study explores the processes that control X/Ca variability of drip waters from Río Secreto cave and the corresponding elemental composition in farmed calcite. In addition, it also examines the $\delta^{18}O$ composition of farmed calcite. Water samples were collected over a 50-month period from 7 drip sites providing > 480 samples, using two different sampling protocols and spanning a marked transition from drought to wet conditions. Farmed calcite was collected on glass plates over 24 months, providing complimentary $\delta^{18}O$, $\delta^{13}C$ compositions and X/Ca ratios of the solid phase. In this chapter the distribution coefficients for Mg, Sr and Ba relative to Ca, and the composition of $\delta^{18}O$ of farmed calcite, are evaluated in light of predicted thermodynamic equilibrium relationships based on published laboratory

experiments of inorganic calcite and/or cave-analog conditions, theoretical calculations and *in situ* calibrations.

3.2 METHODS

3.2.1 Water samples and farmed calcite collection

Rainfall, drip water and groundwater collection methodology is described in Section 1.3 and in Section 2.3.

Calcite from 7 drip sites was grown on 10 x 10cm frosted glass plates wedged in collector funnels (See Fig. 2.1 and Section 2.3). The plates were cleaned with 10% ultraclean HNO_3, and triple rinsed with deionized water. Plates with visible calcite were removed after 4 to 101 days, sealed in new plastic bags, and transported in padded containers.

Cave and surface environmental parameters were logged starting in summer 2017. From July 2017, cave relative humidity was logged at 6-hour intervals using HOBO U23 data loggers with accuracy of ±5% at RH >90% and air temperature accuracy of ± 0.21ºC) at Station LF. Additionally, air temperature at Stations A and B was measured using Cave Pearl Drip Loggers (Beddows and Mallon, 2018) with an accuracy of ± 0.21ºC at 15-minute intervals. Surface temperature at Río Secreto Nature Reserve was logged prior to June 2017 with a Davis Vantage Pro 2 with accuracy of ±0.5ºC, and after June 2017 with a Cave Pearl Logger (Beddows and Mallon, 2018) accurate to ±0.21ºC. CO_2 was measured from October 2016 to November 2018 using a hand held IAQ-CALC Model 8732 with a reading accuracy of ±3% and 1 ppm resolution. CO_2 was measured on the surface and cave Stations A, B and LF during site visits, by averaging records over 5 to 60 minutes in each site.

3.2.2 Analytical Methods

3.2.2.1 Farmed Calcite Sampling

Glass plates with farmed calcite were processed in the Micro-Sampling Laboratory at the Centro de Geociencias, UNAM. Using nitrile gloves, the glass plates were manually scraped with a fine stainless-steel spatula. The recoverable calcite was weighted and collected in Eppendorf vials. Sample growth rate was calculated as mass of the recoverable calcite per cm^2, and reported as (mg/cm^2)/day. For more details, consult Appendix C.

3.2.2.2 Calcite trace elements ratios analysis

Trace elements ratios relative to Ca for Mg, Sr and Ba from single calcite crystals were obtained by laser-ablation ICP-MS, using a Resonetics L-50 excimer laser-ablation Workstation (ArF, λ = 193 nm, 23 ns FWHM, fluence of 4 J/cm^2), attached to a Thermo iCap-Q ICPMS in the Laboratorio de Estudios Isotópicos at the Centro de Geociencias, UNAM, following the general methodology of Bernal et al. (2016). Trace element ratios correspond to the averaged value of various crystals results. See Appendix C for full analytical details.

3.2.2.3 Calcite $\delta^{18}O$ and $\delta^{13}C$ composition determination

Calcite $\delta^{18}O$ and $\delta^{13}C$ determination was undertaken in the Paleoclimatology and Stable Isotopes Laboratory at Auburn University using standard methods with a GasBench II paired with a Thermo Scientific Delta V Plus isotope ratio mass spectrometer (IRMS). Farmed calcite samples were inspected visually to achieve ~3–7 volts on mass 44, and placed into horizontal 12 mL borosilicate vials. Two drops of ~99% phosphoric acid were placed in the neck of vial without interaction with the calcite, then capped with LabCo Chlorobutyl Septum and purged off-line with ultra-high purity (UHP) helium for 7 minutes at a flow rate of 100mL/min. Acidification, producing CO_2 gas, occurred when the vials were placed vertically in the heating block at 70ºC. UHP He carrier gas flowed CO_2 through a PoraPLOT Q GC column to scrub H_2O, and then to the Delta V Plus IRMS. The raw data was normalized and corrected for drift using bracketing IAEA-603 standard ($\delta^{18}O$ = -2.37±0.04 ‰ and $\delta^{13}C$ = 2.45±0.01‰, both V-PDB), as well as two lab standards every 8 samples. Long term analytical precision using the IAEA-603 standard are 0.09 ‰ for $\delta^{18}O$ and 0.07 ‰ for $\delta^{13}C$ PDB. The $\delta^{18}O$ and $\delta^{13}C$ are reported in per mil on the V-Pee Dee Belemnite (V-PDB) scale.

The $\delta^{18}O$ compositions of ~monthly bulk water samples collected after June 2017 were also used for comparison with $\delta^{18}O$ farmed calcite, $\delta^{18}O$ compositions analytical determination of these water samples is described in Section 2.3.3.1.

3.2.2.4 Trace elements determination of water samples

Elemental concentrations for Ca, Mg, Sr, Ba, Al, Mn, Ti and Cl, in drip and rainfall samples was determined using a Thermo Icap-Q ICP-MS in the Laboratorio de Estudios Isotópicos at Centro de Geociencias, UNAM. Standard solutions were prepared from single element standards. Data were corrected for blank intensities and instrumental drift using an internal standard. Relative deviations of identical standard solutions during one day of analysis averaged 4% (n=19) for Ca, Mg, Sr, Ba and 14% (n=16) for Ti, Al and Mn. More details of this analytical procedure are provided in Appendix C.

3.2.3 Data approach

Stable isotopic results in Río Secreto cave show that the epikarst integrates rainfall over monthly timescales and longer for most drip waters (Chapter 2). Weekly bulk water samples were collected prior to June 2017, whereas monthly bulk water samples followed from June 2017 onwards. The higher frequency weekly sampling before June 2017 showes higher variability of drip water characteristics, and it do not as clearly show general seasonal trends. Therefore, the weekly data for elemental concentration, Electrical Conductivity (EC) and drip rates are now aggregated to monthly averages in Table B.2.1 to determine monthly scale descriptive statistics (e.g. Table 3.1) and calculate correlation matrices (e.g. Table B.3).

Distribution coefficients for Mg, Sr, Ba are calculated with:

$$D_X = (X/Ca)_{crystal} \; / \; (X/Ca)_{solution} \qquad \text{Eq. 2}$$

X	concentration of element X, mmol
Ca	calcium concentration, mol
$(X/Ca)_{crystal}$	ratio for modern farmed calcite
$(X/Ca)_{solution}$	ratio for drip water, averaged over the coeval calcite growth time.

Details of calculations for the results shown in Fig. 3.13, Table 3.3 and Table B.6 are in their corresponding captions.

3.3 RESULTS AND DISCUSSION

3.3.1 Temperature and CO_2 variability

A summary of temperature and CO_2 data of cave air and surface air is presented in Table 3.1 and their temporal variability is illustrated in Fig. 3.1 Temperature data variability over this period agree with data from Chapter 1 for the August 2014- July 2017 period from the same sites (Section 1.4.1). Surface air CO_2 concentrations, as expected were low and relatively invariate, averaging 421 ± 32 ppm, n=29 (Fig. 3.1). Cave air CO_2 during the summer from June to October reached up to an order of magnitude higher with max of 3977 ppm, while during the winter months of January and February had a min of 430 ppm and CO_2 values only slightly elevated compared to surface concentrations (Fig. 3.1 and Table 3.1). All cave stations showed the same trend of air CO_2 variations, but with different amplitude due to ventilation differences, in a pattern mirrored in the air temperature variability between chambers and surface and previously described in Section 1.5.1 (Lases-Hernández et al., 2019). Station LF is the most ventilated chamber and closest to the entrance (Fig. 2.1), it showed the lowest CO_2 values and ranged over 1273 ppm, whereas the more isolated Stations A and B had the highest CO_2 values and ranged over 3427 ppm and 2716 ppm, respectively (Fig. 3.1). Seasonal ventilation occurs through Rio Secreto Cave as described in Section 1.5.1. The winter minimum surface temperatures leads to denser cool surface air sinking into the cave, with displacement leading to the exhalation of less dense warmer cave air that also removes the CO_2 accumulated during the warmer summer season when air is mostly stagnant. The seasonal ventilation especially decreases CO_2 concentrations in the more isolated chambers of Stations A and B (Fig. 3.1). Hence, surface temperatures lead to cave air exchange, and surface temperatures thereby control cave CO_2 concentrations (Lases-Hernández et al., 2019).

Average air temperature values and CO_2 concentrations measured at Stations LF, A and B, exhibited significant linear correlations ($r^2 > 0.5$, p-value < 0.001) during the sampling period when calcite was farmed (Table B.5 in Appendix B). It is notable that the warm summer is also the rainy season, such that CO_2 values in the cave are the highest when there is more rainfall, and vice versa (Fig. 3.7).

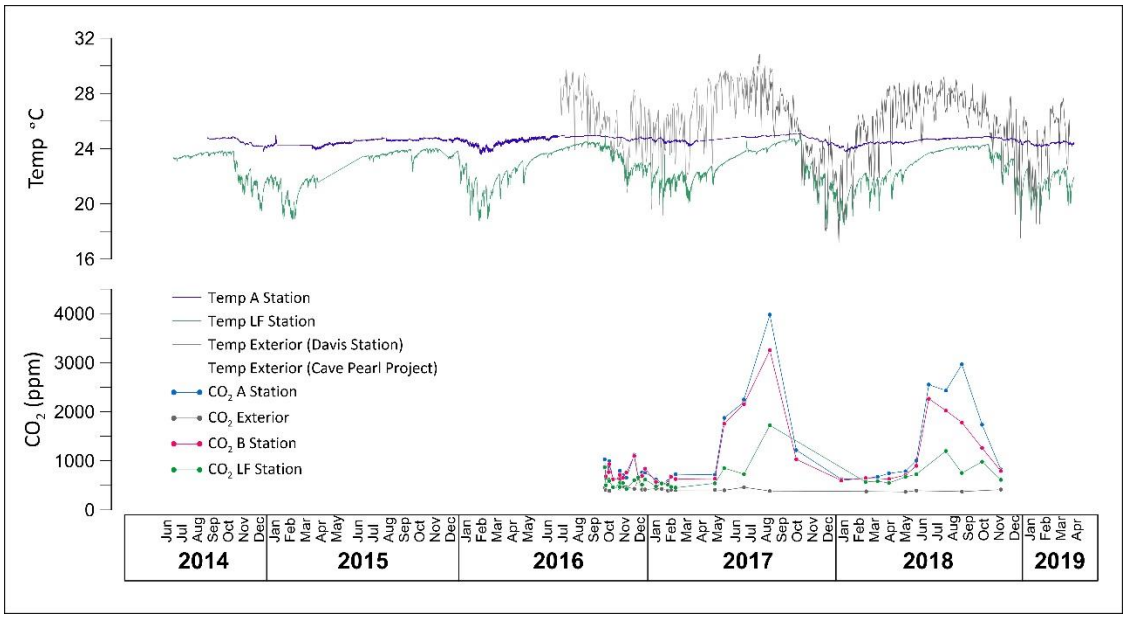

Fig. 3.1 Temperature and CO_2 variability in three different Stations of Río Secreto Cave and the exterior.

Table 3.1 Summary of temperature and CO_2 data measured outside and inside Río Secreto Cave.

Paramater	Station	Period	Frequency	n	AVG	1 SD	MIN	MAX
Air Temp (°C)	A	August 2017 – July 2019	15 minutes	66659	24.6	0.3	23.8	25.1
	LF		6 hours	2841	22.6	1.4	24.9	17.7
	Exterior		daily avg	604	25.4	2.5	17.2	30.9
Air CO_2 (ppm)	A	October 2016 – November 2018	~monthly	35	1118	803	550	3977
	B		~monthly	34	998	626	537	3253
	LF		~monthly	32	652	257	430	1723
	Exterior		~monthly	29	421	32	367	475

3.3.2 Rainwater results and sea-spray contribution

In coastal systems sea-spray can be a source of ions from seawater to groundwater, especially of Ca, Mg and Sr (Goede et al., 1998; Sinclair et al. 2012) and therefore the temporal variability of these elements can be affected reflecting not only cave rock interactions. Río Secreto cave is located ~5 km from the Caribbean coast (Fig. 2.1). In order to assess possible sea-spray influence on trace element ratio variability in drip waters, I analyzed trace elements concentrations and specifically chloride (Cl^-, hereafter Cl) in rainfall to compare with those of drip waters.

The collecting rain gauge was positioned at ground-level and not above the jungle canopy over the cave. I therefore anticipate that some samples may represent not only the elemental concentration of rainwater, but also the washing of accumulated sea-salt off the

vegetation, and potentially some blown dust from the soil/ground over the ~month of collection. However, this methodology was considered adequate to represent the total input of elemental compositions from rainfall in the infiltration water towards the epikarst. A total of 47 monthly rainfall samples were collected over November 2014 to November 2018 above the Rio Secreto Cave, with 34 of those samples analyzed for trace element concentrations. Raw data of rainfall elemental concentrations is presented in Table B.1 (Appendix B). A summary of trace elements concentration in rainfall is presented in Table 3.2.

Fig. 3.2 shows the temporal variation of Cl in rain and drip water. The Cl concentration in rainfall is low and relatively constant ~ 5 ± 5 ppm, while it is higher and with greater variability in drip water.

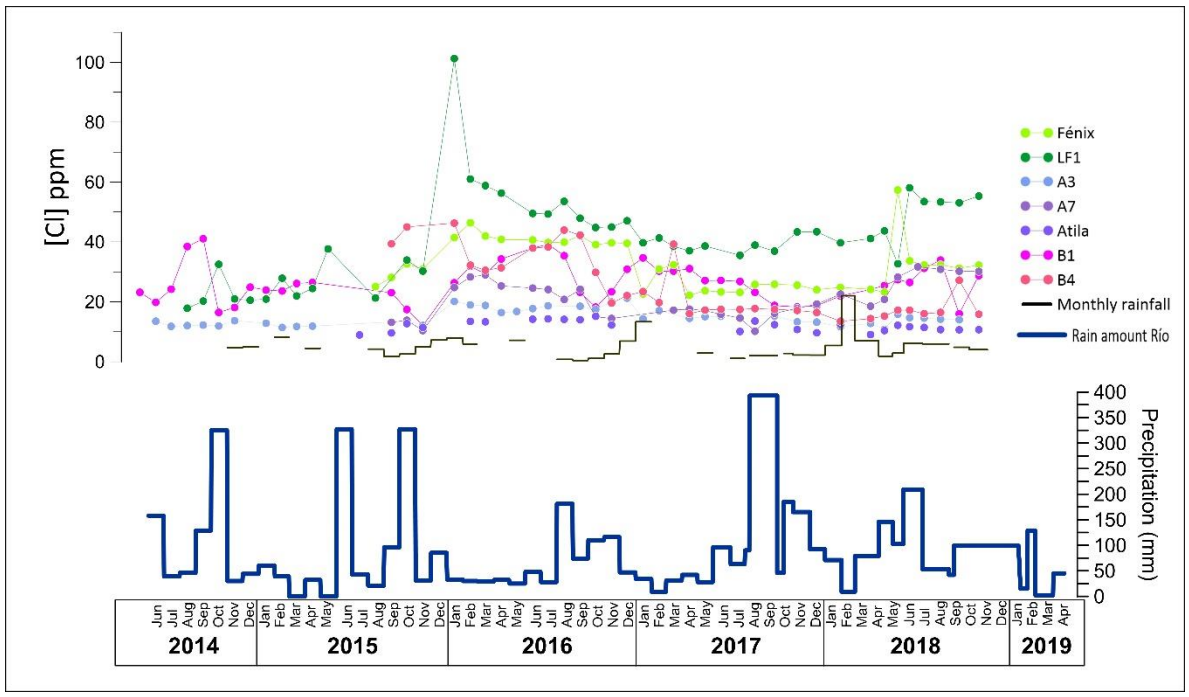

Fig. 3.2 Monthly data for ppm concentration of Cl (Upper) in 7 cave drip sites and precipitation samples, and precipitation amount above the Río Secreto Cave (Lower). Cave drip data spans June 2014 to November 2018 from Stations LF, B and A, with the weekly sampling prior to June 2017 is aggregated here to monthly averages (See Section 3.2.3).

A notable increase in the Cl concentration at LF1, Fénix, B1, B4 and A7 drip sites is observed to occur during January to March 2016 and gradualy decreases after March 2016. The rise in Cl concentration occurred ~3 months the after peak rainfall in October 2015. On the other hand, Cl in drip water at A3 and Atila sites remained constant over the time (Table 3.2, Fig. 3.2).

Table 3.2 Statistical sumary of Electrical Conductivity (EC), pH, elemental compositions and X/Ca ratios for 7 drip water sites and collected over a 50-month period at Río Secreto cave and for monthly rainfall samples colected above the cave. Ca, Mg, Ba and U concentrations are reported in mmol/L. Al. Ti and Mn concentrations are reported in ppm. X/Ca ratios are reported in mmol/mol. Drip waters samples collected at weekly intervals before June 2017 were aggregated to monthly averages before to perform statistical calculations for all samples, see section 3.3.6 for more details and Tables B.1 and B.2 at Appendix B.

Site & Dates		EC (µS/cm)	pH	Ca	Mg	Ba	U	Sr	Cl	Al	Ti	Mn	Mg/Ca	Ba/Ca	Sr/Ca	U/Ca	Al/Ca	Ti/Ca	Mn/Ca
LF1	AVG	288	7.7	0.80	0.16	0.00011	4.4E-06	0.0032	40.8	0.00079	0.00015	7.3E-05	206.4	0.129	4.2	0.0060	0.04	0.0040	0.0016
	SD	33	0.5	0.17	0.02	0.00017	3.5E-06	0.0004	15.3	0.00099	0.00006	1.0E-04	49.7	0.144	0.8	0.0051	0.05	0.0018	0.0021
2014-08-15	RANGE	150	2.2	0.60	0.15	0.00083	1.2E-05	0.0024	83.4	0.00360	0.00027	5.6E-04	247.3	0.695	4.0	0.0159	0.22	0.0073	0.0107
2018-10-28	MIN	229	6.4	0.58	0.11	0.00005	1.1E-06	0.0022	17.8	0.000026	0.00005	2.4E-06	119.5	0.055	2.4	0.0012	0.00	0.0011	0.0001
	MAX	379	8.5	1.18	0.26	0.00088	1.4E-05	0.0046	101.2	0.0036	0.00032	5.6E-04	366.9	0.750	6.4	0.0171	0.22	0.0084	0.0107
	n	34	31	44	44	44	43	44	44	43	41	39	44	44	44	43	40	38	38
Fénix	AVG	404	7.4	1.07	0.11	0.00006	3.0E-06	0.0024	32.5	0.00109	0.00011	3.6E-05	126.6	0.063	2.6	0.0030	0.05	0.0028	0.0007
	SD	98	0.4	0.47	0.01	0.00002	2.6E-06	0.0002	8.4	0.00192	0.00008	5.5E-05	40.3	0.019	0.8	0.0028	0.11	0.0029	0.0009
2015-05-15	RANGE	325	1.6	1.88	0.05	0.00009	7.4E-06	0.0010	35.2	0.01005	0.00052	3.0E-04	133.0	0.068	2.7	0.0097	0.57	0.0165	0.0051
2018-10-28	MIN	267	6.6	0.64	0.10	0.00004	1.1E-06	0.0021	22.2	0.000029	0.00000	3.3E-06	43.0	0.021	0.9	0.0011	0.00	0.0001	0.0000
	MAX	592	8.2	2.53	0.15	0.00013	8.5E-06	0.0031	57.4	0.0101	0.00052	3.0E-04	176.0	0.090	3.6	0.0108	0.57	0.0166	0.0051
	n	38	32	35	35	35	34	35	35	33	34	30	35	35	35	34	33	32	30
A3	AVG	281	7.6	0.87	0.16	0.00006	2.2E-06	0.0026	14.8	0.00971	0.00033	2.0E-03	195.6	0.073	3.2	0.0025	0.41	0.0094	0.0686
	SD	42	0.5	0.22	0.02	0.00002	8.8E-07	0.0002	2.8	0.03158	0.00055	9.0E-03	35.8	0.031	0.6	0.0010	1.32	0.0150	0.2662
2014-06-15	RANGE	170	2.2	1.09	0.11	0.00014	4.1E-06	0.0018	10.3	0.15220	0.00226	5.1E-02	132.6	0.145	2.2	0.0031	5.96	0.0583	1.4688
2018-12-15	MIN	192	5.8	0.46	0.10	0.00004	1.2E-06	0.0018	10.9	0.000068	0.00007	9.8E-06	116.5	0.040	1.9	0.0012	0.00	0.0015	0.0003
	MAX	362	8.0	1.55	0.22	0.00018	5.3E-06	0.0035	21.2	0.1523	0.00233	5.1E-02	249.0	0.186	4.1	0.0043	5.96	0.0599	1.4690
	n	40	34	40	40	40	40	40	40	40	40	40	40	40	40	40	40	40	40
A7	AVG	319	7.5	1.05	0.14	0.00006	3.5E-06	0.0033	20.9	0.03115	0.00050	7.5E-05	154.4	0.066	3.5	0.0033	1.74	0.0149	0.0017
	SD	57	0.4	0.36	0.01	0.00002	3.7E-06	0.0002	6.4	0.10005	0.00109	1.7E-04	50.5	0.022	1.1	0.0032	5.50	0.0337	0.0045
2015-06-15	RANGE	244	1.6	1.18	0.05	0.00011	1.3E-05	0.0011	21.5	0.48778	0.00448	9.2E-04	190.0	0.111	3.2	0.0108	26.50	0.1320	0.0238
2018-10-28	MIN	221	6.4	0.62	0.13	0.00004	1.1E-06	0.0026	10.2	0.000047	0.00004	2.0E-06	81.6	0.032	1.9	0.0009	0.00	0.0008	0.0000
	MAX	465	8.0	1.80	0.18	0.00015	1.4E-05	0.0037	31.7	0.4878	0.00452	9.2E-04	271.6	0.143	5.1	0.0117	26.50	0.1327	0.0239
	n	32	28	30	30	30	30	30	30	30	30	27	30	30	30	30	29	29	27
Atila	AVG	253	7.5	0.92	0.17	0.00006	2.9E-06	0.0028	11.9	0.00472	0.00019	7.2E-05	197.5	0.071	3.2	0.0034	0.20	0.0045	0.0014
	SD	32	0.7	0.24	0.01	0.00002	2.7E-06	0.0002	1.8	0.01946	0.00030	1.0E-04	43.8	0.020	0.7	0.0033	0.81	0.0073	0.0018
2015-05-15	RANGE	125	2.5	1.08	0.05	0.00011	9.8E-06	0.0007	6.2	0.09787	0.00156	3.6E-04	151.8	0.096	2.3	0.0097	4.04	0.0374	0.0070
2018-10-28	MIN	189	5.6	0.61	0.14	0.00005	1.1E-06	0.0025	9.0	0.000027	0.00005	1.5E-07	101.7	0.046	1.8	0.0010	0.00	0.0008	0.0000
	MAX	314	8.1	1.69	0.19	0.00016	1.1E-05	0.0031	15.2	0.0979	0.00161	3.6E-04	253.5	0.142	4.2	0.0108	4.04	0.0382	0.0070
	n	27	22	26	26	26	25	26	26	25	25	24	26	26	26	25	25	25	24
B1	AVG	276	7.6	0.90	0.20	0.00004	4.2E-06	0.0033	26.3	0.00868	0.00026	5.2E-04	228.7	0.046	3.8	0.0048	0.36	0.0064	0.0113
	SD	35	0.5	0.24	0.03	0.00002	3.0E-06	0.0003	6.7	0.02684	0.00042	1.7E-03	48.0	0.023	0.8	0.0033	1.12	0.0105	0.0392
2014-05-15	RANGE	146	2.0	0.96	0.15	0.00010	1.1E-05	0.0014	29.0	0.12441	0.00179	9.5E-03	178.7	0.097	3.0	0.0124	6.08	0.0493	0.2089
2018-10-28	MIN	220	6.1	0.60	0.14	0.00002	1.5E-06	0.0027	12.1	0.000027	0.00005	3.3E-07	124.9	0.016	2.3	0.0014	0.00	0.0011	0.0000
	MAX	366	8.1	1.55	0.29	0.00012	1.3E-05	0.0040	41.1	0.1244	0.00183	9.5E-03	303.6	0.113	5.3	0.0138	6.08	0.0505	0.2090
	n	34	29	46	46	46	46	46	46	46	45	45	46	46	46	46	45	44	44
B4	AVG	435	7.4	1.19	0.30	0.00002	3.3E-06	0.0041	25.2	0.01464	0.00031	4.4E-05	295.9	0.023	4.1	0.0032	0.60	0.0065	0.0007
	SD	110	0.3	0.46	0.03	0.00000	1.1E-06	0.0003	10.7	0.04353	0.00071	5.9E-05	118.1	0.009	1.4	0.0014	1.81	0.0127	0.0007
2015-05-15	RANGE	401	1.7	1.66	0.16	0.00002	4.0E-06	0.0010	32.8	0.17376	0.00368	2.9E-04	369.7	0.041	4.4	0.0053	8.42	0.0458	0.0026
2018-10-28	MIN	233	6.3	0.68	0.20	0.00002	1.7E-06	0.0035	13.5	0.000007	0.00002	1.2E-06	131.8	0.009	1.9	0.0013	0.00	0.0002	0.0000
	MAX	634	7.9	2.34	0.36	0.00004	5.8E-06	0.0046	46.3	0.1738	0.00370	2.9E-04	501.5	0.050	6.3	0.0066	8.42	0.0460	0.0026
	n	37	31	33	33	33	32	33	33	33	33	31	33	33	33	32	32	32	30
RAINFALL	AVG	51		0.17	0.015	3E-05	2E-08	0.0002	4.9	0.005	0.00011	0.0002	136.5	0.17	1.2	0.0002			
	SD	37		0.17	0.010	0.0001	3E-08	0.0001	4.1	0.005	8.3E-05	0.0004	87.9	0.38	0.4	9E-05			
2014-11-15	RANGE	146		0.85	0.051	0.0006	2E-07	0.0005	21.6	0.024	0.00034	0.002	338.1	2.18	2.0	0.0003			
2018-10-27	MIN	13		0.03	0.004	2E-06	5E-09	5E-05	0.4	0.001	2.6E-05	5E-06	19.0	0.01	0.3	5E-05			
	MAX	159		0.88	0.055	0.0006	2E-07	0.0005	22.0	0.024	0.00037	0.002	357.1	2.20	2.3	0.0004			
	n	23		34	34	34	34	34	33	34	34	33	33	33	33	33			

To assess the relative contribution of sea spray to the waters, an Enrichment Factor (EF) was calculated as the average proportion for elemental concentrations and EC between the drip waters of each site and the rainwater (Table 3.3). The average Cl concentrations in drip water resulted to be consistently higher than the monthly rainwater above the cave. Drip waters in this study can be classified into three groups: drips at Station A which are 3 to 5 times the concentration of rainwater, drips at Station B are up to 6 times, and those of Station LF that are 8 to 10 times the concentration of rainwater. Cl can be used as a quasi-conservative tracer reflecting infiltration processes (Tremaine et al. 2016). Tremaine and Froelich (2013) found in their coastal study site that Cl concentrations in drip waters were 4 to 17 times that of rainwater, and they interpreted the elevated Cl as being caused by evapotranspiration that, in their site, were estimated to be between 70% and 93% of annual rainfall.

Table 3.3 Enrichment Factor (EF) denotes how many times drip water is on average more concentrated than rainfall. Enrichment Factor for Electrical Conductivity, and suite of elements calculated as: $EF = Dripwater_{[X]} / Rainfall_{[X]}$ Where, $Dripwater_{[X]}$ is the averaged elemental concentration or EC of monthly samples for 7 individual drip sites. $Rainfall_{[X]}$ is the averaged elemental concentration or EC of monthly rainfall samples. X= Ca, Mg, Ba, U, Sr, Cl , Al,Ti, Mn. Outliers for Ca, Mg, Ba, Cl (n=1), U, Sr, Al, Ti, Mn (n=2) and EC (n=4) from rainfall samples were removed to calculate elemental and CE rainfall averages (i.e. $Rainfall_{[X]}$).

	Electrical Conductivity	Ca	Mg	Ba	U	Sr	Cl	Al	Ti	Mn
LF1	9	6	12	11	252	20	10	0.2	1.4	0.5
Fénix	12	8	9	6	175	15	8	0.3	1.1	0.3
A3	8	6	13	6	125	17	4	2.3	3.1	14.6
A7	10	8	11	6	205	21	5	7.4	4.7	0.6
Atila	8	7	13	6	169	18	3	1.1	1.8	0.5
B1	8	7	15	4	242	21	6	2.1	2.5	3.9
B4	13	9	23	2	189	26	6	3.5	2.9	0.3

As described in Sections 1.5.1 and 3.3.1, the different chambers or Stations are exposed to different degrees of air ventilation and this might lead to different degrees of evaporation. However, multiple lines of evidence indicate that there is no evaporation affecting the stable isotopes composition of drip water samples inside the cave: (i) drip water isotopic values similar to the coeval local meteoric water line during 5 hydrological years; (ii) the isotopic composition of drip water at various drip sites similar to that of rainfall; (iii) drip water mean annual $\delta^{18}O$ compositions from stations A and B closely resembling the annual amount-weighted $\delta^{18}O$ composition of rainfall; (iv) drip water average $\delta^{18}O$ composition from drip site labelled Fénix 1-2‰ more negative than the annual amount-weighted $\delta^{18}O$ composition of rainfall, and; (v) cave air relative humidity at or near 100% during the entire recorded period (Section 1.5.3). Albeit, there is also some evidence from stable isotopes study that drip water from LF1 site experienced evaporation outside of the cave (See Section 2.5.4). Further, proximate drip sites within 5 m-10 m, such as Fénix and LF1, or A3 and A7, exhibit very different Cl concentrations relative to each other (Table 3.2, Fig. 3.2) suggesting that evaporation inside the cave is unlikely the reason that explains dripwater Cl concentration.

LF1 also uniquely has weak but significant correlations of dripwater concentration through the time between Cl relative to Sr and Mg (r^2= 0.43 and 0.35, respectively; p-value<

0.0001), such correlation was not found in any other drip site. Because Sr and Mg are not conservative elements in drip water, it is not expected that their drip water concentration temporal variation varies through the time as a function of evaporation, and it is more likely that their correlation with Cl is related to a dissolution process. I propose that drip water Cl concentration enriched with respect to rainfall may be reflecting drip water dissolving traces of evaporites located in the epikarst overlaying drip sites (Perry et al. 2009), and no evaporation inside the cave. The unique isotopic and hydrological characteristics of each cave drip water sites studied in the current chapter presented in Chapters 1 and 2 are tied to unique complex infiltration paths and variable sizes of the epikarst water reservoirs above each. The epikarst complexity leads to differences in dissolution patterns that seen in elemental concentration variability, even between proximate drips. However, this variability does not follow a simple and predictable behavior. For example, Ba and Cl drip concentration have a comparable fold difference in drip water to rainwater, of 2-11 times for Ba and 3-11 times for Cl. However, Ba and Cl enrichment factors among drip sites are not linearly correlated, as expected if both are reflecting dissolution and this is likely because the different sources of those ions in the epikarst. Ca, Mg, Sr and U presented a higher range of EF values than Ba and Cl (Table 3.3.) and do not show linear correlation among elements and drip sites, except for the relationships between the pairs EC and Ca (r^2=0.71) and Mg and Sr (r^2=0.72). This suggest that Ca, Mg and Sr may present a predictable behavior even at a spatial scale controlled by water-rock interaction within Río Secreto Cave, but other elements such as Cl and Ba will be affected because the infiltration pattern variability, or alternatively because slight epikarst bedrock differences. Future bedrock composition studies will test this hypothesis. Due to the low concentration of Ca, Mg, Sr, U in rainwater relative to drip water (Tables 3.2 and 3.3; Fig. B.2), it is unlikely that seasonal variability in the rainfall contribution to trace element composition of drip water is capable of masking water-rock processes within the epikarst such as PCP.

With the exclusion of 4 outlier EC values from rainwater, likely due to the ground level sampling, the overall rainfall EC values and variability were low 30 ± 10 µS/cm (Fig. 3.6). Rainwater samples presented a positive linear relationship between EC and various elements: Ti (r^2=0.36), Cl (r^2=0.29), Ca (r^2=0.43), Mg (r^2=0.34), Sr (r^2=0.49) (p-value< 0.0001 for all). Additionally, significant linear relationship between different elements in rainfall samples were found and presented in Fig. 3.3 (ABC). Elemental relationships (Figure 3.3) can be explained as either reflecting seawater solutes such as between Mg and Cl, or alternatively by limestone dust from the ground/soil such as between Ca, Sr, and U. Río Secreto Cave is 4 km north of the largest limestone aggregate mine on the Peninsula, that approximately doubled the cleared ground area in 2016 (See Google Earth Historical Imagery). Further evidence that limestone dust from mining activity could be incorporated to the rainfall samples is the linear relationship between Mg/Ca and Sr/Ca ratios in the rainwater samples (r^2=0.68, p-value=0.001; Fig. 3.3D).

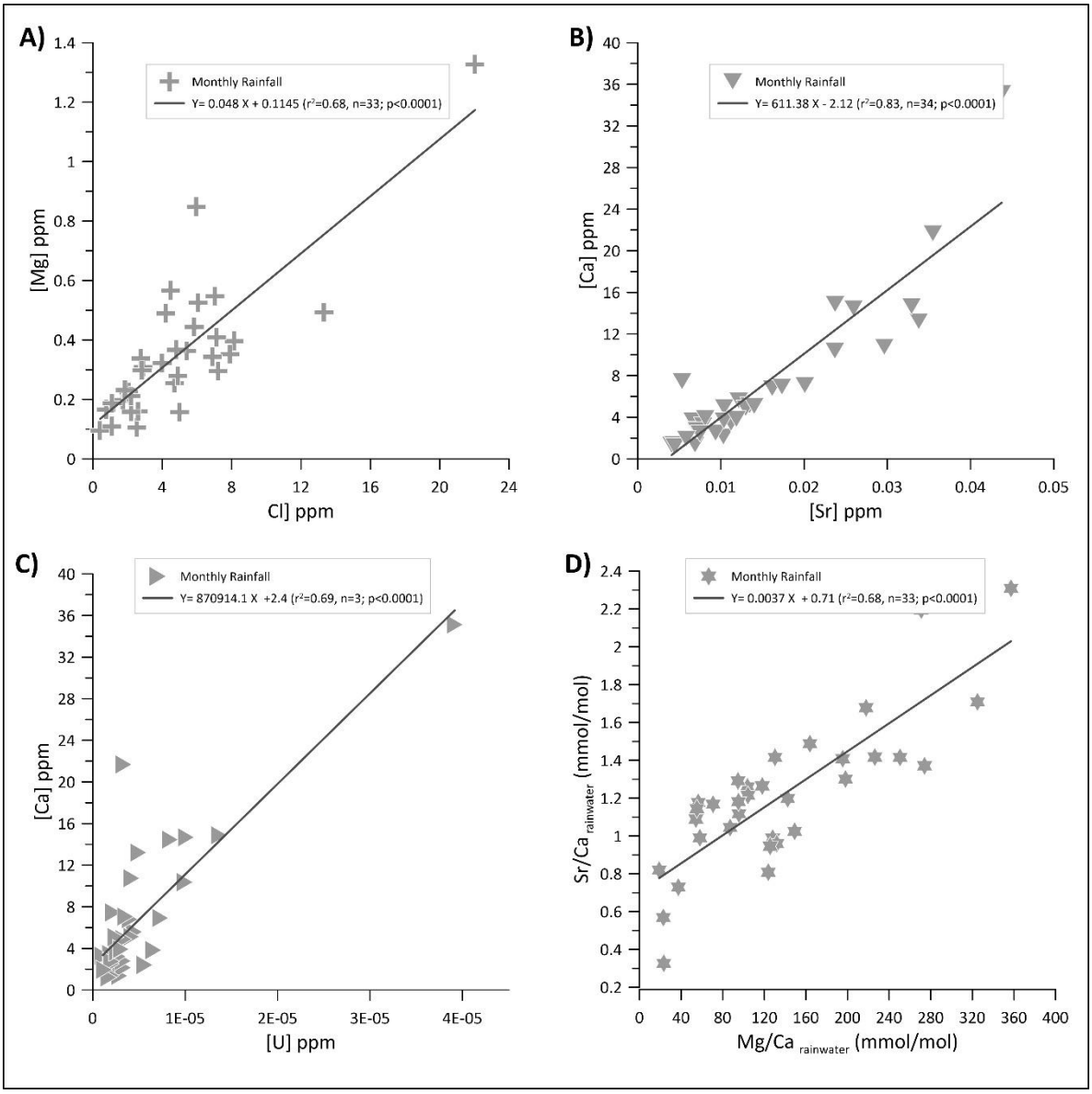

Fig. 3.3 Linear regressions between select elemental ppm concentrations in monthly rainwater samples, with : A) Mg and Cl, B) Ca and Sr, C) Ca and U and D) Mg/Ca and Sr/Ca ratios with no water samples removed as outliers.

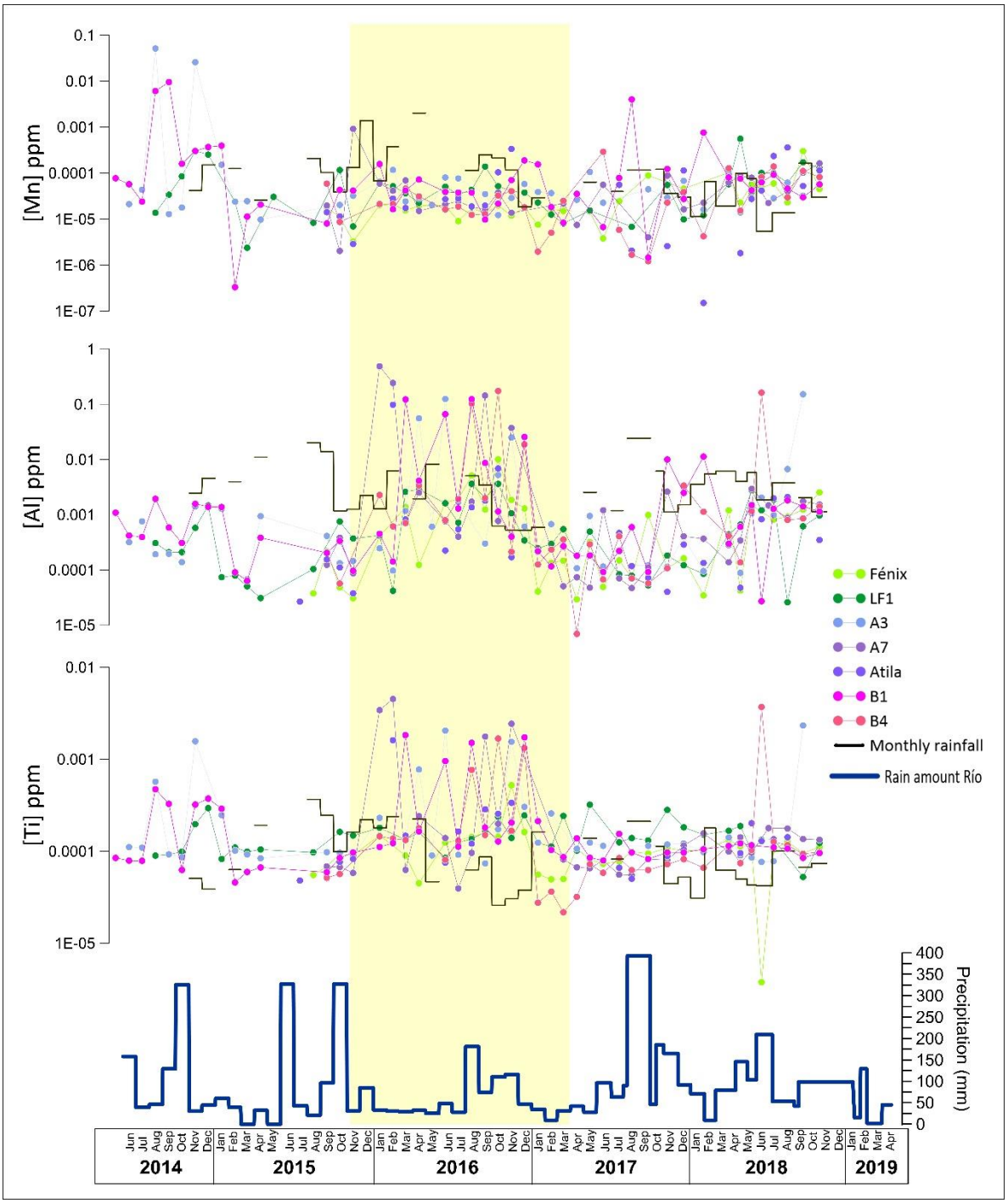

Fig. 3.4 Concentration in ppm of Mn (Upper), Al (Second), and Ti (Third) in 7 cave drips and precipitation samples, and precipitation amount above the Río Secreto Cave (Lower). The Stations A, B, and LF cave drip samples span June 2014 to November 2018, with the weekly samples prior to June 2017 aggregated to monthly averages (See Section 3.2.3). Note that the elemental concentration Y axes are in log scale. A drought from December 2015 to April 2017 (yellow shading) included below average rainfall over summer rainfall 2016, with some drip sites presenting peak values in Al and Ti at that time.

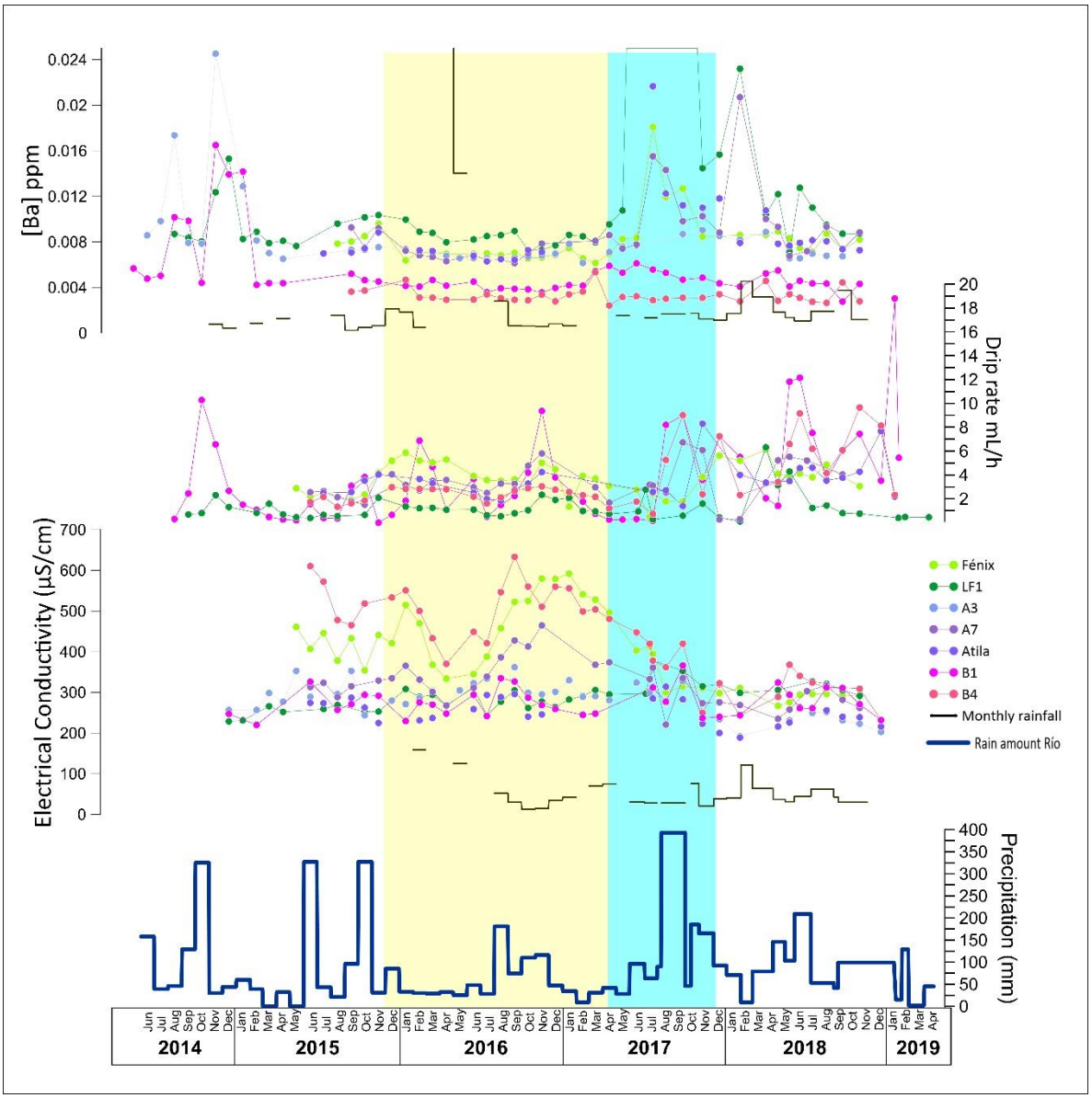

Fig. 3.5 Monthly data Ba concentration (ppm, upper), drip rate (mL/hr, second) and electrical conducitivty (µS/cm; third) for 7 cave drip sites and when available for precipitation samples, and precipitation amount above the Río Secreto Cave (Lower). Cave drip data spans June 2014 to November 2018 from Stations LF, B and A, with the weekly sampling prior to June 2017 aggregated to the shown monthly averages (See Section 3.2.3). A drought (highlighted in yellow) occurred with lower than average summer rainfall 2016, and blue highligted area showing the transition to a wet summer season.

Ti, Al and Mn concentrations in rainfall were very low but above detection limits, and some drips had comparable averaged values (Fig. 3.4, Table 3.2 and Table 3.3). This last result provides further evidence that evaporation is not broadly affecting elemental concentrations in drip waters, as evaporation would have concentrated all drip waters in comparison with rainfall values. Significant linear correlation exists between Al and Ti and between Al/Ca and Ti/Ca ratios in drip water samples (Fig. B.1 at Appendix B) indicating potential for dissolved/suspended clay minerals in drip waters, which have been found to present in the soils of the Yucatan Peninsula (Sedov et al. 2008; Cabadas- Báez et al. 2010). Drip water Al and Ti concentrations show important variability spanning orders of magnitude, mainly over 2016 in the drip sites B1, B4, A3, Fénix (Fig. 3.4). If the elevated Al and Ti is tied to clay mineral particles, then they are transported and precipitated on the Río Secreto cave, and passing through the epikarst to some drip sites. This clay mineral transport appears to be more marked during a meteorological drought. Sources of Al and Ti could be the intensive urban development of Playa del Carmen to the north that relies heavily on cement, or also tied to the expanding mining operation to the south disturbing soil clays in that particular year. Due to the implications of this result, and the high Coefficient of Variation in the analysis of Al, Ti, and Mn when some samples were repeated in different runs, analytical confirmation of these data will be achieved to support this interpretation (See Table 2C at Appendix C).

3.3.3 Temporal variability of Ba concentration and electrical conductivity in drip waters

Statistical summary of Electrical Conductivity, pH, trace elements concentration and X/Ca ratios data for 7 drip sites are presented in Table 3.2. Drip water EC, Ba and discharge time series are show in Fig. 3.5.

Most drip waters EC have slight seasonality similar to that of discharge, with a range of values from 150 to 360 µS/cm (Fig. 3.5). However, the 3 drips of A7, B4, and Fénix, had elevated values of 360-630 µS/cm from May 2015 through to May 2017 (Fig. 3.5). At that time when dripwaters were sampled in 48-hour aliquots at weekly resolution, those three drip sites were found to have seepage flow according to Fairchild et al. (2016) classification (See Fig. 1.6 at Chapter 1). The EC data for A7, B4, and Fénix seepage drips indicates that dissolution was greater during the relatively dry period May 2015-May 2017 (Fig. 3.5). After June 2017, sampling of bulk ~month accumulation of drip water, combined with significant rainfall Summer 2017, the EC from A7, B4, and Fénix, decreased to 150 to 360 µS/cm and was of uniform between drip sites (Fig. 3.5). Despite this logical inference of greater dissolution in seepage drips during dry conditions, it is not clear which elements are creating high EC values at A7, B4, and Fénix sites. Furthermore, there is not apparent covariation between variability in drip EC and of the elemental concentrations analysed in this study (i.e. Ca, Mg, Sr, Ba, Cl) during the drougth period (Figs. 3.2, 3.5 and. B.2). It is possible that the ions elevating EC in these three drips were not measured (e.g. K, Na, SO_4, NO_3) and likely related to soil or sea-spray. Increase ionic concentration in drip waters tied to a drought was also documented by Tremaine et al. (2016) in a coastal cave in Niue Island. Opposite to the multi-element correlation to EC found in rainwater (Section 3.3.2), for the drip waters only the next relationships were found: Cl and EC at B4 site (r^2=0.40), Mg and EC at Atila site (r^2=0.42) and Ba and EC at LF1 site (r^2=0.37), based in monthly integrated data (Table B.3; see also Section 3.2.3). Includying all data integrated in drip water monthly samples

(averaged weekly bulk and monthly bulk, see Section 3.2.3), I only found a linear relationship between dripwater Ca concentration and EC at B1 and LF1 sites with r^2 of 0.27 and 0.43, respectively (Table B.3 in Appendix B). However, I found a strong positive linear correlation at 6 of 7 drip sites between Ca concentration and EC only for the ~monthly drip water samples collected using the second sampling protocol after June 2017 (Fig. 3.6); leading to the appreciation that the monthly bulk water sampling that integrates all drip water during a month or longer is better for the detection of PCP, all while the weekly sampling protocol was most accurate to detect tropical cyclone incursions using $\delta^{18}O$ compositions of drip waters (See Section 2.5.6). This also indicates that the humidity at epikarst reflected as trace elements variability requires a longer time than a week for homogeneization.

Drip Ba concentration is unsurprisingly very low compared to Mg and Sr (Table 3.2), but similar to Baldini et al (2012), and higher than the average Ba reported for drip waters by Tremaine et al. (2016). Variablity of drip Ba concentration was mainly during and proceeding the wet seasons (Table 3.3). In summer 2014, the Ba concentration increased one to two fold in the three drip sites monitored at that time i.e. A3, B1 and LF1 (Fig. 3.5), and in Summer 2017, it increased from one to 4 fold in 4 of the 7 monitored drips i.e. A7, Atila, LF1, Fénix (Fig. 3.5). During Summer 2015 and 2018, most drip waters also had slightly elevated Ba concentration, but during the drought of Summer 2016, the Ba concentrations remained invariable in most drips except LF1 site (Fig. 3.5). The drip Ba concentration of Río Secreto Cave can be affected by seasonal hydrology.

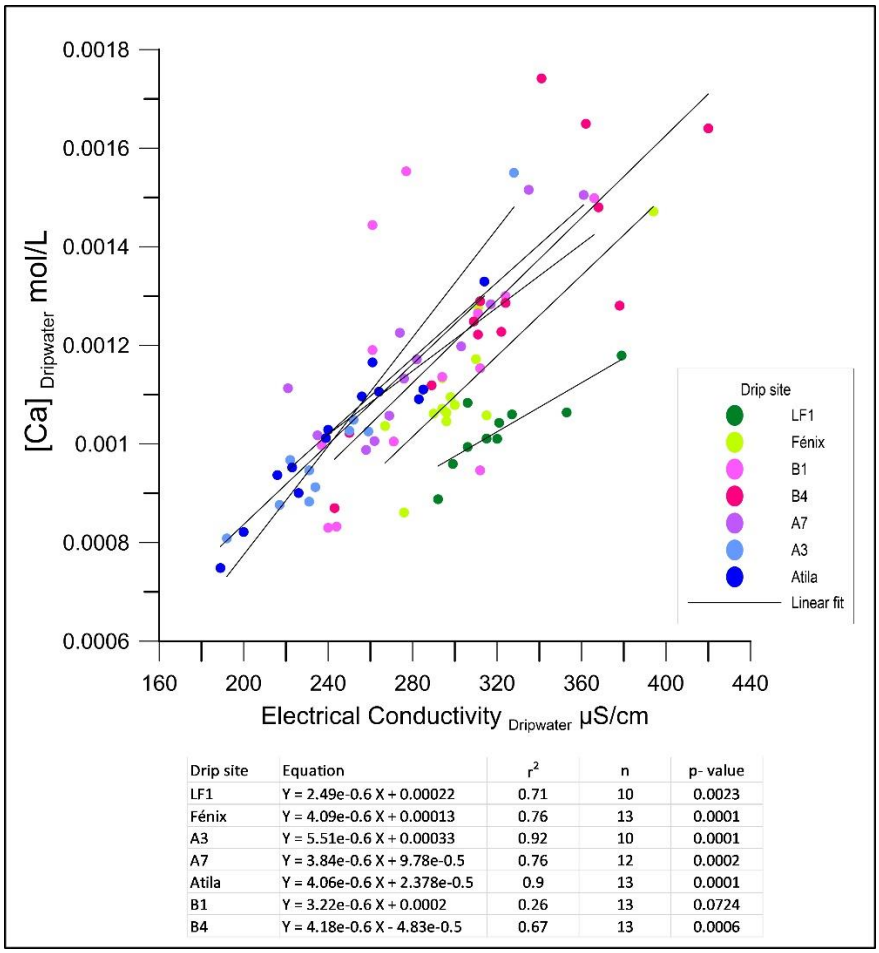

Drip site	Equation	r^2	n	p- value
LF1	Y = 2.49e-0.6 X + 0.00022	0.71	10	0.0023
Fénix	Y = 4.09e-0.6 X + 0.00013	0.76	13	0.0001
A3	Y = 5.51e-0.6 X + 0.00033	0.92	10	0.0001
A7	Y = 3.84e-0.6 X + 9.78e-0.5	0.76	12	0.0002
Atila	Y = 4.06e-0.6 X + 2.378e-0.5	0.9	13	0.0001
B1	Y = 3.22e-0.6 X + 0.0002	0.26	13	0.0724
B4	Y = 4.18e-0.6 X - 4.83e-0.5	0.67	13	0.0006

Fig. 3.6 Linear regressions for Ca concentration vs EC (D) for monthly drip water samples collected after June 2017 at Río Secreto Cave System. Linear regressions results are showed in a Table below plot with no outliers removed from the linear fit.

3.3.4 Prior Calcite Precipitation evidence in drip waters

Linear relationships between ln(Mg) and ln(Sr) and between ln(Sr) and ln(Ba) in drip waters are presented in Fig. 3.7. The regression slopes of ln(Mg/Ca) vs ln(Sr/Ca) for the 7 drip sites fit within error with the theoretical value from Sinclair (2012) and Wassenburg et al. (2020) to diagnose PCP i.e. ln(Mg/Ca) vs ln(Sr/Ca) slopes from 0.709 to1.45 (Fig. 3.7A). Removing from 5% to 15% of outliers in the data of sigle drip sites, it was also found a strong relationship between ln(Ba/Ca) vs ln(Sr/Ca) in all drip sites (Fig. 3.7); with slopes ranging from 0.68-0.87 in 5 drip sites (i.e. Atila, A7, B4, Fénix, LF1) while the slopes of A3 and B1 fit within error to that of the thermodynamic predicted value calculated by Bernal et al. (2016) of 1.02 ± 0.08 for PCP (Fig. 3.7B).

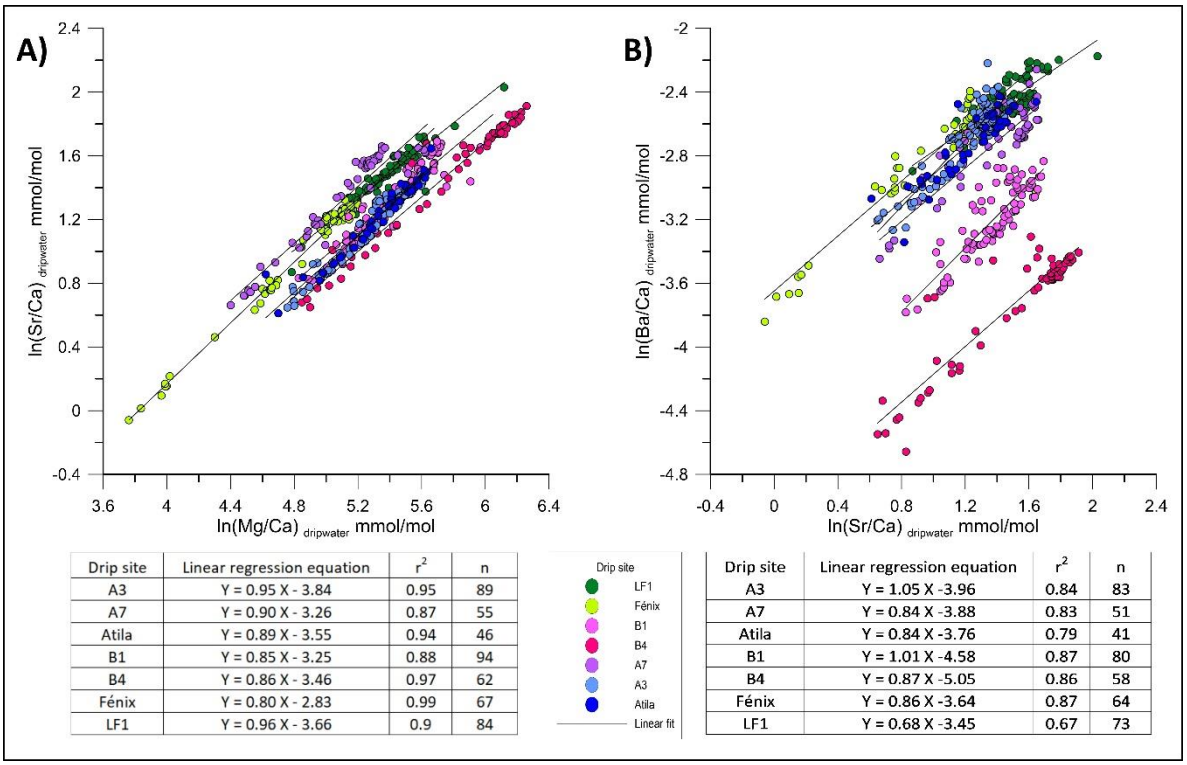

Drip site	Linear regression equation	r^2	n
A3	Y = 0.95 X - 3.84	0.95	89
A7	Y = 0.90 X - 3.26	0.87	55
Atila	Y = 0.89 X - 3.55	0.94	46
B1	Y = 0.85 X - 3.25	0.88	94
B4	Y = 0.86 X - 3.46	0.97	62
Fénix	Y = 0.80 X - 2.83	0.99	67
LF1	Y = 0.96 X - 3.66	0.9	84

Drip site	Linear regression equation	r^2	n
A3	Y = 1.05 X -3.96	0.84	83
A7	Y = 0.84 X -3.88	0.83	51
Atila	Y = 0.84 X -3.76	0.79	41
B1	Y = 1.01 X -4.58	0.87	80
B4	Y = 0.87 X -5.05	0.86	58
Fénix	Y = 0.86 X -3.64	0.87	64
LF1	Y = 0.68 X -3.45	0.67	73

Fig. 3.7 Linear regressions for ln(X/Ca) pairings for all drip water samples in the Río Secreto Cave System: A) is ln(Sr/Ca) and ln(Ba/Ca) and B) is ln(Ba/Ca) and ln(Sr/Ca) for 7 drips, with all concentrations in mmol/mol. All linear regressions have positive slope values, ranging from 0.80 to 0.96 for the ln(Sr/Ca) versus ln(Mg/Ca) in agreement within error to slopes identified as diagnostic of PCP (Sinclair et al. 2012). While the ln(Ba/Ca) versus ln(Sr/Ca) slopes for A3 and B1 are in agreement to that of the thermodynamic predicted value calculated by Bernal et al. (2016) of 1.02 ± 0.08 for PCP. Outliers of 5%-15% data of each drip site were removed in (B) to perform linear regressions.

Mg/Ca, Sr/Ca ratios and drip rates variability of dripwaters along with rainfall amount, CO_2 and temperature time series are presented in Fig. 3.8. Most Mg/Ca and Sr/Ca ratios of drip waters presented a slight seasonal variability synchronous with rainfall amount seasonality and according with PCP modulation. One exception is the seasonal invariate drip Fénix (Fig. 3.8). In some cases, it is possible to distinguish a 1-3 months lag in of trace elements ratios reponse to seasonal rainfall (Fig 3.8). For example, the peak rainfall in October 2014 is followed by a slight decrease in Mg/Ca and Sr/Ca ratios in November 2014, and coincident with a discharge peak at drip A3. This same peak rainfall was paired with a slight and concurrent decrease in Mg/Ca and Sr/Ca ratios during November 2014 at drips B1 and LF1 but in these drip sites the peak of discharge occurred before, during October 2014. This is consisten with the lag in drip discharge variability of Rio Secreto Cave since drip sites can present a lag rainfall by weeks to three months, and the lag is not constant over the time (See Fig. 1.6 and Section 1.4.5). Moreover, the epikarst water reservoirs can integrate from 3 to 15 months of accumulated rainfall (Section 2.5.2). Since PCP is considered to mainly reflect the epikarst humidity, then PCP is expected to also lag in the variability of trace element ratios of drip waters in response to incoming rainfall, that as mentioned for most cases is from 1 to 3 months in Río Secreto Cave.

This study includes the important transition from the drought of 2016, to an anomalosuly wet period starting Summer 2017. Section 2.4.1 elaborates that the third hydrological year of this study (June 2016-May 2017) received 53% of the historical mean annual precipiation, while the fourth hydrological (June 2017-May 2018) was the wettest documented in this study with >1500 mm/year. This transition out of dought is reflected as a conspicous decrease of Mg/Ca and Sr/Ca ratios in the 7 studied drip sites, incuding Fénix (Fig. 3.8). This change caused by an increase in Ca concentration (Fig. B.2) show that Mg/Ca and Sr/Ca ratios of Río Secreto cave drip waters preferentially respond to extreme hydrologycal dry-to-wet transitions. Hence, during the drougth, the drip Mg/Ca and Sr/Ca ratios has weak variation compared to preceeding baseline conditions. This is a similar behaviour to the $\delta^{18}O$ inertia observed in drip waters during drougth years (Section 2.5.3). This may happen because when normal rainfall amount seasonal varibility preveal during years. For example during 2014 and 2015, infiltration leads to similar PCP at a seasonal level on normal and dry years, and this results in very similar Ca concentrations at drip waters during years with average and drier hydrological conditions (Fig. B.2). However, significant larger amount of rainfall infiltrates can interrupt this inertia, because a water saturated epikast inhibits PCP leading to an increase in Ca concentration, and thus decrease in Sr/Ca an Mg/Ca ratios at drips waters. This shift in Sr/Ca and Mg/Ca may be reflected in stalagmites.

Notable occasional inverse variations between drips B1 and B4 for their Mg/Ca and Sr/Ca ratios, but specifically during the weekly sampling prior to June 2017 when aliquots were collected over 48-hr (Fig. 3.8). This is likely related to the sligth differences in residence times when sampling was discrete and at high resolution, compared to the time-averaging after June 2017 implicit with accumulated ~month drip water samples. The Mg/Ca and Sr/Ca variations are consistent for B1 and B4, and even their absolut values converged (Fig. 3.8). This "averaging" with the bulk ~monthly water sampling is also seen in the drip $\delta^{18}O$ compositions (Fig. 2.2); and it is in agreement with the homogeneization of Ca concentration of monthly bulk data and its relationship with EC described in Section 3.3.3.

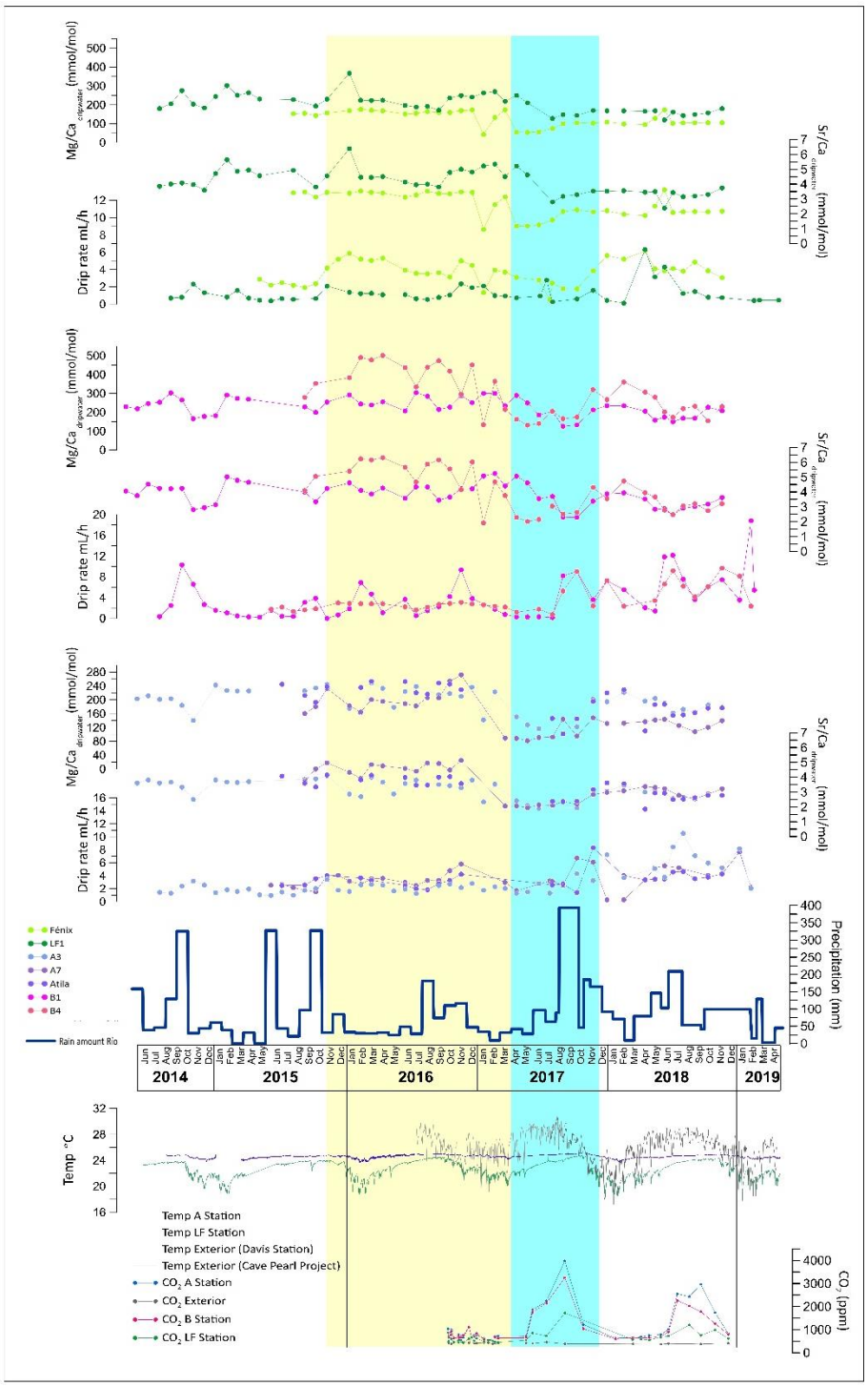

Fig. 3.8 Monthly data for Mg/Ca, Sr/Ca, and drip rate for the 2-3 drips at each of the Stations LF, B, and A (in ordered groupings). Note the Y2 axis for Sr/Ca. Environmental data (lower three panels) include monthly rainfall amount, cave and surface temperature and CO_2. Cave drip data spans June 2014 to November 2018 from Stations LF, B and A, with the weekly sampling prior to June 2017 aggregated to the shown monthly averages (See Section 3.2.3). A drought from December 2015 to April 2017 (yellow shading) included below average rainfall over 2016, followed by the transition to the wet Summer 2017 (blue shading), this transition was reeflected as a shift in Mg/Ca and Sr/Ca ratios in all drip waters.

CO_2 seasonal variability is also an important driver in the PCP process (Treble et al., 2016), particularly in caves where seasonal ventilation drives varibility in cave CO_2 (Wong et al., 2011). In Rio Secreto Cave, CO_2, temperature, and rainfall amount covary seasonally (Section 3.3.1), with summer maxima and winter minima over the dry season. Aditionally to the rapid response of X/Ca ratios to recharge (lagging a max of 3 months), the time covariance between high cave air CO_2 with larger rainfall amounts can lead to think that PCP may be reinforced by CO_2 variability.

One example of the possible reinforcement of PCP due to cave air CO_2 conditions is in Summer 2017, when the high rainfall does not allow dripwater degassification in the epikarst and cave air, as seen had high cave air CO_2 concentrations (Fig. 3.8). This leads to weaker PCP seen in the increase of drip Mg/Ca and Sr/Ca ratios (Fig. 3.8). Nonetheless, cave air CO_2 may play a role in the variability of Mg/Ca and Sr/ Ca of drip waters, even though it is not the main control. Cave air CO_2 was measured over slightly less than two years, and showed a seasonal covariation between cave air temperature and CO_2 (Section 3.3.1). Using cave air temperature as and indicator of cave air CO_2, it is possible to see that the slight decrease in Mg/Ca and Sr/Ca ratios in 6 to 7 dripwaters during December 2014-January of 2015, is likely related either to the recharge of October or December 2014, lagging 1 to 3 months, respectively. The observations can not be related to cave air CO_2 concentration, as the the cave air CO_2 is expected to be low and promoting PCP in the epikarst with cooler winter cave air, also leading to higher X/Ca ratios, (Fig. 3.8). Another example of this same phenomenon was Decembre 2015-February 2016 when the cave air temperature was low, but with rainfall in October to December 2015, the X/Ca ratios decreased (Fig. 3.8). This evidence indicates that the principal control in the modulation of drip waters X/Ca ratios variability is the moisture in the epikarst.

3.3.5 Farmed calcite growth and trace X/Ca variability

Glass plates were placed below 7 drip sites, however, continuous calcite growth throughout the whole sampling period at only three of them, A7, B4 and Fénix. Consequently, results from these three drip sites are reported.

Summary of growth rate for these three sites during January 2017-January 2019 is presented in Table 3.4 and the raw data is presented in Table B.4 (Appendix B).

During the 24 months of calcite farming from January 2017 to January 2019, drip hydrology at A7 and B4 was classified as seepage, whereas Fénix was classified as a seasonal drip (See Section 2.4.7 for drip classifications, and Fig. A in Appendix A). The average calcite growth rate was similar for the three sites at ~0.1 $(mg/cm^2)/d$ (Table 3.3). Fénix site had lower variability and range in calcite precipitation compared to A7 and B4 sites, even though Fénix had the most variable discharge during this sampling period. It can be inferred that drip rate and variability are not necessarily primary controls on calcite growth rate as has been found in other caves (Miorandi, et al 2010).

The growth rate in farmed calcite is usually found to be controlled by cave air CO_2 variability (Banner et al., 2007; Miorandi et al., 2010; Boch et al., 2011; Frisia et al., 2011; Tremaine et al., 2011; Pérez-Mejías et al. 2018) and also by the drip water chemistry and drip

rate (Stoll et al., 2015; Pérez-Mejías et al. 2018). However, this study did not find an obvious correlation between farmed calcite growth rate and cave air CO_2, drip rate, drip elemental concentrations, trace elements ratios, or any other analyzed parameter for the three individual farming sites (Table B.5 in Appendix B, Fig. 3.14). The absence of evidence may relate to the specific method used to quantify farmed calcite growth rates (See Fig. C.1 in Appendix C) or alternatively because it is necessary to have more data to assess this interpretation.

Table 3.4 Statistical summary of stable isotopic composition, calcite growth and X/Ca ratios for farmed calcite samples at 3 different sites of Río Secreto Cave. Raw data is on Table B.4 in Appendix B.

Farmed Calcite								
Sample/ Sampling period		Days of growth	Growth Rate (mg/cm^2)/d	$\delta^{13}C$ (‰ VPDB)	$\delta^{18}O$ (‰ VPDB)	Mg/Ca (mmol/mol)	Sr/Ca (mmol/ mol)	Ba/Ca (mmol/mol)
A7	AVG	46.0	0.127	-9.9	-5.0	2.5	0.47	0.0063
03/04/2017	SD	26.4	0.110	0.9	0.3	0.6	0.07	0.0008
17/01/2019	RANGE	97.0	0.375	2.7	1.0	2.0	0.25	0.0031
	MIN	4.0	0.008	-10.6	-5.4	1.6	0.39	0.0052
	MAX	101.0	0.383	-7.9	-4.4	3.5	0.64	0.0082
	n	13	11	9	10	12	12	12
B4	AVG	52.9	0.084	-11.9	-4.3	5.6	0.87	0.0065
12/01/2017	SD	27.8	0.096	0.8	0.3	0.7	0.07	0.0020
17/01/2019	RANGE	97.0	0.366	2.8	2.0	2.2	0.22	0.0071
	MIN	4.0	0.023	-13.3	-4.8	4.5	0.76	0.0054
	MAX	101.0	0.389	-10.7	-3.7	6.7	0.98	0.0125
	n	14	13	10	10	11	11	11
Fénix	AVG	49.0	0.112	-9.9	-5.6	1.5	0.29	0.0064
12/01/2017	SD	21.4	0.066	1.6	0.3	0.3	0.05	0.0006
14/01/2019	RANGE	73.0	0.191	6.8	1.2	1.0	0.16	0.0022
	MIN	22.0	0.013	-12.1	-6.3	0.9	0.22	0.0055
	MAX	95.0	0.204	-5.3	-5.1	1.9	0.38	0.0077
	n	15	15	14	14	14	14	14

Summary of the farmed calcite X/Ca ratios is presented in Table 3.4 and the raw data is presented in Supplementary Table B.4.

Mg/Ca, and Sr/Ca ratios of farmed calcite at the three drips had distinct and for Sr/Ca largely non-overlapping ranges of values. B4 drip had the highest Mg/Ca and Sr/Ca ratios, while Fénix site presented the lowest values (Fig. 3.9A, and Table 3.4). For Ba/Ca ratios, the 3 sites however have greatly overlapping ranges of values (Fig. 3.9B, and Table 3.4).

In contrast to the observed correlation between Mg/Ca and Sr/Ca ratios for drip waters (Fig. 3.6), no correlation was found for any of the individual farmed calcite sites (Fig. 3.9A).

There is, however, significant positive linear correlation between the ratios Mg/Ca and Sr/Ca for all farmed calcite collectively (r^2=0.86, p-value=0.0001; Fig. 3.9A). The slope of linear regression between ln(Mg/Ca) and ln(Sr/Ca) of all farmed calcite samples is 0.72 (r^2=0.87; n=37, p<0.0001; Fig. 3.9C) which is different from the slopes for drip sites when analyzed individually (Fig. 3.7A) but very similar to the slope of 0.73 (r^2=0.82; n=497, p<0.0001; Fig. 3.9C) for all drip waters collectively for all the sites of this study. The slopes of 0.7-0.8 reflect PCP as proposed for theoretical approaches for Sinclair et al. (2012) and Wassenburg et al. (2020).

Whereas drip water correlation between ln(Sr/Ca) and ln(Ba/Ca) was found at 7 sites (Fig. 3.7B), the farmed calcite samples correlated at 2 of the 3 sites. A7 and Fénix each had a significant positive linear correlation between Sr/Ca and Ba/Ca and very similar slopes (Fig. 3.9B). However, the slopes of ln(Sr/Ca) and ln(Ba/Ca) for farmed calcite at A7 and Fénix sites, despite the strong linear correlation and albeit the resulted slopes are similar to thoes of their corresponding drip waters (Fig. 3.9D and Fig. 3.7B), they did not exhibit the expected slope value for the theoretical approach for PCP by Bernal et al. (2016).

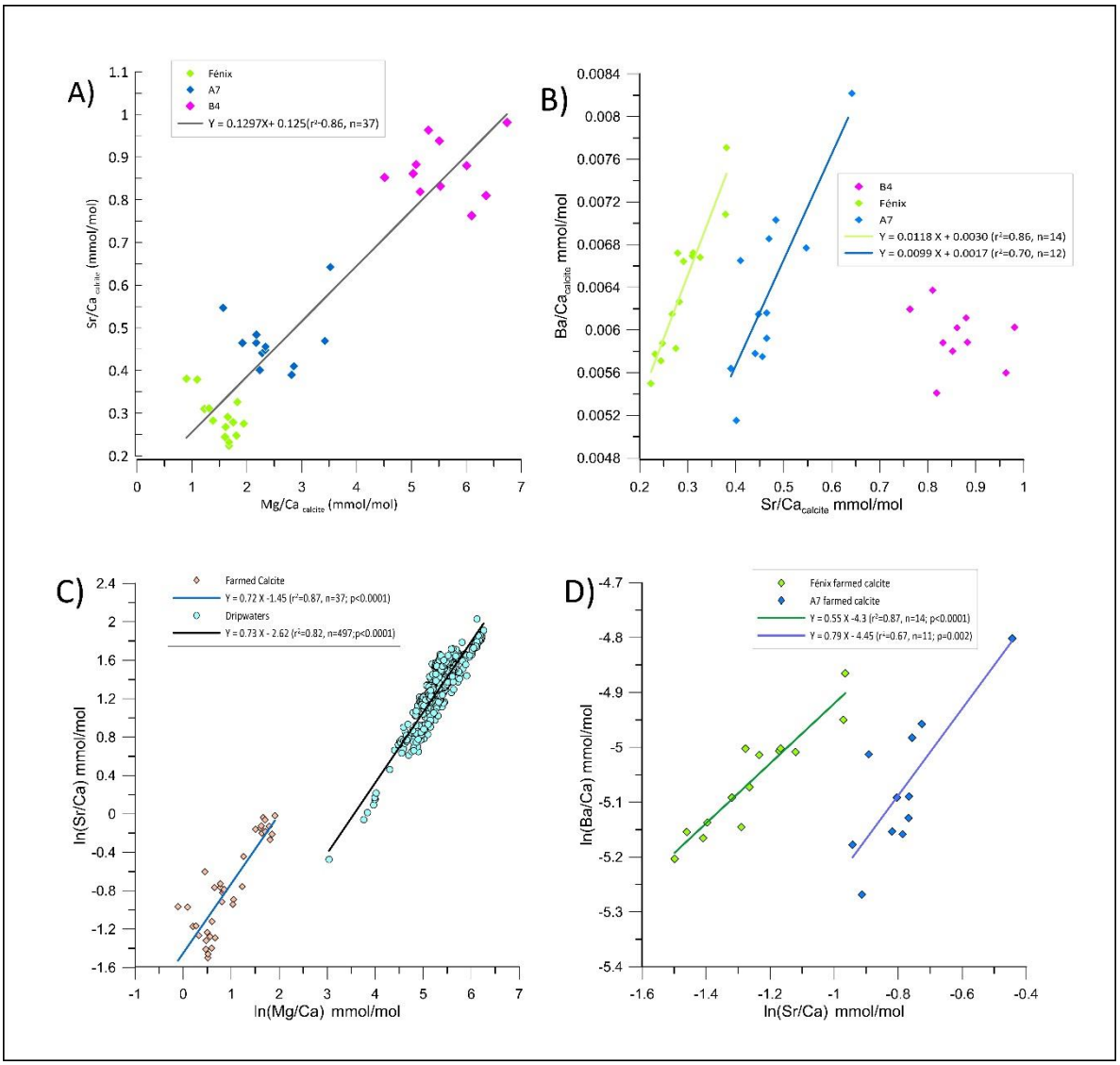

Fig. 3.9 Linear regressions for X/Ca pairings for farmed calcite in the Río Secreto Cave System**.** A) Mg/Ca to Sr/Ca for the 3 sites of A7, B4 and Fénix. B) Sr/Ca to Ba/Ca with linear fit for 2sites of A7 and Fénix. C) ln(Mg/Ca) and ln(Sr/Ca) for all drip water and farmed calcite samples. D) ln(Sr/Ca) and ln(Ba/Ca) for farmed calcite samples at A7 and Fénix individual sites.

The farmed calcite variability of Mg/Ca and Sr/Ca ratios presented some agreement with that of the coeval drip waters, especially for B4 site exhibiting higher values during winter in comparison to summer (Fig. 3.10). However, during farming calcite sampling period, the seasonality of drip Mg/Ca and Sr/Ca ratios was very slight (See Section 3.3.4).

The largest shift of drip Sr/Ca and Mg/Ca occurred at the transition from the 2016 drought to the summer 2017 wet season (Fig. 3.8), which unfortunately occurred prior to calcite farming (Fig. 3.10). The drought-to-wet transition was not observed, and more data will be needed to observe the transfer of X/Ca signals in corresponding calcite, which especially since the drip water Mg/Ca and Sr/Ca results suggest that calcite may preferentialy reflect the drought-to-wet transition (See Section 3.3.4).

The calculated distribution coefficients of D_{Mg}, D_{Sr} and D_{Ba} based on Río Secreto caveempirical data are presented in Table 3.5. It was found that all of the values are in good agreement with others from 19 cave and laboratory studies compiled by Tremaine and Froelich (2013) and values determined for other recent studies such as Day and Henderson, 2013, Drysdale et al., 2019 and Wassenburg et al., 2020 (Table 3.6). One exception is the D_{Ba} at site B4 with values higher than expected (Table 3.6). Notably, no significant relationship between D_{Mg} and cave air temperatures were found at any of the sites (Table B.5 in Appendix B), even though this has been previously reported (Day and Henderson, 2013; Wassenburg et al. 2020). This is likely due to the small temperature variability at Río Secreto cave, and in accordance to observations in similar cave environments Tremaine and Foelich (2013).

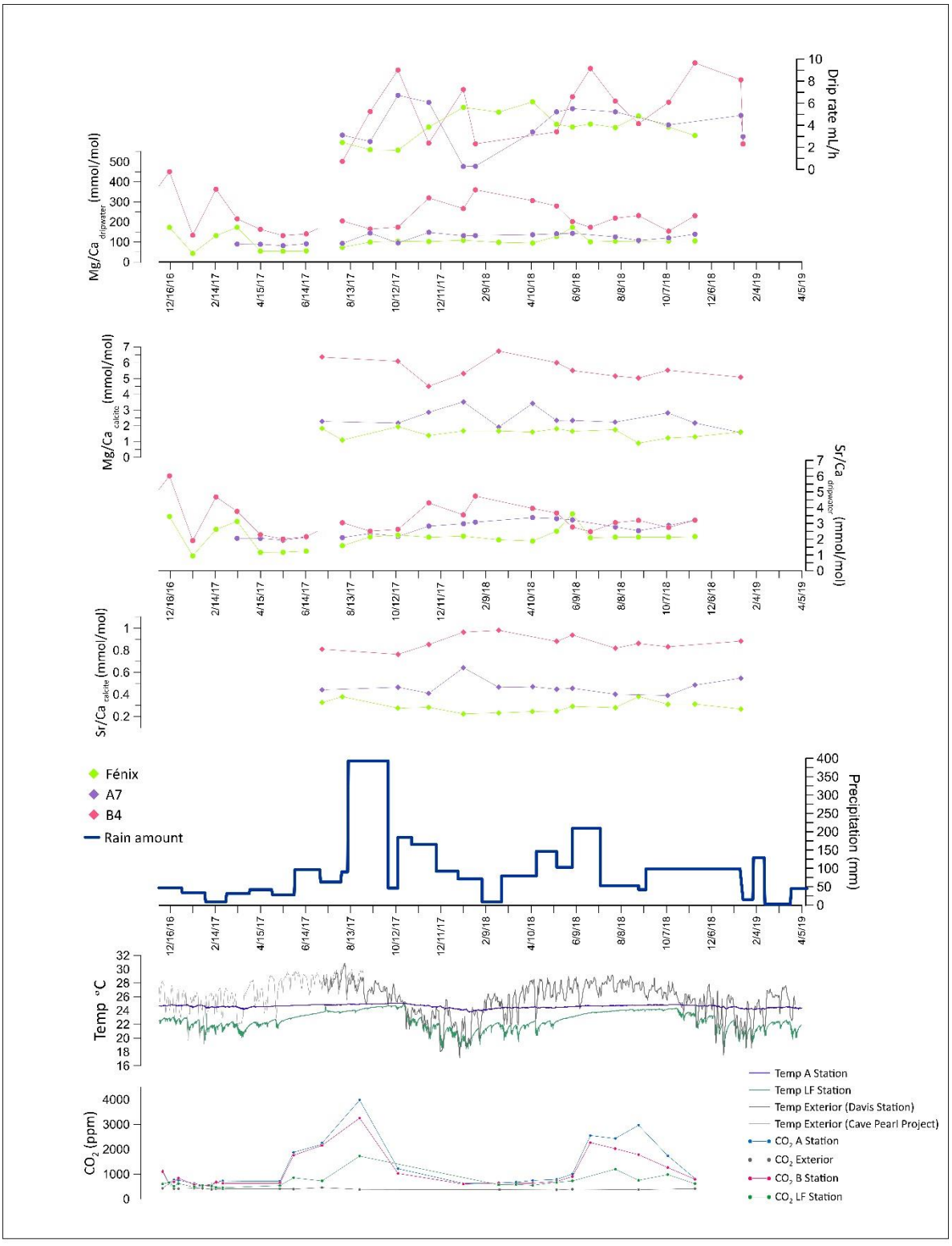

Fig. 3.10 Drip rates, Mg/Ca and Sr/Ca for each of dripwater and farmed calcite (top down) at Sites A7, B4 and Fénix in Río Secreto Cave. Weekly samples prior to June 2017 aggregated to the shown monthly averages. Environmental data (lower three panels) with rainfall amount, temperature and CO_2 measured in Río Secreto cave and on the surface.

Table 3.5 Statistical summary of distributtion coefficients calculated from drip water and farmed calcite empirical data at 3 different sites of Río Secreto Cave using Eq. 2 and reported in units of [mmol mol^{-1} /mmol mol^{-1}]. (See Section 3.2.3) Adittionally, statistically summary of ln(Sr/Ca) vs ln(Mg/Ca) slopes calculated using those distributtion coefficients is showed (sensu Sinclair et al. 2012). Full dataset and calculations provided on Table B.4 in Appendix B.

Site		D_{Mg}	D_{Sr}	D_{Ba}	D_{Sr}-1 / D_{Mg}-1	D_{Ba}-1 / D_{Sr}-1
Fénix	AVG	0.0157	0.14	0.12	0.869	1.032
	1SD	0.0059	0.05	0.04	0.052	0.062
	MIN	0.0086	0.08	0.07	0.751	0.969
	MAX	0.0334	0.27	0.25	0.928	1.228
	n	14	14	14	14	14
A7	AVG	0.0201	0.16	0.11	0.855	1.063
	1SD	0.0045	0.03	0.03	0.032	0.044
	MIN	0.0145	0.14	0.04	0.805	1.014
	MAX	0.0268	0.22	0.17	0.885	1.157
	n	11	11	11	11	11
B4	AVG	0.0262	0.28	0.38	0.742	0.847
	1SD	0.0091	0.06	0.17	0.052	0.205
	MIN	0.0141	0.20	0.23	0.652	0.383
	MAX	0.0438	0.38	0.75	0.813	1.098
	n	10	10	10	10	10

The correlation was not significant between D_{Sr} and calcite growth rate (Table B.5 in Appendix B), except for a weak but significant correlation at Fénix site (r^2=0.30, n=15, p-value>0.0001). Correlation between D_{Sr} and calcite growth rate has been detected in some studies (Tesorio and Pankow, 1996; Huang and Fairchild, 2001), albeit Day and Henderson (2013) suggested that for stalagmite-type growth conditions that are generally in a very low range over short time scales, the growth rate does not exert a significant effect on Sr incorporation.

Figure 3.11 show that, for all drip-sites that yield calcite precipitation, there are significant positive correlations between D_{Mg}, D_{Sr} and D_{Ba} with EC averaged values from drip waters coeval to farming samples in the three studied sites. This is consistent with the correlation found between Ca concentration and EC for monthly bulk drip water samples (Fig. 3.6)., but also suggest that the drip-water ionic strength exterts a control upon D, as expected from classical equilibrium thermodynamics (White, 2013). Moreover, because it was demonstrated previously that EC is modulated by Ca concentration (Fig. 3.6), this result implies that distribution of trace elements between dripwater and calcite is dependant on Ca concentration, and hence, the saturation state of the dripwater. A more extensive database of distribution coefficients and the corresponding solution chemistry showing a similar behaviour, and further calculations using PHREEQ (Parkhurst and Appelo, 2011) might help

demonstrate the thermodynamic effect of ionic strength upon the distribution of trace elements between dripwater and secondary calcite.

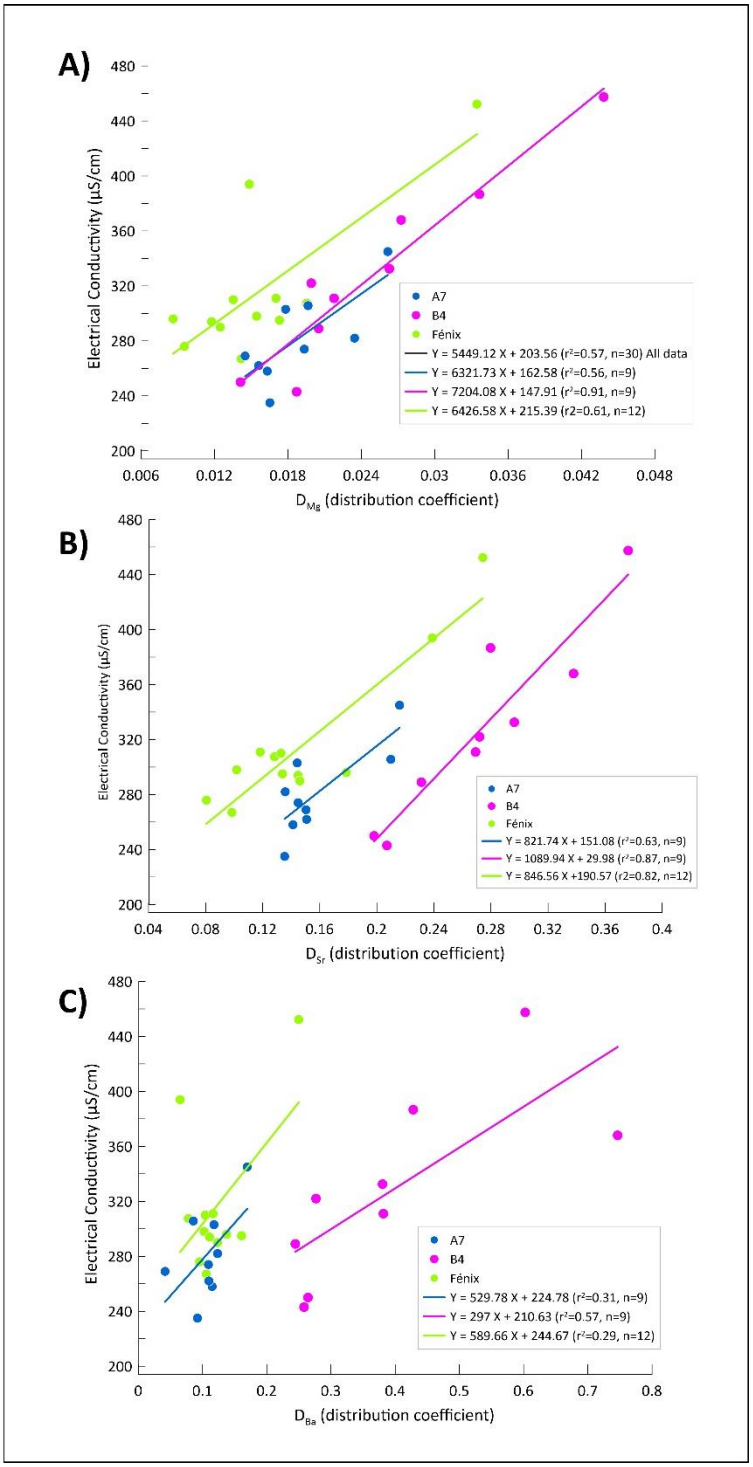

Fig. 3.11 Linear regressions between electrical conductivity (EC) and distribution coefficients (Dx) at drip sites A7, B4 and Fénix, for monthly drip water samples averaged to correspond to farmed calcite sampling period (See Section 3.2.3). Panels are Mg, Sr and Ba for A), B), and C) respectively.

Only in site B4, a weak relationship occurs between averaged drip Ca concentration and calcite growth rate (r^2=0.31, p-value=0.0001; Table B.5). As mentioned, neither the environmental parameters (temperature, CO_2, drip rate, rainfall amount), nor the water chemistry measured in this study can explain the variability of calcite growth of the different sites (See Table B.5), and this may be related either to the sampling methodology, or more data may be required to clarify the relationship.

In further exploration of PCP controlling trace elements composition in Río Secreto Cave, the slopes for ln(Sr/Ca) vs ln(Mg/Ca) and ln(Ba/Ca) vs ln(Sr/Ca) are calculated, but now using the obtained distribution coefficients for this study, and according to Sinclair et al. (2012; See Table 3.5). The slopes for ln(Sr/Ca) vs ln(Mg/Ca) for Fénix, A7 and B4, were 0.87 ± 0.05, 0.86 ± 0.03 and 0.74 ± 0.05 for respectively, and for ln(Ba/Ca) vs ln(Sr/Ca) slopes were 1.03 ± 0.06, 1.06 ± 0.04 and 0.85 ± 0.21. All slopes fit within error to the slope proposed to diagnose PCP by Sinclair (2012) of 0.88 ± 0.13 for ln(Sr/Ca) vs ln(Mg/Ca) and by Bernal et al. (2016) of 1.02 ± 0.08 for ln(Ba/Ca) vs ln(Sr/Ca).

Tremaine and Froelich (2013) observed that variations in drip water Sr/Ca and Mg/Ca ratios are preserved in contemporaneous speleothem calcite at sites with constant bedrock-mixing ratios, seen as constant Sr/Mg ratios. Hence, with constant drip Sr/Mg, coherent and in-phase variations in speleothem Sr/Ca and Mg/Ca may be confidently attributed to wet vs. dry rainfall amount (Tremaine and Froelich, 2013).

Moreover, in a coastal cave on Niue Island, strongly varying Sr/Mg ratios can be attributed to flow path variation and sea-salt input (Tremaine et al. 2016). The Niue drip waters are an order magnitude higher in both Mg and Sr concentrations compared to Río Secreto, but with comparable drip Mg/Sr ratios. In Río Secreto Cave, the the drip and farmed calcite Sr/Mg ratios were largely invariate for A7, B4 and Fénix sites over this study sampling period (Fig. 3.12). The small seasonal variability on Sr/Mg, can be attributed to changes in residence times per the interpretation of Tremaine et al. (2016), all variations remained less than one order of magnitude at the sites. Tremaine et al. (2016) indicate that more than an order of magnitude changes in Sr/Mg ratios reflect significant changes in sea-salt input for the particular very small and low topography island conditions of their study site. Also, the Ba/Sr of drip water and farmed calcite of A7, B4 and Fénix sites had low seasonal variability (Fig. 3.12). Hence, the low variable Sr/Mg ratios at drip waters and farmed calcite at Río Secreto is consistent with the previous demonstration that Sr/Ca and Mg/Ca are modulated by PCP and can be used as indicator of wet vs. dry rainfall amount.

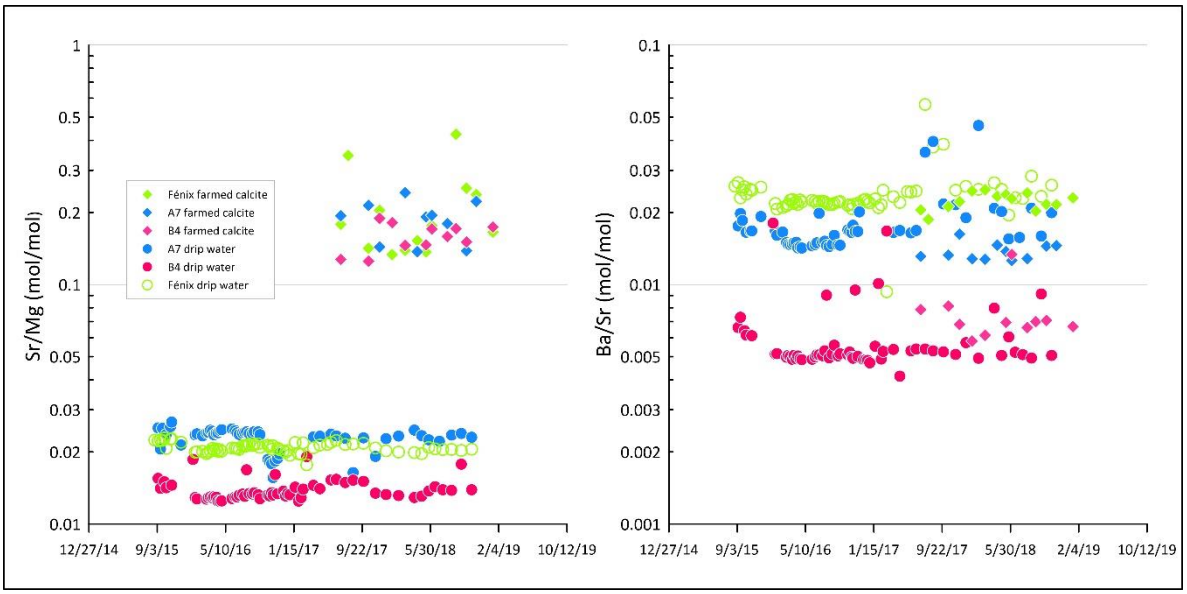

Fig. 3.12 Sr/Mg and Ba/Sr ratios (left and right, respectively) for all drip water samples and for farmed calcite at A7, B4 and Fénix sites in Río Secreto Cave. Y axes are in a log scale.

Table 3.6 Comparison of distributtion coefficients for Sr, Mg and Ba calculated forthis study and other 19 Laboratory inorganic calcite experiments and in situ calibrations. Most of them compiled by Tremaine and Froelich (2013) in their Table 4.

	D_{Mg}	Max Min	D_{Sr}	Max Min	D_{Ba}	Max Min
Cave studies						
Río Secreto cave Fénix site	0.0157	0.0334 0.0086	0.1400	0.27 0.08	0.1200	0.25 0.07
Río Secreto cave A7 site	0.0201	0.0268 0.0145	0.1600	0.22 0.14	0.1100	0.17 0.04
Río Secreto cave B4 site	0.0262	0.0438 0.0141	0.2800	0.38 0.20	0.3800	0.75 0.23
Wassenburg et al. (2020)	0.019	0.025 0.011	0.151	0.08 0.337		
Drysdale et al. (2019)	0.042 ± 0.002 (1 SD)		0.1 ± 0.007 (1 SD)		0.086 ± 0.076 (1 SD)	
Tremain and Froelich (2013)	0.031	0.041 0.019	0.092	0.112 0.061		
Holland et al. (1964)			0.14	0.16 0.12		
Gascoyne (1983)	0.035	0.057 0.013	0.13	0.298 0.088		
Huang and Fairchild (2001)	0.031	0.038 0.014	0.075	0.111 0.057		
Huang et al. (2001)	0.014	0.016 0.012	0.155	0.16 0.15		
Stern et al. (2005)	0.023		0.12			
Karmann et al. (2007)	0.023		0.059			
Fairchild et al. (2010)	0.0177	0.02 0.015	0.11	0.13 0.079		
Laboratory studies						
Holland et al. (1964b)			0.076	0.102 0.056		
Kitano et al. (1971)			0.081	0.4 0.08		
Katz et al. (1972), Katz (1973)	0.097	0.124 0.057	0.07	0.17 0.05		
Lorens (1978, 1981)			0.054	0.126 0.031		
Mucci and Morse (1983)	0.019	0.032 0.01	0.27	0.4 0.15		
Pingitore and Eastman (1984, 1986)			0.08	0.193 0.03		
Tesoriero and Pankow (1996)			0.021	0.14 0.02		
Gabitov and Watson (2006)			0.12	0.35 0.12		
Day and Henderson (2013)		0.029 0.012		0.3 0.12	0.11	0.12 0.1

3.3.6 Farmed calcite isotopic composition and $\delta^{18}O$ predicted values

Table 3.4 shows the summary of isotopic data for A7, B4 and Fénix sites and the raw data for each growth period is shown in Table B.4 in Appendix B.

The B4 farmed calcite had the highest average $\delta^{18}O$ of -4.3 ± 0.3 ‰ (n = 10; range = 2 ‰), while Fénix had the lowest average values for $\delta^{18}O$ (-5.6 ± 0.3 ‰, n = 14, range = 1.6 ‰). The relative values are reversed for average $\delta^{13}C$ values, with B4 being the lowest and also the least variable (-11.9 ± 0.8 ‰, n = 10, range =2.8‰), and now Fénix being less negative (-9.9 ± 1.6 ‰, n = 14) and more variable (range = 6.8 ‰). Average $\delta^{18}O$ and $\delta^{13}C$ values of the farmed calcite at site A7 were -5.0 ± 0.3 ‰ (n = 10; range =1.0 ‰) and -9.9 ± 0.9 ‰ (n = 10; range = 2.7 ‰), respectively.

Farmed calcite $\delta^{18}O$ is expected to be driven by temperature and the $\delta^{18}O$ composition of drip waters (Kim and O'Neil, 1997); in a cave with very low temperature variability as Río Secreto cave, $\delta^{18}O$ values in stalagmites-calcite are ultimately expected to reflect the "amount effect" of rainfall imprinted at various levels in the $\delta^{18}O$ composition of drip water as discussed in Chapters 1 and 2.

The extensively used paradigm in paleo rainfall reconstruction from stalagmites-calcite-$\delta^{18}O$ records, is the assumption that stalagmites are deposited near isotopic equilibrium conditions (Farichild and Baker, 2012; See Section 2.1). Fractionation processes that allow to define kinetic or equilibrium conditions during speleothem formation are still under debate (Riechelmann et al., 2013; Watkins et al., 2013; Hansen et al. 2019). Hendy (1971), suggested that a correlation between $\delta^{18}O$ and $\delta^{13}C$ and their progressive increase along individual growth layers in a stalagmite indicates disequilibrium isotopic fractionation, and this criterion known as the "Hendy Test" is widely used to test suitability of stalagmites for paleoclimatic reconstruction (Fairchild and Baker et al. 2012). However, other studies have found evidence that environmental variations can lead to axially covarying of $\delta^{18}O$ and $\delta^{13}C$ and that it is practically difficult to apply correctly in most cases, and therefore the Hendy test is not an infallible test for disequilibrium detection (Dorale and Liu, 2009). Laboratory experiments of inorganic calcite and/or under cave-analog conditions and theoretical calculations aiming to investigate equilibrium and kinetic fractionation of calcite precipitation have been performed (McCrea, 1950; Epstein et al., 1953; Emiliani, 1966; O'Neil et al., 1969; Kim and O'Neil, 1997;Fantidis and Ehhalt, 1970; Huang and Fairchild, 2001; Wiedner et al., 2008; Polag et al. 2010; Dietzel et al., 2009, Day and Henderson 2011; Affek and Zaarur, 2014; Hansen et al. 2019) and a few *in-situ* studies have reported results of isotopic fractionation between drip water and recent calcite precipitates (Desmarchelier et al., 2000; Plagnes et al., 2002; Genty et al., 2003; Genty, 2008; Mickler et al., 2004; Mangini et al., 2005; Guilfoyle, 2006; Coplen, 2007; Sinha et al., 2007; Boch, 2008; Zhang et al. 2008; Boch et al., 2009; Tremaine et al. 2011; Meyer et al., 2014; Riechelmann et al., 2013; Riechelmann et al., 2011; Van Rampelbergh et al., 2014; Feng et al. 2014; Pu et al. 2016; Pérez-Mejías., 2018). Some of these studies have proposed an empirical relationship for cave-stalagmites water–calcite $\delta^{18}O$ fractionation as a function of temperature.

This study presents calculations of the expected $\delta^{18}O$ values of farmed calcite from Rio Secreto based on the empirical equations presented below and the measured $\delta^{18}O$ composition of drip water and cave air temperature:

$1000 \ln \alpha = 2.78 (10^6 T^{-2}) - 2.89$ (O'Neil et al. 1969, Modified Friedman and O'Neil, 1977) Eq. 3

$1000 \ln \alpha = 18.03 (10^3 T^{-1}) - 32.17$ (Kim and O'Neil, 1997, Modified Kim et al., 2007) Eq. 4

$1000 \ln \alpha = 0.9521 (10^6 T^{-2}) + 18.03 (10^3 T^{-1}) - 21.56$ (Horita and Clayton, 2007) Eq. 5

$1000 \ln \alpha = 2.5733 (10^6 T^{-2}) - 0.869$ (Chacko and Deines, 2008) Eq. 6

$1000 \ln \alpha = 16.1 (10^3 T^{-1}) - 24.6$ (Tremaine et al., 2011) Eq. 7

$1000 \ln \alpha = 15.63 (10^3 T^{-1}) - 23.29$ (Affek and Zaarur, 2014) Eq. 8

$1000 \ln \alpha = 16.516 (10^3 T^{-1}) - 26.141$ (Hansen et al., 2019) Eq. 9

Results of measured and predicted $\delta^{18}O$ calcite values for A7, B4 and Fénix sites are presented in Table B.7 in Appendix B.

This study shows that most $\delta^{18}O$ farmed calcite values from Río Secreto falls within the relationships presented by two of the most recent studies: Affek and Zaarur, (2014) and Hansen et al. (2019) (Fig. 3.13). Río Secreto results agree with several studies based on *in situ* measurements e.g. McDemort et al. 2011; Tremaine et al. 2011), which have higher $\delta^{18}O$ calcite compositions than those predicted by laboratory studies (with the exception of the most recent ones by Affek and Zaarur (2014) and Hansen et al (2019) (See Tale B. 6 in Appendix B).

It has been demonstrated that various processes can lead to disequilibrium fractionation, such as PCP, due to progressive precipitation of speleothem calcite producing $\delta^{18}O$ enrichment with respect to ^{18}O (Hansen et al., 2019) and cave CO_2 variability affecting CO_2 degassing rates (Day and Henderson, 2011). Other parameters such as calcite precipitation rates and pH can also exert control on $\delta^{18}O$ fractionation (Day and Henderson, 2011; Watkins et al., 2014; Hansen et al., 2019). Although, Río Secreto cave has a seasonal ventilation reflected in cave CO_2 variability (See Section 3.3.1), farmed calcite $\delta^{18}O$ variability does not correlate statistically with CO_2 variability and calcite growth rates (Table B.5.) and as metioned above observed calcite isotopic values agree with those predicted from the equilibrium equations examined. Furthermore, the values that fall outside 'equilibrium' do not correspond to the lowest cave CO_2 (Fig. 3.13). Farmed calcite $\delta^{18}O$ of all sites showed very similar trend and amplitude variability (1SD) than coeval drip water (Fig. 3.13 and Table B.4 in Appendix B), revealing that low temporal scale changes in cave conditions (e.g. recharge, air temperature) can be recorded by the isotopic signals of farmed calcite.

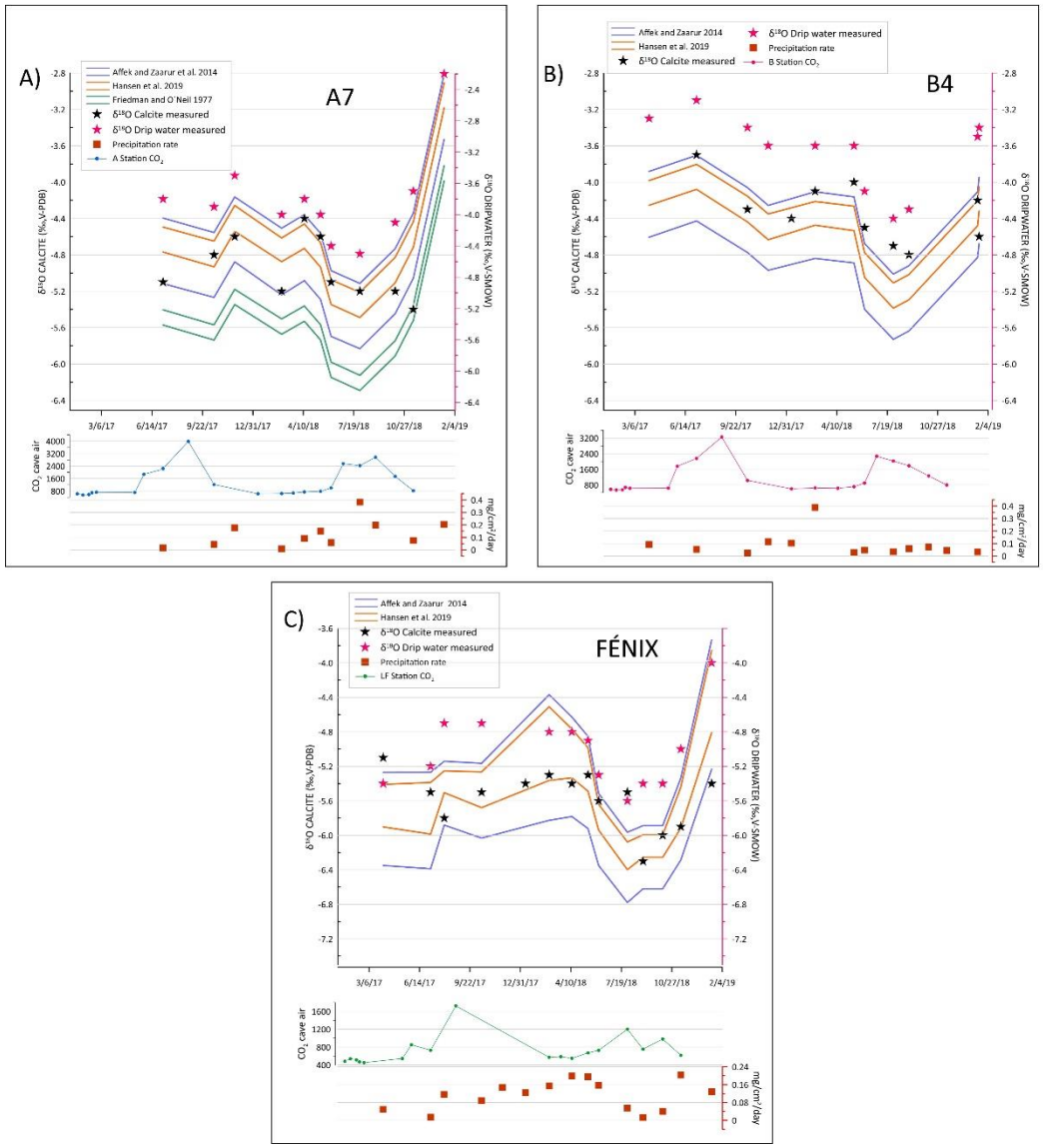

Fig. 3.13. The $\delta^{18}O$ values of farmed calcite, corresponding drip water samples, and edges for range values predicted by Eqs. 8 and 9 (See Section 3.3.6) from laboratory-based inorganic precipitation values under equilibrium conditions. Lower portion of each panel shows CO_2 of the cave air, and calcite growth rate.

A) Cave site A7, with CO_2 for Station A and adding Eq. 3 (See Section 3.3.6).

B) Cave site B4, with CO_2 for Station B.

C) Cave site Fénix, with CO_2 for Station LF.

Details of the predicted values and uncertainties provided in Table B.7.

Line width covers the uncertainties of Eqs. 3, 8 and 9 and the uncertainties due to the measured temperature variability for sampling period (2 SD).

3.3.7 $\delta^{18}O$ calcite correlations

In most cases, $\delta^{18}O$ values from farmed calcite of Río Secreto cave reflected dripwater $\delta^{18}O$ composition and temperature and in turn rainfall $\delta^{18}O$ composition (See Section 3.3.6). However, an influence of kinetic fractionation on calcite $\delta^{18}O$ may still exist. Calcite $\delta^{13}C$ can also reflect environmental processes within the soil including respiration and CO_2, and the epikarst and vadose zones including drip rates and cave ventilation (Fairchild and Baker, 2012). A control of calcite $\delta^{13}C$ also includes the ratio of C3 to C4 type of vegetation above the cave (Dorale et al., 1998; Webb et al., 2004; Burns et al., 2016) and the amount of degassing in the karst (Lachniet et al., 2004). Bedrock dissolution related to rainfall variability and PCP can also influence calcite $\delta^{13}C$ (Fairchild and Baker, 2012; Ridley et al., 2015; Hansen et al. 2019). Correlation between $\delta^{18}O$ and $\delta^{13}C$ has been also related with kinetic effects during rapid calcite precipitation (Hendy, 1971; Lachniet et al. 2014).

This study data shows the existence of a significant relationship between $\delta^{18}O$ and $\delta^{13}C$ of farmed calcite for the three monitored drip sites in Río Secreto cave (Fig. 3.15). Comparison of the measured $\delta^{18}O$ values of farmed calcite and the $\delta^{18}O$ values predicted under equilibrium conditions suggest agreement between this study and studies elsewhere (Section 3.3.6). This suggests that significant statistical correlation between $\delta^{18}O$ and $\delta^{13}C$ of farmed calcite is unlikely the result of kinetic fractionation.

On the other hand, calcite $\delta^{13}C$ is expected to show higher values near cave entrances and more depleted in the most isolated parts of the cave where ventilation is the weakest (Tremaine et al., 2011). The three stations or cave chambers studied in Río Secreto Cave have seasonal ventilation that leads to higher temperatures and CO_2 during the wet Summer of June to October, and lower temperatures and CO_2 during the dry Winter November to May (See Section 3.3.1), presenting the same temporal variability but different values among the three monitored chambers (Fig. 3.1). If CO_2 variability is the principal control of calcite $\delta^{13}C$, the chambers closest to each other (50 m apart) and most isolated would be expected to show similar calcite $\delta^{13}C$ values (i.e. Stations A and B) and different from those of the most ventilated chamber (i.e. Fénix in Station LF). The highest calcite $\delta^{13}C$ values were found at Fénix and A7 drip sites, located in the two more distant cave chambers (300 m apart) with different intra-annual temperature, different ventilation regimes and seasonal CO_2 amplitude variability (Table 3.1, Figs. 2.1 and 3.1). In contrast, site B4 presents the lowest average calcite $\delta^{13}C$ values (Table 3.3, Fig. 3.15) despite being intermediate in distance and relative ventilation regime. Furthermore, a comparison of seasonal calcite $\delta^{13}C$ variability between the low ventilation wet summer (June-October) versus high ventilation dry winter (November-May) does not suggest ventilation influences calcite $\delta^{13}C$ (Fig. 3.14).

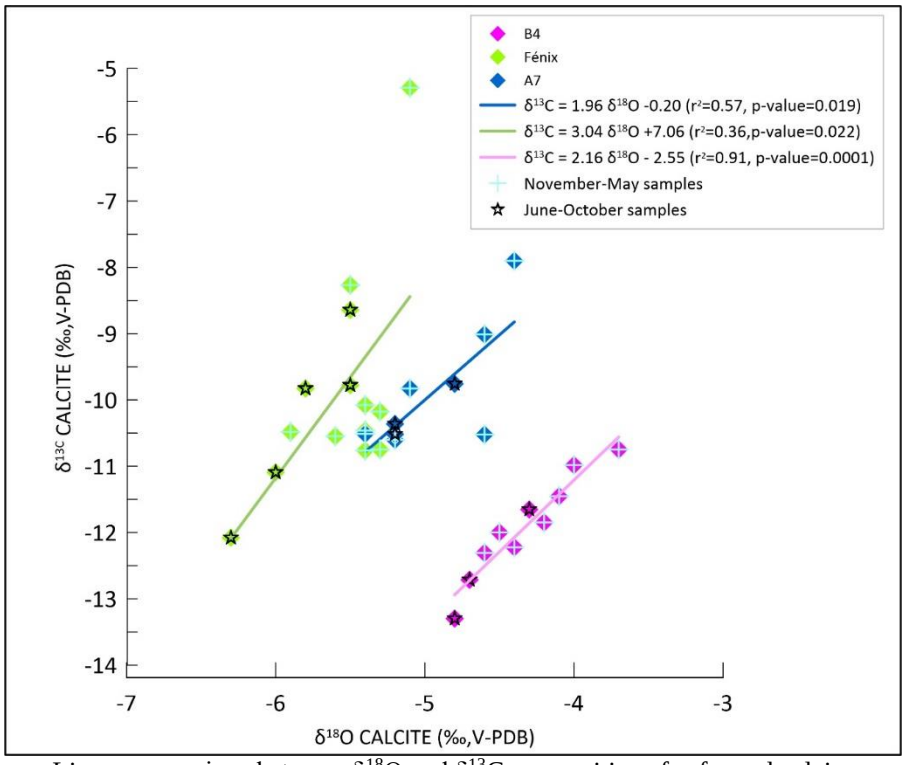

Fig. 3.14 Linear regressions between $\delta^{18}O$ and $\delta^{13}C$ compositions for farmed calcite samples for Sites A7, B4 and Fénix in Río Secreto Cave. Symbols coded for wet Summer season June-October that has higher CO_2 and temperature, and dry Winter season November-May that has lower CO_2 and temperature.

Tremaine et al. (2011) suggest that ventilation effects will be reflected as a calcite $\delta^{13}C$ vs $\delta^{18}O$ slope steeper relative to that corresponding to equilibrium conditions, based on a homogeneous aquatic reservoir of fixed isotopic composition under specific temperature (i.e. slope of 0.44). However, when they studied not a single sample but a whole cave in time and space, Tremaine et al. (2011) obtained similar $\delta^{13}C$ vs $\delta^{18}O$ slopes (~1.8) with a large offset of ~2‰ for $\delta^{13}C$ between farmed calcite presumably precipitated in carbon equilibrium with drip water, and farmed calcite precipitated in a strongly ventilated flow path. The present study shows similar $\delta^{13}C$vs $\delta^{18}O$ slopes of 2.16 and 1.96 for B4 and A7 sites respectively with an offset of ~2 ‰ for $\delta^{13}C$, while Fénix site presents a steeper slope of ~3 and an offset of only 1 ‰ relative to A7 drip site (Fig. 3.14). These results are incompatible with an effect of ventilation on calcite $\delta^{13}C$ and $\delta^{18}O$, because an offset is observed even between two poorly ventilated chambers that have temperature variations <1 ^{o}C over the course of the year.

In low latitude regions such as the Yucatan Península, where the vegetation has been consistent over recent time, stalagmite $\delta^{13}C$ can reflect effective rainfall amount and the drip hydrology, such as has been proposed for Belize (Ridley et al. 2015). Dry intervals would lead to PCP, increased bedrock carbon contributions and a reduction of soil organic matter remineralization, all contributing to less depleted drip water $\delta^{13}C$ values, and the opposite during wet periods. An enrichment of $\delta^{13}C$ associated to longer residence time, such as during persisting dry intervals, has also been demonstrated in cave-analog calcite precipitation experiments (Hansen et al. 2019).

Evidence presented in this study also suggests a link between rainfall variability and $\delta^{18}O$ of drip water and expected also in calcite (Section 2.5.3). Due to the above, and because the current evidence does not suggest that CO_2 or other processes are controlling the $\delta^{13}C$ values of farmed calcite, the most likely explanation for the strong relationship between $\delta^{18}O$ and $\delta^{13}C$ in farmed calcite is that both are reflecting hydrological variability (Fig. 3.15). It would be expected that a shift from drought to wet conditions will be recorded by those proxies (See Section 2.5.3). In this regard, only site B4 recorded a shift for $\delta^{18}O$ and $\delta^{13}C$ in the farmed calcite of -0.5‰ and -0.9 ‰ respectively, at the time of a change form dry to wet conditions corresponding with 166 mm for April-June 2017, and 569 mm for July-October 2017 (Table B.4 in Appendix B). The other two sites have higher rainfall integration times and lower isotopic variability in drip water compared to B4 (Section 2.5.2, Fig. 2.2), and A7 and Fénix presented higher isotopic inertia in their farmed calcite isotopic compositions for the mentioned dry to wet transition periods.

This study reports results from 21 to 24 months of calcite growth. It would be ideal to continue the monitoring effort to better understand the processes that control the transferring of proxy variability from drip waters to stalagmite calcite. Several lines of evidence presented indicate that PCP takes place in Río Secreto Cave and may be controlling Mg/Ca and Sr/Ca variability in both drip waters and calcite samples (Sections 3.3.4 and 3.3.5). Interestingly, a significant positive linear relationship between calcite Mg/Ca relative to both $\delta^{13}C$ and $\delta^{18}O$ support a strong connection between hydrological variability and PCP (Fig. 3.15). Moreover, in the case of calcite Mg/Ca relative to $\delta^{18}O$ there is a significant correlation based on comparing calcite samples by site individually and all the samples together (n=31; Fig. 3.15).

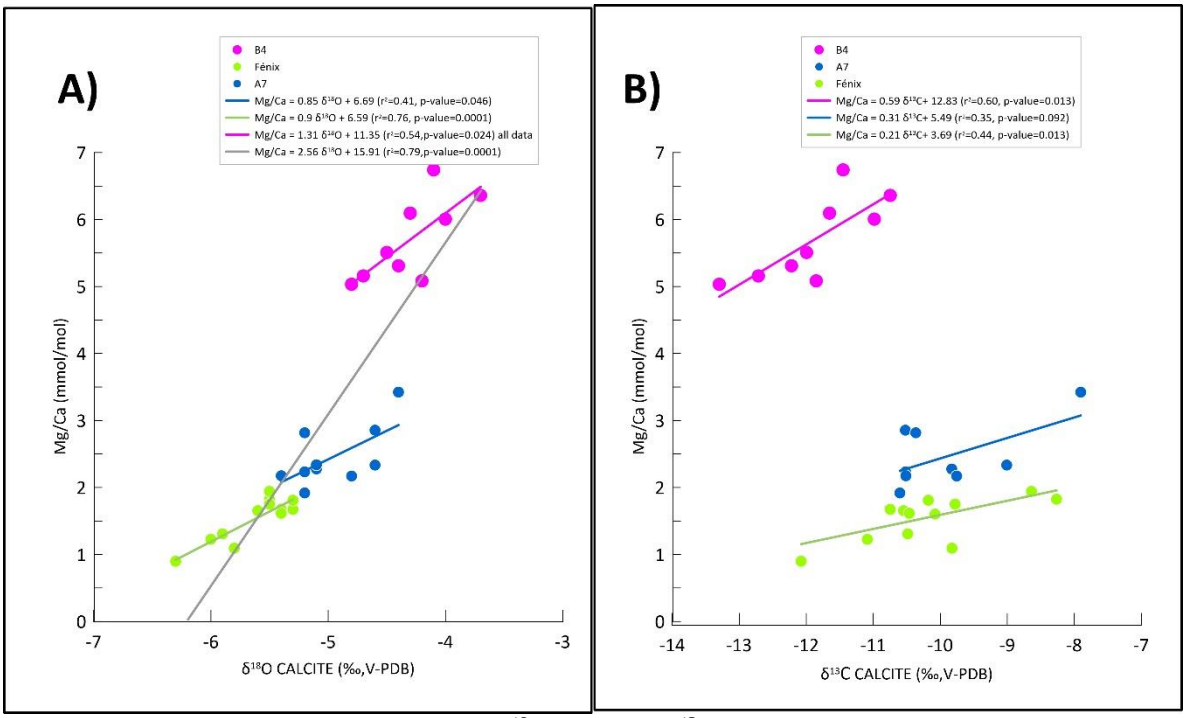

Fig. 3.15 Linear regressions between $\delta^{18}O$ (left) and $\delta^{13}C$ (right) compositions and Mg/Ca ratios for farmed calcite samples for Sites A7, B4 and Fénix in Río Secreto Cave. Panel A includes regression lines plotted for each individual sites and for all data for $\delta^{18}O$.

These results support the use of Mg/Ca, $\delta^{13}C$ and $\delta^{18}O$ in stalagmites from Río Secreto cave to reconstruct past rainfall variability as independent proxies. Mg/Ca, $\delta^{13}C$ and $\delta^{18}O$ values are imprinted on calcite-stalagmites through different processes, and this work suggest that all of them reflect hydroclimate variability. Despite the observed correlation between Mg/Ca and Sr/Ca, and between Sr/Ca and Ba/Ca in both drip waters and calcite (Section 3.3.4 and 3.3.5; Figs. 3.7 and 3.9), there is no positive correlation between calcite $\delta^{13}C$ and $\delta^{18}O$ relative to Sr/Ca and Ba/Ca ratios.

The only stalagmite from Río Secreto Cave at this time analyzed for both stable isotopes and trace elements ratios (i.e. Yáax Stalagmite) exhibited synchronous visible spikes in $\delta^{18}O$, $\delta^{13}C$ and Mg/Ca but not in Sr/Ca over certain time windows (Serrato-Marks et al., submitted). However, these four proxies were strongly correlated with each other when the stalagmite proxy records were examined at high resolution, suggesting that because the processes that control their variability are different, their degree of correlation with each other varies over the time (Serrato-Marks et al. submitted). However, it is very likely that when hydroclimate changes from very dry to wet conditions it would be possible to observe a coherent response in all of them (Section 3.3.4).

3.3.8 Implications for Paleoclimatic Reconstructions

In Río Secreto Cave several lines of evidence indicate that drip water Mg/Ca and Sr/Ca are influenced by water-rock interactions, likely reflecting hydrological variability controlling PCP. There is evidence that Ba/Ca may also potentially be a suitable proxy of hydroclimate variability from stalagmites. Drip water trace element ratios have minor seasonal variability in Mg/Ca and Sr/Ca, and the transition from a dry period to a wet season is more likely to be recorded by these proxies than a transition from a normal hydrological year to a dry period because of the inertia of epikarst discharge. These trace element results agree with those found for $\delta^{18}O$ drip water regarding their value as proxies to detect drought events in Río Secreto cave (Section 2.5.3).

The work with farmed calcite spanning 21 to 24 months of calcite growth did not allow to properly characterize the main controls of calcite growth rates in this cave. Results of farmed calcite $\delta^{18}O$ agree with those predicted for the thermodynamic relationships proposed, recently by Affek and Zaarur (2014) and Hansen et al. (2019). This is important considering that the three different chambers analyzed in this study exhibited a wide range of chemical, temperature, isotopic and air CO_2 conditions. Correlation between calcite $\delta^{18}O$ and $\delta^{13}C$ relative to calcite Mg/Ca ratios suggests that these different chemical tracers can be used as proxies of hydroclimate conditions, although they are also influenced by different dynamics within the epikarst. Future paleoclimatic records from stalagmites from the Yucatan Peninsula region would benefit from measurement of Mg/Ca, Sr/Ca and Ba/Ca to complement hydroclimate inferences from $\delta^{18}O$ and $\delta^{13}C$.

3.4 CONCLUSIONS

This study examined trace element variability of rainfall and drip water samples from 7 individual drip sites, distributed between 3 chambers, collected over a 50-month period at Río Secreto cave. The study also examined $\delta^{18}O$, $\delta^{13}C$ and X/Ca of farmed calcite samples collected from 7 sites over a ~24-month period.

Drip water from sites classified as seepage flow or seasonal drips both exhibited similar concentration and variability of Ca, Mg and Sr. Only 1 of 7 drip sites exhibited higher Mg and Sr water concentrations. Seasonal variability in drip water Mg/Ca and Sr/Ca is very low, and therefore may not be perceptibly transferred to stalagmites in most cases. Sea spray does not significantly influence the concentration of Mg and Sr of drip water, despite the cave being located ~5 km from the Caribbean Sea.

The transition from a drought period to a wet period was recorded, however, in all drip water sites in agreement with PCP. Slope of ln(Mg/Ca) vs ln(Sr/Ca) based on drip water data for individual drip sites, or by using the empirical distribution coefficients obtained in this study, agree with theoretical values indicating the occurrence of PCP (Sinclair et al. 2012; Wassenburg et al. 2020). Most drip water data from 7 drip sites suggested also potential for the use of Ba/Ca variability as a PCP proxy, based in the drip water slopes values of ln(Sr/Ca) vs ln(Ba/Ca) in which 2 of 7 drip sites are in agreement with the thermodynamic slope value proposed by Bernal et al. (2016) for PCP occurrence.

The calcite growth rates and drip water chemistry, drip rate and cave air CO_2 do not have a significant relationship. Farmed calcite $\delta^{18}O$ is near or within the expected $\delta^{18}O$ values predicted for the thermodynamic relationships proposed by Affek and Zaarur (2014) and Hansen et al. (2019).

Correlation between calcite $\delta^{18}O$, $\delta^{13}C$ and Mg/Ca ratios suggest they can be interpreted as hydroclimate proxies. This study provides a valuable *in situ* calibration of stalagmite proxies, in support of the interpretation of stalagmite hydroclimate records. This comprehensive monitoring work should be extended in order to improve our understanding of the controls of calcite growth, and to test the hypothesis posed by the results here presented.

REFERENCES

Affek H. P. and Zaarur S. (2014) Kinetic isotope effect in CO_2 degassing: Insight from clumped and oxygen isotopes in laboratory precipitation experiments. *Geochim. Cosmochim Acta* **143**, 319-330.

Baldini J., McDermot F., Baldini L., Otley C., Linge K., Clipson B. and Jarvis K. (2012) Identifying short-term and seasonal trends in cave drip water trace element concentrations based on a daily-scale automatically collected drip water dataset. *Chem. Geol.* **330**, 1–16.

Banner J. L., Guilfoyle A., James E. W., Stern L. A. and Musgrove M. (2007) Seasonal variations in modern speleothem calcite growth in Central Texas, U.S.A. *J. Sediment. Res.* **77**, 615–622.

Beddows P. A. and Mallon E. K. (2018). Cave Pearl data logger: A Flexible Arduino-based logging platform for long-term monitoring in harsh environments. *Sensors* **18**, 530.

Bernal J. P., Cruz F. W., Stríkis N. M., Wang X., Deininger M., Catunda M. C. A., Ortega-Obregón C., Cheng H., Edwards R. L. and Auler A. S. (2016) High-resolution Holocene South American monsoon history recorded by a speleothem from Botuverá Cave, Brazil. *Earth Planet. Sci. Lett.* **450**, 186–196 doi.org/10.1016/j.epsl.2016.06.008.

Boch R. (2008) Stalagmites from Katerloch Cave, Austria: Growth dynamics and high-resolution records of climate change. PhD thesis Leopold-Franzens University of Innsbruck, Austria. Available from: http://www.uibk.ac.at/geologie/staff/ boch_en.html

Boch R., Spötl C. and Frisia S. (2011) Origin and palaeoenvironmental significance of lamination in stalagmites from Katerloch Cave, Austria. *Sedimentology* **58**, 508-531. doi.org/10.1111/j.1365-3091.2010.01173.x

Boch R., Spötl C. and Kramers J. (2009) High-resolution isotope records of early Holocene rapid climate change from two coeval stalagmites of Katerloch Cave, Austria. *Quat. Sci. Rev.* 28, 2527–2538.

Breitenbach, S. F., Adkins, J. F., Meyer, H., Marwan, N., Kumar, K. K., & Haug, G. H. (2010). Strong influence of water vapor source dynamics on stable isotopes in precipitation observed in Southern Meghalaya, NE India. *Earth Planet. Sci. Lett.* **292**, 212-220.

Burns, S. J., Godfrey, L. R., Faina, P., McGee, D., Hardt, B., Ranivoharimanana, L., and Randrianasy, J. (2016). Rapid human-induced landscape transformation in Madagascar at the end of the first millennium of the Common Era. *Quat. Sci. Rev.***134**, 92–99. doi.org/10.1016/j.quascirev.2016.01.007

Cabadas-Báez, H., Solleiro-Rebolledo E., Sedov S., Pi-Puig T., Gama-Castro J. (2010) Pedosediments of karstic sinkholes in the eolianites of NE Yucatán: A record of Late Quaternary soil development, geomorphic processes and landscape stability. *Geomorphology* **122**, 323–337.

Chacko T. and Deines P. (2008) Theoretical calculation of oxygen isotope fractionation factors in carbonate systems. *Geochim. Cosmochim. Acta* **72**, 3642–3660.

Coplen, T.B., 2007. Calibration of the calcite–water oxygen-isotope geothermometer at Devils Hole, Nevada, a natural laboratory. *Geochim. Cosmochim. Acta* **71**, 3948–3957.

Day, C.C., Henderson, G.M. (2011). Oxygen isotopes in calcite grown under cave-analogue conditions. *Geochim. Cosmochim. Acta* **75**, 3956–3972.

Day, C.C., Henderson, G.M. (2013). Controls on trace-element partitioning in cave- analogue calcite. *Geochimica Cosmochim. Acta* 120, 612-627.

Desmarchelier J., Hellstrom J. and McCulloch M. (2006) Rapid trace element analysis of speleothems by ELA-ICP-MS. *Chem. Geol.* **231**, 102–117.

Dietzel, M., Tang, J., Leis, A., Köhler, S.J. (2009) Oxygen isotopic fractionation during inorganic calcite precipitation — Effects of temperature, precipitation rate and pH. *Chem. Geol.* **268**, 107–115.

Dorale J.A., Edwards R.L., Ito E. and GonzaHlez L.A. (1998). Climate and vegetation history of the midcontinent from 75 to 25 ka: A Speleothem record from Crevice Cave. Missouri, USA. *Science* **282**, 1871–1874.

Dorale J.A. and Liu Z. (2009) Limitations of Hendy test criteria in judging the paleoclimatic suitability of speleothems and the need for replication. *J. Cave Karst Stud.* **71**, 73–80.

Drysdale R. N., Zanchetta G., Baneschi I., Guidi M., Isola I., Couchoud I., Piccini L., Greig A., Wong H., Woodhead J. D., Regattieri E., Corrick E., Paul B., Spötl C., Denson E., Gordon J., Jaillet S., Dux F. and Hellstrom J. C. (2019) Partitioning of Mg, Sr, Ba, and U into a subaqueous calcite speleothem. *Geochim. Cosmochim. Acta* **264**, 67–91.

Duan W., Ruan J., Luo W., Li T., Tian L., Zeng G., Zhang D., Bai Y., Li J., Tao T., Zhang P., Baker A. and Tan M. (2016) The transfer of seasonal isotopic variability between precipitation and drip water at eight caves in the monsoon regions of China. *Geochim. Cosmochim. Acta* **183**, 250–266.

Emiliani, C. (1966). Isotopic paleotemperatures. *Science*, **154**, 851-857.

Epstein S., Buchsbaum R., Lowenstam H. and Urey H. C. (1953) Revised carbonate-water isotopic temperature scale. *Bull. Geol. Soc. Am.* **64**, 1315–1326.

Fairchild, I. J. and Treble, P. C. (2009). Trace elements in speleothems as recorders of environmental change. *Quat. Sci. Rev.* **28**, 449-468.

Fairchild, I.J. and Baker, A. (2012) *Speleothem Science*. John Wiley & Sons.

Fairchild I.J., Borsato A., Tooth A.F., Frisia S., Hawkesworth C.J., Huang Y., McDermott F. and Spiro B. (2000) Controls on trace element (Sr-Mg) compositions of carbonate cave waters: Implications for speleothem climatic records. *Chem. Geol.* **166**, 255-269.

Fantidis J. and Ehhalt D.H. (1970) Variations of the carbon and oxygen isotopic composition in stalagmites and stalactites: Evidence of non-equilibrium isotopic fractionation. *Earth Planet. Sci. Lett.* **10**, 136–144.

Feng W., Casteel R. C., Banner J. L. and Heinze-Fry A. (2014) Oxygen isotope variations in rainfall, drip-water and speleothem calcite from a well-ventilated cave in Texas, USA: Assessing a new speleothem temperature proxy. *Geochim. Cosmochim. Acta* **127**, 233–250.

Friedman I. and O'Neil J. R. (1977) Compilation of stable isotope fractionation factors of geochemical interest. *Geolog. Surv. Prof. Paper 440-KK*, pp. 117.

Frisi S., Fairchild I.J., Fohlmeister J., Miorandi R., Spötl C. and Borsato A. (2011) Carbon mass-balance modelling and carbon isotope exchange processes in dynamic caves. *Geochimica Cosmochim. Acta* **75**, 380–400.

Gabitov R. and Watson E. (2006) Partitioning of strontium between calcite and fluid. *Geochem. Geophys. Geosyst.* **7**, 1–12.

Gascoyne M. (1983) Trace-element partition coefficients in the calcite-water system and their paleoclimatic significance in cave studies. *J. Hydrol*. **61**, 213–222.

Genty D. (2008) Palaeoclimate research in Villars Cave (Dordogne, SW-France). *Int. J. Speleol*. **37**, 173–191.

Genty D., Blamart D., Ouahdi R., Gilmour M., Baker A., Jouzel J., Van-Exter S. (2003). Precise dating of Dansgaard-Oeschger climate oscillations in western Europe from stalagmite data. *Nature* **421**, 833–837.

Goede A., McCulloch M., McDermott F. and Hawkesworth C. (1998) Aeolian contribution to strontium and strontium isotope variations in a Tasmanian speleothem. *Chem. Geol.* **149**, 37–50.

Guilfoyle A. (2006) Temporal and spatial controls on cave water and speleothem calcite isotopic and elemental chemistry, Central Texas. Master's thesis, The University of Texas at Austin.

Hansen M., Scholz, D. Schöne, B. R. and Spötl C. (2019). Simulating speleothem growth in the laboratory: Determination of the stable isotope fractionation ($\delta^{13}C$ and $\delta^{18}O$) between H_2O, DIC and $CaCO_3$. *Chem. Geol.* **509**, 20-44.

Hendy C.H. (1971). The isotopic geochemistry of speleothems—I. The calculation of the effects of different modes of formation on the isotopic composition of speleothems and their applicability as palaeoclimatic indicators. *Geochim. Cosmochim. Acta* **35**, 801–824.

Horita J. and Clayton R. N. (2007) Comment on the studies of oxygen isotope fractionation between calcium carbonates and water at low temperatures by Zhou and Zheng (2003, 2005). *Geochim. Cosmochim. Acta* **71**, 3131–3135.

Huang Y., Fairchild I., Borsato A., Frisia S., Cassidy N., McDermott F. and Hawkesworth C. (2001) Seasonal variations in Sr, Mg, and P in modern speleothems (Grotta di Ernesto, Italy). *Chem. Geol*. **175**, 429–448.

Ishikawa M. and Ichikuni M. (1984) Uptake of sodium and potassium by calcite. *Chem. Geol*. **42**, 137–146.

Katz A. (1973) The interaction of magnesium with calcite during crystal growth at 25–90 ºC and one atmosphere. *Geochim. Cosmochim. Acta* **37**, 1563–1586.

Kennett D.J., Breitenbach S.F., Aquino V.V., Asmerom Y., Awe J., Baldini J.U., Bartlein P., Culleton B.J., Ebert C. and Jazwa C. (2012) Development and disintegration of Maya political systems in response to climate change. *Science* **338**, 788–791.

Kim S. T. and O'Neil J. R. (1997) Equilibrium and nonequilibrium oxygen isotope effects in synthetic carbonates. *Geochim. Cosmochim. Acta* **61**, 3461–3475.

Kim S. T., Mucci A. and Taylor B. (2007) Phosphoric acid fractionation factors for calcite and aragonite between 25 and 75 C: Revisited. *Chem. Geol.* **246**, 135–146.

Kowalczk A. J. and Froelich P. N. (2010) Cave air ventilation and CO_2 outgassing by radon-222 modeling: How fast do caves breathe? *Earth Planet. Sci. Lett*. **289**, 209–219.

Lachniet M. S., J. P. Bernal, Y. Asmerom, V. Polyak, and D. Piperno (2012) A 2400-yr Mesoamerican rainfall history links climate and cultural change in Mexico. *Geology* **40**, 259–26.

Lachniet M. S., Asmerom Y., Polyak, V. and Bernal J. P. (2017). Two millennia of Mesoamerican monsoon variability driven by Pacific and Atlantic synergistic forcing. *Quat. Sci. Rev.***155**, 100-113. https://doi.org/10.1016/j.quascirev.2016.11.012

Lambert J. and Aharon P. (2010) Oxygen and hydrogen isotopes of rainfall and dripwater at DeSoto Caverns (Alabama, USA): Key to understanding past variability of moisture transport from the Gulf of Mexico. *Geochim. Cosmochim. Acta* **74**, 846–861.

Lorens R. (1978) A study of biological and physical controls on the trace metal content of calcite and aragonite. PhD thesis. University of Rhode Island, USA.

Luo W., Wang S., Zeng G., Zhu X. and Liu W. (2014) Daily response of drip water isotopes to precipitation in Liangfeng Cave, Guizhou Province, SW China. *Quat. Int.* **349**, 153–158.

Mangini A., Spötl C. and Verdes P. (2005). Reconstruction of temperature in the Central Alps during the past 2000 yr from a $\delta^{18}O$ stalagmite record. *Earth Planet. Sci. Lett*. **235**, 741–751.

Mattey D. P., Fairchild I. J., Atkinson T. C., Latin J.-P., Ainsworth M. and Durell R. (2010) Seasonal microclimate control of calcite fabrics, stable isotopes and trace elements in modern speleothem from St Michaels Cave, Gibraltar. *Geolog. Soc., London, Spec. Publ*. **336**, 323–344.

McCrea, J.M. (1950). On the isotopic chemistry of carbonates and a paleotemperature scale. *J. Chem. Phys*. **18**, 849–857.

Medina-Elizalde M., Burns S.J., Lea D.W., Asmerom Y., von Gunten L., Polyak V., Vuille M. and Karmalkar A. (2010) High resolution stalagmite climate record from the Yucatán Peninsula spanning the Maya terminal classic period. *Earth Planet. Sci. Lett*. **298**, 255-262.

Medina-Elizalde M., Burns S.J., Polanco-Martinez J., Lases-Hernández F., Bradley R., Wang H. –C. and Shen C. –C. (2017) Synchronous precipitation reduction in the American Tropics associated with Heinrich 2. *Sci. Rep*. **7**, 11216.

Meyer K. W., Feng W., Breecker D. O., Banner J. L. and Guilfoyle A. (2014) Interpretation of speleothem calcite $\delta^{13}C$ variations: Evidence from monitoring soil CO_2, drip water, and modern speleothem calcite in central Texas. *Geochim. Cosmochim. Acta* **142**, 281–298.

Mickler, P.J., Banner, J.L., Stern, L., Asmerom, Y., Edwards, R.L., Ito, E. (2004). Stable isotope variations in modern tropical speleothems: Evaluating equilibrium vs. kinetic isotope effects 1. *Geochim. Cosmochim. Acta* **68**, 4381–4393.

Miorandi R., Borsato A., Frisia S., Fairchild I. J. and Richter D. K. (2010) Epikarst hydrology and implications for stalagmite capture of climate changes at Grotta di Ernesto (NE Italy): results from long-term monitoring. *Hydrol. Process*. **24**, 3101– 3114.

Mischel S.A., Scholz D., Spötl C., Jochum K.P., Schröder-Ritzrau A. and Fiedler S. (2016). Holocene climate variability in central Germany and a potential link to the polar North Atlantic: A Replicated record from three coeval speleothems. *The Holocene* **27**, 509–525.

Mucci A. and Morse J. (1983) The incorporation of Mg2+ and Sr2+ into calcite overgrowths: influences of growth rate and solution composition. *Geochim. Cosmochim. Acta* **47**, 217–233.

Mucci A. and Morse J. (1990) Chemistry of low-temperature abiotic calcites: Experimental studies on coprecipitation, stabil- ity and fractionation. *Rev. Aquat. Sci*. **3**, 217–254.

O'Neil, J.R., Clayton, R.N., Mayeda, T.K. (1969). Oxygen isotope fractionation in divalent metal carbonates. *J. Chem. Phys*. **51**, 5547–5558.

Parkhurst D. and Appelo C. A. J. (2011). PHREEQC (Version 3)—A computer program for speciation, batch-reaction, one-dimensional transport, and inverse geochemical calculations. *Water Resources Div., Denver, CO*.

Perez-Mejias C., Moreno A., Sancho C., Bartolome M., Stoll H.M., Osacar M.C., Cacho I. and Delgado-Huertas A. (2018) Transference of isotopic signal from rainfall to dripwaters and farmed calcite in Mediterranean semi-arid karst. *Geochim. Cosmochim. Acta*, **243**, 66–98.

Perry E., Paytan A., Pedersen B. and Velazquez-Oliman G. (2009). Groundwater geochemistry of the Yucatan Peninsula, Mexico: constraints on stratigraphy and hydrogeology. *J Hydrol*, **367**, 27-40.

Plagnes V., Causse C., Genty D., Paterne M. and Blamart D. (2002). A discontinuous climatic record from 187 to 74 ka from a speleothem of the Clamouse Cave (south of France). *Earth Planet. Sci. Lett*. 20, 87-103.

Polag D., Scholz D., Mühlinghaus C., Spötl C., Schröder-Ritzrau A., Segl M. and Mangini A. (2010). Stable isotope fractionation in speleothems: laboratory experiments. *Chem. Geol*. **279**, 31–39.

Pu J., Wang A., Shen L., Yin J., Yuan D. and Zhao H. (2016) Factors controlling the growth rate, carbon and oxygen isotope variation in modern calcite precipitation in a subtropical cave, Southwest China. *J. Asian Earth Sci*. **119**, 167–178.

Ridley H.E., Asmerom Y., Baldini J.U.L., Breitenbach S.F.M., Aquino V.V., Prufer K.M., Culleton B.J. Polyak V., Lechleitner F.A., Kennett D.J., Zhang M., Marwan N., Macpherson C.G., Baldini L.M., Xiao T., Peterkin J.L., Awe J. and Haug G.H. (2015). Aerosol forcing of the position of the intertropical convergence zone since ad1550. *Nat. Geosci*. **8**, 195–200.

Riechelmann, D.F.C., Deininger, M., Scholz, D., Riechelmann, S., Schröder-Ritzrau, A., Spötl, C., Richter, D.K., Mangini, A., Immenhauser, A. (2013). Disequilibrium carbon and oxygen isotope fractionation in recent cave calcite: Comparison of cave precipitates and model data. Geochim. Cosmochim. Acta 103, 232–244.

Riechelmann, D.F.C., Schröder-Ritzrau, A., Scholz, D., Fohlmeister, J., Spötl, C., Richter, D.K., Mangini, A. (2011). Monitoring Bunker Cave (NW Germany): A Prerequisite to interpret geochemical proxy data of speleothems from this site. *J. Hydrol*. **409**, 682–695.

Scholz D., Frisia S., Borsato A., Spötl C., Fohlmeister J., Mudelsee M., Miorandi R. and Mangini, A. (2012) Holocene climate variability in north-eastern Italy: Potential influence of the NAO and solar activity recorded by speleothem data. *Clim. Past* **8,** 1367–1383.

Sedov S., Solleiro-Rebolledo, E. Fedick, S. L. Pi-Puig T., Vallejo-Gómez E. and de Lourdes Flores-Delgadillo M. (2008) Micromorphology of a soil catena in Yucatán: Pedogenesis and geomorphological processes in a tropical karst landscape. In *New trends in soil micromorphology* (pp. 19-37). Springer, Berlin, Heidelberg.

Serrato-Marks et al. (submitted) Evidence for decreased precipitation variability in the Yucatán Peninsula during the mid-Holocene doi.org/10.1002/essoar.10502455.1

Shevenell L. and McCarthy J.F. (2002) Effects of precipitation events on colloids in a karst aquifer. *J Hydrol* **255** (1–4), 50–68.

Sinclair D. J. (2011) Two mathematical models of Mg and Sr partitioning into solution during incongruent calcite dissolution Implications for dripwater and speleothem studies. *Chem. Geol*. **283**, 119–133.

Sinclair D. J., J. L. Banner, F. W. Taylor, J. Partin, J. Jenson, J. Mylrole, E. Goddard, T. Quinn, J. Jocson, and B. Miklavic (2012) Magnesium and strontium systematics in tropical speleothems from the Western Pacifi. *Chem. Geol.* **294**, 1– 17. doi:10.1016/j.chemgeo.2011.10.008

Stoll H., Mendez-Vicente A., Gonzalez-Lemos S., Moreno A., Cacho I., Cheng H. and Edwards R. L. (2015) Interpretation of orbital scale variability in mid-latitude speleothem $d^{18}O$: Significance of growth rate controlled kinetic fractionation effects. *Quat. Sci. Rev*. **127**, 215–228.

Tesoriero A. and Pankow J. (1996) Solid solution partitioning of Sr^{2+}, Ba^{2+}, and Cd^{2+} to calcite. *Geochim. Cosmochim. Acta* **60**, 1053–1063.

Treble P., Chappell J. and Shelley J. (2005) Complex speleothem growth processes revealed by trace element mapping and scanning electron microscopy of annual layers. *Geochim. Cosmochim. Acta* **69**, 4855–4863.

Treble P., Shelley J. and Chappell J. (2003) Comparison of high resolution sub-annual records of trace elements in a modern (1911–1992) speleothem with instrumental climate data from southwest Australia. *Earth Planet. Sci. Lett*. **216**, 141–153.

Treble P. C., Fairchild I. J., Griffiths A., Baker A., Meredith K. T., Wood A. and McGuire E. (2015). Impacts of cave air ventilation and in-cave prior calcite precipitation on Golgotha Cave dripwater chemistry, southwest Australia. Quaternary Science Reviews, 127, 61-72.

Tremaine D. M. and Froelich P. N. (2013) Stalagmite trace element signatures: A hydrologic geochemical study of modern cave dripwaters and farmed calcite. *Geochim. Cosmochim. Acta* **121**, 522–545.

Tremaine, D. M., D. J. Sinclair, H. M. Stoll, M. Lagerström, C. P. Carvajal and R. M. Sherrell (2016) A two-year automated dripwater chemistry study in a remote cave in the tropical south Pacific: Using [Cl-] as a conservative tracer for seasalt contribution of major cations. *Geochim. Cosmochim. Acta* **184**, 289– 310, doi:10.1016/j.gca.2016.03.029.

Tremaine D.M., Froelich P.N. and Wang Y. (2011) Speleothem calcite farmed in situ: Modern calibration of $\delta^{18}O$ and $\delta^{13}C$ paleoclimate proxies in a continuously-monitored natural cave system. *Geochim. Cosmochim. Acta* **75**, 4929–4950.

Van Rampelbergh, M., Verheyden, S., Allan, M., Quinif, Y., Keppens, E., Claeys, P. (2014). Monitoring of a fast-growing speleothem site from the Han-sur-Lesse cave, Belgium, indicates equilibrium deposition of the seasonal $\delta^{18}O$ and $\delta^{13}C$ signals in the calcite. *Clim. Past* **10**, 1871–1885.

Wassenburg J. A., Riechelmann, S., Schröder-Ritzrau, A., Riechelmann, D. F. C., Richter, D. K., Immenhauser, A., Terente, M., Constantin, S., Hachenberg, A., Hansen, M. and Scholz, D. (2020). Calcite mg and Sr partition coefficients in cave environments: Implications for interpreting prior calcite precipitation in speleothems. *Geochim. Cosmochim. Acta* **269**, 581–596. https://doi.org/10.1016/j.gca.2019.11.011

Watkins J.M., Nielsen L.C., Ryerson F.J. and DePaolo D.J. (2013). The influence of kinetics on the oxygen isotope composition of calcium carbonate. *Earth Planet. Sci. Lett.* **375**, 349–360.

White, W. M. (2013). *Geochemistry*. John Wiley & Sons.

Wiedner E., Scholz D., Mangini A., Polag D., Mühlinghaus C. and Segl M. (2008) Investigation of the stable isotope fractionation in speleothems with laboratory experiments. *Quat. Int*. **187**, 15–24.

Williams P. W. (2008), The role of the epikarst in karst and cave hydrogeology: A review. *Int. J. Speleol.* **37**, 1–10.

Wong C.I., Banner J.L. and Musgrove M. (2011). Seasonal dripwater Mg/Ca and Sr/Ca variations driven by cave ventilation: Implications for and modeling of speleothem paleoclimate records. *Geochim. Cosmochim. Acta* **75**, 3514-3529.

Zhan L., Chen J. and Zhang S. (2016). Spatial and temporal characteristics of 2H and ^{18}O in the basin of Dongting Lake: Impact of monsoon precipitation. *J. Radioanal. Nucl. Chem*. **307**, 479-490.

Zhang R., Schwarcz H. P., Ford D. C., Schroeder F. S. and Beddows P. A. (2008) An absolute paleotemperature record from 10 to 6 ka inferred from fluid inclusion D/H ratios of a stalagmite from Vancouver Island, British Columbia, Canada. *Geochim. Cosmochim. Acta* **72**, 1014–1026

CONCLUSION AND PERSPECTIVE

This work presents a comprehensive long term *in-situ* calibration work to understand the hydrological controls on the variability of various proxies used to perform paleoclimatic reconstructions from stalagmites. This study reports results from a five-year monitoring effort that included quantification of various physicochemical variables that have the potential to control the formation of stalagmites in the Río Secreto cave located in the northeastern coast of the Yucatan Peninsula. The project included several research stages that resulted from the natural evolution of the data-based knowledge generated progressively from this monitoring work. This thesis is organized according to the narrative that followed this evolution. The sequence of this thesis chapters reflect the response to questions that led to new ones and that needed to be answered even at the expense of modifying the sampling protocol in order to best adjust it to the demands of the problem. For example, the first years of monitoring of environmental variables within the cave allowed us to observe that the different cave chambers or stations studied presented differences in the air temperature of the cave and that the seasonal air temperature variability of the cave was coupled to the surface air temperature variability, which implied seasonal differences in the degree of gas exchange with the surface (ventilation) and among the studied sites that were located at different distances form the cave entrance. These observations triggered the measurement of CO_2 variability in the cave air and on the surface in October 2016, which then allowed improving of understanding of processes that may be affected by it, for example; Prior Calcite Precipitation.

In Chapter 1, the results of the first three years of monitoring of stable isotopic compositions of rain, dripping water and groundwater were analyzed and their paleoclimatic implications fully explored. In particular, an important finding reported in Chapter 1 is the first empirical evidence of the existence of an "amount effect" on a seasonal scale in the Yucatan Peninsula; essential to support paleorainfall reconstruction from stalagmites. Additionally, this chapter examines the role of drip water integration of the rainfall isotopic signal, qualitatively, and the implications of epikarst water reservoir size for the detection of the isotopic signals of drought and tropical cyclone events. Analyzing up to 16 drip sites in this period, it was found that a drip site labeled as LF1 recorded closely the isotopic amplitude

variability of rainfall at a monthly scale and this was an unprecedented result regarding what was reported in available literature and it made this drip site especially promising for the reconstruction of short-lived meteoric events such as tropical cyclones (TCs). However, this site also had a bias towards enriched isotopic values and due to the type of discrete sample drip water collection carried out during the first 3 years, it was not possible to determine if this bias was caused by the sampling method or by some other process, such as evaporation. A crucial finding reported in Chapter 1 with implications for water management in the Yucatan Peninsula and other regions with similar karst topography, relates to evidence that evaporation plays a negligible role on the effective recharge of groundwater and aquifers, despite that most of this region experiences a deficit of precipitation annually.

In Chapter 2, I shifted the sampling protocol to collect continuous water samples in order to be able to calculate an amount-weighted isotopic composition of drip water and test the hypothesis that the isotopic composition of LF1 reflected evaporation on the surface or the sampling protocol. This new sampling protocol also enabled to examine the role of discrete versus continuous water sampling in the characterization of the annual amount-weighted isotopic composition of drip water, which is important because most calibration studies use one or the other; and the results here obtained revealed that if the discrete sampling is carried out at high temporal resolution and this resolution is higher than the rainfall integration time by the drip reservoir (e.g. bi-weekly), both drip water sampling methodologies are valid to approximate the amount-weighted isotopic composition of a drip.

The new monitoring effort: (i) enabled to produce estimates of rainfall integration times and degree of homogenization, stratified by reservoir, of most drip sites analyzed, from bi-weekly, monthly and annual drip water samples, and; (ii) help test the notion that the isotopic composition of drip water at different drip sites converge into a single value when drip water is integrated over a sufficiently long period and provided they reflect the same water source and no other process, such as evaporation, has altered the isotopic composition of the water source. In addition, this second chapter explored the implications of observed drip water variability and residence times for the detection of significant precipitation reductions (i.e. meteorological droughts) and TCs from stalagmite $\delta^{18}O$ records; and it provided the first instrumental evidence of the existence of a rainfall "amount effect" on

interannual timescales for the Yucatan Peninsula. The first two chapters provide therefore a thorough assessment of the processes that affect the isotopic signal of rainfall and the role of the epikarst characteristics and cave environmental conditions in influencing the transferring of this signal into drip water sites that ultimately provide the "ingredients" to form a stalagmite. These chapters present, furthermore, a fundamental understanding of the impact of epikarst drip water reservoirs on the magnitude and temporal representation of hydroclimate variability inferred from stalagmite $\delta^{18}O$ records. The results from the chapters have important implications to our understanding of the role of climate change for the development and collapse of the Maya civilization. Results from Chapters 1 and 2 indicate that annual rainfall reconstruction from stalagmites from Río Secreto cave are possible but they are expected to underestimate the magnitude of short-term droughts, including those found to be coeval with the collapse of the Maya civilization during the Classic Period (Medina-Elizalde et al., 2010).

Chapter 3 explores the processes that control Mg/Ca, Sr/Ca and Ba/Ca variability of drip water from Río Secreto cave based on a 4-year monitoring work using two different sampling protocols; discrete and continuous sampling of drip water. Sampling methodology that integrates the accumulation of drip water for a month or longer, resulted more effective for characterizing the seasonal variability of the elemental concentrations of Ca, Mg and Sr in the drip water and therefore for the detection of processes controlled by water-rock interaction such as Prior Calcite Precipitation.

In addition this chapter presents results of farmed calcite collected on glass plates over 24 months, providing complimentary $\delta^{18}O$, $\delta^{13}C$ compositions and Mg/Ca, Sr/Ca and Ba/Ca ratios of the solid phase. Several lines of evidence suggest that the Mg/Ca and Sr/Ca variability in drip water is being controlled by a process known as Prior Calcite Precipitation and thus can be used as proxies of wet and dry conditions when measured in stalagmites samples.

Chapter 3 also presents distribution coefficients for Mg, Sr and Ba, and $\delta^{18}O$ empirical values from drip water and calcite and compares them with those predicted by published thermodynamic relationships based on laboratory experiments of inorganic calcite and/or under cave-analog conditions, theoretical calculations, and *in situ* calibrations. This last

chapter offers the first *in situ* calibration evidence of the feasibility of using $\delta^{13}C$ and X/Ca values as proxies of wet and dry conditions in stalagmites from this region. However, the ~two-year analysis of farmed calcite data was not sufficient to understand the environmental controls on modern calcite growth. This monitoring effort should be continued and extended to better understand the processes that control the transferring of proxy variability from drip waters to stalagmite calcite at different time scales. For example, since the preliminary data presented in this study suggests that $\delta^{13}C$-calcite composition has the potential to reflect conditions of hydrological variability, the stable carbon isotopes of the chemical species involved in the reaction of modern calcite deposition should be more thoroughly monitored (e.g. CO_{2aq} and DIC). Furthermore, the data suggest that the ionic strength of the solution may be slightly influencing the deposition of some trace elements (e. Mg and Sr), therefore, experiments to address these and other questions may be carried out to continue refining our understanding of proxies of climatic variability based on stalagmites from this cave and region.

APPENDIX A

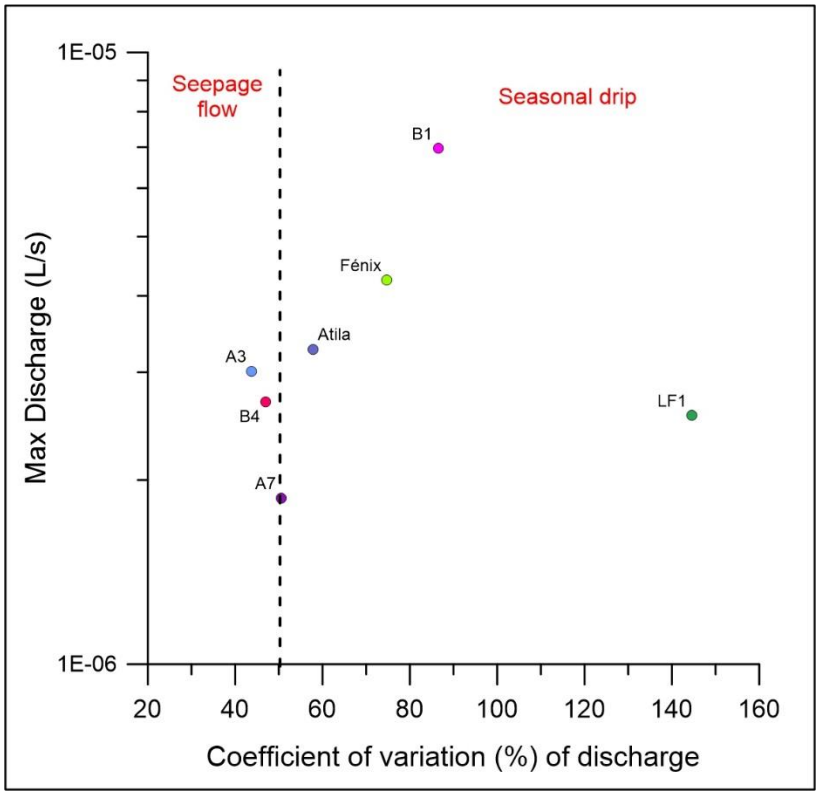

Fig. A. (a) Hydrological behavior of Rio Secreto cave drip sites from July 2017 to April 2019 expressed in terms of maximum discharge versus variability in discharge defined by Fairchild et al. (2006). The coefficient of variation is the quotient of the standard deviation over the mean drip rate value expressed as a percentage (See Section 2.4.7 of main article).

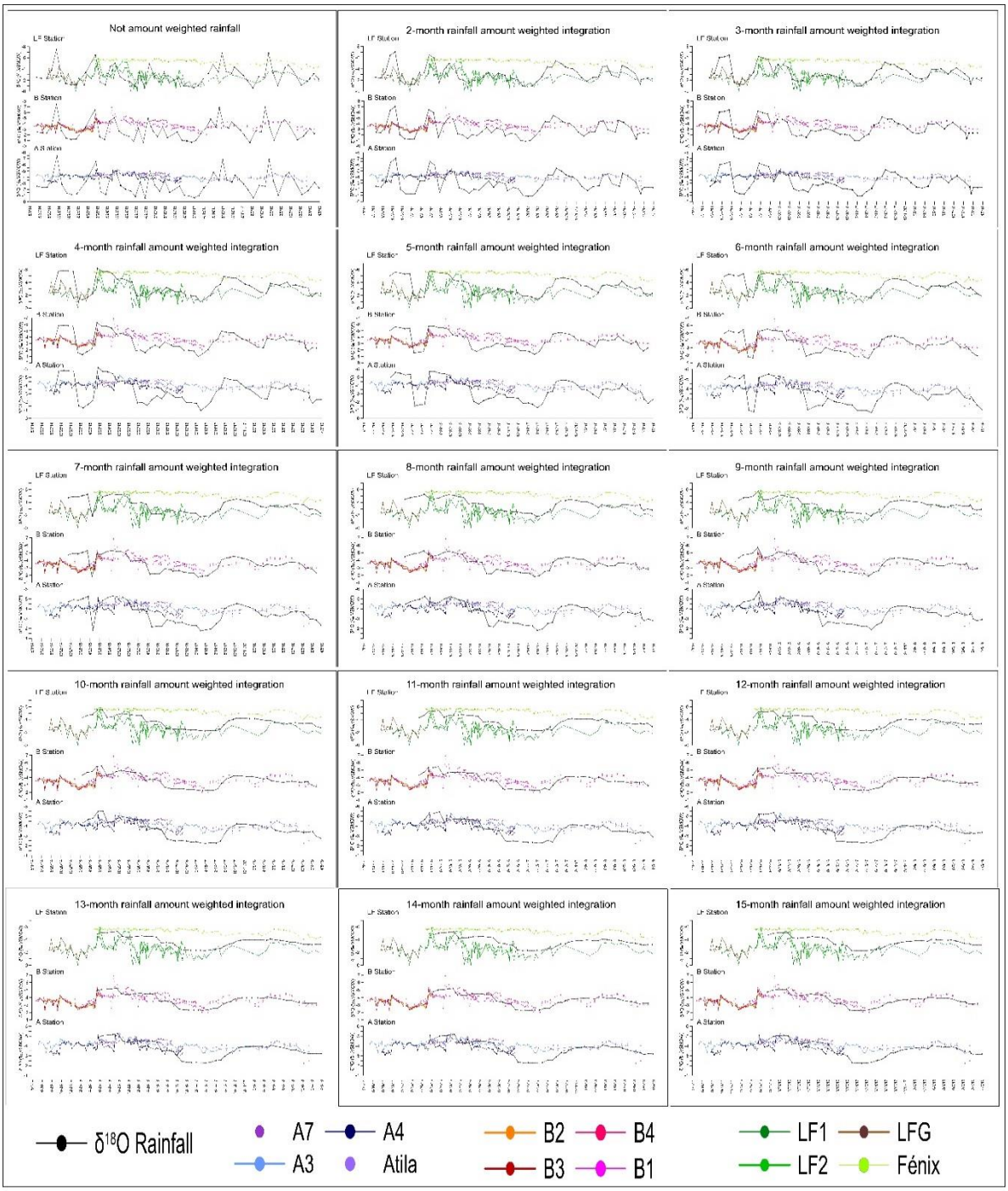

Fig. B Tests for the determination of the rain integration time by the reservoirs of drip sites of Río Secreto. Each plot shows the $\delta^{18}O$ data of 12 drip sites at stations A, B and LF (panels) during five hydrological years. The results of the integration of the amount-weighted $\delta^{18}O$ composition of rainfall from 2 to 15 months is plotted (black dots gray line) (see Methods section 2.3 for details). Data before June 2017 was obtained from Lases Hernández et al. (2019). Cross correlations between $\delta^{18}O$ series of different rainfall integrations and the monthly $\delta^{18}O$ averages of three drip sites (i.e. A3, B1 and LF1) in Rio Secreto Cave were determined using the Analyzer software (Paillard et al., 1996). Value of cross correlation maximum coefficients founded for each drip site are presented in Fig. 2 of main manuscript, additionally it was found that in no case there is a phase lag in the time series. See also Sections 2.3.3.2 and 2.5.2 in Chapter 2. [PLEASE SEE THE DIGITAL FILES FOR A LEGIBLE SET OF FIGURES]

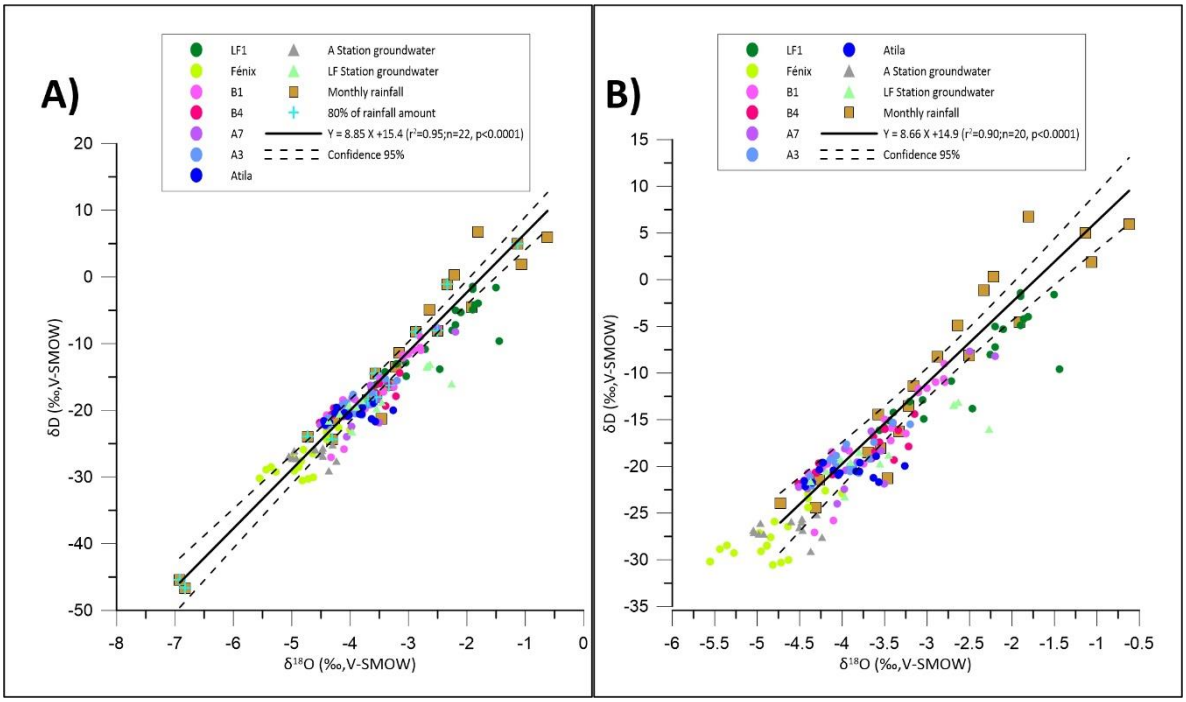

Fig. C. $\delta^{18}O$ vs δD of montly rainfall, drip water and groundwater samples for the period July 2017-April 2019. A) LMWL was calculated using values of all samples includiying two samples associated tropical cyclones incursions that exhibited a very low composition. Rain samples with turquoise cross symbols had an associated rainfall higher than 90 mm and together represent 80% of the precipitation of the sampling period. B) Same as A but missing the rainfall samples associated with tropical cyclones. Note that slopes in both cases are very similar. It is noticeable that most samples of LF1 drip site do not exhibit a different deviation to the rainfall values in comparison with the other 6 drip sites also plotted. Confidence Interval at 95% were calculated by 5000 iterations using Grapher^{TM} (Golden Software, LLC) .

Table A Isotopic composition ($\delta^{18}O$ and δD) of monthly and partial rainfall samples collected at Río Secreto reserve during 5 hydrological years. Amount of rainfall recorded at Rio Secreto and CONAGUA weather station are presented for comparison (See Fig. 2.1-A).

Initial Date	Final Date	Number of collection days	mm Rio	mm Playa	$\delta^{18}O$	δD	Date in the graph	Rain
01/06/2014	30/06/2014	30	158	77	-2.5	-11.1	15/06/2014	Monthly
01/07/2014	31/07/2014	31	39	7	-2.3	-9.5	15/07/2014	Monthly
01/08/2014	31/08/2014	31	46	45	-2.3	-8.5	15/08/2014	Monthly
01/09/2014	30/09/2014	30	129	152	-3.7	-18.5	15/09/2014	Monthly
01/10/2014	31/10/2014	31	325	452	-7.4	-45.8	15/10/2014	Monthly
01/11/2014	30/11/2014	30	30	50	-2.8	-12.8	15/11/2014	Monthly
01/12/2014	31/12/2014	31	44	24	-1.4	-0.1	15/12/2014	Monthly
01/01/2015	31/01/2015	31	60	37	-1.2	3.1	15/01/2015	Monthly
01/02/2015	28/02/2015	28	39	39	-1.3	5.2	15/02/2015	Monthly
01/03/2015	31/03/2015	31	0	32			15/03/2015	Monthly
01/04/2015	30/04/2015	30	32	3	-3.3	-10.8	15/04/2015	Monthly
01/05/2015	31/05/2015	31	0	3			15/05/2015	Monthly
01/06/2015	30/06/2015	30	327	292	-6.5	-40.1	15/06/2015	Monthly
01/07/2015	31/07/2015	31	43	45	-1.6	-7.0	15/07/2015	Monthly
01/08/2015	31/08/2015	31	21	41	-1.2	-0.7	15/08/2015	Monthly
01/09/2015	30/09/2015	30	96	40	-4.4	-24.6	15/09/2015	Monthly
01/10/2015	31/10/2015	31	327	243	-5.0	-26.6	15/10/2015	Monthly
01/11/2015	30/11/2015	30	31	288	-2.6	-6.5	15/11/2015	Monthly
01/12/2015	31/12/2015	31	85	50	-2.0	-4.0	15/12/2015	Monthly
01/01/2016	31/01/2016	31	33	70	-1.8	2.4	15/01/2016	Monthly
01/02/2016	28/02/2016	28	30	41	-0.9	7.9	15/02/2016	Monthly
01/03/2016	31/03/2016	31	29	33	-3.2	-15.8	15/03/2016	Monthly
01/04/2016	30/04/2016	30	32	0	-0.6	12.3	15/04/2016	Monthly
01/05/2016	31/05/2016	31	25	1	-4.9	-31.0	15/05/2016	Monthly
01/06/2016	30/06/2016	30	48	48	-2.7	-11.0	15/06/2016	Monthly
01/07/2016	31/07/2016	31	28	15	-1.7	-4.1	15/07/2016	Monthly
01/08/2016	31/08/2016	31	181	145	-3.4	-12.9	15/08/2016	Monthly
01/09/2016	30/09/2016	30	74	116	-1.5	-0.8	15/09/2016	Monthly
01/10/2016	31/10/2016	31	110	175	-2.0	-2.7	15/10/2016	Monthly
01/11/2016	30/11/2016	30	116	46	-2.5	-3.3	15/11/2016	Monthly
01/12/2016	31/12/2016	31	47	51	-1.0	3.2	15/12/2016	Monthly
01/01/2017	31/01/2017	31	34	54	-0.9	7.6	15/01/2017	Monthly
01/02/2017	28/02/2017	28	9	23	-0.7	10.0	15/02/2017	Monthly
01/03/2017	31/03/2017	31	31	24	-1.0	4.5	15/03/2017	Monthly
01/04/2017	30/04/2017	30	42	34	-2.3	-7.3	15/04/2017	Monthly
01/05/2017	30/05/2017	30	28	16	-3.1	-19.3	15/05/2017	Monthly
31/05/2017	03/07/2017	33	96	97	-4.8	-32.2	15/06/2017	Monthly
04/07/2017	31/07/2017	27	63	46	-3.5	-21.3	17/07/2017	Monthly

01/08/2017	09/08/2017	9	90	83	-6.8	-46.6	09/08/2017	Monthly
10/08/2017	02/10/2017	53	393	393	-3.5	-18.0	05/09/2017	Monthly
02/10/2017	15/10/2017	13	46	117	-3.2	-13.5	07/10/2017	Monthly
15/10/2017	02/11/2017	18	185	70	-4.3	-24.4	25/10/2017	Monthly
02/11/2017	05/12/2017	33	165	148	-3.7	-18.5	19/11/2017	Monthly
05/12/2017	03/01/2018	29	92	70	-2.9	-8.3	19/12/2017	Monthly
03/01/2018	04/02/2018	32	71	82	-1.9	-4.5	14/01/2018	Monthly
04/02/2018	02/03/2018	26	9	19	-0.6	5.9	17/02/2018	Monthly
02/03/2018	17/04/2018	46	79	71	-2.6	-4.9	25/03/2018	Monthly
17/04/2018	14/05/2018	27	146	99	-2.5	-8.1	01/05/2018	Monthly
14/05/2018	04/06/2018	21	103	84	-6.9	-45.4	25/05/2018	Monthly
04/06/2018	11/07/2018	37	209	190	-3.3	-16.3	22/06/2018	Monthly
11/07/2018	31/08/2018	51	53	53	-1.1	1.9	21/07/2018	Monthly
31/08/2018	10/09/2018	10	42	52	-4.3	-21.5	05/09/2018	Monthly
10/09/2018	10/10/2018	30	99	172	-4.7	-24.0	25/09/2018	Monthly
10/10/2018	14/11/2018	35	99	112	-3.6	-14.4	27/10/2018	Monthly
16/11/2018	13/01/2019	59	99	129	-1.1	5.0	15/12/2018	Monthly
17/01/2019	30/01/2019	14	15	39	-1.8	6.8	23/01/2019	Monthly
31/01/2019	14/02/2019	15	129	264	-2.3	-1.1	07/02/2019	Monthly
15/02/2019	21/03/2019	35	2	2	-3.2	-11.4	03/03/2019	Monthly
22/03/2019	12/04/2019	22	45	25	-2.2	0.3	01/04/2019	Monthly
21/10/2014	21/10/2014	1	79		-9.5	-61.4	21/10/2014	Partial
12/06/2016	19/06/2016	8	38		-2.3	-8.4	12/06/2016	Partial
28/08/2016	30/08/2016	3	157		-2.9	-10.7	28/08/2016	Partial
27/09/2016	29/09/2016	3	168		-2.0	-1.4	27/09/2016	Partial
15/10/2016	23/10/2016	9	11		-0.8	9.5	15/10/2016	Partial
27/10/2016	29/10/2016	3	19		-1.6	0.0	27/10/2016	Partial
29/10/2016	29/10/2016	1	9		-4.0	-18.3	29/10/2016	Partial
30/10/2016	30/10/2016	1	27		-3.9	-17.0	30/10/2016	Partial
01/11/2016	01/11/2016	1	27		-3.3	-13.2	01/11/2016	Partial
02/11/2016	07/11/2016	6	53		-2.5	-2.1	07/11/2016	Partial
09/11/2016	09/11/2016	1	29		-0.7	9.5	09/11/2016	Partial
10/11/2016	16/11/2016	7	1		-1.1	4.2	10/11/2016	Partial
11/12/2016	13/12/2016	3	28		-1.4	-0.5	11/12/2016	Partial
22/12/2016	22/12/2016	1	6		-1.0	3.3	22/12/2016	Partial
26/12/2016	02/01/2017	8	19		-0.5	7.7	26/12/2016	Partial
07/01/2017	10/01/2017	4	8		-0.2	11.7	07/01/2017	Partial
13/01/2017	17/01/2017	5	37		-1.1	6.7	13/01/2017	Partial
21/02/2017	21/02/2017	1	12		-0.9	9.0	21/02/2017	Partial
11/04/2017	11/04/2017	1	3		1.6	17.9	11/04/2017	Partial
19/04/2017	20/04/2017	2	16		-1.5	-0.7	19/04/2017	Partial
20/04/2017	20/04/2017	1	25		-3.5	-18.2	20/04/2017	Partial
22/04/2017	10/05/2017	19	7		-1.3	-4.8	30/04/2017	Partial
03/05/2017	03/05/2017	1	36		-1.5	4.4	03/05/2017	Partial

30/05/2017	05/06/2017	7	4		-1.5	-9.3	30/05/2017	Partial
06/06/2017	09/06/2017	4	8		-2.7	-12.8	06/06/2017	Partial
10/06/2017	13/06/2017	4	29		-3.0	-16.0	10/06/2017	Partial
13/06/2017	19/06/2017	7	35		-7.6	-54.0	13/06/2017	Partial
20/06/2017	03/07/2017	14	22		-4.2	-26.8	25/06/2017	Partial
05/07/2017	06/07/2017	2	39		-5.0	-33.4	05/07/2017	Partial
05/07/2017	06/07/2017	1	39	27	-5.0	-33.4	06/07/2017	Partial
07/07/2017	31/07/2017	24	13	19	-0.6	-0.4	17/07/2017	Partial
07/07/2017	31/07/2017	25	13		-0.6	-0.4	20/07/2017	Partial
22/08/2017	02/10/2017	41	373	370	-4.5	-26.7	10/09/2017	Partial
26/10/2017	02/11/2017	7	185	70	-4.3	-24.4	25/10/2017	Partial
05/12/2017	22/12/2017	17	96	64	-2.7	-7.5	13/12/2017	Partial
22/12/2017	03/01/2018	12	9	6	-1.2	6.0	28/12/2017	Partial
04/06/2018	19/06/2018	15	160	137	-3.7	-19.6	11/06/2018	Partial
19/06/2018	11/07/2018	22	53	53	-2.6	-6.6	30/06/2018	Partial
10/10/2018	31/10/2018	21	49	215	-3.9	-17.8	21/10/2018	Partial
31/10/2018	14/11/2018	14	37	28	-2.9	-7.7	07/11/2018	Partial
14/01/2019	17/01/2019	3	5	116	-2.9	-3.0	15/01/2019	Partial

Table B. Drip water $\delta^{18}O$, δD, volume and drip rate data at 7 drip sites of Rio Secreto cave collected during July 2017–April 2019.

Drip Site	Initial Date	Final Date	Number of collection days	Volume (mL)	$\delta^{18}O$	δD	Date in the graph	Drip rate (mL/hour)
A3	08/09/2017	15/10/2017	37	3835	-3.8	-20.7	27/09/2017	4.3
A3	15/10/2017	25/11/2017	41	3205	-3.9	-20.5	10/11/2017	3.3
A3	25/11/2017	10/01/2018	46	8000	ND	ND	18/12/2017	7.2
A3	10/01/2018	26/01/2018	16	4165	-3.9	-20.0	02/02/2018	10.8
A3	26/01/2018	21/03/2018	54	ND	-3.6	-17.4	10/03/2018	ND
A3	21/03/2018	12/04/2018	22	ND	-3.9	-19.9	01/04/2018	ND
A3	12/04/2018	14/05/2018	32	3915	-3.7	-19.2	28/04/2018	5.1
A3	14/05/2018	04/06/2018	21	1900	-4.1	-19.7	24/05/2018	3.8
A3	04/06/2018	28/06/2018	24	4860	-4.4	-22.1	16/06/2018	8.4
A3	28/06/2018	31/07/2018	33	8335	-4.4	-21.1	14/07/2018	10.5
A3	31/07/2018	31/08/2018	31	5270	-4.1	-19.3	15/08/2018	7.1
A3	31/08/2018	10/10/2018	40	5710	-3.9	-17.6	20/09/2018	5.9
A3	10/10/2018	14/11/2018	35	4370	-4.1	-18.8	28/10/2018	5.2
A3	14/11/2018	14/01/2019	61	5885	-3.2	-15.5	15/12/2018	4
A3	14/01/2019	17/01/2019	3	197	-3.4	-15.3	15/01/2019	2.7
A7	11/07/2017	02/08/2017	22	1641	-4.1	-23.9	22/07/2017	3.1
A7	02/08/2017	08/09/2017	37	2250	-4.1	-24.0	20/08/2017	2.5
A7	08/09/2017	15/10/2017	37	5970	-3.5	-21.9	27/09/2017	6.7
A7	15/10/2017	25/11/2017	41	5991	-3.5	-18.4	10/11/2017	6.1
A7	25/11/2017	10/01/2018	46	296	ND	ND	18/12/2017	0.3
A7	10/01/2018	26/01/2018	16	335	-4.0	-20.4	02/02/2018	0.9
A7	21/03/2018	12/04/2018	22	2600	-3.8	-19.5	01/04/2018	4.9
A7	12/04/2018	14/05/2018	32	4010	-4.0	-22.4	28/04/2018	5.2
A7	14/05/2018	04/06/2018	21	2780	-4.4	-22.4	24/05/2018	5.5
A7	04/06/2018	31/07/2018	57	7135	-4.5	-22.2	02/07/2018	5.2
A7	31/07/2018	31/08/2018	31	ND	-4.0	-18.1	15/08/2018	ND
A7	31/08/2018	10/10/2018	40	3875	-4.1	-19.1	20/09/2018	4
A7	10/10/2018	14/11/2018	35	ND	-3.7	-16.2	28/10/2018	ND
A7	14/11/2018	14/01/2019	61	3525	-2.2	-8.2	15/12/2018	2.4
A7	14/01/2019	17/01/2019	3	285	-2.5	-7.7	15/01/2019	4
Atila	11/07/2017	02/08/2017	22	1359	-3.6	-21.2	22/07/2017	2.6
Atila	02/08/2017	08/09/2017	37	2410	-3.6	-21.7	20/08/2017	2.7
Atila	08/09/2017	15/10/2017	37	1235	-3.3	-20.0	27/09/2017	1.4
Atila	15/10/2017	25/11/2017	41	8175	-3.8	-20.6	10/11/2017	8.3
Atila	25/11/2017	10/01/2018	46	ND	ND	ND	18/12/2017	ND
Atila	10/01/2018	26/01/2018	16	4525	-4.0	-20.7	02/02/2018	11.8
Atila	26/01/2018	21/03/2018	54	ND	-3.8	-19.6	10/03/2018	ND
Atila	21/03/2018	12/04/2018	22	2575	-4.0	-20.9	01/04/2018	4.9
Atila	12/04/2018	14/05/2018	32	2650	-3.8	-20.5	28/04/2018	3.5
Atila	14/05/2018	04/06/2018	21	1760	-4.4	-21.8	24/05/2018	3.5
Atila	04/06/2018	28/06/2018	24	2630	-4.4	-22.1	16/06/2018	4.6
Atila	28/06/2018	31/07/2018	33	3660	-4.4	-21.6	14/07/2018	4.6
Atila	31/07/2018	31/08/2018	31	2630	-4.2	-19.6	15/08/2018	3.5
Atila	31/08/2018	10/10/2018	40	3620	-4.2	-19.6	20/09/2018	3.8
Atila	10/10/2018	14/11/2018	35	3585	-4.3	-20.4	28/10/2018	4.3
Atila	14/11/2018	14/01/2019	61	5525	-3.6	-18.9	15/12/2018	3.8

Atila	14/01/2019	17/01/2019	3	210	-4.1	-20.4	15/01/2019	2.9
B1	11/07/2017	02/08/2017	22	80	-3.2	-16.5	22/07/2017	0.2
B1	02/08/2017	08/09/2017	37	7282	-4.1	-25.8	20/08/2017	8.2
B1	08/09/2017	15/10/2017	37	8000	-4.3	-27.1	27/09/2017	9
B1	15/10/2017	25/11/2017	41	3535	-3.7	-19.7	10/11/2017	3.6
B1	25/11/2017	10/01/2018	46	8000	ND	ND	18/12/2017	7.2
B1	10/01/2018	26/01/2018	16	6210	-3.4	-15.9	02/02/2018	16.2
B1	26/01/2018	21/03/2018	54	ND	-2.8	-10.6	10/03/2018	ND
B1	21/03/2018	12/04/2018	22	1575	-2.8	-11.0	01/04/2018	3
B1	12/04/2018	14/05/2018	32	1075	-3.4	-17.2	28/04/2018	1.4
B1	14/05/2018	04/06/2018	21	5960	-3.9	-18.4	24/05/2018	11.8
B1	04/06/2018	28/06/2018	24	7000	-4.3	-20.2	16/06/2018	12.2
B1	28/06/2018	31/07/2018	33	5960	-4.2	-19.7	14/07/2018	7.5
B1	31/07/2018	31/08/2018	31	2686	-4.1	-18.4	15/08/2018	3.6
B1	31/08/2018	10/10/2018	40	5790	-4.4	-20.7	20/09/2018	6
B1	10/10/2018	14/11/2018	35	6250	-4.2	-20.2	28/10/2018	7.4
B1	14/11/2018	14/01/2019	61	2545	-2.9	-11.0	15/12/2018	1.7
B1	14/01/2019	17/01/2019	3	1805	-3.5	-15.0	15/01/2019	25.1
B1	17/01/2019	30/01/2019	13	1695	-2.8	-9.0	23/01/2019	5.4
B1	30/01/2019	14/02/2019	15	2180	-3.1	-11.7	07/02/2019	6.1
B1	14/02/2019	21/03/2019	35		-3.1	-12.1	03/03/2019	ND
B1	21/03/2019	12/04/2019	22	1540	-3.0	-11.6	01/04/2019	2.9
B4	11/07/2017	02/08/2017	22	385	-3.7	-19.1	22/07/2017	0.7
B4	02/08/2017	08/09/2017	37	4666	-3.2	-17.9	20/08/2017	5.3
B4	08/09/2017	15/10/2017	37	8000	-3.4	-19.3	27/09/2017	9
B4	15/10/2017	25/11/2017	41	2355	-3.6	-17.4	10/11/2017	2.4
B4	25/11/2017	10/01/2018	46	8000	ND		18/12/2017	7.2
B4	10/01/2018	26/01/2018	16	2620	-3.6	-16.8	02/02/2018	6.8
B4	26/01/2018	21/03/2018	54	ND	-3.2	-14.4	10/03/2018	ND
B4	21/03/2018	12/04/2018	22	ND	-3.3	-16.1	01/04/2018	ND
B4	12/04/2018	14/05/2018	32	2620	-3.6	-18.4	28/04/2018	3.4
B4	14/05/2018	04/06/2018	21	3325	-4.1	-20.9	24/05/2018	6.6
B4	04/06/2018	28/06/2018	24	5270	-4.4	-21.5	16/06/2018	9.1
B4	28/06/2018	31/07/2018	33	4911	-4.3	-20.6	14/07/2018	6.2
B4	31/07/2018	31/08/2018	31	3090	-4.3	-19.6	15/08/2018	4.2
B4	31/08/2018	10/10/2018	40	5850	-4.5	-21.9	20/09/2018	6.1
B4	10/10/2018	14/11/2018	35	8115	-4.3	-20.7	28/10/2018	9.7
B4	14/11/2018	14/01/2019	61	5855	-3.5	-16.0	15/12/2018	4
B4	14/01/2019	17/01/2019	3	223	-3.4	-15.3	15/01/2019	3.1
Fénix	11/07/2017	02/08/2017	22	1287	-4.7	-30.3	22/07/2017	2.4
Fénix	02/08/2017	08/09/2017	37	1595	-4.6	-30.0	20/08/2017	1.8
Fénix	08/09/2017	15/10/2017	37	1555	-4.8	-30.5	27/09/2017	1.8
Fénix	15/10/2017	25/11/2017	41	3780	-5.0	-29.1	10/11/2017	3.8
Fénix	25/11/2017	10/01/2018	46	6210	ND	ND	18/12/2017	5.6
Fénix	10/01/2018	26/01/2018	16	5865	-4.8	-27.6	02/02/2018	15.3

Fénix	26/01/2018	21/03/2018	54	ND	-4.9	-28.4	10/03/2018	ND
Fénix	21/03/2018	12/04/2018	22	4705	-4.6	-26.5	01/04/2018	8.9
Fénix	12/04/2018	14/05/2018	32	3145	-4.9	-28.5	28/04/2018	4.1
Fénix	14/05/2018	04/06/2018	21	1945	-5.3	-29.3	24/05/2018	3.9
Fénix	04/06/2018	28/06/2018	24	2375	-5.6	-30.2	16/06/2018	4.1
Fénix	28/06/2018	31/07/2018	33	3015	-5.6	-30.2	14/07/2018	3.8
Fénix	31/07/2018	31/08/2018	31	3613	-5.4	-28.9	15/08/2018	4.9
Fénix	31/08/2018	10/10/2018	40	3695	-5.4	-28.5	20/09/2018	3.8
Fénix	10/10/2018	14/11/2018	35	2575	-5.0	-27.1	28/10/2018	3.1
Fénix	14/11/2018	14/01/2019	61	4725	-4.0	-22.9	15/12/2018	3.2
Fénix	14/01/2019	17/01/2019	3	200	-4.8	-25.9	15/01/2019	2.8
Fénix	17/01/2019	30/01/2019	13	905	-4.4	-22.9	23/01/2019	2.9
Fénix	30/01/2019	14/02/2019	15	865	-4.4	-23.4	07/02/2019	2.4
Fénix	14/02/2019	21/03/2019	35	1580	-4.2	-22.6	03/03/2019	1.9
Fénix	21/03/2019	12/04/2019	22	1145	-4.4	-24.4	01/04/2019	2.2
LF1	11/07/2017	02/08/2017	22	140	-1.4	-9.6	22/07/2017	0.3
LF1	02/08/2017	08/09/2017	37	ND	-2.5	-13.8	20/08/2017	ND
LF1	08/09/2017	15/10/2017	37	520	-3.0	-14.9	27/09/2017	0.6
LF1	15/10/2017	25/11/2017	41	1570	-2.7	-10.8	10/11/2017	1.6
LF1	25/11/2017	10/01/2018	46	480	ND	ND	18/12/2017	0.4
LF1	10/01/2018	26/01/2018	16	123	-1.9	-4.2	02/02/2018	0.3
LF1	26/01/2018	21/03/2018	54	ND	-1.5	-1.6	10/03/2018	ND
LF1	21/03/2018	12/04/2018	22	4845	-1.8	-4.0	01/04/2018	9.2
LF1	12/04/2018	14/05/2018	32	2415	-2.3	-8.0	28/04/2018	3.1
LF1	14/05/2018	04/06/2018	21	2160	-3.4	-15.1	24/05/2018	4.3
LF1	04/06/2018	28/06/2018	24	ND	-3.5	-15.8	16/06/2018	ND
LF1	28/06/2018	31/07/2018	33	980	-3.6	-16.2	14/07/2018	1.2
LF1	31/07/2018	31/08/2018	31	1080	-3.2	-13.0	15/08/2018	1.5
LF1	31/08/2018	10/10/2018	40	760	-3.4	-14.2	20/09/2018	0.8
LF1	10/10/2018	14/11/2018	35	630	-3.1	-12.9	28/10/2018	0.8
LF1	14/11/2018	14/01/2019	61	915	-2.1	-5.3	15/12/2018	0.6
LF1	14/01/2019	17/01/2019	3	30	-1.9	-1.4	15/01/2019	0.4
LF1	17/01/2019	30/01/2019	13	125	-1.9	-1.8	23/01/2019	0.4
LF1	30/01/2019	14/02/2019	15	166	-2.2	-5.0	07/02/2019	0.5
LF1	14/02/2019	21/03/2019	35		-2.2	-7.2	03/03/2019	ND
LF1	21/03/2019	12/04/2019	22	240	-1.9	-4.9	01/04/2019	0.5
Showerhead A					-3.2	-8.1	14/01/2019	
Showerhead B					-3.1	-7.6	14/01/2019	
Showerhead entrada de ensueño					-3.2	-13.0	14/02/2019	
Showerhead LF1					-3.1	-9.3	14/01/2019	
Showerhead pond B					-2.4	-5.6	14/02/2019	

Table C. Groundwater $\delta^{18}O$ and δD data collected at stations LF and A during August 2017 to January 2019.

Site	$\delta^{18}O$	δD	Date
LF STATION POND	-2.3	-16.0	02/08/2017
LF STATION POND	-4.0	-23.3	15/10/2017
LF STATION POND	-3.6	-19.7	25/11/2017
LF STATION POND	-2.7	-13.3	26/02/2018
LF STATION POND	-2.6	-13.1	21/03/2018
LF STATION POND	-2.7	-13.5	12/04/2018
LF STATION POND	-3.5	-18.8	14/05/2018
LF STATION POND	-3.8	-18.5	04/06/2018
LF STATION POND	-4.0	-19.3	31/07/2018
LF STATION POND	-4.2	-20.5	31/08/2018
LF STATION POND	-4.4	-21.6	10/10/2018
LF STATION POND	-3.9	-19.5	14/11/2018
A STATION GROUNDWATER	-4.4	-29.1	08/09/2017
A STATION GROUNDWATER	-4.2	-27.6	15/10/2017
A STATION GROUNDWATER	-4.5	-26.6	25/11/2017
A STATION GROUNDWATER	-4.3	-25.2	26/02/2018
A STATION GROUNDWATER	-4.5	-26.0	21/03/2018
A STATION GROUNDWATER	-4.5	-25.6	12/04/2018
A STATION GROUNDWATER	-4.5	-26.9	14/05/2018
A STATION GROUNDWATER	-4.9	-27.2	04/06/2018
A STATION GROUNDWATER	-5.0	-26.1	31/07/2018
A STATION GROUNDWATER	-5.0	-26.9	31/08/2018
A STATION GROUNDWATER	-5.0	-27.1	10/10/2018
A STATION GROUNDWATER	-5.0	-27.2	14/11/2018
A STATION GROUNDWATER	-4.60	-25.90	14/01/2019

Table D Isotopic ($\delta^{18}O$) shifts associated with rainfall from three topical cyclones at Rio Secreto in cave drip water and rainfall.

$\delta^{18}O$ shifts asociated with topical cyclones rainfall at Rio Secreto cave drip waters and rainfall				
Previous period	2-9 October 2014	7-9 June 2015	11 July-2 August 2017	12 April-14 May 2018
Cyclone ocurrence period	18-25 October 2014	14-16 June 2015	2 August-8 September 2017	14-May-4 June 2018
Sample	Hanna	Bill	Franklin	Alberto
A2	-1	-1.5	ND	ND
A3	-0.6	-1.5	ND	-0.4
A4	-1	-1.4	ND	ND
A7	ND	0.1	0.0	-0.4
Atila	ND	-0.6	0.1	-0.6
B1	-0.8	-2.1	-0.9	-0.5
B4	ND	-0.5	0.4	-0.5
Fénix	ND	0	0.1	-0.4
LF1	-0.8	-1.8	-1.0	-1.2
LF2	ND	-1.3	ND	ND
LFG	-1.8	ND	ND	ND
Rainfall	-5.8	-3.2	-3.4	-4.4

Table E Hystorical record of monthly precipitation amount at CONAGUA weather station, Playa del Carmen (See Fig. 1A).

MONTHLY PRECIPITATION (MM)

STATION (23163 CONAGUA CODE); *PLAYA DEL CARMEN,* *MPIO. DE SOLIDARIDAD*

YEAR	JAN	FEB	MAR	APR	MAY	JUN	JUL	AUG	SEP	OCT	NOV	DIC	TOTAL ANNUAL
1998	174.9	2.7	13.5	53.5	218.0	148.0	266.0	117.5	66.5	487.5	130.5	73.7	**1,752.3**
1999	35.3	0.0	51.0	0.0	10.2	228.8	172.6	297.6	235.9	464.3	128.5	124.3	**1,748.5**
2000	30.9	16.8	22.3	36.9	45.2	110.6	7.6	91.1	391.6	147.2	165.0	17.6	**1,082.8**
2001	19.0	19.0	58.0	21.0	102.5	25.2	43.1	78.0	215.2	295.3	149.0	230.0	**1,255.3**
2002	5.5	241.0	14.0	0.0	134.0	248.0	31.0	67.2	222.9	167.4	24.0	157.9	**1,312.9**
2003	60.0	390.0	22.0	45.4	28.6	253.5	108.6	142.3	202.0	183.9	176.8	22.9	**1,636.0**
2004	24.5	88.9	7.6	69.4	84.4	556.0	66.4	15.5	94.9	244.2	50.4	16.0	**1,318.2**
2005	31.0	6.5	25.0	21.9	66.8	148.1	219.6	101.5	86.9	538.0	92.0	74.0	**1,411.3**
2006	107.0	133.0	71.0	22.0	59.2	71.7	131.7	388.8	198.5	168.8	213.7	196.6	**1,762.0**
2007	75.3	162.7	18.9	45.0	112.1	62.0	60.5	118.7	126.0	95.0	135.5	*	**1,011.7**
2008	98.5	60.5	25.5	2.0	17.5	129.5	68.0	31.0	98.2	478.5	9.0	37.9	**1,056.1**
2009	68.5	16.1	14.0	5.0	42.1	67.3	18.4	56.7	114.0	142.4	275.1	28.1	**847.7**
2010	8.5	50.5	2.0	286.0	98.8	127.0	335.0	92.7	230.1	66.5	84.5	1.5	**1,383.1**
2011	28.3	45.0	63.0	2.1	45.0	303.9	119.8	45.4	72.1	683.5	80.3	34.3	**1,522.7**
HIST. 1998-2011	**54.8**	**88.1**	**29.1**	**43.6**	**76.0**	**177.1**	**117.7**	**117.4**	**168.2**	**297.3**	**122.5**	**78.1**	**1,352.1**
												MIN	847.7
												MAX	1,762.0
												AVG	1,391.5

Table F Comparison between observed and expected shifts in drip water $\delta^{18}O$ of A3, B1 and LF1 drip sites resulting from the influence of TC Alberto (2018). The observed drip water shift was calculated from the difference between the isotopic composition at each drip site during and prior to the occurrence of TC Alberto. The expected drip water $\delta^{18}O$ shift was calculated based on comparing the drip water $\delta^{18}O$ composition of the sample prior to the event to the expected drip water $\delta^{18}O$ composition resulting from mixing TC Alberto rainfall ($\delta^{18}O$= -6.9‰, rainfall amount =103 mm) to this sample. The size of the reservoir (in mm) of the sample prior to the event was approximated by our estimates of rainfall integration times (Fig. 2). For this analysis, however, rainfall integration times were re-calculated to produce the closest match to the drip water $\delta^{18}O$ value of the specific sample prior to the event. For A3 the integration time was 15 months and for LF1 this was 3 months, similar to what was obtained using the full time series of these drips (Fig. 2). For B1, however, the rainfall integration time that provided the best match to the observed drip water value prior to the event was 8 months and not 4 months estimated using the full time series. This difference is a reflection of the non-stationary nature of the reservoir sizes (Lases-Hernandez et al., 2019). Results suggest that the observed drip water negative isotopic shifts reflect well-mixed TC rainfall with the water reservoir prior to this event. Note that all $\delta^{18}O$ values are in per mil (V-SMOW).

Drip Sample Site + relative to TC		Dates Start-End All 2018	Drip water $\delta^{18}O$ ‰	$\delta^{18}O$ shift ‰	Rainfall timespan (months)	Integrated rainfall $\delta^{18}O$ amount-weighted ‰	Amount of rainfall from integrated rainfall (mm)	$\delta^{18}O$ amount weighted (expected from mixing) ‰	$\delta^{18}O$ Shift in drip water (expected from mixing) ‰
A3	Prior	April 12 – May 14	-3.7	-0.4	15	-3.7	1542		
	After	May 14 – June 4	-4.1					-3.9	-0.2
LF1	Prior	April 12 – May 14	-2.3	-1.2	3	-2.5	233		
	After	May 14 – June 4	-3.4					-3.8	-1.4
B1	Prior	April 12 – May 14	-3.4	-0.5	8*	-3.2	789		
	After	May 14 – June 4	-3.9					-3.6	-0.4
Alberto TC rainfall		May 14 - June 4	$\delta^{18}O$ = -6.9 ‰ Rainfall amount = 103 mm						

APPENDIX B

PLEASE CONTACT THE AUTHOR TO GET THE RESEARCH DATA OF THIS APPENDIX <flases@geociencias.unam.mx>

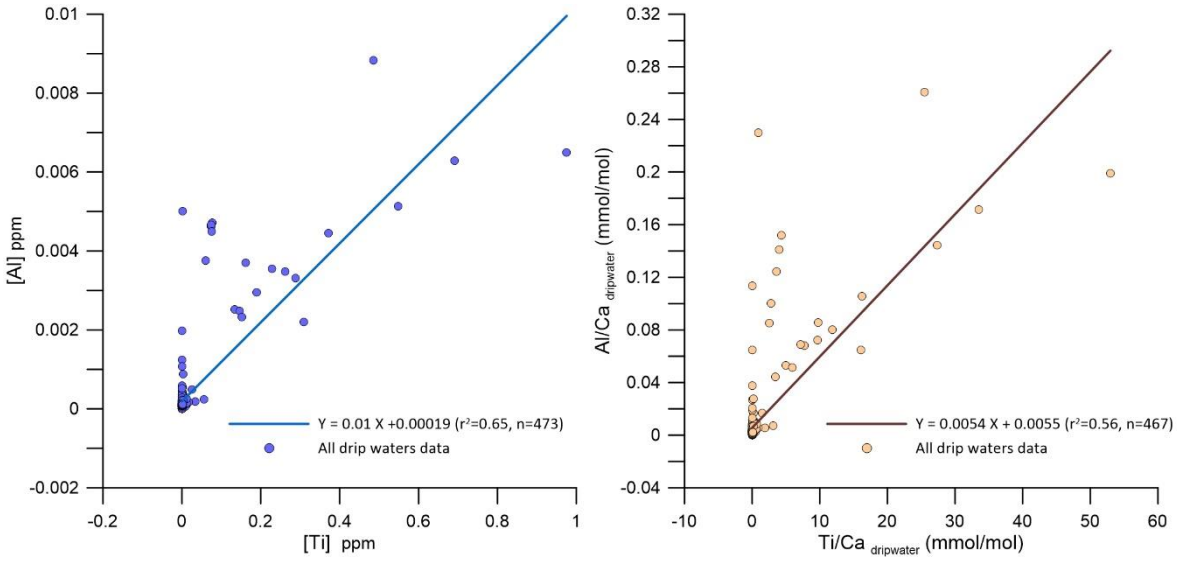

Fig. B.1 Linear regressions between Al and Ti concentrations (left) and X/Ca ratios (right) of drip water samples in Río Secreto Cave.

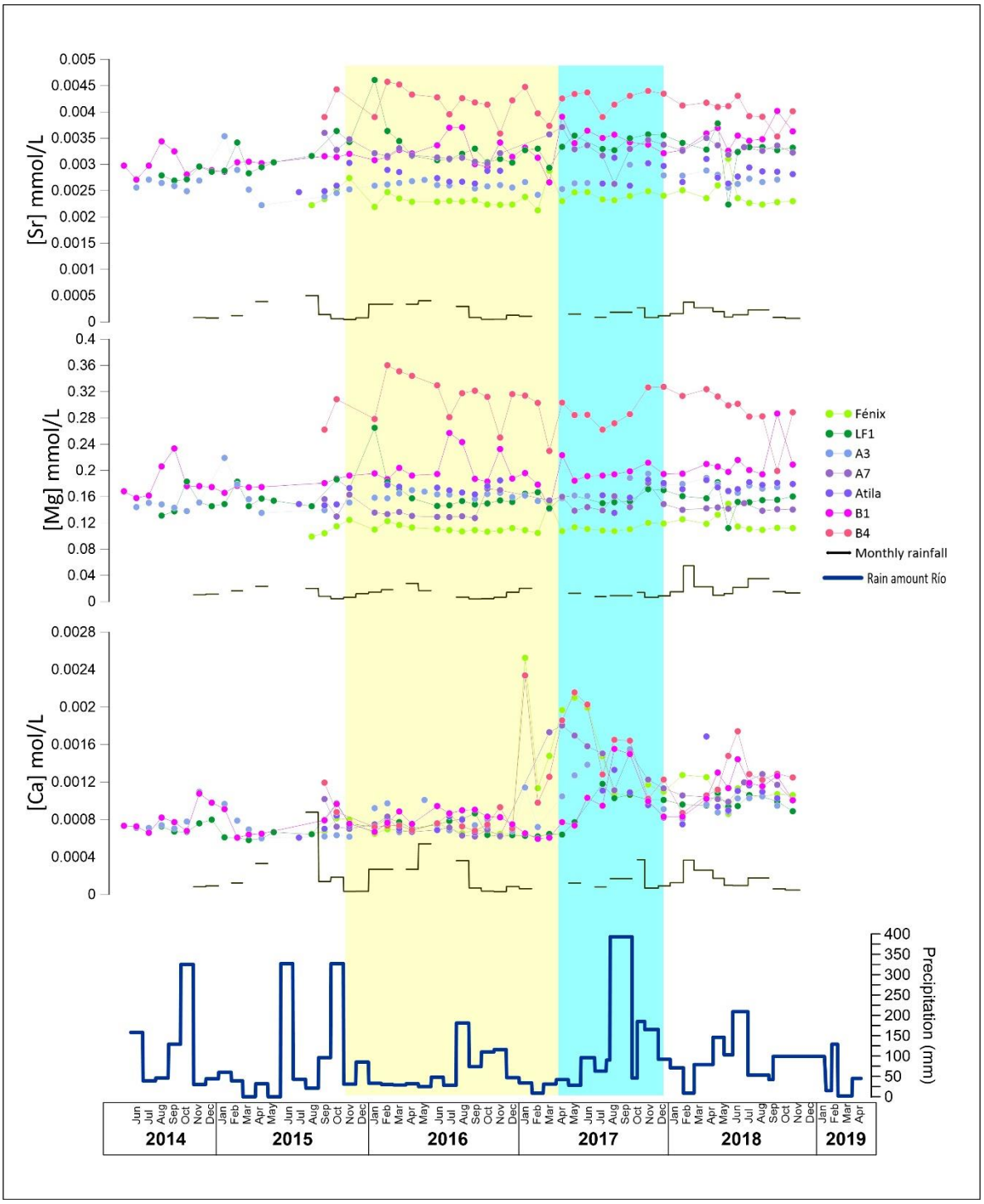

Fig. B.2 Upper three panels: Drip waster Sr, Mg and Ca concentration time series from June 2014 to November 2018, data before June 2017 were agregated in monthly averages (See Section 3.2.3). Aditionally Sr, Mg and Ca concentration of monthly rainwater is showed (black). Lower panel shows rainfall amount measured above Río Secreto cave. Yellow rectangle is higthligting a drougth period when summer rainfall was lower than average and blue rectangle is highligting the transition to a wet summer season.

APPENDIX C

Analysis of elemental concentrations of water samples

All materials used for trace element determination were leached in 1 N reagent grade HCl in deionized water for 12-hours, then leached in deionized water for 12-hours, and finally triple rinsed with deionized water. Materials included the Nalgene bottles for water sampling, Eppendorf vials, and plasticware used for sample handling and solution preparation. This material was prepared in the Ultra-Clean Laboratory at Centro de Geociencias, UNAM. All analytical HNO_3 solutions also used deionized water.

Water samples taken after June 2017 for trace elements were acidified *in situ* with 1 to 3 drops of clean 50% HNO_3. Raw rainfall samples were taken to the Centro de Geociencias UNAM for preparation in the Ultra-Clean Laboratory, with 1 mL of sample diluted 1:1 with 5% HNO_3 and the tube closed with parafilm until analysis. Samples were spiked with 0.1 mL of 0.1 ppm concentration of Ge, Tm and Bi of the Internal Standard solution, to obtain a final volume of 2.1 mL with a 0.005 ppm concentration of Ge, Tm and Bi.

Standard solutions were prepared from distilled, deionized water and ultrapure 16 N HNO_3. Primary high purity mono-element standards from Inorganic Venture, 3% HNO_3 v/v, were used to gravimetrically prepare multi-elemental stock standard mixtures using a Mettler Toledo XSR analytical balance readable to 0.1 mg. I used 5 standards with different concentrations of Ca, Sr, Mg, Ba, 5 standards with different concentrations of Al, Mn, Ti and 4 standards with different concentrations of Cl. The 0.005 ppm Internal Standard of Ge+Tm+Bi was added to have the same concentration in blanks and samples.

Elements concentrations for Ca, Mg, Sr, Ba, Al, Mn, Ti, and Cl were determined using a Thermo Icap-Q-ICP-MS at the Laboratorio de Estudios Isotópicos, Centro de Geociencias. The acidified samples were nebulized with a pneumatic nebulization assisted by a peristaltic pump that controlled the sample flow to 500 µL/min. Data were corrected for blank intensities and instrumental drift using the variability of the Ge+Tm+Bi internal standard, and by bracketing the analysis of every 15 samples with measuring 3 different standards that included the elements of interest, and correcting each element by their corresponding standard solution deviation factor. The relative standard deviation (RSD) of the same standard solutions during one day of analysis and of repeated samples between runs are presented in Table 1C and Table 2C, respectively. With the assumption that isotopic abundances of single measured elements are practically constant in the water samples, data was converted into different concentration units using their correspondent standard calibration curves from measured standards and the dilution factor. The same monitored isotopes (listed in Table 3C) were analyzed in farmed calcite.

Table 1C. ICPMS Elemental Determination Coefficient of Variation (CV) of standards. Repeated measurements (n) for each element on the same day for three different elemental standards during one day of analysis. CV is the ratio of standard deviation to the arithmetic average.

Element	CV %	n
Ca	4	19
Mg	3	19
Ba	5	19
Sr	3	19
Ti	22	16
Mn	6	16
Al	8	16
Cl	23	19

Table 2C. ICPMS Elemental Determination Coefficient of Variation (CV) for three replicate water sample analyses over two run days. CV is the ratio of standard deviation to the arithmetic average.

Element	CV %	n
Mg	3	3
Ca	3	3
Ba	7	3
Sr	6	3
Al	22	3
Ti	8	3
Mn	24	3

Farmed calcite laboratory sampling.

Farmed calcite samples were taken to the Centro de Geociencias, UNAM. Glass plates were handled with nitrile gloves and carefully scraped with a stainless-steel spatula to collect calcite in the acid-cleaned eppendorf vials for trace element and stable isotopes compositions analysis. The sampling is illustrated in Figure C.1 using the glass plate from Fenix, with 37 days of growth.

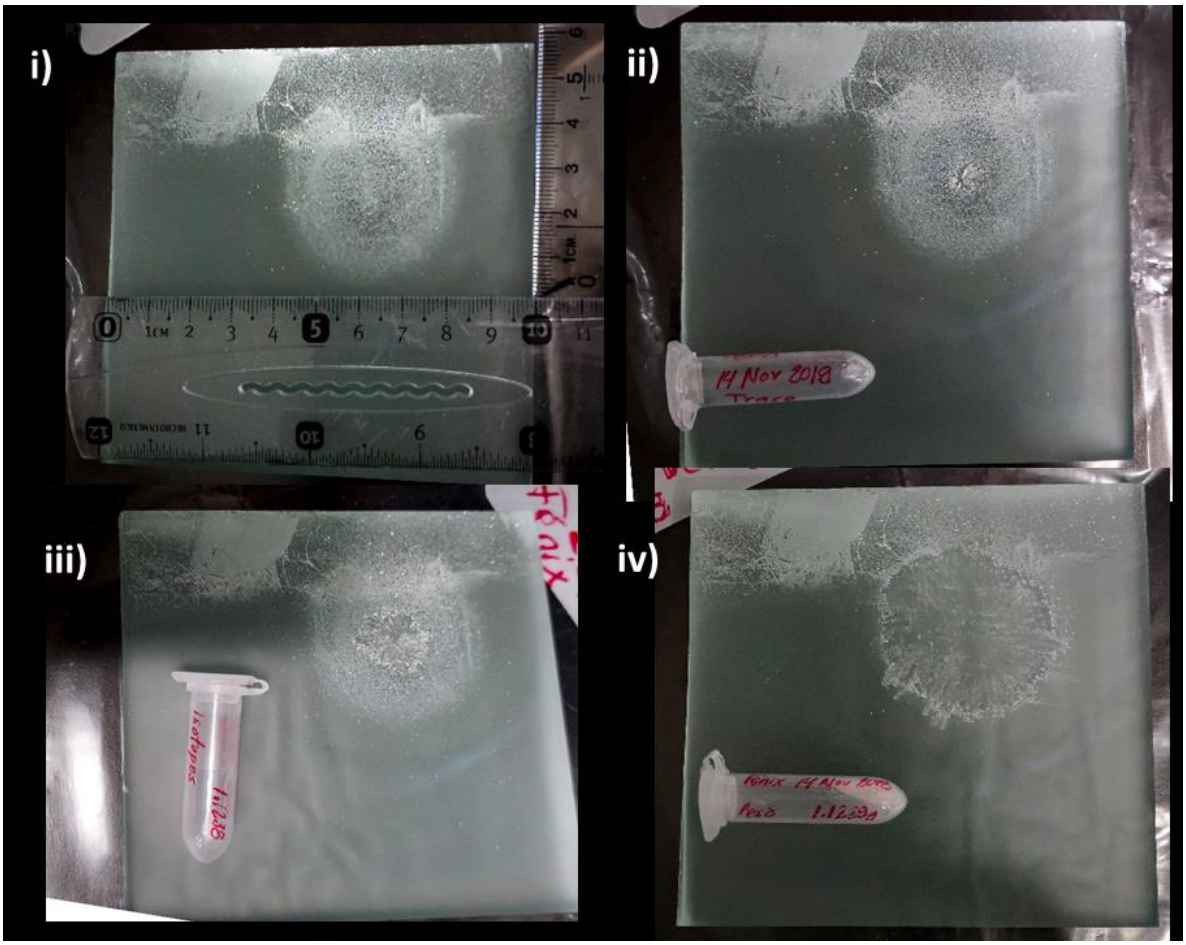

Figure C.1. Sampling procedure of farmed calcite on frosted glass plates. Example from Fénix drip site which grew over 37 days (October 9 to November 14, 2018).

i) The circular growth of 9.6 cm^2 of calcite that grew around the drip point.

ii) Select crystals are taken from the circle center and placed in an eppendorf vial, for determination of trace elements ratios.

iii) At least 1 mg is placed in an eppendorf vial for $\delta^{18}O$ and $\delta^{13}C$ determination.

iv) All remaining circular is placed in a third eppendorf vial. Calcite outside the primary circular drop growth, such as runoff of the water on the edges of the glass plate, is not considered, and not included in the mass determination. The runoff calcite is left on the glass, and stored in a ziploc bag as a back up.

The eppendorf vials are pre-weighed, and all mass determinations completed on a Mettler Toledo XSR analytical balance with resolution of 0.1 mg.

The growth rate of farmed calcite is reported as (mg/cm^2)/day based on the sum of the calcite in the Eppendorf vials, divided between the primary circular drip area, and the number of days of growth.

Farmed calcite elements measurement

Analysis of calcite crystals was carried out using LA-ICPMS at the Laboratorio de Estudios Isotópicos, Centro de Geociencias, UNAM, following the method of Bernal et al. (2016). Calcite crystals from 37 glass plates, ranging 10-100 µm in size, were arranged on 11 mounts with epoxy resin, that was then polished with 1-6 µm diamond paste until the crystals were exposed allowing for laser ablation. Each sample analysis included 7-9 crystals large enough to be ablated with a 33 µm diameter laser beam, with 5 Hz sampling rate and 4 J/cm^2 fluence. Examples of the ablation craters are shown in Fig. C.2.

Element/Ca molar ratios were standardized with NIST SRMs 612 glass using values per Jochum et al. (2011). The glass standard was ablated for 30 s, bracketing every 16 calcite crystal ablations, to support correction of potential drift due to material accumulation in the ICP cones. Relative standard deviation (RSD) of elemental ratios of NIST SRMs 612 glass standard (Table 4C) have <3% variability for Mg/Ca, Sr/Ca, and Ba/Ca. The monitored isotopes are reported in Table 3C. A similar approach has produced X/Ca ratios with < 5% variability (Evans and Müller, 2013). Inter-crystal variation in trace element ratios is likely controlled by variation in crystal size. Table 5C shows the standard error of the mean relative to each sample measurements for the Mg/Ca, Sr/Ca and Ba/Ca ratios. The crystal values of each sample were averaged and the result is reported in Table B4 of Appendix B.

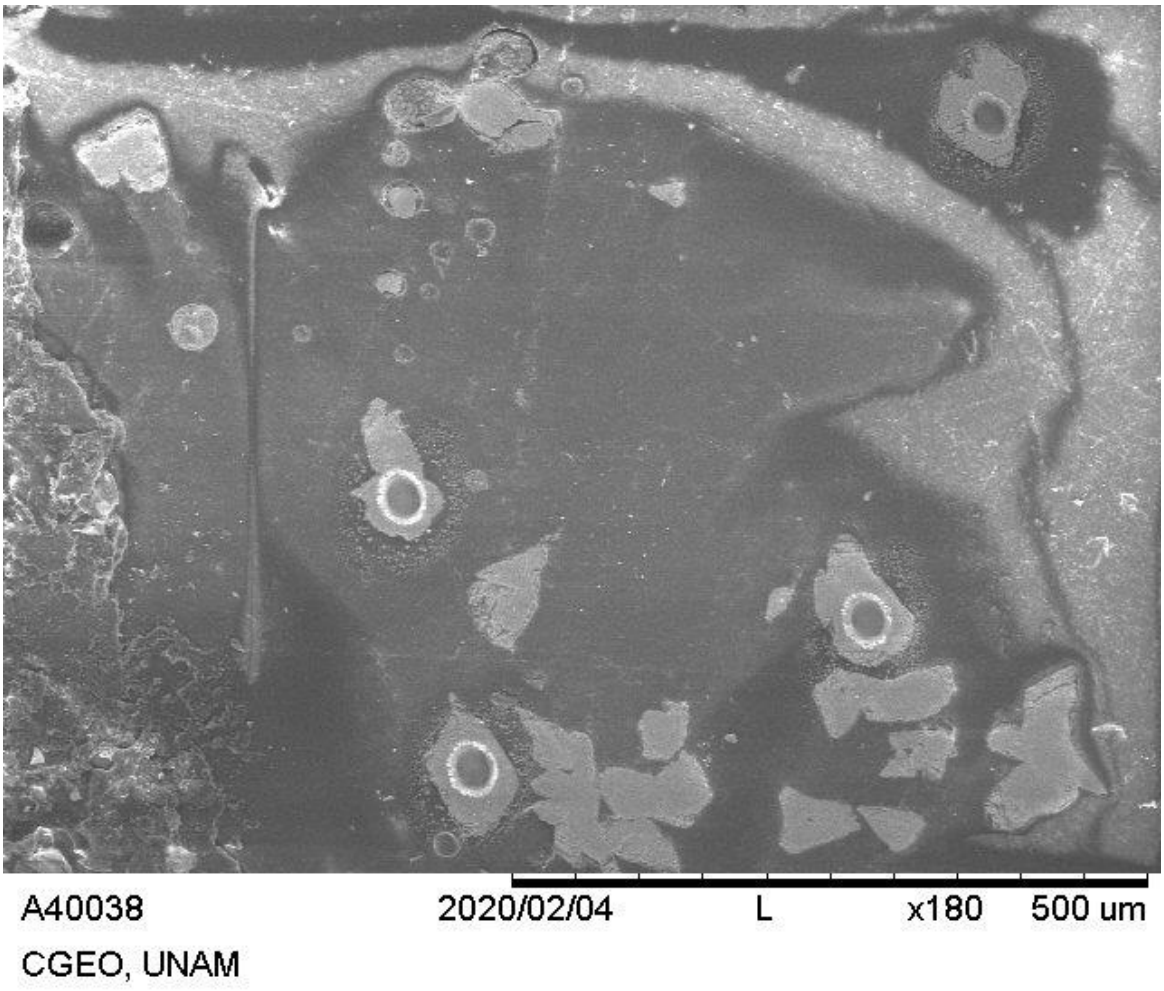

Figure C2. Calcite crystals and 4 craters after laser ablation corresponding to a B4 drip site farmed calcite sample. Image was obtained using a Hitachi TM-1000 Scanning Electron Microscope, operated at 15 KV and using a backscattered electron detector from Centro de Geociencias, UNAM.

Table 3C. Elements and isotopes monitored for the analysis of X/Ca ratios in farmed calcite and/or water samples.

Element	Monitored masses (m/z+)
Mg	26
Ca	43
Sr	88
Ba	137, 138
Al	27
Mn	55
Fe	57
U	238
Ti	47
Cl	35

Table 4C. Variation Coefficients (ratio of standard deviation to the arithmetic average) calculated for different elemental ratios during 20 bracketing measurements of NIST SRMs 612 during analysis of farmed calcite crystals.

Ratio	**VC (%)**
Mg/Ca	2.5
Sr/Ca	0.9
Ba/Ca	1.3

Table 5C- Standard error of the mean (SEM) for Mg/Ca, Sr/Ca and Ba/Ca of the measurement of individual crystals of farmed calcite sample.

	Growth Timeframe			Standard Error of the Mean		
Station Name	**Start Date**	**End Date**	**Number crystals ablated**	**Mg/Ca**	**Sr/Ca**	**Ba/Ca**
B4	03/04/2017	06/07/2017	8	0.09	0.0154	0.000132
B4	06/07/2017	15/10/2017	5	0.32	0.0072	0.000152
B4	15/10/2017	25/11/2017	9	0.14	0.0104	0.00012
B4	25/11/2017	10/01/2018	7	0.09	0.0224	0.000175
B4	10/01/2018	26/02/2018	8	0.24	0.0331	0.000300
B4	12/04/2018	14/05/2018	8	0.03	0.0114	0.000103
B4	14/05/2018	04/06/2018	8	0.12	0.0397	0.002666
B4	04/06/2018	31/07/2018	8	0.21	0.0363	0.000130
B4	31/07/2018	31/08/2018	8	0.12	0.0220	0.000168
B4	31/08/2018	09/10/2018	8	0.10	0.0171	0.000208
B4	14/11/2018	14/01/2019	8	0.09	0.0145	0.000245
A7	03/04/2017	06/07/2017	8	0.15	0.0248	0.000500
A7	06/07/2017	15/10/2017	7	0.22	0.0370	0.000406
A7	15/10/2017	25/11/2017	8	0.15	0.0153	0.000207
A7	25/11/2017	10/01/2018	3	0.00	0.0053	0.000833
A7	10/01/2018	26/02/2018	7	0.10	0.0114	0.000318
A7	26/02/2018	12/04/2018	6	0.15	0.0185	0.000501
A7	12/04/2018	14/05/2018	8	0.11	0.0162	0.000347
A7	14/05/2018	04/06/2018	8	0.17	0.0252	0.000300
A7	04/06/2018	31/07/2018	8	0.10	0.0152	0.000196
A7	31/08/2018	09/10/2018	7	0.12	0.0103	0.000224
A7	09/10/2018	14/11/2018	9	0.13	0.0166	0.000123
A7	14/11/2018	14/01/2019	8	0.14	0.0331	0.000507
Fénix	03/04/2017	06/07/2017	8	0.12	0.0240	0.000261
Fénix	11/07/2017	02/08/2017	8	0.08	0.0240	0.000342
Fénix	02/08/2017	15/10/2017	8	0.13	0.0135	0.000217
Fénix	15/10/2017	25/11/2017	8	0.11	0.0158	0.000199
Fénix	25/11/2017	10/01/2018	9	0.05	0.0041	0.000153
Fénix	10/01/2018	26/02/2018	8	0.03	0.0046	0.000104
Fénix	26/02/2018	12/04/2018	9	0.07	0.0058	0.000286
Fénix	12/04/2018	14/05/2018	8	0.05	0.0047	0.000087
Fénix	14/05/2018	04/06/2018	8	0.05	0.0154	0.000272
Fénix	04/06/2018	31/07/2018	8	0.09	0.0131	0.000384
Fénix	31/07/2018	31/08/2018	9	0.06	0.0252	0.000601
Fénix	31/08/2018	09/10/2018	8	0.10	0.0181	0.000509
Fénix	09/10/2018	14/11/2018	9	0.10	0.0169	0.000461
Fénix	14/11/2018	14/01/2019	7	0.13	0.0035	0.000392